

**Investigating the control of inter-homologue
recombination and synapsis during meiosis in
*Arabidopsis thaliana***

by

MAHEEN FERDOUS

A thesis submitted to
The University of Birmingham
for the degree of
DOCTOR OF PHILOSOPHY

School of Biosciences
University of Birmingham
September 2012

UNIVERSITY OF
BIRMINGHAM

University of Birmingham Research Archive

e-theses repository

This unpublished thesis/dissertation is copyright of the author and/or third parties. The intellectual property rights of the author or third parties in respect of this work are as defined by The Copyright Designs and Patents Act 1988 or as modified by any successor legislation.

Any use made of information contained in this thesis/dissertation must be in accordance with that legislation and must be properly acknowledged. Further distribution or reproduction in any format is prohibited without the permission of the copyright holder.

Abstract

During meiosis, axis formation and synapsis of homologous chromosomes are tightly co-ordinated with meiotic recombination. This study investigates the influence of chromosome axis and synaptonemal complex proteins on meiotic crossover formation.

The study involved the characterization of a novel protein, AtASY3, required for normal meiosis in *Arabidopsis*. Analysis of *Atasy3* mutants revealed that loss AtASY3 compromises chromosome axis formation, synapsis and normal levels of crossover formation. Further analysis revealed that loss of AtASY3 disrupts the axial organization of AtASY1. In separate studies, colleagues found that AtASY3 and AtASY1 are able to interact. Together, these results suggest that AtASY3 is a functional homologue of the budding yeast axis protein, Red1. Since studies in budding yeast indicate that Red1 and Hop1 (homologue of AtASY1) play a key role in establishing a bias to favour inter-homologue recombination, this study suggests that AtASY3 and AtASY1 may have a similar role in *Arabidopsis*.

The study also involved the analysis of the putative phosphorylation site, residue T295, on AtASY1. This revealed that T295 is essential for AtASY1-mediated crossover formation during meiosis. Additionally, a potential meiotic role for the RECQ DNA helicase, AtRECQ4B was investigated, however, the protein does not appear to be essential for *Arabidopsis* meiosis.

Acknowledgements

I would like to thank Prof. Chris Franklin for providing me the opportunity to do such a challenging and rewarding project. I am highly grateful for his exceptional supervision, guidance and support towards my project and academic development.

I would like to especially thank Dr. James Higgins for his excellent supervision, guidance and support on all aspects of my project throughout my PhD. I am thankful to Dr. Kim Osman for helping me with protein gel analysis and Dr. Richard Tudor for assistance with molecular biology techniques. I am grateful to Dr. Gareth Jones for his help with *Crepis* and advice regarding my project. I would also like to thank Dr. Eugenio Sanchez-Moran, Dr. Susan Armstrong and Prof. Noni Franklin-Tong for helpful scientific discussions and guidance throughout my PhD. I am grateful to Ruth Perry and Steve Price for technical assistance and Karen Staples for horticultural support. I am also thankful to all members, past and present, of the Franklin, Armstrong, Franklin-Tong, Sanchez-Moran and Coates labs for their help and support during my PhD.

I would like to thank my family, my wife Niki and her family and my friends, especially Rashed Hossain and Mohammad Ahasan, for their love and support over the past few years, which helped me through both the good and difficult times of my PhD.

List of Contents

ABSTRACT	II
ACKNOWLEDGEMENTS.....	III
CHAPTER 1	1
INTRODUCTION	1
1.1. OVERVIEW OF MEIOSIS	2
1.1.1. <i>Meiosis I: The first meiotic division</i>	2
1.1.2. <i>Meiosis II: The second meiotic division</i>	3
1.2. SISTER CHROMATID COHESION	6
1.3. PAIRING AND SYNAPSIS OF HOMOLOGOUS CHROMOSOMES	8
1.3.1. <i>Homologous chromosome pairing</i>	9
1.3.2. <i>Homologous chromosome synapsis</i>	13
1.3.3. <i>Role of meiotic recombination in homologous chromosome pairing and synapsis</i>	18
1.4. MEIOTIC RECOMBINATION.....	21
1.4.1. <i>DNA double-strand break formation</i>	23
1.4.2. <i>Processing of double-strand breaks</i>	25
1.4.3. <i>Strand invasion and exchange</i>	26
1.4.4. <i>Pathways to meiotic crossover formation</i>	34
1.4.4.1. <i>MSH4-dependent pathway for crossover formation</i>	35
1.4.4.2. <i>MSH4-independent pathway for CO formation</i>	43
1.4.5. <i>Double-Holliday junction resolution</i>	45
1.4.6. <i>Crossover homeostasis</i>	48
1.4.7. <i>Crossover control</i>	50
1.5. INTER-RELATIONSHIP BETWEEN CHROMOSOME AXES AND MEIOTIC RECOMBINATION	56
1.5.1. <i>Co-ordination between chromosome axis maturation and recombination</i>	56
1.5.2. <i>Spatial association between recombination and chromosome axis/SC</i>	58
1.5.3. <i>Role of axis proteins in recombination</i>	59

1.6. <i>ARABIDOPSIS THALIANA</i> - A MODEL PLANT FOR MEIOSIS RESEARCH	60
1.7. AIMS AND OBJECTIVES	62
CHAPTER 2	64
MATERIALS AND METHODS	64
2.1. PLANT MATERIAL AND GROWTH CONDITIONS.....	65
2.2. NUCLEIC ACID MANIPULATIONS.....	65
2.2.1. <i>Isolation of plant DNA</i>	65
2.2.2. <i>RNA extraction from plant tissue</i>	66
2.2.3. <i>cDNA synthesis</i>	67
2.2.4. <i>Nucleic acid quantification</i>	67
2.2.5. <i>DNA agarose gel electrophoresis</i>	67
2.2.6. <i>RNA agarose gel electrophoresis</i>	68
2.2.7. <i>Primer design</i>	68
2.2.8. <i>Polymerase chain reaction (PCR)</i>	69
2.2.9. <i>PCR for genotyping plants</i>	70
2.2.10. <i>Reverse transcription (RT)-PCR</i>	70
2.2.11. <i>3' -rapid amplification of cDNA ends (RACE)</i>	71
2.2.12. <i>Cloning</i>	71
2.2.12.1. <i>Amplification of insert DNA</i>	71
2.2.12.2. <i>Gel extraction of DNA bands</i>	72
2.2.12.3. <i>Ligation of DNA fragments into vectors</i>	72
pCR®-Blunt	73
pET21b	74
pPF408	74
2.2.12.4. <i>Preparation of competent E. coli cells</i>	75
2.2.12.5. <i>Transformation into competent E. coli by heat shock</i>	76
2.2.12.6. <i>Preparation of electro-competent A. tumefaciens</i>	76
2.2.12.7. <i>Transformation into electro-competent A. tumefaciens</i>	77
2.4.12.8. <i>Bacterial growth media</i>	77

2.2.12.9. Colony PCR	78
2.2.12.10. Extraction of plasmid DNA using boil preparation	78
2.2.12.11. Purification of plasmid DNA using wizard preparation	79
2.2.12.12. Restriction digestion	80
2.2.12.13. DNA sequencing	80
2.2.12.14. DNA sequence analysis	80
2.3. PROTEIN MANIPULATIONS.....	81
2.3.1. Recombinant protein production	81
2.3.1.1. Test induction and purification	81
2.3.1.2. Large scale protein production.....	82
2.3.2. Protein extraction from plant tissue	83
2.3.3. Protein quantification	84
2.3.4. Sodium dodecyl sulfate polyacrylamide gel electrophoresis (SDS-PAGE)	84
2.3.5. Two dimensional-polyacrylamide gel electrophoresis (2D-PAGE)	85
2.3.6. Coomassie staining.....	87
2.3.7. Western blotting	87
2.3.8. Antibody labelling	88
2.3.9. Protein detection using enhanced chemiluminescence (ECL).....	88
2.4. CYTOLOGICAL PROCEDURES.....	89
2.4.1. Meiotic chromosome spreading.....	89
2.4.2. Preparation of fluorescence in situ hybridization (FISH) probes	89
2.4.3. Fluorescence in situ hybridization (FISH).....	90
2.4.4. Meiotic timecourse	91
2.4.5. Immunolocalization.....	92
2.4.6. Immunolocalization coupled with timecourse	93
2.4.7. Assessing pollen viability using Alexander's staining	93
2.4.8. Fluorescence microscopy and image analysis	94
2.5. TRANSFORMATION INTO ARABIDOPSIS	94

2.6. GENETIC CROSSING OF PLANTS.....	95
2.7. STATISTICAL PROCEDURES.....	96
CHAPTER 3	97
INVESTIGATION OF THE ARABIDOPSIS RECQ HELICASE, ATRECQ4B	97
3.1. INTRODUCTION.....	98
3.2. <i>ATRECQ4A</i> AND <i>ATRECQ4B</i> EXPRESSION IS MEIOSIS-SPECIFIC.....	100
3.3. ANALYSIS OF <i>ATRECQ4A</i> AND <i>ATRECQ4B</i> EXPRESSION IN THEIR CORRESPONDING MUTANT LINES.....	102
3.4. ANALYSIS OF <i>ATRECQ4B</i> FERTILITY	103
3.5. CYTOLOGICAL ANALYSIS OF WILD-TYPE AND <i>ATRECQ4B</i> MEIOTIC STAGES.....	104
3.6. <i>ATRECQ4B</i> IS NOT ESSENTIAL FOR CO FORMATION	108
3.7. DISCUSSION	109
3.7.1. <i>AtRECQ4A</i> and <i>AtRECQ4B</i> are expressed during meiosis.....	109
3.7.2. Disruption of <i>AtRECQ4B</i> does not lead to meiotic defects.....	109
3.7.3. Loss of <i>AtRECQ4B</i> does not affect chiasma formation.....	111
CHAPTER 4	113
MOLECULAR CHARACTERIZATION OF ASY3 IN ARABIDOPSIS THALIANA AND BRASSICA OLERACEA	113
4.1. INTRODUCTION.....	114
4.2. IDENTIFICATION OF <i>ARABIDOPSIS ASY3</i>	115
4.3. <i>ATASY3</i> IS EXPRESSED IN REPRODUCTIVE TISSUES.....	119
4.4. MOLECULAR CHARACTERIZATION AND ANALYSIS OF <i>ATASY3</i> T-DNA INSERTION MUTANTS	120
4.5. MOLECULAR CHARACTERIZATION OF <i>BRASSICA ASY3</i>	123
4.5.1. Determining <i>BoASY3</i> 3'-end nucleotide sequence using 3'-RACE	124
4.5.2. Cloning the full length coding sequence of <i>BoASY3</i>	126
4.6. PRODUCTION OF AN ANTI-ASY3 ANTIBODY.....	133
4.6.1. Cloning the <i>AtASY3</i> C-terminal region for recombinant protein production.....	133
4.6.2. Production of the recombinant protein for anti-ASY3 antibody preparation.....	134
4.6.3. Validation of anti-ASY3 antiserum.....	136
4.7. DISCUSSION	140
4.7.1. <i>ASY3</i> is a putative meiotic axis protein in <i>Arabidopsis</i> and <i>Brassica</i>	140

4.7.2. <i>AtASY3</i> is expressed in <i>Arabidopsis</i> meiocytes	141
4.7.3. <i>Atasy3</i> mutants display reduced fertility	142
4.7.4. Anti-ASY3 antibody is capable of detecting recombinant ASY3	142
CHAPTER 5	144
CYTOLOGY AND IMMUNOLocalIZATION OF ASY3	144
5.1. INTRODUCTION	145
5.2. CYTOLOGICAL ANALYSIS OF <i>ATASY3</i> MUTANTS	145
5.3. VERIFICATION OF <i>ATASY3</i> MUTANT PHENOTYPE	149
5.3.1. <i>Allelism test</i>	149
5.3.2. <i>Complementation test</i>	149
5.3.2.1. Cloning <i>AtASY3</i> cDNA for complementation of <i>Atasy3</i> mutants	150
5.3.2.2. Transformation of <i>AtASY3</i> cDNA into <i>Atasy3</i> mutants and analysis of subsequent transformants	152
5.4. <i>ATASY3</i> LOCALIZES TO MEIOTIC CHROMOSOME AXES IN EARLY PROPHASE I	156
5.5. <i>BoASY3</i> LOCALIZES TO MEIOTIC CHROMOSOME AXES SIMILARLY TO <i>ATASY3</i>	159
5.6. ANALYSIS OF MEIOTIC CHROMOSOME AXIS AND SC PROTEINS IN <i>ATASY3-1</i> MUTANT	161
5.6.1. <i>Meiotic cohesin components AtSMC3 and AtSYN1 localize normally in Atasy3-1</i>	161
5.6.2. <i>AtASY1 localization is disrupted in Atasy3-1</i>	162
5.6.3. <i>AtZYP1 fails to polymerize in Atasy3-1</i>	164
5.7. CHIASMA FREQUENCY IS SIGNIFICANTLY REDUCED IN <i>ATASY3</i> MUTANTS	166
5.8. ANALYSIS OF RECOMBINATION PROTEINS IN <i>ATASY3-1</i> MUTANT	169
5.8.1. <i>DSB formation is reduced in Atasy3-1</i>	169
5.8.2. <i>Number of foci of strand exchange proteins is reduced in Atasy3-1</i>	170
5.8.3. <i>Localization of AtMSH4 and AtMLH1 is reduced in Atasy3-1</i>	171
5.9. THE RESIDUAL <i>ATASY1</i> FOCI STABILIZES <i>AtDMC1</i> IN <i>ATASY3-1</i>	175
5.10. <i>ATASY1</i> IS EPISTATIC TO <i>ATASY3</i> WITH REGARD TO CO FORMATION	178
5.11. LOSS OF <i>ATASY3</i> DOES NOT AFFECT PROGRESSION OF MEIOSIS	178
5.12. DISCUSSION	180
5.12.1. <i>Loss of AtASY3 results in asynapsis and other meiotic defects</i>	180

5.12.2. ASY3 is a meiotic chromosome axis protein in Arabidopsis and Brassica	181
5.12.3. Normal AtASY1 localization is dependent on AtASY3	183
5.12.4. AtASY1 localization in Atasy3-1 is DSB-independent	185
5.12.5. DSBs appear reduced in Atasy3-1	186
5.12.6. AtASY3 is required for normal levels of CO formation	189
5.12.7. Residual AtASY1 mediate AtDMC1-dependent inter-homologue recombination in Atasy3-1	190
5.12.8. SC nucleation is sufficient to prevent ectopic recombination during meiosis	193
CHAPTER 6	195
ANALYSIS OF ARABIDOPSIS ASY1-T295A MUTANTS	195
6.1. INTRODUCTION	196
6.2. MOLECULAR CHARACTERIZATION OF ATASY1-T295A	198
6.3. ANALYSIS OF ATASY1-T295A	202
6.4. CYTOLOGICAL ANALYSIS OF ATASY1-T295A	204
6.5. NORMAL ATASY1 LOCALIZATION MAY BE DISRUPTED ATASY1-T295A	206
6.6. ANALYSIS OF ATASY1 ^{T295A} PROTEIN EXPRESSION IN ATASY1-T295A	206
6.6.1. Detection of AtASY1 in wild-type and Atasy1 mutant	207
6.6.2. Detection of AtASY1 ^{T295A} in Atasy1-T295A	208
6.7. PRELIMINARY ANALYSIS OF ASY1 PHOSPHORYLATION USING 2D GEL ELECTROPHORESIS	212
6.8. DISCUSSION	214
6.8.1. Mutation of T to A at residue 295 of AtASY1 leads to meiotic defects	214
6.8.2. Residue T295 may be essential for the normal AtASY1 localization	216
6.8.3. AtASY1T295A is unable to promote normal levels of inter-homologue recombination in Atasy1-T295A	217
6.8.4. Preliminary analysis suggests that BoASY1, homologue of AtASY1, may be a likely substrate for phosphorylation	219
CHAPTER 7	222
GENERAL DISCUSSION	222
7.1. INTRODUCTION	223
7.2. ATRECQ4B IS NOT ESSENTIAL FOR NORMAL MEIOSIS	223
7.3. ATASY3, A NOVEL MEIOTIC AXES COMPONENT, IS REQUIRED FOR SYNAPSIS AND CO FORMATION DURING MEIOSIS	227

7.3.1. ASY3 is a novel component of meiotic chromosome axes.....	227
7.3.2. AtASY3 is required for normal levels of meiotic DSB and CO formation	229
7.3.4. AtASY3 is required for normal AtASY1 localization	230
7.3.5. ASY3 interacts with ASY1 in Arabidopsis and Brassica.....	232
7.3.6. AtASY3 shares functional similarities with RED1	234
7.3.7. Putative roles of the axis protein AtASY3 in CO formation	236
7.3.8. Future perspectives	238
7.3.8.1. Putative interaction of SUMO with AtASY3	238
7.3.8.2. Putative phosphorylation of AtASY3	242
7.4. ATASY1 PHOSPHORYLATION IS ESSENTIAL FOR MEDIATING INTER-HOMOLOGUE RECOMBINATION.....	247
7.4.1. Atasy1-T295 mutants exhibit defective meiosis.....	247
7.4.2. AtASY1 T295 is essential for normal levels of inter-homologue recombination	248
7.4.3. Further work.....	250
7.5. FINAL WORD	253
REFERENCES.....	254
APPENDIX	270
9.1. GENERAL BUFFERS AND SOLUTIONS	271
CYTOLOGY.....	271
NUCLEIC ACID MANIPULATIONS	272
PROTEIN MANIPULATIONS	273
9.2. LIST OF PRIMERS	275
9.3 LIST OF PUBLICATIONS AND PRESENTATIONS	282
Publications.....	282
Oral presentations	282
Poster presentations	283
Other scientific activities.....	283

List of Figures

Figure 1. Diagrammatic representation of meiosis.	5
Figure 2. (A) Dual loop organization and (B) structure of the SC.	20
Figure 3. Schematic representation of meiotic DSB repair pathway.....	22
Figure 4. Expression analysis of <i>AtRECQ4A</i> and <i>AtRECQ4B</i> in flower buds.	101
Figure 5. Meiotic atlas of WT <i>Arabidopsis</i>	106
Figure 6. <i>Atrecq4B</i> mutant cytology.	107
Figure 7. Structure of <i>AtASY3</i> and its predicted product and <i>AtASY3</i> expression analysis.	118
Figure 8. Comparison between WT and <i>Atasy3</i> fertility.....	122
Figure 9. (A,D,E,F) ClustalW2 alignment of various sequences, (B) 3' RACE PCR products and (C) Amplification of <i>BoASY3</i>	132
Figure 10. Cloning and detection of <i>AtASY3</i> -C recombinant protein and validation of anti-ASY3 antibody.....	139
Figure 11. Representative meiotic stages from <i>Atasy3-1</i> PMCs.	147
Figure 12. Representative meiotic stages of <i>Atasy3-2</i> (A-F) and <i>Atasy3-3</i> (G-L)....	148
Figure 13. (A) Allelism and (B, C) complementation analysis.....	155
Figure 14. Immunolocalization of <i>AtASY3</i> in WT.....	158
Figure 15. Immunolocalization of <i>BoASY3</i> using anti-ASY3 antibody.....	160
Figure 16. Immunolocalization of axis and SC proteins in <i>Atasy3-1</i>	165
Figure 17. Cytological and FISH analysis of WT, <i>Atasy3-1</i> and various other mutants.	168
Figure 18. Immunolocalization of various recombination proteins in WT and <i>Atasy3-1</i>	174
Figure 19. Time-course analysis of <i>AtDMC1</i> localization in WT, <i>Atasy1</i> and <i>Atasy3</i> and of meiotic progression in <i>Atasy3-1</i>	177
Figure 20. Analysis of the nucleotide and amino acid sequence of the transgene in <i>Atasy1T295A</i>	201
Figure 21. Cytology of <i>Atasy1T295A</i> and <i>AtASY1</i> localisation in the mutant.	205

Figure 22. Western blotting analysis of ASY1 in extracts from WT, *Atasy1*, *Atasy1T295A* and *Brassica*.211

List of Tables

Table 1. Standard PCR.	70
Table 2. Components of the resolving and stacking gels and their amounts for SDS-PAGE.	85
Table 3. Conditions for rehydration and IEF for 2D-PAGE.	87
Table 4. Number of transgenic plants and the percentage of their fertility (mean seed-set) relative to the wild-type.	154
Table 5. Comparison of lengths of siliques from WT, <i>Atasy1</i> and <i>Atasy1-T295A</i> mutants.	203
Table 6. Comparison of mean seed-sets of WT, <i>Atasy1</i> and <i>Atasy1-T295A</i> mutants.	203

List of Abbreviations

AE	Axial element
ASY1	Asynaptic 1
At	<i>Arabidopsis thaliana</i>
ATP	Adenosine tri-phosphate
BIO	Biotin
BLAP75	BLM-associated polypeptide
BLM	Bloom syndrome protein
BRCA2	Breast cancer 2
BrdU	Bromodeoxyuridine
BSA	Bovine serum albumin
C-terminal	Carboxyl-terminal
cDNA	Copy DNA
CO	Crossover
Col-0	<i>Arabidopsis thaliana</i> ecotype columbia
DAPI	4,6-diaminido-2-phenylindole
DEPC	Diethyl procarbonate
dHj	Double holliday junction
DIG	Digoxigenin
D-loop	Displacement loop
DMC1	Disruption of meiotic control 1
DNA	Deoxyribonucleic acid
DSB	Double-strand break
ECL	Enhanced chemiluminescence
EM	Electron microscopy
FISH	Fluorescent <i>in situ</i> hybridisation
FITC	Fluorescein isothiocyanate
GAPD	Glyceraldehyde-3-phosphate dehydrogenase
GFP	Green fluorescent protein
HOP1	Homologue pairing 1
HORMA	Domain common in: Hop1p, Rev7p and MAD2
HRP	Horseradish peroxidase
H2AX	Histone variant H2AX
IPTG	Isopropyl β -D-1-thiogalactopyranoside

JM	Joint molecule
LE	Lateral element
MEK1	Meiotic kinase 1
MLH1	MutL homologue 1
MLH3	MutL homologue 3
MMS4	Methyl methanesulfonate sensitive 4
MND1	Meiotic nuclear division 1
MRE11	Meiotic recombination 11
mRNA	Messenger RNA
MS	Murashige and Skoog
MSH4	MutS homolog 4
MSH5	MutS homolog 5
MUS81	MMS and UV sensitive 81
NASC	National Arabidopsis Stock Center
NCO	Non crossover
NE	Nuclear envelope
N-terminal	Amino-terminal
O/N	Overnight
PBS	Phosphate buffered saline
PCR	Polymerase chain reaction
PMC	Pollen mother cell
rDNA	Ribosomal DNA
RED1	Reduction division defective 1
RMI1	RecQ mediated genome instability 1
RNA	Ribonucleic acid
RPA	Replication protein A
RT	Room temperature
RT-PCR	Reverse transcription polymerase chain reaction
SEI	Single end invasion
SC	Synaptonemal complex
SDS-PAGE	Sodium-dodecyl-sulfate polyacrylamide gel electrophoresis
SDSA	Synthesis-dependant strand annealing
SDW	Sterile distilled water
SMC	Structural maintenance of chromosomes
SPO11	Sporulation specific protein 11
SSC	Saline sodium citrate

ssDNA	Single stranded DNA
SYCP	Synaptonemal complex protein
SYN1	Synapsis 1
T-DNA	Transfer DNA
TF	Transverse filament
TOP3 α	Topoisomerase 3 alpha
WT	Wild-type
ZYP1	Synaptonemal complex protein 1

CHAPTER 1

Introduction

1.1. Overview of Meiosis

Meiosis is a specialized cell division in eukaryotes, involving two rounds of nuclear division known as meiosis I and meiosis II, after one round of DNA replication. Both meiosis I and meiosis II consist of four stages – prophase, metaphase, anaphase and telophase. During meiosis I homologous chromosomes separate and during meiosis II sister chromatids separate to produce haploid gametes. These divisions reduce the chromosome number by half thereby compensating for fertilization, which involves the conjugation of two haploid sets of genetic information for the formation of a diploid offspring. Meiosis thus ensures chromosome number from generation to generation and is therefore essential for sexual reproduction. An important aspect of meiosis is homologous recombination, a process that allows the exchange of genetic material between paternal and maternal homologous chromosomes resulting in the formation of new combinations of alleles. Therefore, meiosis is also crucial for producing genetic variation. Meiosis is highly conserved throughout evolution and its duration lasts about 33h in *Arabidopsis* (Armstrong et al., 2003).

1.1.1. Meiosis I: The first meiotic division

Prior to meiosis, DNA replication occurs during pre-meiotic S phase. Prophase I is the first and longest stage of meiosis lasting ~21 hours in *Arabidopsis* (Armstrong et al., 2003). It is divided into five cytologically distinct substages – leptotene, zygotene, pachytene, diplotene and diakinesis. Figure 1 is a diagrammatic representation of all the stages of meiosis. Early during leptotene, chromosomes condense into thin thread-like structures called chromatids. Sister chromatids are held together by a

protein complex called cohesin (Sjogren and Nasmyth, 2001). Homologous chromosomes start to pair and synapse along their axis via the assembly of a proteinaceous structure known as the synaptonemal complex (SC). Meiotic recombination is also initiated at certain regions of the chromosomes at this stage. Pairing and synapsis is more apparent during zygotene, where chromosomes appear relatively thicker. Zygotene is followed by pachytene during which homologous chromosomes appear fully synapsed. During diplotene, the SC disassembles and at diakinesis, crossovers (COs), which are products of meiotic recombination, are visible as chiasmata (singular - chiasma) on paired homologues, also referred to as bivalents. Bivalents progressively condense and desynapse along most of their lengths except at chiasmata. Subsequently, kinetochore microtubules, a type of spindle fibre become attached to specialized protein structures called kinetochores, formed on the centromere of each chromosome. The kinetochore microtubules then start to align the bivalents within the cell and at metaphase I bivalents are arranged at the equatorial region of the meiotic cell. During anaphase I homologous chromosomes separate and move towards either poles of the cell due to shortening of spindle fibres. This process is known as disjunction and is followed by telophase I which leads to the formation of the dyad stage, in which the cell contains two polar groups of partially decondensed chromosomes. The cell then initiates a second round of nuclear division.

1.1.2. Meiosis II: The second meiotic division

The second meiotic division is very similar to a mitotic division. During prophase II, each of the two poles of the meiotic cell consist of a pair of sister chromatids. At

metaphase II, the sister chromatids align on the equatorial plate while remaining attached to the spindle fibres. During anaphase II, sister chromatids separate and migrate towards the poles of the cell. This leads to telophase II, where one member of each chromosome is present at each pole. This is followed by the formation of a nuclear envelope around each set of chromosome and subsequently cytokinesis, which generates four haploid cells.

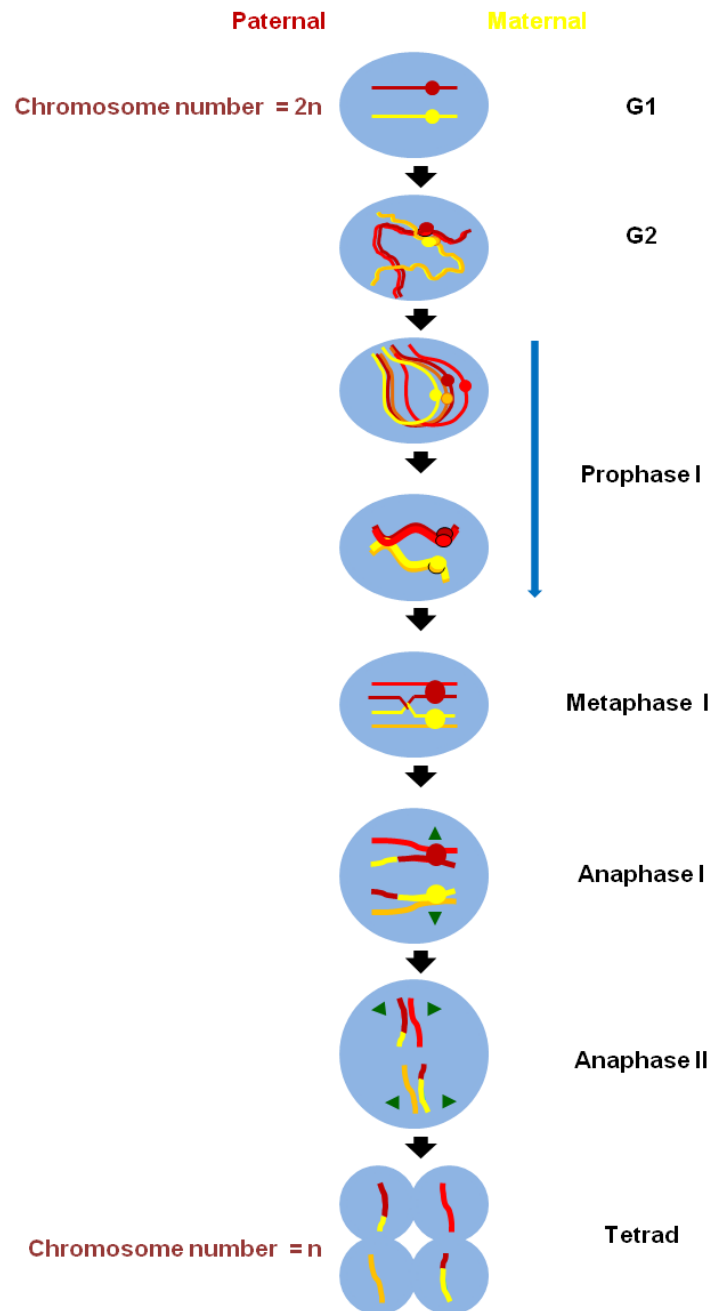


Figure 1. Diagrammatic representation of meiosis.

DNA synthesis occurs in the diploid parent cell prior to meiosis. During prophase I of meiosis homologous chromosomes pair and synapse and recombination events take place between them. Homologous chromosomes align during metaphase I, followed by their separation at anaphase I. This is followed by a second division at anaphase II which separates the sister chromatids leading to the formation of four haploid gametes.

1.2. Sister chromatid cohesion

Prior to the onset of mitosis and meiosis sister chromatid cohesion is established following DNA replication in S phase (Guacci et al., 1994). Sister chromatid cohesion is essential for the attachment of the kinetochores of sister chromatids to microtubules emanating from the opposite spindle poles in both mitotic and meiotic cell. This attachment allows pairs of chromatids to be recognized and aligned at the equator of the metaphase spindle leading to the subsequent correct segregation of sister chromatids during both mitosis and meiosis II (Uhlmann and Nasmyth, 1998). Sister chromatid cohesion is maintained by a ring-like multi-protein complex known as the cohesin (Michaelis et al., 1997, Uhlmann and Nasmyth, 1998). Cohesin ranges around 40nm in diameter and holds sister chromatids together during both mitosis and meiosis (Gruber et al., 2003). Cohesin accumulates at ~50kb region around each centromere and at AT rich and intergenic regions along chromosome arms during S phase (Uhlmann, 2004). Studies in budding yeast have revealed that the mitotic cohesin complex consists of four core proteins – the SMC proteins SMC1 and SMC3, the Kleisin family member SCC1 and SCC3, while the meiotic cohesin complex contains the same proteins, with the exception that SCC1 is replaced by another Kleisin member, REC8 (Guacci et al., 1997, Michaelis et al., 1997). SMC1 and SMC3 have five structural domains – two α helices, a globular hinge domain and N and C terminal globular domains containing nucleotide binding motifs called Walker A and Walker B respectively (Losada and Hirano, 2005). SMC1 and SMC3 are thought to fold in half at the hinge domain producing anti parallel coil interaction, bringing the Walker A and Walker B motifs together to create a region with ATPase activity, which is thought to be required for the association of SMC proteins with DNA

(Arumugam et al., 2003, Haering et al., 2002, Nasmyth and Haering, 2005). Biochemical studies in which yeast recombinant proteins were co-expressed in insect cells showed that SMC1 and SMC3 monomers interact with each other in the hinge region to form a stable V-shaped heterodimer (Haering et al., 2004). Further studies suggest that the head of SMC1 interacts with the carboxyl (C) -terminal of SCC1 and the head of SMC3 interacts with the amino (N) -terminal of SCC1 to form a ring structure that is proposed to hold the sister chromatids together (Gruber et al., 2003, Haering et al., 2002, Haering et al., 2004). REC8, component of the meiotic cohesion complex shares functional similarities in its N and C termini with its mitotic counterpart SCC1 (Gruber et al., 2003). Furthermore, biochemical studies revealed that REC8 can bind to SMC1 and SMC3 via interactions with its C and N termini respectively thus attributing to a structural role of REC8 in the meiotic cohesion complex (Gruber et al., 2003). SCC3 is the fourth subunit of the cohesin complex and studies in yeast have shown that it binds directly to the C-terminal of SCC1, presumably to stabilise the cohesin complex (Haering et al., 2002). The cohesin complex is highly conserved among organisms. SMC1 β , SMC3, REC8 and STAG3 (homologue of SCC3) have been identified as components of the mammalian cohesin complex and shown to interact with each other (Eijpe et al., 2003, Lee et al., 2003, Prieto et al., 2001, Revenkova et al., 2001). *Arabidopsis* AtSMC1 and AtSMC3 have similar structural properties as their yeast homologues and loss of these proteins result in defects in embryo and endosperm development (Lam, 2005, Liu Cm et al., 2002). Immunolocalization studies revealed that AtSMC3 localizes along the entire length of chromosomes by pachytene. AtSMC3 remains associated with sister chromatids until diakinesis after which a substantial AtSMC3 signal is observed

at microtubule spindle until telophase I suggesting a role of AtSMC3 in spindle assembly as well as sister chromatid cohesion (Lam, 2005). In *Arabidopsis*, AtSYN1 has been identified as a homologue of the yeast REC8 (Bai et al., 1999). Cytological analysis revealed that *Atsyn1* mutants possess abnormal chromosomes along with extensive chromosome fragmentation and bridges at anaphase I resulting in the formation of polyads and the subsequent defect in reproductive growth (Bai et al., 1999). Immunolocalization studies indicated that AtSYN1 localizes along the full length of meiotic chromosomes arms in early prophase I. (Cai, 2003). Recently, AtSCC3 has also been shown to be involved in sister-chromatid cohesion (Chelysheva, 2005). Cytological analysis showed that *Atsc3* mutants exhibit low levels of chromosome fragmentation and bridges at metaphase I suggesting that AtSCC3 is required for normal reproductive development (Chelysheva, 2005). Immunolocalization studies indicate that AtSCC3 associates with meiotic chromosomes from leptotene through to metaphase I, supporting a role for the protein as a component of the cohesin complex (Chelysheva, 2005).

1.3. Pairing and synapsis of homologous chromosomes

Pairing and synapsis of homologous chromosomes are essential for the correct recognition, juxtaposition and alignment of homologues during meiosis.

1.3.1. Homologous chromosome pairing

Telomeres are thought to play an important role during early chromosome pairing. Telomeres are composed of tandem repeat sequences at chromosome ends thereby protecting them from shortening or degradation. Telomeric repeats are highly conserved although their numbers vary enormously between organisms. *Arabidopsis* telomeres are composed of the repeat sequence 5'-TTTAGGG-3' and range between 2-5kb in length (Riha and Shippen, 2003). Prior to meiosis in eukaryotes, the centromeres of chromosomes are found clustered near spindle poles while their telomeres are scattered across the other side of nucleus. This is known as the 'Rabl' orientation of chromosomes (Zickler and Kleckner, 1998). Eventually, during early prophase I telomeres become attached to the inner nuclear envelope (NE) and subsequently move along the NE to form a cluster towards the microtubule organizing centre (MTOC) This orientation of telomeres is known as the 'bouquet' arrangement (Bass et al., 2000, Scherthan, 2001). Bouquet formation has been proposed to facilitate homologue recognition and pairing by bringing homologous chromosomes into close association with each other (Bass et al., 2000, Golubovskaya et al., 2002, Harper et al., 2004). In hexaploid wheat, chromosome pairing depends on the Ph1 locus, which ensures pairing between homologues and not homoeologues (Riley et al., 1959). Nevertheless, bouquet formation during early wheat meiosis has been proposed to facilitate pairing of sub-telomeric regions, which subsequently facilitates pairing along homologous chromosomes (Lukaszewski, 1997). Similarly, recent FISH analysis in barley (*Hordeum vulgare L*) using telomere probes suggests that telomeres pair to form a bouquet in late G2 (Higgins et al., 2012). At this stage, the axis protein ASY1 formed continuous signal at subtelomeric

but remained as foci or short stretches in the interstitial regions. Subsequent SC formation was also found to initiate in the subtelomeric regions, from where it polymerized to linear stretches as prophase I progressed. Interestingly, telomeres were found to be clustered until late zygotene. This suggests that pairing and synapsis in Barley initiate from subtelomeric regions which are in close proximity, possibly due to telomere clustering (Higgins et al., 2012). However, studies in *Sordaria macrospora* revealed that homologue pairing occurs prior to the formation of the bouquet suggesting that it is not necessary for homologue pairing (Storlazzi et al., 2003). Therefore, the significance of the bouquet is currently a topic of debate. Additionally, it has been suggested that the bouquet may have a role in the regulation of recombination and interlock resolution, although these too remain unclear (Zickler and Kleckner, 1998). In *Arabidopsis*, telomeres do not form a classical 'bouquet' orientation and are instead found to cluster while remaining associated with the nucleolus rather than the NE throughout meiotic interphase (Armstrong et al., 2001). FISH analysis using sub-telomeric probes revealed that telomeres of homologous chromosomes in *Arabidopsis* pair at the G2-leptotene transition while remaining associated with the nucleolus. It is thought that this pairing is mediated by similar unique sequences present in the sub-telomeric regions of homologous chromosomes, although the exact mechanism of homologue recognition is not yet understood (Armstrong et al., 2001). These observations led Armstrong et al. (2001) to propose that the clustering of telomeres while remaining associated with the nucleolus in *Arabidopsis* may be equivalent to the bouquet of other species and may facilitate homologue pairing.

More recent studies suggest that meiotic chromosome pairing is promoted by telomere-led rapid meiotic prophase chromosome movements (RPMs) independent of bouquet formation (Lee et al., 2012). Studies in *S. pombe* revealed that dynamic movement (~5µm/min) of telomeres clustered them at the spindle pole body within the meiotic cell during zygotene and early pachytene (reviewed in Koszul and Kleckner, 2009). In maize, live imaging studies revealed that the telomere-led movements were involved in movements of individual chromosome segments as well as rotations of the entire chromatin during early prophase I (Sheehan and Pawlowski, 2009). It has been proposed that these telomere-led movements could bring homologues into close proximity thereby promoting their pairing by aiding in homologue search and recognition. The movements have also been proposed to play a role in resolving chromosomal interlocks (Koszul and Kleckner, 2009). Telomere movements have also been reported in a wide variety of organisms. Molecular studies showed that telomere movements are mediated by cytoskeletal motion-generating components that are directly linked to the chromosome ends via SUN protein-mediated bridges that span the NE (Chikashige et al., 2006). Defects in budding yeast SUN protein, MPS3 and the telomere-cytoskeleton bridge proteins, NDJ1 and CMS4 were found to cause defects both in RPMs and homologue pairing (Conrad et al., 2008, Conrad et al., 2007, Trelles-Sticken et al., 2000). A recent study further analysed the role of RPMs by analysing pairing between between lacI-GFP tagged chromosome segments in RPM-defective mutants (Lee et al., 2012). This revealed that in *cms4*Δ and *mps3-dAR* the number of paired signals was significantly reduced compared to the wild-type. Furthermore, time-lapse analysis revealed a graded decrease in telomere movements in relation to the severity of chromosome

pairing defects in *mps3* Δ , *ndj1* Δ and *cms4* Δ , suggesting that RPMs are involved in chromosome pairing. Interestingly, Mps3, Ndj1 and Csm4 have previously shown to be required for bouquet formation (Lee et al., 2012). This raised the possibility that RPMs directly promote homologue pairing but separately from any role in bouquet formation. In agreement with this, chromosome pairing was found to be less defective in *mps3-dAR* than in *ndj1* Δ even though telomere clustering appears more defective in *mps3-dAR* than in *ndj1* Δ . This suggests that homologue pairing is correlated with RPMs rather than bouquet formation (Lee et al., 2012).

Intriguingly, homologous chromosome recognition and pairing in *C. elegans* depend on heterochromatic repeats, known as pairing centres (PCs) that are present at one end of each chromosome (MacQueen et al., 2005). PCs mediate interaction between chromosomes and the mammalian zinc-finger proteins HIM-8 and ZIM 1, 2, 3. This is followed by the tethering of these proteins and their bound chromosome sites in a patch on the NE during early prophase I. This arrangement has been proposed to facilitate homologue recognition by promoting association of homologous PCs (Hiraoka and Dernberg, 2009, Osman et al, 2011 and the reference therein). The PC-NE attachment sites consist of nuclear membrane spanning complexes composed of SUN- and KASH-domain proteins SUN-1 and ZYG-12 which link PCs to cytoskeletal microtubules (Hiraoka and Dernburg, 2009). It is proposed that ZYG-12 directly interacts with dynein motor protein which in turn interacts with microtubules to pull apart the associations between PCs. The forces generated are thought to separate only non-homologous interactions while leaving the correctly linked robust

homologous PCs attached. These events are also thought to release a block imposed by SUN-1 which subsequently facilitates chromosome synapsis (Osman et al, 2011 and the references within). Both SUN and KASH domain proteins are widely conserved among organisms. In addition to MPS3 in *S. cerevisiae* studies in *S.pombe* have shown that the SUN domain protein, SAD1 mediates telomere clustering to spindle pole body via interaction with RAP1/TAZ1/BQT1/BQT2 protein complex (Chikashige et al., 2006). *Arabidopsis* has two SUN domain proteins, although their meiotic roles have not yet been characterized (Graumann et al., 2010). Thus it is plausible that a similar mechanism involving NE, bridge proteins and cytoskeletal microtubules may mediate telomere clustering which may promote homologue pairing during *Arabidopsis* meiosis.

1.3.2. Homologous chromosome synapsis

Homologous chromosome synapsis during early prophase I is thought to stabilize homologue pairing and facilitate homologous recombination. Homologous chromosomes synapsis is achieved by the formation of a highly conserved proteinaceous structure known as the synaptonemal complex (SC) between each pair of homologues. The SC consists of two lateral elements (LEs), each of which are formed at the base of each homologue and are connected to each other via transverse filaments (TFs) forming a zipper-like tripartite structure (Figure 2B). The LEs of the SC are thought to be derived from axial elements (AEs), which comprises of axis proteins and components of the cohesin complex (Blat et al., 2002, Klein et al., 1999). Immunolocalization studies in yeast revealed that cohesin components

REC8 and SMC3 localize along the chromosome axes during early prophase I (Klein et al., 1999). Similar observations have been reported for the *Arabidopsis* cohesin components AtSYN1 and AtSMC3 (Cai, 2003, Lam, 2005). In addition, the coiled-coil protein RED1 and HORMA domain protein HOP1 have been identified as LE components in budding yeast (Hollingsworth et al., 1990, Smith and Roeder, 1997). Immunofluorescence studies in wild type *S. cerevisiae* revealed that RED1 localizes along the entire length of chromosomes at pachytene, where it co-localizes with ZIP1, the TF protein component of the SC (Smith and Roeder, 1997). Furthermore, RED1 localizes to unsynapsed chromosomes present in yeast *zip1* mutant which lacks TFs. In addition, cytological studies involving wild-type *S. cerevisiae*, where pachytene chromosomes were digested with DNase I and then labelled with histone H2B and anti-RED1 antibodies along with 4',6-diamidino-2-phenylindole (DAPI) showed significant levels of RED1 staining but greatly reduced histone and DAPI staining in the meiocytes. This indicated that RED1 is associated with core of the SC and not with chromatin (Smith and Roeder, 1997). These observations suggest that RED1 is a component of the axial region of the SC (Smith and Roeder, 1997). It has been suggested that yeast RED1 and mammalian SYCP3 are structurally analogous. SYCP3, like RED1 also has a coiled-coiled domain in its C-terminus and has been shown, together with SYCP2, to localize to LEs of mammalian SC during pachytene (Fraune et al., 2012, Yuan et al., 2000). Furthermore, male *sycp3* mice mutants fail to form SC and are completely sterile (Yuan et al., 2000). A recent study has also identified a coiled-coil protein, PAIR3, which is essential for pairing and synapsis of homologous chromosomes in rice. The rice *pair3* mutant displays asynaptic chromosomes at pachytene and fail to form bivalents at diakinesis resulting in a loss

of recombination (Yuan et al., 2009). Immunolocalization studies indicate that PAIR3 localizes along the length of meiotic chromosomes during pachytene in a ZEP1 (TF protein of rice SC) – independent manner (Wang et al., 2010a). These results suggest that PAIR3 is associated with the LE of the rice SC (Wang et al., 2010a, Yuan et al., 2009). Immunolocalisation studies in *S. cerevisiae* revealed that the HORMA domain protein HOP1 also localizes along the entire length of meiotic chromosome axes at early prophase I (Hollingsworth et al., 1990, Smith and Roeder, 1997). Moreover, HOP1 has been shown to co-localize with RED1 at early prophase I in wild-type cells. Additionally, HOP1 has been reported to be able to localize to unsynapsed AEs in *zip1* mutant suggesting that HOP1 associates with AE regions of the SC. In accord, *hop1* mutant have been reported to lack SC (Hollingsworth et al., 1990). Recently, two HORMA domain proteins, HORMAD1 and HORMAD2 have been shown to be associated with the AEs of mammalian SC (Wojtasz et al., 2009). Immunolocalisation studies in mice revealed that both HORMAD1 and HORMAD2 co-localized with SYCP3 during early prophase I (Wojtasz et al., 2009). In rice, immunocytological and electron microscope (EM) analyses suggest that the HORMA domain protein PAIR2 associates with AEs at leptotene and zygotene. Mutation in *pair2* completely eliminates synapsis indicating that PAIR2 plays an essential role in homologous chromosome synapsis during rice meiosis (Nonomura et al., 2004). The *Arabidopsis* HORMA domain protein AtASY1 show limited homology to yeast HOP1 (Caryl et al., 2000). Although AtASY1 is not an AE component, it has been shown to associate with the AE by immunolocalisation and immunogold electron microscopy (Armstrong et al., 2002). Immunolocalisation studies revealed that AtASY1 localizes to meiotic chromosome in early leptotene, when AE first become visible.

Subsequently, AtASY1 forms a continuous LE-associated signal by leptotene-zygotene transition, persisting until pachytene when synapsis is complete (Armstrong et al., 2002). *Atasy1* mutant fails to form the SC indicating that AtASY1 is important for synapsis during *Arabidopsis* meiosis (Caryl et al., 2000).

Soon after the formation on AEs in early leptotene, each AE is thought to bind a pair of sister chromatids, which are organized into parallel sets of loops (Kleckner, 2006). Two AEs are then held together by TFs which assemble progressively between AEs in a zipper-like manner during early prophase I to form the tripartite SC. The SC is fully formed by pachytene, when homologous chromosomes are fully aligned, paired and synapsed. In budding yeast, the coiled-coil protein ZIP1 has been identified as the TF component of the SC (Sym et al., 1993). Immunolocalization studies on wild-type chromosome spreads revealed that ZIP1 localizes along the entire length of synapsed homologous chromosomes during pachytene. Additionally, electron microscopy showed that *zip1* mutants are able to form full-length AEs that can undergo homologous pairing but are defective in synapsis (Sym et al., 1993). Unlike in yeast, the LEs of the mammalian SC are connected to each other by the central region, which consists of TF and central elements (CEs) (reviewed in Fraune et al, 2012). SYCP1 has been identified as the TF protein that interacts, via its coiled-coil domain with the CE, composed of the proteins SYCE1, SYCE2, SYCE3 and TEX12 to make up the central region of mammalian SC (Fraune et al, 2012 and the references therein). Studies of *sycp1* knockout mice revealed that although AEs were able to form and align normally homologous chromosomes failed to synapse in the mutants. In addition, analysis of the CE protein knockout mice suggests that the proteins are involved in synapsis initiation and/or propagation (Fraune et al, 2012 and

the references therein). In contrast, the LEs of the rice SC are connected to each other via only TFs, similarly to the LEs of the yeast SC. Recently, ZEP1 has been identified as the TF protein of the rice SC (Wang et al., 2010b). Rice *zep1* mutants display normal alignment and pairing of homologous chromosomes at leptotene and zygotene but fail to form the SC at pachytene (Wang et al., 2010b). Furthermore, immunolocalisation studies in wild type revealed that ZEP1 forms a continuous linear signal along the entire length of chromosomes at pachytene, when the SC is fully formed (Wang et al., 2010b). The *Arabidopsis* transverse filaments are composed of coiled-coil proteins called AtZYP1a and AtZYP1b, encoded by two genes *AtZYP1a* and *AtZYP1b* respectively (Higgins et al., 2005). The AtZYP1 proteins bind LEs with their C-terminals and attach head-to-head with their N-terminals thus bringing LEs within close proximity (Higgins et al., 2005). Immunolocalization studies show that AtZYP1 initially localizes to meiotic chromosomes during leptotene as numerous foci. At zygotene AtZYP1 polymerizes to form a continuous linear signal along the entire length of the pachytene chromosomes, indicating that AtZYP1 is a SC component (Higgins et al., 2005). Dual-immunolocalization revealed that AtASY1 signals flank both sides of the AtZYP1 signal along the synapsed homologues at pachytene, suggesting that AtZYP1 forms part of the central region of the SC (Higgins et al., 2005). In *Atzyp1* RNAi mutant, where both *Atzyp1a* and *Atzyp1b* are disrupted, synapsis fails to occur suggesting that AtZYP1 is essential for the formation of the central region of *Arabidopsis* SC (Higgins et al., 2005).

1.3.3. Role of meiotic recombination in homologous chromosome pairing and synapsis

Many studies have implicated meiotic recombination in playing an important role in the process of chromosome pairing and synapsis in addition to its role in crossover (CO) formation. Studies conducted using chromosome painting in *S. cerevisiae* *spo11* and *rad50* mutants, both of which are defective in double-strand break (DSB) formation (the first step of recombination) indicate that chromosome pairing in these mutants is drastically reduced (Loidl et al., 1994). Similarly, in *Sordaria macrospora* lack of SKI8, a protein required for DSB formation, leads to severe defects in homologue identification, pairing and subsequent synapsis in the *ski8* mutant (Tesse et al., 2003). These defects in the *ski8* mutant can be recovered via induction of exogenous DSBs, hence meiotic recombination (Tesse et al., 2003). Similarly, several studies in various organisms have shown that both early and late recombination intermediates are found to be spatially associated with the chromosome axis (Osman et al., 2011 and the references within). These observations collectively suggest that recombination is required for normal levels of homologous chromosome pairing and synapsis. A mechanism for how recombination promotes chromosome pairing and eventual synapsis has also been suggested. It is proposed that early during the process of recombination in leptotene the recombination regions of homologous chromosomes are brought into close proximity of each other. The resulting close association of homologues has been suggested to facilitate pairing and synapsis of homologous chromosomes (Zickler and Kleckner, 1998). However, chromosome pairing in some organisms has been shown to be recombination independent. Live imaging studies of chromosomes in *Drosophila*

male meiosis revealed that homologue pairing and synapsis occur in the absence of recombination (Vazquez et al., 2002). Furthermore, homologue pairing and synapsis in *C. elegans* have also shown to be independent of DSB formation and recombination (MacQueen et al., 2005). These observations support the notion that although recombination may facilitate pairing of homologous chromosomes in some organisms the dependence of homologue pairing on recombination is not universal.

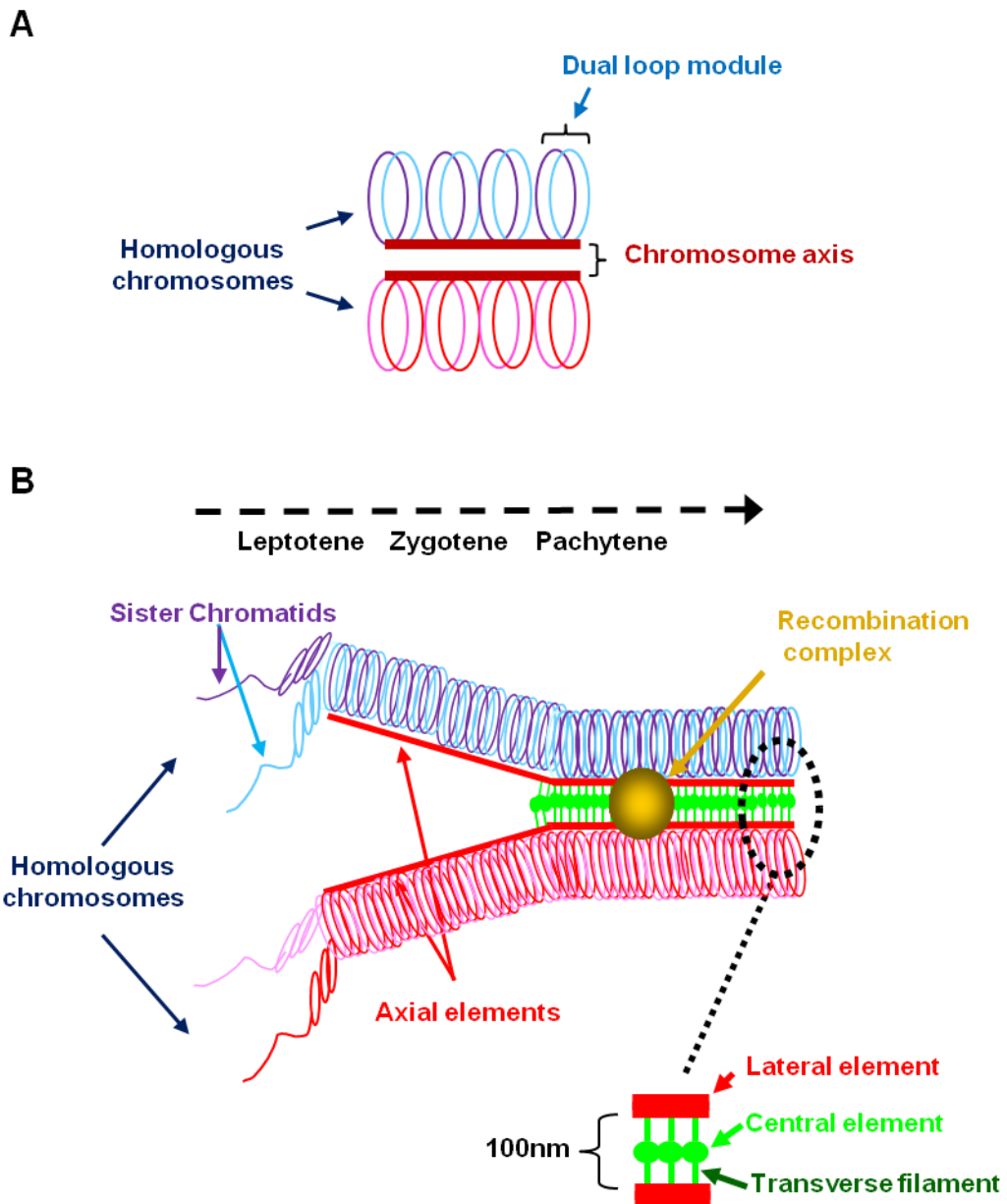


Figure 2. (A) Dual loop organization and (B) structure of the SC.

(A) During early prophase I sister chromatids of each set of homologous chromosomes are organized into sets of chromatin loops. The loops are anchored and aligned along a linear proteinaceous axis. (B) In *Arabidopsis*, homologous chromosomes become associated with axial elements at early leptotene and align at a distance of 400nm. At late leptotene/early zygotene, synapsis is initiated. Lateral elements of homologous chromosomes are connected by the polymerizing transverse filaments. By early pachytene the SC is completely formed between the homologues which become fully synapsed at a distance of 100nm. Modified from Alberts et al, (1983).

1.4. Meiotic Recombination

Recombination is a process that generates COs between homologous chromosomes during meiosis. It is required for the correct segregation of chromosomes at anaphase I as well as to generate genetic variation in the offspring. The mechanisms involved in meiotic recombination have been primarily established from various studies in budding yeast and is believed to be canonical amongst most eukaryotes including *Arabidopsis*. Meiotic recombination involves the formation of double-strand breaks (DSBs), followed by strand resection and invasion which leads to the formation of intermediate structures. Some of these structures are stabilized and subsequently resolved to generate meiotic COs (Figure 3).

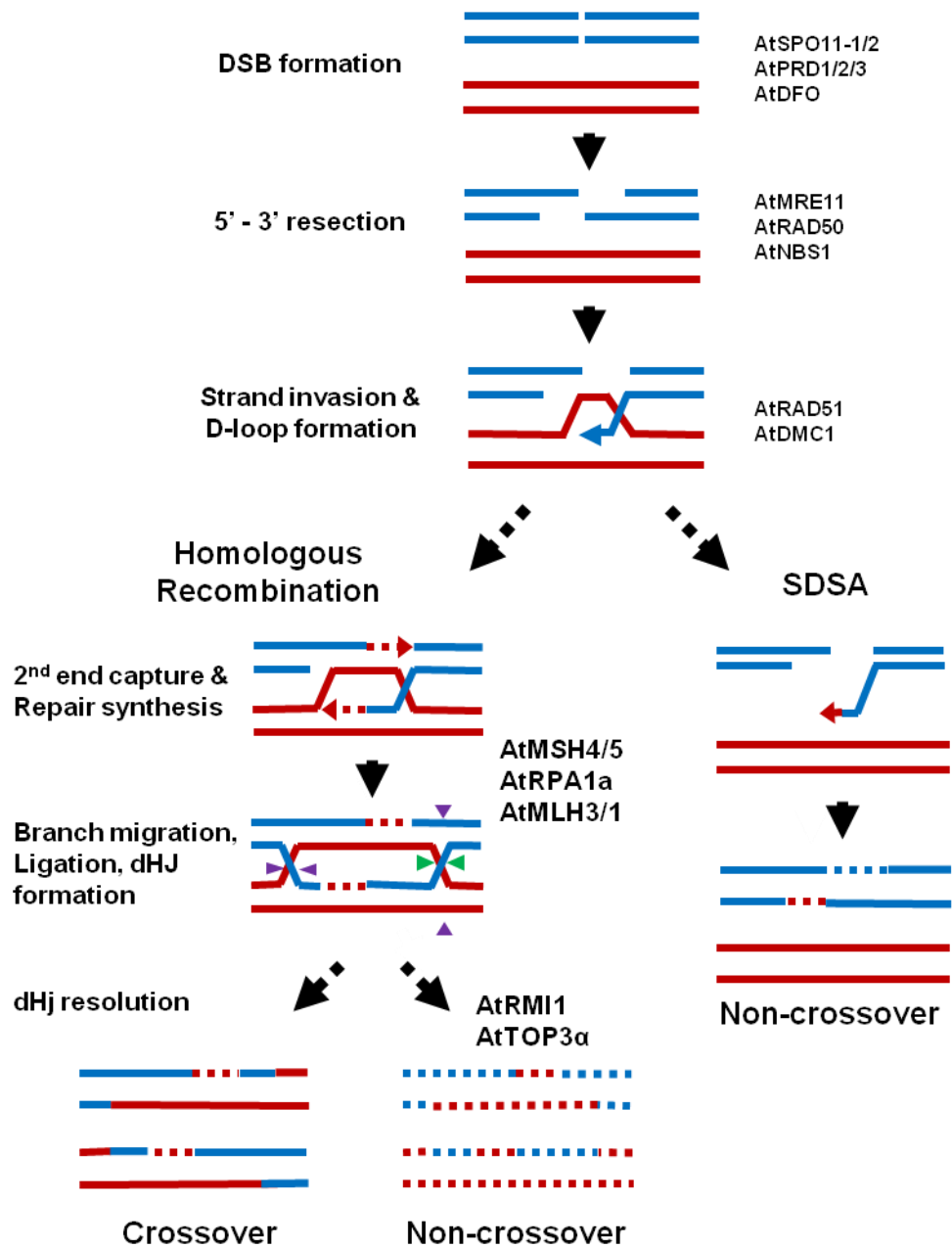


Figure 3. Schematic representation of meiotic DSB repair pathway.

Following DSB formation the 5' -end is resected to 3' end. This is followed by strand invasion which leads to the formation of D-loop. A portion of the overall D-loops are repaired via the SDSA pathway to form NCOs while the remaining undergo 2nd end capture, repair synthesis and ligation. These latter intermediates are then stabilized to form dHJs. A substantial portion of the dHJs are resolved to generate COs while some of them may also undergo dissolution to generate NCOs.

1.4.1. DNA double-strand break formation

Meiotic recombination is initiated by the formation of DNA DSBs during leptotene. DSBs are generated by a topoisomerase II – related transesterase, SPO11 which catalyses DSB formation by nucleophilic attack on meiotic DNA via its catalytically active tyrosine residues (Keeney et al., 1997). During this process SPO11 becomes covalently attached to the 5' ends of DNA on either side of each DSB site and remains attached until further processing in the subsequent step of recombination (Keeney et al., 1997). SPO11 is widely conserved among organisms and three paralogues of SPO11, AtSPO11-1, AtSPO11-2 and AtSPO11-3 have been identified in *Arabidopsis* (Grelon et al., 2001, Hartung and Puchta, 2001). However, only AtSPO11-1 and AtSPO11-2 have been shown to be essential for meiotic DSB formation (Grelon et al., 2001, Stacey et al., 2006). *Atspo11-1-3* mutant is sterile and cytological analysis revealed that the mutant lacks synapsis at pachytene and bivalents and chiasmata at metaphase I (Sanchez-Moran et al., 2007). In addition, immunolocalization studies showed that the mutant had no γ H2AX foci, which is a marker for DSBs, indicating the absence of DSB formation in the mutant (Sanchez-Moran et al., 2007). Similarly, *Atspo11-2* mutant displays severe sterility along with the absence of synapsis at pachytene and bivalents at metaphase I (Stacey et al., 2006). Interestingly, the complete lack of DSB formation in *Atspo11-1-3* mutants suggests that AtSPO11-2 is unable to catalyse DSB formation without AtSPO11-1, indicating that AtSPO11-1 and AtSPO11-2 may act non-redundantly as a heterodimer to catalyze DSB formation (Sanchez-Moran et al., 2007, Stacey et al., 2006). In budding yeast SPO11 alone is not sufficient to initiate recombination. Accessory proteins MRE11, RAD50, XRS2, MER2, MIE4, SKI8, REC102, REC104

and REC114 have all been proposed to be involved in the initiation of meiotic recombination (Cole et al., 2010). Many of these accessory proteins are yet to be identified in *Arabidopsis* due to the lack of homology at sequence level between species. However, recent fertility screens of mutant lines have identified three mutants *Atprd1*, *Atprd-2* and *Atprd-3* whose phenotypes are reminiscent of the *Atspo11-1-3* mutant (De Muyt et al., 2009, De Muyt et al., 2007). Further analysis revealed that each of the three *Atprd* mutants can suppress phenotypes of mutants of proteins involved downstream in the meiotic DNA repair process. These observations suggest that AtPRD1, AtPRD2 and AtPRD3 are required for DSB formation during meiotic recombination in *Arabidopsis*. In concert with this, AtPRD1 have been shown to interact with AtSPO11-1 directly in a yeast two-hybrid assay (reviewed in Osman et al., 2011). Additionally, a recent study suggests that a novel protein, AtDFO, is also required for DSB formation during *Arabidopsis* meiosis (Zhang et al., 2012). *Atdfo* mutants exhibit extensive defects in homologue pairing and synapsis along with a severe reduction in recombination which leads to nearly complete sterility. Moreover, *Atdfo/Atmre11* which is deficient in both AtDFO and AtMRE11, a DSB processing protein, was found to suppress the fragmentation phenotype of *Atmre11* single mutant. This suggests that AtDFO is involved in DSB formation, although its functional mechanism remains unresolved (Zhang et al., 2012).

1.4.2. Processing of double-strand breaks

After DSB formation, H2AX, a histone variant is phosphorylated at C-terminal serine, S139, at sites of DSB to form γ H2AX. γ H2AX is formed over a large region surrounding each DSB but is absent in the vicinity of the DSB (Shroff et al., 2004). It has been suggested that γ H2AX produces structural changes to facilitate the subsequent DNA repair process at the DSB site (Fernandez-Capetillo et al., 2003). The DNA repair process begins with the nucleolytic removal of the SPO11 which remains attached to 5' ends of DNA on either side of DSB. This is followed by the subsequent resection of the 5' ends to 3' single stranded DNA (ssDNA), each approximately 0.5-1 kb in length. In budding yeast these processes are carried out by the MRE11-RAD50-XRS2/NBS1 (MRX/N) complex together with COM1/SAE2 (Mimitou and Symington, 2009). *S. cerevisiae* *mrx* mutants have low spore viability and are defective in recombination and synapsis (Connelly and Leach, 2002). Mutants of *Arabidopsis* MRN proteins *Atmre11* and *Atrad50* exhibit defective synapsis and extensive fragmentation at prophase I (Bleuyard et al., 2004a, Puizina, 2004). Analysis of an *Atmre11/Atspo11-1* double mutant revealed that the fragmentation phenotype observed in the *Atmre11* mutant was suppressed in the double mutant indicating that AtMRE11 is involved in DSB repair rather than its induction (Puizina, 2004). Furthermore, co-immunoprecipitation studies showed that AtMRE11 can interact with AtRAD50 *in vitro* (Daoudal-Cotterell et al., 2002). In addition, the *Arabidopsis* AtNBS1 has been proposed to play a role in DNA cross-link repair and shown to possess an AtMRE11 interaction site in its C-terminal (Waterworth et al., 2007). These observations suggest that AtMRE11, AtRAD50 and AtNBS1 may form a protein complex which is involved in early DSB repair

processing. Additionally, *Arabidopsis* AtCOM1, a homologue of the budding yeast COM1/SAE2 is also thought to be involved in DSB processing (Uanschou et al., 2007). Immunolocalization studies of the *Atcom1* mutant revealed that the mutant is able to accumulate AtSPO11 but not downstream recombination intermediates. Furthermore, the *Atcom1* mutant exhibits extensive chromosome fragmentation which is not suppressed in the *Atcom1/Atdmc1* double mutant, suggesting that AtCOM1 is involved in the early stages of DSB processing (Uanschou et al., 2007). Therefore, based on above observations it is plausible that similarly to budding yeast, the *Arabidopsis* AtMRE11-AtRAD50-AtNBS1 complex along with AtCOM1 are involved in the early steps meiotic DSB processing.

1.4.3. Strand invasion and exchange

Strand resection during early DSB processing generates 3' – ended ssDNA on either side of the DSB. This is followed by the assembly of bacterial RecA-related recombinases RAD51 and DMC1 via mediator proteins on the 3' ssDNA tail to form a nucleoprotein filament. This nucleoprotein filament then invades duplex DNA, performs a homology search and initiates strand exchange (Bishop and Zickler, 2004). In budding yeast RAD51 has been shown to be involved in the mitotic DNA repair between sister chromatids of the same chromosome, whereas DMC1 plays a role in inter-homologue recombination during meiosis (Bishop et al., 1992, Shinohara et al., 1992). Initially it was thought that in addition to RAD51, the meiosis specific DMC1 is necessary to make the switch from inter-sister to inter-homologue recombination during meiosis in budding yeast (Bishop et al., 1992). However,

studies show that over-expression of RAD51 in *S. cerevisiae dmc1* mutant can restore inter-homologue recombination suggesting that RAD51 and DMC1 work as partners to promote inter-homologue recombination (Bishop, 1994). Interestingly, recent studies in budding yeast suggest that although both the recombinases are capable of strand-exchange only DMC1 catalyzes homology search and strand exchange in essentially all meiotic recombination events (Cloud et al., 2012). Analysis of a separation of function mutant form of *S. cerevisiae* RAD51, that retains filament-forming but not joint molecule (JM) forming activity, suggests that RAD51's strand exchange activity is fully dispensable for normal meiotic recombination. Furthermore, analysis of a similar mutant of DMC1 suggests that loss of DMC1 causes a severe defect in inter-homologue JM formation. These findings suggest that the JM activity of DMC1 alone is responsible for meiotic recombination (Cloud et al., 2012). Nevertheless, biochemical studies suggest that RAD51 acts with MEI5-SAE3 as an accessory factor that stimulates DMC1 activity, suggesting that the recombinase catalyzes recombination indirectly, via DMC1, during meiosis (Cloud et al., 2012). *Arabidopsis Atrad51* mutants are sterile and exhibit extensive chromosome fragmentation suggesting that AtSPO11-induced DSBs are not repaired in the absence of AtRAD51 (Li, 2004). On the other hand, *Arabidopsis Atdmc1* mutants fail to form any COs resulting in the formation of univalents which segregate randomly at anaphase I. Interestingly, chromosome fragmentation was not observed in *Atdmc1* mutants suggesting that DSBs are repaired in these mutants, probably by using the sister chromatid as the repair template (Couteau et al., 1999). These observations indicate that the recombinases AtRAD51 and AtDMC1 function together to mediate inter-homologue recombination during *Arabidopsis* meiosis. A recent

study using BrdU pulse-labelling and dual-immunolocalisation suggest that AtDMC1 loading slightly precedes AtRAD51 indicating an asymmetry in the loading of the recombinases in *Arabidopsis* (Sanchez-Moran et al., 2007). This observation supports previous reports in budding yeast, where it has been proposed that RAD51 and DMC1 loading are asymmetrical (Hunter and Kleckner, 2001). It has been suggested that the asymmetrical loading of the two recombinases in *Arabidopsis* might be a mechanism to promote inter-homologue recombination (Sanchez-Moran et al., 2007). Consistent with this, recent immunolocalisation studies in *Arabidopsis* early prophase I chromosome spreads revealed that AtRAD51 and AtDMC1 foci do not co-localize with each other, instead, they form doublets which co-localize with γ H2AX foci. This suggests that DSBs are flanked by two different nucleoprotein filaments, comprised of either AtRAD51 or AtDMC1 (Kurzbauer et al., 2012). Additionally, the study also revealed that AtDMC1-coated nucleoprotein filaments are impeded from DSB repair using the sister chromatid as a template presumably by the axis protein AtASY1, which has been shown to mediate inter-homologue recombination during *Arabidopsis* meiosis (Kurzbauer et al., 2012, Sanchez-Moran et al., 2007).

Arabidopsis has five other paralogues of AtRAD51: AtRAD51B, AtRAD51C, AtRAD51D, AtXRCC2 and AtXRCC3 (Bleuyard et al., 2004b). However, only AtRAD51C and AtXRCC3 have been shown to possess a role in meiosis (Bleuyard and White, 2004, Li, 2005). Both *Atrad51c* and *Atxrcc3* mutants exhibit extensive chromosome fragmentation. Analysis of *Atrad51c/Atspo11* and *Atxrcc3/Atspo11* double mutants revealed that the fragmentation phenotype of *Atrad51c* and *Atxrcc3* are suppressed in double mutants indicating that AtRAD51C and AtXRCC3 are involved in meiotic recombination (Bleuyard and White, 2004, Li, 2005). In addition,

yeast-two hybrid studies have showed AtXRCC3 directly interacts with AtRAD51C and also with AtRAD51. These observations led to the proposal that AtRAD51C forms a complex with XRCC3 which may mediate the assembly of RAD51 during meiotic recombination (Osakabe et al., 2002).

In budding yeast, mediator proteins are thought to be involved in the assembly of strand exchange proteins. RPA is one of the mediator proteins involved in nucleofilament formation (San Filippo et al., 2008). Biochemical studies in yeast have shown that RPA can remove secondary structures within the DNA thereby promoting the assembly of RAD51 onto the 3' – ended ssDNA. Furthermore, RPA is thought to coat the 3'-ended ssDNA and prevent incorrect RAD51-mediated strand exchange (reviewed in San Filippo et al., 2008). Yeast RPA is thought to form a heterotrimer composed of subunits: RPA1 (~70kDa), RPA2 (~32kDa) and RPA3 (~14kDa) (Wold, 1997). In budding yeast mutants where *rfa1*, the gene encoding the large subunit of RPA had been mutated, a complete loss of recombination was observed implying that RPA is crucial for meiotic recombination (Soustelle et al., 2002). In mammals, *RPA1* has been identified as a homologue of the yeast *RFA1* gene. Mice with a heterozygous point mutation in *rpa1* accumulate lymphoid tumours and their offspring exhibit early embryonic lethality (Wang and Haber, 2004). In *Arabidopsis*, although five paralogues of RPA1 subunit have been identified, only AtRPA1a has been shown to possess a role in meiosis (Osman et al., 2009, Shultz et al., 2007). Analysis of *Atrpa1a* mutants revealed that the protein is involved in downstream steps of strand exchange and is dispensible for meiotic DNA repair suggesting that AtRPA1a is not essential for nucleoprotein filament formation. However, immunolocalisation studies showed that AtRPA1a is associated with meiotic chromosomes from

leptotene to early pachytene. These observations led to the suggestion that in addition to a role in strand exchange AtRPA1a may be involved in AtRAD51-filament formation, although in its absence the latter role is performed by one or more of its paralogues with functional redundancy (Osman et al., 2009).

In budding yeast the RAD52 epistasis group, composed of the proteins RAD52, RAD55 and RAD57 have been proposed to play a role in nucleoprotein filament formation (Symington, 2002). It is thought that RAD55 and RAD57 form a heterodimeric complex that binds ssDNA and remove the inhibitory block on RAD51-mediated strand exchange imposed by RPA. This is thought to promote the initiation of strand exchange by the recombinases (Sung, 1997). *S. cerevisiae* RAD55 and RAD57 share sequence homology with *Arabidopsis* AtRAD51B and AtRAD51C respectively, although there is no evidence of conservation of any functional homology (Osman et al., 2011). Also *Arabidopsis* does not have a RAD52 orthologue but possesses two paralogues of the mammalian tumour suppressor protein BRCA2 (Siaud et al., 2004). In mammals, BRCA2 has been shown to act as a mediator protein and help recruit RAD51 to 3'-ended ssDNA with the help of another mediator protein DSS1. Mammalian BRCA2 is thus considered a functional analogue of budding yeast RAD52 (Jensen et al., 2010, Thorslund et al., 2007). The *Arabidopsis* *Atbrca2* mutant where both paralogues of *AtBRCA2* are disrupted exhibit defects in synapsis as well as localization of the recombinases AtRAD51 and AtDMC1. Furthermore, yeast two hybrid assay and co-immunoprecipitation studies showed that either paralogue of *AtBRCA2* is able to physically interact with AtRAD51 and AtDMC1 suggesting that it may be involved in the recruitment of the recombinases during early DSB repair (Dray et al., 2006).

Additionally in budding yeast, the mediator proteins RAD54 and RDH54/TID1, both members of the SWI2/SNF2 chromatin remodelling protein family, are thought to help the recombinases promote strand exchange (Shinohara et al., 1997). Analysis of the *rad54* mutant revealed that there is a reduction of somatic homologous recombination suggesting that RAD54 is involved in promoting exchanges between sister chromatids. Whereas, *rdh54* mutants exhibit severely reduced spore viability suggesting that RDH54 is involved in the DMC1-dependent exchange between homologous chromosomes (Shinohara et al., 2003, Shinohara et al., 1997). In *Arabidopsis* AtRAD54, is not involved during meiosis and a homologue of budding yeast RDH54 has not been found yet. Since *Arabidopsis* has at least 40 SWI2/SNF2 family members it is possible that many share functional redundancy with respect to nucleoprotein filament formation and strand exchange initiation (reviewed in Osman et al., 2011).

In *S. cerevisiae* the MND1/HOP2 complex has been shown to be important in facilitating strand invasion (Chi et al., 2007). Both *mnd1* and *hop2* mutants fail to sporulate and exhibit a severe reduction in pairing and undergo meiotic arrest at pachytene checkpoint (Tsubouchi and Roeder, 2002). Immunolocalisation studies revealed that although RAD51 and DMC1 accumulate at prophase I in both mutants DSBs remain unrepaired in them. Hence it is thought that the recombination defects in both mutants occur during strand exchange step after loading of the recombinases (Tsubouchi and Roeder, 2002). Furthermore, the two proteins have been shown to interact in co-immunoprecipitation studies suggesting that MND1 and HOP2 may work as a complex along with RAD51 and DMC1 to promote homology search and promote strand invasion (Tsubouchi and Roeder, 2002). Biochemical studies in

mammals showed that mouse MND1-HOP2 complex can interact with both DMC1 and RAD51 *in vitro* (San Filippo et al., 2008). *Arabidopsis Atmnd1* and *Athop2* fail to undergo pairing and synapsis, display possible non-homologous interactions and fail to repair DSBs (Kerzendorfer, 2006, Panoli et al., 2006, Schommer et al., 2003). Co-immunoprecipitation studies showed that AtMND1 and AtHOP2 are able to physically interact with each other and with AtRAD51 and AtDMC1 (Kerzendorfer, 2006, Vignard et al., 2007). These observations led to the proposal that *Arabidopsis* AtMND1-AtHOP2 may perform similar roles to their budding yeast counterparts (Vignard et al., 2007).

An important aspect during strand-exchange is the choice of DSB repair template. As discussed earlier, in both *S. cerevisiae* and *Arabidopsis*, RAD51 has been shown to mediate DNA repair using sister-chromatids while both RAD51 and DMC1 are necessary for inter-homologue recombination during meiosis (reviewed in Bishop 2004, Osman et al., 2011). Additionally, in budding yeast a protein complex, composed of the axis proteins RED1 and HOP1 and the kinase MEK1, is essential for establishing a bias towards DMC1-mediated inter-homologue recombination by forming a barrier to inter-sister repair during the strand exchange step (Niu et al., 2005). In *Arabidopsis*, although AtASY1 has been characterized as a functional homologue of budding yeast HOP1, identification of homologues of RED1 and MEK1 still remain unreported. Nevertheless, AtASY1 has recently been shown to mediate AtDMC1-dependent inter-homologue recombination in *Arabidopsis* (Sanchez-Moran et al., 2007). More recently HED1 has also been shown to promote DMC1-mediated inter-homologue recombination by attenuating inter-sister exchanges in budding yeast (Busygina et al., 2008). Evidence for this comes from the observation that

spore viability is restored in *hed1/dmc1* double mutants in contrast to *dmc1* single mutants which have the option of DSB repair via inter-sister pathway but still fails to do so. Hence it is thought that the high spore viability in *hed1/dmc1* double mutants is presumably due to the absence of HED1-mediated blockage to inter-sister repair (Busygina et al., 2008). In support, both yeast two-hybrid and pull down assays indicate that HED1 can interact with RAD51 but not DMC1. Furthermore, biochemical studies using affinity pull-down assays revealed that HED1 strongly interferes with RAD51-RAD54 interaction but not with DMC1-RAD54 interaction (Busygina et al., 2008). Hence, it has been proposed that HED1 attenuates RAD51-mediated inter-sister recombination by disrupting the interaction between RAD51 and its strand-exchange efficacy mediator RAD54 during the strand exchange step, thereby promoting inter-homologue recombination (Busygina et al., 2008). A homologue of the budding yeast HED1 is yet to be identified in other eukaryotes.

Soon after its assembly the RAD51/DMC1-containing nucleoprotein filament initiates strand exchange via single-end invasion. Initially during single-end invasion the functional nucleoprotein filament performs a homology search and locates complementary sequences on either of the two homologous chromosomes. It then invades the intact duplex and displaces similar ssDNA from one of the donor strand. As the invading strand polymerizes the displaced DNA strand extends to form loop-like structure known as the 'displacement loop' (D-loop) (reviewed in Bishop and Zickler., 2004). At this stage a proportion of the single-end invasions are repaired via DNA synthesis and ligation without undergoing any genetic exchange. This pathway of repair is called synthesis-dependent strand annealing (SDSA) and leads to a non-crossover event. In the remaining single-end invasions, after displacing similar

ssDNA from the target donor strand the invading strand base pairs with complementary DNA on the other strand of the donor duplex. This result in the formation of a stable single end invasion intermediate (SEI) which is subsequently resolved into a CO through one of the pathways for CO formation (reviewed in Bishop and Zickler, 2004).

1.4.4. Pathways to meiotic crossover formation

Following strand invasion during early DSB repair the invading strand in the D-loop interacts with the intact duplex to form a stable intermediate called SEI, as mentioned earlier. The second invading strand then associates with donor duplex and DNA synthesis occurs from the 3' end joining newly synthesised DNA with the resected 5' ends. This gives rise to a more stable structure known as the double Holliday junction (dHj) (Holliday, 1964). The dHj is subsequently stabilized and resolved to form CO (reviewed in Bishop and Zickler., 2004).

Studies in budding yeast have led to the proposal that meiotic COs can be formed by at least two different pathways (Borner et al., 2004, de los Santos et al., 2003). The first is dependent on the bacterial MutS homologue MSH4, which is involved in the stabilization of recombination intermediates while the second is the MSH4-independent pathway. In *S. cerevisiae*, approximately 85% of the COs are formed by MSH4-dependent pathway and exhibit CO interference, a mechanism which ensures that two COs do not form in adjacent regions in a chromosome (Borner et al., 2004). The remaining COs are found to be randomly distributed throughout the genome indicating that they are formed via a different pathway which does not involve MSH4

and does not exhibit CO interference (de los Santos et al., 2003, Hollingsworth, 2004). Interestingly, *Arabidopsis* too has been reported to possess an interference-sensitive MSH4-dependent and an interference-insensitive MSH4-independent pathway for meiotic CO formation (Copenhaver et al., 2002, Higgins, 2004).

1.4.4.1. MSH4-dependent pathway for crossover formation

In budding yeast the MSH4-dependent pathway for CO formation is associated with a complex of proteins including MSH4, MSH5, MER3, ZIP1, ZIP2, ZIP3 and ZIP4, collectively referred to as ZMM proteins (Borner et al., 2004). Putative homologues of *S. cerevisiae* ZMM proteins have also been identified in *Arabidopsis* (reviewed in Osman et al., 2011).

The MutS homologues MSH4 and MSH5 play a key role in promoting CO formation and CO interference during meiotic recombination in eukaryotes (Ross-Macdonald and Roeder, 1994, Zalevsky et al., 1999). Budding yeast *msh4* and *msh5* mutants exhibit ~85% reduction in COs while the remaining COs have been reported to be interference insensitive. Furthermore, the mutants also fail to form intermediate structures such as the SEI and dHj (Ross-Macdonald and Roeder, 1994). *In vitro* biochemical studies using recombinant human hMSH4/5 and suggest that MSH4 and MSH5 work as a heterodimer that can bind to Holliday junctions (Hjs) and pro-Hjs such as D-loops. These observations led to the hypothesis that during human meiotic recombination, hMSH4-hMSH5 heterodimer encompass two DNA duplexes side by side via a sliding clamp mechanism to convert and stabilize them into dHjs, which are subsequently resolved to COs or NCOs (Snowden et al., 2004). Homologues of

MSH4/MSH5 have also been identified in *Arabidopsis* (Higgins, 2004, Higgins et al., 2008b). *Atmsh4* and *Atmsh5* displayed a severe reduction in CO formation. In contrast to 9.86 chiasmata per cell *Atmsh4* and *Atmsh5* mutants were reported to possess 1.25 and 1.15 chiasmata per cell respectively, representing only ~15% of wild-type levels. The remaining COs observed in the mutants did not display CO interference (Higgins, 2004, Higgins et al., 2008b). Immunolocalization studies revealed that in wild-type both AtMSH4 and AtMSH5 localized to meiotic chromosomes as numerous foci (>100) during leptotene. Their numbers gradually decreased through until pachytene when only 8 or 9 foci were present, corresponding to the number of chiasmata reported in wild-type. These observations suggest that AtMSH4 and AtMSH5 possess similar roles to their counterparts in budding yeast (Higgins, 2004, Higgins et al., 2008b). Immunolocalization studies further revealed that AtMSH5 localization during meiosis require AtMSH4 suggesting the two proteins may work as a complex. In agreement, AtMSH4 and AtMSH5 were found to exhibit extensive co-localisation during prophase I in immunolocalization studies (Higgins et al., 2008b).

A recent study has revealed that AtMSH4 localization depends on the tumour suppressor protein retinoblastoma (RBR) (Chen et al., 2011). Analysis of its mutant, *Atrbr-2*, revealed that it displays incomplete synapsis and a reduction in chiasma frequency to 1.7 in contrast to 9-10 in the wild-type, a phenotype reminiscent of *Atmsh4* mutant (Chen et al., 2011). Immunolocalization studies revealed that AtMSH4 failed to localize at all in majority of the meiocytes from *Atrbr-2*. Since strand exchange proteins AtRAD51 and AtDMC1 were able to localize in *Atrbr-2* mutant, it is speculated that AtRBR may play a role during early DSB repair prior to AtMSH4

loading (Chen et al., 2011). In animals, pRB has been found to interact with chromatin modifiers, DNA repair proteins and condensin complexes (Longworth et al., 2008). It is speculated that AtRBR may influence meiotic chromosomal organization to allow proper recombination progression, although its exact function during meiosis still remains to be determined (Chen et al., 2011).

In budding yeast the ZMM protein MER3 have been suggested to be involved in processing recombination intermediates (Borner et al., 2004). MER3 is a DExH-box type DNA helicase that can unwind DNA in a 3' to 5' direction and stimulate extension of DNA heteroduplex in the direction relative to incoming ssDNA (Mazina et al., 2004, Nakagawa, 2001). Furthermore, *mer3* mutants exhibit severe defects in DNA synthesis during meiotic recombination (Terasawa et al., 2007). In *Arabidopsis* AtMER3/RCK has been identified as a homologue MER3 (Chen et al., 2005, Mercier et al., 2005). Analysis of the *Atmer3/rck* mutant revealed that although pairing and synapsis is normal during early prophase I chiasma frequency per cell was severely reduced to 2.25 compared to 9-10 in the wild-type. The remaining chiasmata did not display CO interference suggesting that MSH4-dependent COs were absent in the mutant (Mercier et al., 2005). These observations suggest that AtMER3/RCK is important for the stabilization of intermediate heteroduplex structures during CO formation via the MSH4-dependent pathway (Mercier et al., 2005).

In budding yeast, the small ubiquitin-like modifier (SUMO) ligase protein ZIP3 and ZIP4 have been implicated in the assembly of the SC (Agarwal and Roeder, 2000, Tsubouchi et al., 2006). Budding yeast *zip3* mutants lack homologue pairing and recombination but are able to form SC. It is suggested that ZIP3 regulates ZIP1

assembly by suppressing ZIP1 polymerization via sumoylation of axis or SC components (Agarwal and Roeder, 2000). ZIP4 on the other hand has been shown to function with ZIP2 to promote ZIP1 polymerization (Tsubouchi et al., 2006). Additionally, both ZIP3 and ZIP4 have been shown to be epistatic to all ZMM proteins in CO formation (Agarwal and Roeder, 2000, Tsubouchi et al., 2006). A putative *Arabidopsis* AtZIP3 has been identified but does not appear to have a role in SC assembly. Instead, it was reported to be epistatic to AtMSH4/5 in CO formation via means of preliminary observations (Osman et al., 2011). Similarly, *Arabidopsis* AtZIP4 does not have a role in AtZIP1 polymerization (Chelysheva et al., 2007). However, *Atzip4* mutants exhibit a severe reduction in chiasma frequency forming 2.55 chiasmata per cell compared to 9-10 in the wild-type. The remaining COs were found to be CO interference insensitive suggesting that AtZIP4 functions similarly to other ZMM proteins during CO formation (Chelysheva et al., 2007).

ZIP2, a protein with a XPF domain has been shown to be epistatic to other ZMM proteins in budding yeast (Chua and Roeder, 1998). *zip2* mutants are reported to be defective in single strand invasion during meiotic recombination. Recently, AtSHOC1, a novel XPF endonuclease was identified in *Arabidopsis* which may be functionally similar to ZIP2 in budding yeast (Macaisne et al., 2008). In *Atshoc1* mutants the chiasma frequency was reduced from 9.2 in wild-type to 1.27, representing ~15% of wild-type levels. This observation was similar to *Atmsh4/5* mutant. Furthermore, the chiasma frequency of *Atshoc1/Atmsh5* double mutant showed no significant difference from that observed in *Atmsh4* single mutant suggesting that AtSHOC1 functions epistatic to other ZMM proteins during CO formation in *Arabidopsis* (Macaisne et al., 2008). In *Arabidopsis*, another novel protein AtPTD has been found

to function similarly to ZMM proteins (Wijeratne, 2005). *Atptd* mutants display a reduction in chiasma frequency from wild-type levels of 9.7 to 2.5. Further analysis revealed that MSH4-dependent COs were absent in the mutant and the residual COs did not display interference and were distributed at random (Wijeratne, 2005). AtPTD protein displays sequence similarities with a protein called ERCC1, which has been shown to form a complex with XPF to cleave intermediate structures *in vitro* (Sancar et al., 2004, Wijeratne, 2005). In support, AtPTD has been shown to interact with AtSHOC1 in a two-hybrid assay. These observations suggest that AtSHOC1 and AtPTD may work as a complex in the formation of MSH4-dependent COs (Macaisne et al., 2008).

Studies in *S. cerevisiae zip1/red1* double mutant suggest that in addition to its role as the TF component of SC ZIP1 also plays a separate role in CO formation (Storlazzi et al., 1996). As discussed earlier, Red1 is an AE component of the budding yeast SC and its mutant lacks SC and displays a reduction in recombination to ~25% of wild-type levels (Rockmill and Roeder, 1988, Smith and Roeder, 1997). In *zip1* mutant SEIs and dHjs are reduced to ~15% of wild-type levels (Sym et al., 1993). Since *zip1* mutants also lack the SC its subsequent recombination defects should be similar to that observed in the *red1* mutant. However, analysis of the *zip1/red1* double mutant revealed the double mutant displayed a sum of the two single mutant phenotypes including a specific deficit of CO recombinants observed exclusively in the *zip1* mutant (Storlazzi et al., 1996). These observations led to the suggestion that ZIP1 plays an additional role in meiotic recombination. In agreement, the remaining COs in *zip1* mutant were found to be interference insensitive similarly to other *zmm* mutants (Borner et al., 2004). Intriguingly, in *Arabidopsis* AtZYP1 has been observed to

localize as numerous foci early in leptotene, well before SC formation during zygotene suggesting it may play a role in CO formation in addition to SC formation (Higgins et al., 2005). Although *Atzyp1* RNAi knock out mutants display only a mild reduction in the chiasma frequency from 9-10 in the wild-type to 7.3, the remaining COs have been reported to occur between both homologous and non-homologous chromosomes. These COs result in the formation of multivalents, homologous and non-homologous bivalents and univalents during metaphase I suggesting that CO control is compromised in *Atzyp1* RNAi mutants (Higgins et al., 2005). Similarly, the rice *zep1* mutants exhibit an increase in chiasma frequency suggesting that ZEP1 plays a separate role in CO formation in addition to its structural role in SC (Wang et al., 2010b).

In addition to the ZMM proteins studies in budding yeast have shown that the MutL mismatch repair proteins MLH1 and MLH3, which function as a heterodimer, are also essential for promoting CO formation (Nishant et al., 2008, Wang et al., 1999). Both *mlh1* and *mlh3* mutant exhibits reduced spore viability and reduction in CO frequency. Analysis of *S. cerevisiae msh4/mlh1* double mutant revealed that it displayed similar defects in CO formation to the *msh4* single mutant suggesting that MLH1-MLH3 heterodimer functions following MSH4-MSH5 in the recombination pathway (Hunter and Borts, 1997). Mouse male and female *mlh1* mutants fail to form COs leading to the formation of unpaired univalents at metaphase I (Baker et al., 1996, Woods et al., 1999). Additionally, both male and female mouse *mlh3* mutants fail to undergo meiosis and are completely infertile (Lipkin et al., 2002). Homologues of AtMLH1 and AtMLH3 have also been identified in *Arabidopsis*. AtMLH1 is required for recombination in both somatic and meiotic cells whereas AtMLH3 is meiosis-

specific (Dion et al., 2007, Jackson et al., 2006). Immunolocalization studies revealed that both AtMLH1 and AtMLH3 formed approximately 9 foci during pachytene, corresponding to the number of chiasmata observed in wild-type meiocytes. AtMLH1 localization during meiosis has been found to be dependent on AtMLH3. *Atmlh3* mutants exhibit a reduction of chiasmata from ~9.8 in the wild-type to ~3.9. Immunocytological analysis revealed that AtMSH4 is able to localize in *Atmlh3* suggesting that dHJs are formed but are not resolved in the mutant (Jackson et al., 2006). These observations led to the proposal that in *Arabidopsis* the AtMLH1/AtMLH3 complex is required to maintain dHJs in a conformation that promotes their resolution into COs (Franklin et al., 2006, Jackson et al., 2006).

Analysis of the *Atrpa1a* mutant revealed that in addition to its role in nucleoprotein filament assembly, AtRPA1a also possess a role in MSH4-dependent CO formation (Osman et al., 2009). *Atrpa1a* mutant exhibit 3.98 chiasmata per cell compared to 9.86 in the the wild-type. Analysis of *Atrpa1a/Atmsh4* double mutant revealed that its chiasma frequency was reduced to 1.08 which was not significantlt different from that of the *Atmsh4* single mutant, suggesting that AtRPA1a is required for MSH4-dependent CO formation. Interestingly, the *Atrpa1a/Atmlh3* double mutant was found to have a slightly higher mean CO frequency of 1.76 per cell suggesting that AtRPA1a functions after AtMSH4 but before AtMLH3 during CO formation (Osman et al., 2009). *In vitro* studies *S. cerevisiae rfa1-t11* mutant revealed that the loss of RPA protein in budding yeast causes defects in RAD52-mediated strand annealing and second-end capture after D-loop formation (Sugiyama et al., 2006). These observations led to the proposal that in *Arabidopsis* AtRPA1a may play a similar role

in strand annealing and second-end capture during the formation intermediate structures (Osman et al., 2009).

Soon after the formation of dHJs, they are then resolved to form CO recombinants. However, recent analysis in *Arabidopsis* suggests that the proteins AtRMI1/BLAP75 and AtTOP3 α are involved in the dissolution of some dHJs as NCOs (Chelysheva et al., 2008, Hartung et al., 2008). This pathway of dHj dissolution is supported by the presence of a tripartite protein complex referred to as RTR (RECQ/TOP3 α /RMI) or BTB (Blooms/TOP3 α /BLAP75) complex in yeast and mammals (Raynard et al., 2008). The RTR/BTB complex has been shown to resolve dHJ and D-loop via a hemicatenane intermediate (Raynard *et al.*, 2008). *S.cerevisiae*, *rmi1* mutants show reduced sporulation and spore viability and *top3* mutants show hyper-recombination, chromosome instability and do not sporulate (Chang et al., 2005, Mullen et al., 2005). *S. pombe top3* mutants are lethal and *D. melanogaster* and mice *top3 α* mutants display early embryogenic lethality (White, 2008 and the references therein). Analysis of these mutants led to the proposal that BLAP75/RMI1 is involved in the loading and stabilisation of the RTR/BTB complex and TOP3 α catalyses the dissolution of recombination intermediates (White, 2008). *Arabidopsis Atrmi1/blap75* mutant exhibits drastic chromosome fragmentation at anaphase I although all pachytene stages were normal with no disruption to homologue recognition and synapsis (Chelysheva et al., 2008). *Arabidopsis Attop3 α* mutants exhibit absolute sterility and chromosome fragmentation in metaphase I and absence of second meiotic division (Hartung et al., 2008). These observations led to the proposal that AtRMI1/BLAP75 and AtTOP3 α promote the dissolution of some dHJs as NCOs via a hemicatenane intermediate (Chelysheva et al., 2008, Hartung et al., 2008). In *Arabidopsis* only 5-

10% of DSBs are resolved as COs while the rest are repaired as NCOs. It is thought that most of the NCOs arise via the SDSA pathway early during DSB repair. Interestingly, immunolocalization studies suggest that at zygotene the number of intermediate structure stabilization protein AtMSH4 is found to be three fold higher than the number of COs formed eventually. Hence it has been suggested that the remaining intermediate structures which do not form COs may be resolved as NCOs by the AtRMI1/BLAP75-AtTOP3 α complex (reviewed in Osman et al., 2011).

1.4.4.2. MSH4-independent pathway for CO formation

Studies in yeast revealed that ~15% of COs in budding yeast and all or most COs in fission yeast form via a pathway independent of MSH4. The COs formed via this pathway do not exhibit interference and are distributed randomly throughout the genome (Borner et al., 2004, de los Santos et al., 2003, Smith et al., 2003). The MSH4-independent pathway it is thought to be dependent partially on MUS81-MMS4 in budding yeast and completely on MUS81-EME1 in fission yeast (de los Santos et al., 2003, Smith et al., 2003). MUS81 is a structure-specific highly conserved endonuclease that can cleave a variety of DNA structures (Haber and Heyer, 2001). *S. cerevisiae mus81* mutants exhibit reduction in spore viability while *S. pombe mus81* mutants are completely sterile (de los Santos et al., 2003, Smith et al., 2003). Although the mechanism of MUS81 function is still poorly understood it is proposed that in *S. cerevisiae*, MUS81 and MMS4 are thought to function as a heterodimer which cleaves D-loop to yield a branched structure. The branched structure then captures the second free DSB end and extends it via DNA synthesis. This is followed

by a second cleavage by MUS81-MMS4 complex which resolves the structure into CO recombinants (Bishop, 2006). In *S. pombe* EME1 is thought to partner MUS81 for mediating CO formation probably via a similar mechanism. Genetic analysis in *Arabidopsis* revealed the existence of two pathways to CO formation, later confirmed by analysis of *Atmsh4* mutant (Copenhaver et al., 2002, Higgins, 2004). Analysis of the *Atmsh4* mutant revealed the presence of an AtMSH4-independent pathway for CO formation in *Arabidopsis*. This pathway accounted for ~15% of COs which did not exhibit interference (Higgins, 2004). Biochemical analysis revealed that *Arabidopsis* AtMUS81 and AtEME1 can form a heterodimer, which cleaved intact or nicked Hjs (Higgins et al., 2008a). Immunolocalization studies on wild-type chromosome spreads suggest that AtMUS81 localizes in a DSB-dependent manner to every recombination site during leptotene probably at the same time as AtRAD51. Since AtMUS81 may not be required for CO formation at many of these sites it is suggested that AtMUS81 may play a role in resolving aberrant joint molecules that arise during strand invasion (reviewed in Osman., 2011). Interestingly, *Atmus81* mutant did not exhibit any reduction in fertility. However, there was a 90% decrease in CO frequency in the *Atmsh4/Atmus81* double mutant indicating that AtMUS81 is required for approximately 5%, but not all, of the 15% COs formed by the AtMSH4-independent pathway. The residual 10% of the COs may be formed by an entirely different pathway(s) (Higgins et al., 2008a). The existence of more than two recombination pathways is supported by analysis of the budding yeast *msh5/mms4* double mutant, which exhibit a six-fold reduction in CO frequency compared to wild-type, although not complete elimination of COs (de los Santos et al., 2003).

1.4.5. Double-Holliday junction resolution

Previous biochemical studies in budding yeast identified three structure-selective nucleases that have been shown to possess joint molecule (JM) resolution capabilities. These are MUS81 (which partners with MMS4), SLX1 (which partners with SLX4) and YEN1 (Schwartz and Heyer, 2011). MUS81 is related to the XPF subunit of the ERCC1-XPF family of endonucleases that possess H_j resolving abilities (Boddy et al., 2001). In budding yeast MUS81 activity is responsible for ~5% of the total COs suggesting the presence of other resolvases that are involved in dH_j resolution (de los Santos et al., 2003). SLX1 is a GIY domain nuclease which partners with the scaffold protein Slx4. Recombinant SLX1-SLX4 complexes from budding yeast and humans have been shown to cleave Y junctions, 5' flaps and H_js implicating the complex in JM resolution (Fricke and Brill, 2003, Munoz et al., 2009, Svendsen et al., 2009). Additionally, studies showed that the budding yeast Rad2/XPG family endonuclease, YEN1, also possess H_j resolving abilities (Ip et al., 2008). Expression of YEN1 in affinity purification studies revealed that the nuclease was able to resolve H_js by a symmetrical cleavage mechanism analogous to that shown by bacterial resolvase RUVF (Ip et al., 2008). Similar observations were made for its homologue, GEN1, in humans (Ip et al., 2008). Furthermore, a recent study showed that loss of YEN1 in *mus81* background resulted in roughly 2-fold decrease in H_j resolution efficiency *in vivo*. In contrast, loss of MUS81 alone did not reduce H_j resolution efficacy *in vivo* suggesting that in budding yeast YEN1 acts redundantly with MUS81 during CO formation (Tay and Wu, 2010). Similarly, expression of GEN1 in *S. pombe mus81* mutant was shown to promote H_j resolution and CO formation in the mutant (Lorenz et al., 2009). In addition, the XPG/RAD2 nuclease family

member, EXO1 and DNA mismatch repair components the MUTLY complex MLH1-MLH3 are also thought to possess a role in dHj resolution (Zakharyevich et al., 2010). Although, the above nucleases were implicated in JM resolution their exact roles in resolving meiotic JMs remained unclear. Nevertheless, recent studies in budding yeast have provided interesting data regarding JM resolution. In budding yeast, the BLM helicase homologue SGS1 has been shown to be a central regulator of JM resolution pathways (De Muyt et al., 2012, Zakharyevich et al., 2012). A *sgs1/slx4/yen1/mms4* quadruple mutant exhibits a 6 fold reduction in COs and 3.6 fold reduction in NCOs whereas the *slx4/yen1/mms4* triple mutant was found to display wild-type levels of product formation. This suggests that SGS1 can resolve JMs efficiently into both COs and NCOs. Further analysis of various quadruple mutants of structure-specific nucleases suggest that SGS1 specifically promotes CO formation in conjunction with EXO1-MUTLY complex while in the absence of the latter SGS1 mediates JM disassembly into NCOs (De Muyt et al., 2012, Zakharyevich et al., 2012). In accord, SGS1 has previously been shown to be a member of the RTR complex, which is involved in the dissolution of JMs to form NCOs (Gilbertson and Stahl, 1996, Martini et al., 2011). Interestingly, recent studies indicate that YEN1 and SLX1-SLX4 are cryptic resolvases that are revealed specifically in the absence of MUS81-MMS4 and SGS1 respectively. YEN1 mutation in a *mus81* background caused an additional 21% reduction in total COs than *mus81* single mutant, however, this effect was not observed in any other double mutant involving YEN1. This suggests that YEN1 makes a significant contribution in crossing over in *mus81*. Similarly, *sgs1/slx4* and *sgs1/slx1* double mutants exhibit meiotic catastrophe and unresolved JMs, which were not observed in any other double mutants involving

SLX4 and SLX1 (Zakharyevich et al., 2012). Taken together, the data suggests that in budding yeast SGS1 is the major JM resolvase during wild-type meiosis. In the absence of SGS1, JM resolution occurs normally but depends on MUS81-MMS4 and SLX1-SLX4 and on YEN1 when MUS81 is disrupted (De Muyt et al., 2012, Zakharyevich et al., 2012).

JM resolution appears to be dependent of varying resolvases between organisms. In contrast to budding yeast, MUS81 is required for the formation of most if not all COs in fission yeast (Hollingsworth, 2004, Smith et al., 2003). The complete sterility phenotype displayed by *S. pombe mus81* mutants can be rescued by bacterial H_j resolvase RUSA suggesting that MUS81 is involved in the resolution of intermediate structures in fission yeast (Hollingsworth, 2004). Additionally, *S. pombe* SGS1 orthologue, RQH1 was also found to be important for CO and NCO formation, although a meiotic resolvase activity is yet to be shown (Cromie et al., 2006). In *C. elegans*, the FANCDJ-related DNA helicase RTEL1 has been functionally compared to SGS1 and *rtel1-1* mutant appears to promote JM resolution via MUS81-dependent pathway (Youds et al., 2010). In *Arabidopsis*, a functional homologue of SGS1 is yet to be found. Additionally, two homologues of GEN1 have been identified in *Arabidopsis*. However, the double knockout line was found to be fertile suggesting possible redundancy of proteins in dH_j resolution (Osman et al., 2011). Nevertheless, ~85% of the meiotic COs are dependent on the MUTL complex AtMLH1-AtMLH3 while the rest are partially dependent on AtMUS81 (Franklin et al., 2006, Higgins, 2004, Higgins et al., 2008a, Higgins et al., 2008b). Hence, it is plausible that dH_j resolution in *Arabidopsis* may be similar to that in budding yeast, although this remains to be validated.

1.4.6. Crossover homeostasis

In budding yeast, a study was carried out using a series of *S. cerevisiae spo11* hypomorphs where DSB formation was induced at different levels (~80%, ~30%, and ~20% of wild-type levels) in order to understand CO/NCO designation (Martini et al., 2006). The study measured recombination frequency at eight different intervals across three chromosomes in the *spo11* hypomorphs. These revealed that reducing the number of DSBs does not cause a parallel reduction in the number of COs, instead, there is a tendency for COs to be maintained at the expense of NCOs. This phenomenon is termed crossover homeostasis and is thought to be important for assuring the formation of at least one CO between each chromosome pair, which is essential for the proper segregation of chromosomes during meiotic divisions (Martini et al., 2006).

Various studies of meiotic recombination revealed that although recombination is initiated by the formation DSBs at a number of sites along the chromosomes, only a subset of DSBs mature to form COs, while the rest are resolved as NCOs. The ratio of DSBs to COs has been observed to vary among organisms. In budding yeast, number of DSBs was found to be approximately three times more than COs whereas in mouse only ~10% of DSBs are resolved as COs (Kauppi et al., 2004). Immunolocalization studies on wild-type *Arabidopsis* meiocytes using anti-AtSPO11 antibody, that detects DSB catalyzing protein AtSPO11, revealed that DSBs are formed at ~150 sites during early leptotene (Sanchez-Moran et al., 2007). This is in agreement with the number of early recombination intermediates, AtRAD51 and AtDMC1 observed during early prophase I in wild-type meiotic chromosome spreads using similar studies (Sanchez-Moran et al., 2007). However, FISH studies revealed

that only 9-10 COs are present at wild-type metaphase I suggesting that only 5-10% of the DSBs are subsequently repaired to form COs in *Arabidopsis* while the rest are repaired as NCOs (Franklin et al., 2006). The importance of such a variation between DSB and CO numbers is currently unknown, although it is speculated that the high number of DSBs is required to promote homologous chromosome pairing and synapsis (Baudat and de Massy, 2007, Osman et al., 2011). Interestingly, the observation that only a few DSBs are eventually repaired to form COs suggest the presence of anti-CO factors. In *Arabidopsis*, recent studies suggest that mutation of the helicase AtFANCM in the *zmm* mutant *Atzyp4* results in an increase in mean bivalent numbers to ~4.5 from ~1.5 in *Atzyp4*. Furthermore, analysis of eight genetic intervals using tetrad analysis revealed that in *Atfancm-1/Atzyp4* the genetic distances were increased by a factor of 1.9 to 3.1 compared to the wild type (Crismani et al., 2012). In an *Atfancm-1* single mutant the recombination frequency was increased by ~12% compared to the wild-type. Interestingly, an *Atfancm-1/Atzyp4/Atmus81* triple mutant exhibits an absence of bivalents at metaphase I and chromosome fragmentation at anaphase I suggesting that the extra COs in *Atfancm-1* are AtMUS81-dependent and interference-insensitive. These findings suggest that AtFANCM acts as an anti-CO factor during *Arabidopsis* meiosis (Crismani et al., 2012). Similar anti-CO activity has been described for RTEL1 in *C. elegans* and SGS1 in budding yeast (Oh et al., 2007, Youds et al., 2010). *rtel-1* mutant exhibits significantly increased meiotic recombination in five genetic intervals on three chromosomes (Youds et al., 2010). Similarly, loss of SGS1 increases meiotic COs and causes transient accumulation of inter-homologue, inter-sister chromatid and multi-chromatid joint molecules during meiosis (Jessop et al., 2006, Oh et al., 2007,

Oh et al., 2008a). AtFANCM, RTEL1 and SGS1 have all been proposed to act as anti-recombinases that can resolve intermediate structures which lead to the formation of NCOs, thereby constraining the formation of excess COs (De Muyt et al., 2012, Oh et al., 2008b, Youds et al., 2010).

So far, it is unclear how DSBs are designated as COs and NCOs, although analysis in budding yeast *zmm* mutants have led to the proposal that CO/NCO decision takes place early in the DSB repair process (Borner et al., 2004). Budding yeast *zmm* mutants form normal levels of DSBs but are defective in strand invasion and dHj and CO formation. However, NCOs have been observed to form at normal levels in *zmm* mutants. Since strand invasion is the earliest step which is aberrant in *zmm* mutants, it is proposed that the CO/NCO decision takes place at or before this step in the DSB repair process (Borner et al., 2004). This proposal is referred to as 'Early Crossover Decision' (ECD) model of CO formation and is likely to be the case for *Arabidopsis* meiotic recombination (Bishop and Zickler, 2004, Borner et al., 2004).

1.4.7. Crossover control

Various studies have revealed that meiotic COs are not randomly distributed across the genome and their numbers are tightly regulated in all organisms (Jones, 1984). Interestingly, the number and distribution of COs in all organisms are such that they ensure the formation of at least one CO per chromosome pair. This is known as the obligate CO and is essential for correct segregation of chromosomes during meiotic divisions (Jones, 1984, Jones and Franklin, 2006, Shinohara et al., 2008). Formation of a CO reduces the formation of another CO in adjacent region. This is due to the

presence of interference between COs. Interference is the phenomenon by which the formation of one CO reduces the possibility of the formation of another CO in close proximity (Jones and Franklin, 2006). This therefore increases the chance of a second CO occurring in the areas most distal to the initial CO. Interference was first observed in *Drosophila* chromosomes where the number of observed double COs on a chromosome was less than the expected number (Sturtevant, 1915). In budding yeast, tetrad analysis in quartet mutants in which the four pollen grains remain attached after meiotic recombination showed that ~85% of the COs formed exhibited interference based on their fit to chi-square distribution (Copenhaver et al., 2002). As discussed earlier, this is also the case in *Arabidopsis* (Higgins, 2004).

The mechanism of how interference is established between COs is still poorly understood. It was thought that interference was controlled and transmitted by the SC which runs the whole length of homologous chromosomes (Sym et al., 1993). This was supported by the observation that budding yeast *zmm* mutants which lacked SC also lacked interference (Borner et al., 2004). However, a more recent study suggests that CO interference is established before the formation of the SC (Fung et al., 2004). Furthermore, *Arabidopsis Atzyp1* mutants which lack SC still have nearly wild-type distribution of COs and hence the presence of interference, indicating that the SC does not have a role in transmitting interference signals (Higgins et al., 2005). A model for establishing CO interference is the 'counting model', which proposes that adjacent COs are separated by a fixed number of NCOs (Stahl, 2004). This model accounts well for the pattern of CO distribution in various organisms including *Arabidopsis*. A prediction of the counting model is that a reduction in DSBs would cause a corresponding reduction in both CO and NCO

products. However, studies in budding yeast suggests that a reduction in DSB does not result in reduction in COs, instead COs are maintained at the expense of NCOs (Martini et al., 2006). Another model proposed that CO interference is transmitted by the local release of tension across a chromosome by the induction of COs (Kleckner, 2004). Kleckner et al., (2004) suggested that during the formation of a CO the chromosome axis twists due to a build up of tension. This tension is relieved locally and no other CO is formed in close vicinity due to a lack of tensional stress. However, there is a build-up of stress further away from the CO due to constant expansion and contraction of chromatin throughout meiosis. This stress is proposed to be relieved at a CO site far away from the initial CO site (Kleckner, 2004). Nevertheless, the exact mechanism of establishing CO interference still remains unknown.

More recently, analysis of the distribution of recombination events in mammals and budding yeast revealed that meiotic COs tend to occur at specific regions along chromosomes. These regions have been termed recombination hotspots are approximately 1-2kb in length (Kauppi et al., 2004). Since all recombination events initiate by the formation of DSBs recombination hotspots are also known as DSB hotspots. Studies in yeast and mice showed that DSB hotspot designation requires the post-translational chromatin modification, the tri-methylation of histone H3 on lysine 4, H3K4me3 (Borde et al., 2009, Buard et al., 2009). This epigenetic modification has been proposed to serve as a marker for the initiation of recombination. Analysis of the *S. cerevisiae* mutants which lack the H3K4 methyltransferase protein SET1 revealed drastic changes in hotspot usage in the mutant compared to the wild-type (Borde et al., 2009). Furthermore, two separate studies in mice independently identified PRDM9, which is involved in hotspot

regulation through chromatin modification (Grey et al., 2009, Parvanov et al., 2010). PRDM9 was found to be meiosis-specific and possess a SET domain that trimethylates H3K4. Mice lacking PRDM9 exhibit meiotic arrest at prophase I and hence complete sterility (Hayashi et al., 2005). PRDM9 possesses a DNA-binding zinc-finger domain comprising of several zinc-finger repeats in its C-terminus (Baudat et al., 2009). Intriguingly, computational analysis predicts that the C-terminus zinc-finger domain of both mouse and human PRDM9 may bind to a 13-mer sequence motif (CCnCCnTnnCCnC), found enriched in DSB hotspots. This prediction has been confirmed by *in vitro* analysis suggesting that the H3K4 modifier is recruited to DSB hotspots (Baudat et al., 2009, Grey et al., 2011). Studies involving experimental and population genetics suggest that variation in the C-terminus zinc-finger domain of PRDM9 may lead to variation in the usage of DSB hotspot (Segurel et al., 2011). Analysis of a selection of *Prdm9* alleles from 20 mouse strains revealed extensive variation in repeat numbers of the zinc-finger domains in PRDM9 between the strains (Parvanov et al., 2010). Similar observations were reported in studies of human PRDM9 C-terminus zinc-finger repeats using DNA from several different sources and spanning multiple ethnicities (Baudat et al., 2009, Parvanov et al., 2010). The extensive variation of PRDM9 C-terminal zinc-finger repeats is thought to account for the differences in hotspot usage between individuals in both mice and human. Consistent with this suggestion, transgenic mice with varying levels of PRDM9 zinc fingers exhibit differences in hotspot activity, H3K4me3 levels, and the genome-wide distribution of crossovers (Grey et al., 2011). These findings implicate PRDM9 in playing a role in CO control. So far, an orthologue of PRDM9 has not been identified in *Arabidopsis*. However, recent studies suggest that chromatin modifications

mediated by the methyltransferase AtMET1, which is required to maintain CG DNA methylation, also plays an important role in CO distribution during *Arabidopsis* meiosis (Yelina et al., 2012). Loss of *Atmet1* results in loss of DNA methylation and associated histone modifications which lead to increased transcription of repetitive sequences (Kankel et al., 2003). Analysis of the segregation of polymorphic markers revealed an increase in centromere-proximal meiotic CO frequency in *Atmet1*. This was not observed in the wild-type as centromeric repeat regions are densely methylated and hence exhibit low CO frequency. Furthermore, pollen-typing assays revealed a coincident decrease in CO frequency at pericentromeric regions but an increase at the distal regions of chromosomes in *Atmet1*. Interestingly, the total number of COs were found to be similar between the wild-type and *Atmet1*. These observations suggest that regional epigenetic organization play an important role in CO distribution along eukaryotic chromosomes (Yelina et al., 2012). Additionally, the SWI2/SNF2-like chromatin remodelling protein, AtDDM1 has also been shown to be involved in CO control in *Arabidopsis* (Melamed-Bessudo and Levy, 2012). Analysis of fluorescent seed markers from *DDM1/ddm-1* revealed that its meiotic recombination rate was 59% higher than that of the wild-type. Additionally, analysis of molecular markers within chromosome 5 showed that recombination was 60-90% more in euchromatic regions than heterochromatic regions in *DDM1/ddm-1* compared to the wild-type. Similar results were observed for *MET1/met1-3* (Melamed-Bessudo and Levy, 2012).

Histone acetylation and deacetylation have also been shown to be involved in meiotic recombination. Disruption of *S. cerevisiae* histone acetyltransferase (HAT), *SpGcn5* leads to a partial loss of DSBs in *ade6-M26* hotspot locus (Yamada et al., 2004).

Additionally, disruption of histone deacetylase (HDAC), ScRpd3p increases HIS4 hotspot activity (Merker et al., 2008). Furthermore, in budding yeast disruption of the HDAC, SIR2 changes the genomic distribution of meiosis-specific DSBs (Mieczkowski et al., 2007). In *Arabidopsis*, a recent study revealed that mutation of the GCN5-related HAT gene *AtMCC1* leads to ~68% reduction in fertility and the formation of univalents in 8% of the *Atmcc1* nuclei. Interestingly, all of these univalents involved chromosome 2 indicating the loss of the obligate CO in the chromosome. Additionally, there was a significant decrease in ring bivalents (contains 2-3 COs) for chromosome 1 and a significant increase for chromosome 4 in *Atmcc1* compared to the wild-type. This corresponded to a significant increase in distal chiasmata in chromosome 4. Altogether, these changes increased the formation of ring bivalents by 12% in *Atmcc1* compared to the wild-type, although there was no significant difference in the overall chiasma frequency between the two. These findings suggest that histone acetylation plays an important role in CO control in *Arabidopsis* (Perrella et al., 2010).

The findings discussed in the above sections highlight the importance of chromatin modifications in CO control. It is likely that controlled chromatin condensation and decondensation may make the DNA more accessible for recombination proteins. Alternatively, these may regulate the expression of recombination proteins such that they influence CO formation. However, the mechanisms underlying CO control still remains poorly understood.

1.5. Inter-relationship between chromosome axes and meiotic recombination

1.5.1. Co-ordination between chromosome axis maturation and recombination

In many organisms, normal juxtaposition of the homologous axes at early prophase I requires meiotic recombination, which in turn requires the former to generate normal levels of COs, suggesting that the two processes are tightly linked (Kleckner, 2006). The basis of this inter-relationship is still poorly understood, however, it can be best explained by the 'axis to loop capture' model. (Zickler and Kleckner, 1999). It is proposed that during early prophase I meiotic chromosomes are arranged as so-called 'dual-loop modules' (Figure 2A), where meiotic sister chromatids are organized into a set of chromatin loops. The loops are anchored and aligned along a linear proteinaceous axis at a density of approximately 20 loops per μm of axis. The density of loops along chromosome is thought to be conserved between organisms, evident from the observation that organisms with larger genomes have either larger loop size or longer axis but no change in their loop density (reviewed in Kleckner, 2006). Zickler and Kleckner (1999) proposed that in leptotene DSBs form towards the base of chromatin loops which are in close proximity to the chromosome axis. At some point soon after the formation of DSBs, the DSB ends become tethered to their underlying axis along with RecA homologues and other recombination proteins that are loaded onto the DNA ends. One of the protein-associated DSB end then identify and capture a homologous DNA sequence located within the chromatin loop of its corresponding homologue. This mechanism of homologue identification is termed

'axis to loop capture' and is thought to allow homology search over a distance of the length of one chromatin loop (Zickler and Kleckner, 1999). It is suggested that following loop capture by the axis-associated DSB, the ends of DNA around DSB which are coated with various early recombination proteins form a rigid rod-like structure. The rod on one side is proposed to grow outward, carrying the DSB and the associated axis towards the homologue axis. This is followed by the rod on the other side which is also thought to grow outward but swing $\sim 180^\circ$ about the DSB to capture the homologue axis. These actions are proposed to pull the homologues together to close proximity of each other (Zickler and Kleckner, 1999). The resulting close association of homologues is thought to facilitate pairing and synapsis of homologous chromosomes (reviewed in Kleckner, 2006).

Indeed, recombination has been shown to be tightly co-ordinated with axis maturation. Initially, Blat *et al* (2002) proposed that recombination machinery assembles within the chromatin loop and then gets tethered onto the chromosome axis prior to DSB formation in the axis-associated loop (Blat *et al.*, 2002). Other scientists argued that DSBs are formed prior to the loop-axis association or that DSB formation and axis assembly occur concomitantly (Kleckner, 2006, Lorenz *et al.*, 2006). In *Arabidopsis*, dual-immunolocalization along with time course studies suggest that DSB formation and axis maturation are indistinguishable events (Sanchez-Moran *et al.*, 2007). The studies revealed that although the number of AtSPO11 (DSB catalyzing protein) foci was maximum at 3h post BrdU pulse labelling at S-phase, the number of γ H2AX (DSB marker) foci did not peak till 5h post pulse-labelling. This indicates that there is a considerable delay in the actual formation of DSBs after AtSPO11 loading. In addition, the study reported that appearance of

γ H2AX signal is concomitant with transition of AtASY1, AtSMC3 and AtSCC3 signals from chromatin to the axis. These observations suggest that DSB formation, hence recombination does not occur till the axis has matured (Sanchez-Moran et al., 2007).

In *Arabidopsis*, further evidence of the tight co-ordination between recombination and chromosome axis maturation are emphasized by analysis of progression of prophase I in recombination mutants. Time-course experiments using BrdU pulse-labelling at S-phase and the subsequent detection of labeled meiotic stages using FITC-conjugated anti-BrdU antibody and DAPI-stained DNA revealed that completion of prophase I takes ~29 hours post pulse-labeling in wild-type (Armstrong et al., 2003). However in mutants such as *Atmsh4*, *Atzyp1* and *Atmlh3* in which recombination is defective, completion of prophase I takes considerably longer, ~38, ~54 and ~35 hours post pulse-labeling in S phase respectively, than in wild-type (Higgins, 2004, Higgins et al., 2005, Jackson et al., 2006). These observations suggest the presence of an intra-prophase I surveillance mechanism that ensures DSBs are repaired before proceeding with the divisions of meiosis (Jackson et al., 2006).

1.5.2. Spatial association between recombination and chromosome axis/SC

An important aspect of meiotic recombination is that it occurs in the context of the chromosome axis and the SC. Early EM studies of *Schizophyllum commune*, *Coprinus*, *Bombyx mori* and human spermatocytes revealed that 'recombination nodules', containing a complex of recombination proteins were found to be associated with the SC at pachytene (von Wettstein et al., 1984). Furthermore, the

number and distribution of these nodules were consistent with the number of eventual chiasmata observed in the corresponding organism. More recent studies in mammals involving immunocytological techniques revealed that these nodules correspond to MLH1 and MLH3, which are thought to mark CO sites (Barlow and Hulten, 1998, Lipkin et al., 2002). Furthermore, mouse and budding yeast recombination proteins RAD51 and DMC1 have been observed to localize to homologous axes (Moens et al., 2002 and the references therein). In *Arabidopsis*, the recombination proteins AtRAD51, AtDMC1, AtMSH4 and AtMLH3 all exhibit axis-associated foci-like signals supporting the notion that recombination is spatially coupled with the axis (reviewed in Osman et al., 2011).

1.5.3. Role of axis proteins in recombination

Cohesins form an integral component of the meiotic chromosome axes. In addition to their role in maintaining sister-chromatid cohesion, cohesins are also thought to play a role in meiotic CO formation. Studies involving human cells where DSBs were induced using a laser microbeam and assembly of repair proteins were tracked *in vivo* by immunofluorescent detection revealed that cohesin accumulates at DSB sites (Kim et al., 2002). It has been proposed that the accumulation of cohesin at break sites following their formation is required to stabilize broken DNA ends and facilitate DSB repair (Strom et al., 2004). *S. cerevisiae* *rec8* mutants which lack the meiotic REC8 cohesin subunit fail to repair DSBs. Similarly, *Arabidopsis* *Atsyn1* mutants lacking the yeast REC8 homologue AtSYN1 also fail to repair DSBs (Bai et al., 1999, Klein et al., 1999). In addition to cohesins, certain structural components of the SC

have also been shown to play a role in promoting meiotic recombination. The SC TF component ZIP1 in *S. cerevisiae* and AtZYP1 in *A. thaliana* has also been shown to be required for normal levels of CO formation (Borner et al., 2004, Higgins et al., 2005, Storlazzi et al., 1996). In addition, RED1 and HOP1, the AE components of the SC in budding yeast, have been shown to be essential for the formation of DMC1-mediated interference-dependent COs (Niu et al., 2005). Similarly, *Arabidopsis* meiotic axis protein, AtASY1 has recently been shown to play a key role in mediating inter-homologue recombination (Sanchez-Moran et al., 2007). Time-course studies coupled with immunolocalization studies showed that in the absence of AtASY1, AtDMC1 is destabilized soon after loading leading to a loss of inter-homologue recombination in *Atasy1* (Sanchez-Moran et al., 2007). It is presumed that AtASY1 promotes CO formation via interaction with yet unknown members using a mechanism similar to the one in budding yeast.

1.6. *Arabidopsis thaliana* - a model plant for meiosis research

In *Arabidopsis*, male meiosis occurs in the anther. Early during anther development several adjacent hypodermal cells within the anther primordium undergo periclinal divisions to form archesporial cells. The archesporial cells then divide mitotically to form primary sporogenous cells. The sporogenous cells subsequently differentiate into pollen mother cells (PMCs) and primary parietal cells, which differentiate mitotically to form the wall of the anther (reviewed in Wilson and Yang, 2004). Female meiosis on the other hand occurs in the ovule housed in gynoecium in

Arabidopsis. Hypodermal cells at the top of ovule primordium differentiate during early ovule development to form an archesporial cell, which give rise to the spore bearing tissue, megaspore mother cell (MMC). Female meiosis occurs in the MMC giving rise to four haploid megaspores, three of which degenerate via programmed cell death and only one develops into the female gametophyte (reviewed in Osman et al., 2011, Wilson and Yang 2004).

The first description of meiosis in *Arabidopsis* was reported over a century ago. However, due to the small size of chromosomes in *Arabidopsis* and the limited cytological procedures available at that time meiotic research in *Arabidopsis* proved to be challenging. Nevertheless, recent advances in the development of cytological and molecular biology tools have made *Arabidopsis* an ideal model organism for studying meiosis. *Arabidopsis* has a relatively small genome (~125MB) which has been completely sequenced (*Arabidopsis* Genome Initiative, 2000). In addition, there is a wide selection of T-DNA insertional mutants available for identification and characterization of meiotic genes in *Arabidopsis*. Furthermore, the anther locules in *Arabidopsis* contain synchronized meiocytes which allow the cytological analysis of chromosomes at different stages of meiosis. Recent advances have also enabled the ultra-structural analysis of meiotic chromosome synapsis using electron microscopy and the analysis of chromosome-specific chiasma frequency and distribution using FISH (Albini and Jones, 1984, Armstrong and Jones, 2003, Jones et al., 2003). The availability of antibodies against various meiotic proteins allows efficient immunocytological analysis of the localization of various proteins during meiosis. (Sanchez-Moran, 2007 and the references therein). Time course experiments using BrdU pulse labelling of meiotic chromosomes allow the study of the chronology and

duration of the different meiotic stages in *Arabidopsis* (Armstrong et al., 2003). The use of BrdU pulse labelling in conjunction with immunolocalization also allows the study of the distribution of meiotic proteins at different time points (Armstrong et al., 2003, Sanchez-Moran et al., 2007). In addition, the ability to transform and express a desired gene *in vivo* during *Arabidopsis* meiosis using *Agrobacterium* is highly advantageous for the characterization of meiotic proteins (Zhang *et al.*, 2006). More recent advances have led to the development of proteomics studies involving co-immunoprecipitation and mass spectrometry using meiocytes from *Arabidopsis* and its close relative *Brassica* (Sanchez-Moran et al., 2005). These have allowed the analysis of interactions between meiotic proteins and raised the possibility of identifying novel proteins involved in meiosis. Finally, there is generally no meiotic arrest in *Arabidopsis* meaning that meiosis proceeds to the end in most mutants allowing defects to be tracked along the meiotic stages (reviewed in Sanchez-Moran, 2007). These characteristics make *Arabidopsis* an ideal model organism for studying meiosis.

1.7. Aims and objectives

Chromosome axis formation, synapsis and meiotic recombination are essential for normal meiosis. Recent evidence suggests that these processes are closely inter-linked, although their inter-relationship still remains poorly understood. This project aims to investigate this inter-relationship in order to study the control of meiotic

recombination and chromosome synapsis during meiosis in *A. thaliana*. The objectives of this project are as follows:

Elucidation of the role of the RECQ family DNA helicase, AtRECQ4B, during meiosis.

Molecular and cytological characterization of a novel axis component, AtASY3, that is required for normal synapsis and recombination.

Investigation of the effect of post-translational modification of the axis-associated protein, AtASY1, by analysing a putative phosphorylation site, T295, in the protein.

CHAPTER 2

Materials and methods

2.1. Plant material and growth conditions

Arabidopsis thaliana seeds including those of the T-DNA insertion lines used in this study were obtained from European Arabidopsis Stock Centre (NASC) (www.arabidopsis.info). Seeds for *Atasy1-T295A* transgenic lines were provided by Eduardo Corredor and Ruth Perry. The ecotype Columbia-0 (Col-0) was used as a wild-type control in all experiments.

Plants were grown in soil based compost in a glasshouse at 18-25°C with a 16 hour light cycle and watered twice daily. For growing plants in MS media (see appendix for recipe), seeds were initially sterilized in 20% bleach (Parazone™) for 15 minutes followed by three 15 minute washes in sterile distilled water (SDW) on a rotating wheel. Seeds were then dried, placed on MS plate and vernalized 48 hours at 4°C before moving the MS plate to a growth chamber, maintained at 22°C with a day length of 16 hours.

2.2. Nucleic acid manipulations

2.2.1. Isolation of plant DNA

DNA was isolated for genotyping plants using the Extract-N-Amp™ Plant PCR kit (Sigma). A small portion of nascent leaf (~2x2mm) was collected into a 0.5 ml microfuge tube. 40µl of extraction buffer was added to the tube and the leaf was broken up with the tip of a pipette. The sample was then incubated at 95°C for 10 minutes in a PCR machine. Subsequently, 40µl of dilution buffer was added and the

tube flicked in order to further break up the tissues. The sample was then centrifuged for 15 seconds at 13,000 rpm to separate the plant DNA into the supernatant. The tube containing the extracted DNA was stored at -20°C .

2.2.2. RNA extraction from plant tissue

All microfuge tubes, pipette tips and pestles that were used for handling RNA were treated with diethyl pyrocarbonate (DEPC) to remove any RNase contamination in them. All equipments were immersed in DEPC (1:1000 with SDW) and left overnight before being subsequently autoclaved to inactivate DEPC. Total RNA from the desired plant tissue was extracted using RNase easy minikit (Qiagen) as per the manufacturer's protocol. A suitable amount (50-100mg) of the desired plant tissue was snap frozen in liquid nitrogen upon collection and ground in a 1.5ml tube using a pestle. Subsequently, the RLT buffer (Qiagen) was added to the sample and the tube vortexed to break open cells and denature RNases. The sample was then passed through a QIAshredder spin column (Qiagen) to remove cellular debris and then through a RNeasy mini column (Qiagen) where the RNA binds to a silica membrane. The membrane was then washed with RW1 buffer (Qiagen) containing ethanol followed by RNase free (DEPC treated) water to elute the RNA. Eluted RNA was stored at -70°C .

2.2.3. cDNA synthesis

First-strand cDNA synthesis was carried out using the Superscript™ II reverse transcriptase (Invitrogen). 1µl of Oligo(dT)₂₄ was added together with ~2µg of total RNA and 1µl of dNTP mix (10mM each) and made up to 12µl with RNase free water. The sample was then heated at 65°C for 5 minutes and instantly chilled on ice. Subsequently, 5µl of 5X FSB, 2µl of 0.1M DTT and 1µl of the RNase inhibitor RNasein (Promega) was added to the sample. This was then subjected to reverse transcription PCR (see section 2.2.10) for generating cDNA. cDNA was stored at -20°C.

2.2.4. Nucleic acid quantification

DNA was diluted to 1:100 with SDW and RNA to 1:200 with DEPC treated water. Each sample was transferred to a quartz cuvette before measuring its absorbance with a spectrophotometer (Jenway 6305) at a wavelength of 260nm. The concentration of the sample was then calculated given that a DNA sample of 50µg/ml and an RNA solution of concentration 40 µg/ml each has an absorbance (OD₂₆₀) of 1.0.

2.2.5. DNA agarose gel electrophoresis

1% agarose gels were used in all cases. To prepare a gel, agarose (Sigma) was dissolved in 0.5X TBE by heating in a microwave. The molten gel was briefly cooled and 0.5µg/ml of ethidium bromide was added for subsequent visualisation of DNA

before being allowed to set. The gel was covered with loading buffer (0.5X TBE) before loading any DNA. For estimation of molecular weights, all DNA was run next to a 1kb DNA ladder (15 µl 1Kb Ladder {Invitrogen, 50µl DNA loading buffer {40% [v/v] glycerol, 0.25% [w/v] Bromophenol blue, 0.25% [w/v] xylene cyanol}, 135µl SDW). DNA loading buffer was added to DNA if not already included in the sample. Gels were run using Hybaid or Biorad electrophoresis kits. Images of gels were captured using a FluorS Max multi-imager or a Gel-Doc XR imager using QuantityOne Software.

2.2.6. RNA agarose gel electrophoresis

Agarose gels for resolving RNA samples were prepared run and visualized using similar techniques as used for DNA gels. However, before loading RNA samples onto a gel, RNA loading dye (Invitrogen) was added to each sample at a ratio of 1:1 and incubated at 65°C to prevent the formation of any secondary structures of RNA.

2.2.7. Primer design

Primers were designed by selecting appropriate regions from the desired nucleotide sequence. Primers were obtained from Eurofins MWG Operon (Germany). A complete list of primers used in this study can be found in the Appendix.

2.2.8. Polymerase chain reaction (PCR)

PCRs were used to amplify genomic DNA, cDNA and plasmid DNA using desired primers. Most PCRs were carried out using *Taq*DNA polymerase ReddyMix (ThermoScientific) following the manufacturer's instructions. Primers were used at a final concentration of 0.1 μ M. In a typical PCR reaction (Table 1), DNA was denatured at 95°C before allowing primers to anneal. The annealing temperature was generally 5°C below the average melting temperatures of the primers being used. Nucleotide sequence was then elongated from the primers by *Taq* polymerase in the ReddyMix. The duration of this elongation stage was 1 minute per kb of sequence to be amplified. Each cycle consisting of the above stages was usually carried out 35 times. This was followed by a final elongation stage to complete the amplification process. PCRs were carried out in a ThermoHybaid Omnigene, Techne TC-412 or ThermoHybaid PCR Sprint thermo-cycler.

In some cases where accurate amplification of nucleotide sequence were necessary, PCRs were carried out using Pfu DNA polymerase (Promega) according to the manufacturer's protocol. All solutions were prepared on ice and reactions were subjected to a hot start. DNA elongation times were extended as per the protocol to allow proof reading by the polymerase. All other aspects of the PCRs were similar to those described in the above paragraph.

Temperature (°C)	Time (minutes)	Number of cycles
94	2	1
94	1	35
5°C below T _m of primers	1	
72	1 minute per kb	
72	10	1

Table 1. Standard PCR. (T_m = Melting temperature)

2.2.9. PCR for genotyping plants

Plants were genotyped by PCRs using gene specific primers in conjunction with a primer specific to the left border of T-DNA. 1µl of genomic DNA extracted from plant leaf was added to 9µl primer mix (final concentration 2pmol/µl) and 10µl of *Taq*DNA ReddyMix (ThermoScientific). PCRs were carried out as described in section 2.2.8.

2.2.10. Reverse transcription (RT)-PCR

RT-PCRs were used for cDNA preparation for gene expression analysis and other purposes. RT-PCRs were carried out using SuperScript™ II reverse transcriptase enzyme (Invitogen) as per the manufacturer's instructions. Sample preparation is detailed in section 2.2.3. During the RT-PCRs, samples were heated at 42°C for 50 minutes to allow elongation of cDNA using the RNA template. This was followed by heating at 70°C for 15 minutes to inactivate the reaction.

2.2.11. 3' -rapid amplification of cDNA ends (RACE)

3'-RACE, involving three rounds of PCRs, was used to amplify the unknown nucleotide sequence at the 3' end of *Brassica ASY3* from an mRNA template. The first round of PCR was essentially a RT-PCR (section 2.2.10) which generated cDNA. However, instead of using the usual oligo-dT primer the reaction was carried out using a modified oligo dT-adaptor primer, which consists of a short sequence of deoxy-thymine nucleotides and an adaptor sequence. The second and third rounds of PCRs were carried out similarly to that described in section 2.2.8. The second round of PCR involved the amplification of the 3' end of the cDNA using a gene specific primer (GSP) complementary to a known location and an anti-sense primer complementary to the oligo(dT)-adaptor sequence. The final round of PCR used a nested GSP in conjunction with the primer complementary to the adaptor sequence to amplify the 3' end of the cDNA increasing specificity of the desired product.

2.2.12. Cloning

2.2.12.1. Amplification of insert DNA

For cloning, the desired nucleotide fragments were initially amplified by PCRs using specific primers as described in 2.2.8. In case of cloning of fragments into expression vectors, PCRs were carried out using primers with specific restriction sites incorporated in them. Amplified fragments were separated using gel electrophoresis as described in section 2.2.5.

2.2.12.2. Gel extraction of DNA bands

DNA fragments in agarose gel were illuminated using weak UV light. A small portion of the gel containing the DNA fragment of interest was cut using a sterile blade. Extraction of the DNA fragment from the gel was carried out using QIAquick Gel Extraction Kit (QIAGEN) following the manufacturer's guidelines. The gel containing the DNA fragment was dissolved in three volumes (w/v) of QG buffer by heating at 50°C for 10 minutes. The solution was then transferred to a QIAquick spin column and centrifuged at 13,000 rpm for 1 minute. During this process DNA binds to the membrane in the column. The column is then washed with PE buffer and the DNA is subsequently eluted in nuclease free water.

2.2.12.3. Ligation of DNA fragments into vectors

pDrive

pDrive (Qiagen) is a 3.85kb easy cloning vector. The plasmid has a multiple cloning site (MPC) within the *lacZ* gene, which allows blue/white selection of colonies using X-gal. The plasmid also permits ampicillin and kanamycin selection. For ligation, 2-4µl of purified DNA was mixed with 1µl of pDrive and 5µl of 2x ligation buffer. Samples were incubated overnight at 15°C.

pZErO™-2

pZErO™-2 (Invitrogen) is a 3.3 Kb plasmid with a *lacZ* gene containing a MPC. The *lacZ* gene is fused with *ccdB* which encodes a lethal protein. Expression of *ccdB* results in death of cells containing non-recombinant vector. Therefore, cloning into the MPC disrupts *ccdB* expression allowing growth of recombinants only. The plasmid also contains kanamycin resistance gene. For ligation of cohesive ends a 2:1 molecular ratio of insert:vector was used while a 10:1 ratio of insert:vector was used for blunt-end ligation. Molecular ratio for ligation of cohesive ends was calculated as follows:

$$X \text{ ng insert} = (2)(\text{bp insert})(10 \text{ ng linearized pZErO}^{\text{TM}}\text{-2}) / (3297 \text{ bp pZErO-2})$$

For blunt-end ligation, the 2 in the above equation was replaced with 10. Ligation samples were prepared as per manufacturer's instructions. Ligations were carried out at 16°C for 30 minutes for cohesive-end ligation and 60 minutes for blunt-end ligation.

pCR®-Blunt

pCR®-Blunt (Invitrogen) is a 3.5kb vector used for blunt-end cloning. The plasmid has similar properties to pZErO™-2. For ligation into pCR®-Blunt, a 10:1 molar ratio of insert:vector was used. Molecular ratio was calculated as follows:

$$X \text{ ng insert} = (10)(\text{bp insert})(25 \text{ ng linearized pCR}^{\text{®}}\text{-Blunt}) / (3500 \text{ bp pCR}^{\text{®}}\text{-Blunt})$$

Ligation samples were prepared as per manufacturer's instructions. Ligations were carried out at 16°C for 60 minutes.

pET21b

pET21b (Novagen) is a 5.4 Kb plasmid with MPC downstream of a T7 promoter. Expression from the T7 promoter is under the control of a Lac operator (*lacI*), which allows isopropylthio-β-D-galactosidase (IPTG) inducible expression. The plasmid also contains 6 repeats of the CAC codon, which codes for histidine, downstream of the MPC. This histidine tag is attached to the C-terminus of the recombinant protein and allows easy protein purification. The plasmid also contains an ampicillin resistance gene for selection. For preparation of each ligation sample a molar ratio of 3:1 insert:vector was used. Molecular ratio was calculated as follows:

$$X \text{ ng insert} = (3)(\text{bp insert})(10 \text{ ng linearized vector}) / (\text{bp vector})$$

The insert and vector mix was added to 4μl of 5x ligation buffer and 1μl T4 ligase (Invitrogen). Each sample was then made up to a final volume of 20μl with SDW. Ligations were performed over night at 14°C.

pPF408

pPF408 is a 11.5 Kb binary plasmid which contains a MPC downstream of a meiosis specific DMC1-promoter (Siaud et al., 2004). The plasmid allows the expression of a fragment of interest during meiosis *in vivo*. The plasmid also contains BASTA and

chloramphenicol resistance genes for selection. Sample preparation and ligation were carried out similarly to the methods mentioned above for pET21b.

2.2.12.4. Preparation of competent *E. coli* cells

Ready-competent *E. coli* BL21 (DE3) was obtained from Novogen. However, competent *E. coli* DH5 α was prepared in house. *E. coli* DH5 α from a glycerol stock was streaked on a Lysogeny Broth (LB) agar plate (for recipe see appendix), which was then incubated overnight at 37 °C. After incubation a single colony was used to inoculate 5 ml of LB, which was then grown for 16 hours at 37 °C while shaking at 200-225 rpm. 100 μ l of the resulting culture was then added to 100ml of LB in a 2 litre flask and grown further at the above conditions until the optimal density of the culture at OD₅₅₀ was between 0.3-0.4. The flask was cooled on ice for 10 minutes before transferring its contents to a pre-cooled 250ml centrifugation tube. The tube was then centrifuged for 5 minutes at 3000 rpm at 4°C (SORVALL[®] RC26). After discarding the supernatant the pellet containing cells were re-suspended by swirling in 20 ml of ice-cold TFB1 (30mM potassium acetate, 100mM rubidium chloride, 10mM calcium chloride, 50mM magnesium chloride, 15% (v/v) glycerol pH5.8 filter sterilised). The sample was then allowed to incubate on ice for 2 hours after which it was centrifuged for 5 minutes at 2000 rpm in 4°C. The supernatant was discarded and the cells were re-suspended by swirling in 4ml ice-cold TFBII (10mM MOPS, 75mM calcium chloride, 10mM rubidium chloride, 15% (v/v) glycerol, pH 6.5, filter sterilised). The sample containing the bacterial cells were left overnight on ice at 4°C

before being aliquoted (50µl) into 1ml microcentrifuge tubes. The tubes were then snap frozen in liquid nitrogen and stored at -80°C.

2.2.12.5. Transformation into competent *E. coli* by heat shock

A 50µl aliquot of competent cells was thawed on ice for 10 minutes. Subsequently, 2µl of ligation reaction was added twice and gently mixed by stirring the pipette tip. The tube with the mixture was then left on ice for 30 minutes. Subsequently, the mixture was subjected to a heat shock at 42°C for 45 seconds after which the tube was quickly transferred on ice. After 2 minutes of recovery on ice, 200µl of LB was added to the heat shocked culture. The tube containing the culture was then incubated at 37°C for 45 minutes, shaking at 200 rpm. After incubation, cells were then plated on LB agar plates containing the appropriate selective media and grown inverted overnight at 37°C.

2.2.12.6. Preparation of electro-competent *A. tumefaciens*

5µl of bacterial culture from a glycerol stock of *A. tumefaciens* was added to 10ml of LB containing rifampicin and grown for 48 hours at 28°C in a shaking tray. This was then used to inoculate 200ml of LB containing rifampicin in a 2 litre flask. The culture was grown further in the above conditions until it reached an OD₆₀₀ of 0.5-0.8. The culture was transferred to a centrifugation flask and cooled on ice before being centrifuged at 500 rpm for 5 minutes at 4°C. The pellet containing cells was then washed once with each of 1.0, 0.5, 0.2 and 0.02 culture volumes of 10% glycerol by

repeated resuspension and centrifugation. Cells were then divided into 100µl aliquots, snap frozen in liquid nitrogen and stored at -70°C.

2.2.12.7. Transformation into electro-competent *A. tumefaciens*

A 100µl aliquot of electro-competent *A. tumefaciens* (LBA4404) cells was thawed on ice for 10 minutes. 2µl of plasmid DNA was added to the cells twice, each time mixing gently using the pipette tip. The mixture was allowed to incubate on ice for 20 minutes before being transferred to a 0.2cm electroporation cuvette (BioRad) at 4°C.

The cells in the cuvette were then electroporated using a BioRad micropulser set to EC1 (2.5 KV, 5-6 ms) at 4°C. After electroporation, the cells were left to recover on ice for 1 minute. Subsequently, 1ml of LB was added to the cuvette and mixed gently with the cells. The cells were then incubated at 28°C for 2 hours before being plated onto LB agar plates containing appropriate selection antibiotics and grown for 2 days at 28°C.

2.4.12.8. Bacterial growth media

The recipe for LB broth and LB agar media can be found in Appendix. All media was prepared using SDW and sterilised by autoclaving at 15 psi and 121°C for 20 minutes. For preparation of selective media, ampicillin was used at a final concentration of 100µg/ml, kanamycin at a final concentration of 50µg/ml and chloramphenicol at a final concentration of 12.5µg/ml for *E. coli* and 100µg/ml for *A.*

tumefaciens. Handling and inoculations of liquid broth and agar plates were carried out under aseptic conditions.

2.2.12.9. Colony PCR

Colony PCRs were used to test bacterial colonies following transformation to verify whether they contained plasmids cloned with the desired inserts. PCRs were carried out using a primer specific to the insert and another specific to a region in the plasmid. In case of *E. coli*, a small amount of each bacterial colony was picked with a separate sterile toothpick and mixed with 9 μ l of primer mix (final concentration 2pmol/ μ l) and 10 μ l of *Taq*DNA ReddyMix (ThermoScientific) in a 0.5ml microfuge tube. For *Agrobacterium*, after picking, each colony was dipped into 10 μ l of SDW in a 0.5ml microfuge tube and boiled for 5 minutes to lyse the cells. Subsequently, 1 μ l of each sample was added to a separate tube containing primer and PCR mix as mentioned earlier. All bacterial DNA were subjected to PCR as described in section 2.2.8.

2.2.12.10. Extraction of plasmid DNA using boil preparation

Boil preparation was used to extract crude DNA to check for the presence of a fragment of interest in transformed cells. For this procedure, 10ml of LB broth was inoculated with bacterial cells from a single colony. The culture was grown overnight at 37°C, shaking at 200 rpm. Subsequently, 1ml of the culture was centrifuged at 13,000 rpm for 1 minute to pellet the cells. The supernatant was discarded and cells

were resuspended in 100µl of STET buffer (8% Sucrose, 0.5% Triton X100, 50mM NaEDTA pH 8, 10mM Tris-HCl pH 8). 10µl of lysozyme (10 mg/ml) was added to the mixture, which was then boiled for 45 seconds to lyse the cells. The mixture was then immediately centrifuged at 13,000 rpm for 10 minutes to pellet cellular debris. The pellet was then removed and 500µl of ice cold 100% ethanol was added to the supernatant together with 10µl of 3M sodium acetate. The sample was then incubated in -20°C to precipitate DNA before being centrifuged at 13,000 rpm for 10 minutes at 4°C. The supernatant was removed and pellet was then washed with 500µl of 70% ethanol. The pellet containing DNA was then allowed to air dry for 15 minutes before re-suspending in 100µl of SDW containing RNaseA (40 µg/ml).

2.2.12.11. Purification of plasmid DNA using wizard preparation

Plasmid DNA was purified from bacterial cultures using Wizard plus SV Minipreps DNA purification system (Promega). DNA purification was carried out using the manufacturer's guidelines for the microcentrifuge protocol. 9ml of bacterial culture grown overnight was centrifuged at 13,000 rpm for 5 minutes to pellet the cells. The pellet was re-suspended in 250µl Cell Resuspension Solution before adding 250µl of Cell Lysis Solution to lyse the cells. Subsequently, 10µl of alkaline protease was added to remove unwanted proteins followed by 350µl of Neutralization Solution. The mixture was then centrifuged at 13,000 rpm to bind plasmid DNA in a spin column. The column was then washed with ethanol before eluting the plasmid DNA in 100µl of nuclease-free SDW. Purified plasmid DNA was stored at -20°C.

2.2.12.12. Restriction digestion

Restriction enzymes were obtained from New England Biolabs or Fermentas. Restriction digests were carried out in appropriate buffers supplied with the enzymes following instructions from the manufacturer. Plasmid DNA was digested at 37°C for 2 hours or overnight as per requirement. In some cases, restriction enzymes were inactivated after digestion by heating at 65°C for 30 minutes.

2.2.12.13. DNA sequencing

For DNA sequencing 300-500ng of plasmid DNA, purified using wizard preparation, was added to 1µl of 3.2 pmol/µl primer (M-13 forward, M-13 reverse, T7 promoter) and made up to a 10µl final volume with SDW. DNA sequencing reactions were carried out by the Functional Genomics Laboratory in University of Birmingham.

2.2.12.14. DNA sequence analysis

DNA sequencing results were analysed using Chromas software. Homology searches were carried out using the BLAST program on the National Centre for Biotechnology Information (NCBI) website (www.ncbi.nlm.nih.gov) and the ClustalW program (www.ebi.ac.uk/Tools/msa/clustalw2). Reverse complementation was carried out using the website www.bioinformatics.org/sms/rev_comp.html. Nucleotide sequences were translated to putative amino acid sequences using BCM Search Launcher (<http://searchlauncher.bcm.tmc.edu>).

2.3. Protein manipulations

2.3.1. Recombinant protein production

The AtASY3-C recombinant protein was used to produce an antibody against ASY3. A test induction was initially carried out to verify *AtASY3-C* expression before a large scale production of the recombinant protein.

2.3.1.1. Test induction and purification

E.coli BL21 (DE3) containing the pET-21b vector with AtASY3-C was grown in 10ml LB containing ampicillin (100µg/ml), which was incubated overnight at 37°C on a shaker (200 rpm). The culture was then separated into two halves and 5ml of fresh LB containing ampicillin (100µg/ml) was added to each half. For induction of AtASY3-C expression, 10µl of Isopropyl β-D-1-thiogalactopyranoside (IPTG) (final concentration of 1mM) was added to one half of bacterial culture while the other half was left uninduced. The cultures were then grown for 4 hours at 37°C on a shaker (200 rpm). For protein purification 1ml of each culture was centrifuged at 13,000 rpm for 1 minute. The supernatants were removed while the cells from each culture were resuspended in 75µl Bugbuster Mastermix (Novagen) and incubated at room temperature for 30 minutes. The solutions were then centrifuged at 13,000 rpm for 1 minute. Supernatants containing the soluble proteins were separated while each pellet containing insoluble proteins was resuspended in 75µl SDW. Both soluble and insoluble protein solutions were then loaded onto SDS-PAGE gels for further analysis.

2.3.1.2. Large scale protein production

Large scale protein production was performed by growing *E.coli* BL21 (DE3) containing the pET-21b vector with AtASY3-C in 200ml LB containing ampicillin (100µg/ml) in a 2L flask. The culture was incubated overnight at 37°C on a shaker (200 rpm). Subsequently, 200ml of fresh LB containing ampicillin (100µg/ml) was added to culture. Recombinant protein expression was induced by adding IPTG (final concentration of 1mM) and subsequently incubating the culture for 4 hours at 37°C on a shaker (200 rpm). The bacterial culture was then divided into two halves and centrifuged in 250ml centrifuge flasks using a floor centrifuge (SORVALL® RC26) for 10 minutes at 5000 rpm at 4°C. The supernatants were discarded and each culture pellet was re-suspended in 200ml of cold lysis buffer (see appendix) by gentle swirling. Samples were then centrifuged as before and each pellet re-suspended in 20ml cold lysis buffer. 400µl of 10mg/ml lysozyme and 100µl of 50mM phenylmethanesulfonylfluoride (PMSF) were added to each sample and incubated at 4°C for 1.5 hours. This was followed by the addition of sodium deoxycholate (26 mg) together with 50µl of 50mM PMSF to each sample, which were subsequently incubated at 37°C for 30 minutes. Cells were then sonicated 5x (30 seconds pulse each) with 30 seconds on ice to cool between each pulse. Samples were subsequently centrifuged at 5,000 rpm (SORVALL® RC26) for 20 minutes at 4°C and the supernatant discarded. The resulting pellets containing recombinant proteins were re-suspended in 20ml of lysis buffer followed by sonication and centrifugation approximately 5-7 times until pellet appeared white with black spots. The pellet containing the AtASY3-C recombinant protein was then resuspended in 10ml 1x PBS (Sigma). The recombinant protein solution was quantified, tested using SDS-PAGE

and coomassie staining before sending 2mg of it to BioGenes (Germany) for antibody production. Purified proteins were stored at -20°C .

2.3.2. Protein extraction from plant tissue

Anthers from *B. oleracea* and *A. thaliana* buds that are expected to contain early prophase I meiocytes were extracted, snap frozen in liquid nitrogen and stored in an eppendorf tube at -80°C until required. Immediately before protein extraction one protease inhibitor tablet (Roche) was dissolved in 10ml IP buffer (see appendix). For protein extraction, $\sim 250\mu\text{l}$ of frozen meiotic tissue was transferred to a 1.5ml microfuge tube and ground using a pestle for 5 minutes. While grinding, the tube was continuously refrozen in liquid nitrogen to prevent the tissues from thawing. Once the tissues were suitably ground, $250\mu\text{l}$ of IP buffer containing protease inhibitor was added. The tissues were then further ground for 10 minutes while being continuously refrozen. When completely ground, the tissues were allowed to thaw before adding another $250\mu\text{l}$ of IP buffer containing protease inhibitor. For extraction of proteins from $\sim 100\mu\text{l}$ of frozen meiotic tissues the amount of IP buffer containing protease inhibitor was reduced to $150\mu\text{l}$ per addition after each grinding step to make a final volume of $300\mu\text{l}$. The solution containing the ground tissues was then centrifuged at 13,000 rpm for 20 minutes at 4°C . The resulting supernatant containing soluble meiotic proteins was carefully extracted to a fresh tube, quantified and used for further analysis. Both the supernatant and the pellet (containing insoluble proteins) were stored at -20°C (or -70°C for long-term storage).

2.3.3. Protein quantification

Protein concentrations were quantified using BioRad assays performed according to the manufacturer's instructions. 200µl of Bradford reagent was added to an appropriate amount of each protein sample before making up to a final volume of 1ml using SDW. Each mixture was incubated at room temperature for 5 minutes, then transferred to a plastic cuvette before measuring its absorbance using a spectrophotometer (Jenway 6305) at 595 nm. The absorbance of BSA (10 mg/ml) was used as standard. Protein concentrations were estimated using the following:

$$\text{x mg/ml Protein} = (\{\text{Abs. Protein} / \text{Abs. BSA}\} \times \text{Conc. BSA}) / (\text{Vol. Protein})$$

2.3.4. Sodium dodecyl sulfate polyacrylamide gel electrophoresis (SDS-PAGE)

Proteins were analysed by SDS-PAGE using 3rd generation BioRad self-assembly kits. A resolving gel was prepared first as per Table 2. 7ml of the resolving gel was poured into the glass plates and a layer of absolute butanol was added over the gel to prevent the formation of air bubbles before allowing the gel to set. The butanol was then rinsed off and 2.5ml of stacking gel, prepared as per Table 2, was added on top of the resolving gel along with a comb containing wells. The stacking gel was then allowed to set. For both gels the TEMED was added immediately before pouring as it causes the gels to polymerise quickly. The gel tank was then assembled as described in the manufacturer's instructions and filled with 1x reservoir buffer (see Appendix). Prior to their loading proteins were mixed with 5x protein loading buffer and boiled for 5 minutes. Protein samples along with a protein weight marker

(PageRuler™ prestained protein ladder, Fermentas) were then loaded onto the SDS-PAGE gel. The gel was initially run at 80V to allow proteins to enter the resolving gel before being run at 150V until the proteins were resolved.

Contents	Resolving gel		Stacking gel
	10%	15%	
SDW	6.1ml	3.6ml	3ml
Resolving buffer (1.5M Tris, pH 8.8)	3.75ml	3.75	0
Stacking buffer (1M Tris, pH 6.6)	0	0	1.25ml
Acrylamide (Protogel)	5ml	7.5ml	625µl
SDS (10% w/v)	150µl	150µl	50µl
APS (15% w/v)	75µl	75µl	25µl
TEMED (Sigma)	15µl	15µl	5µl
Final volume	15ml	15ml	5ml

Table 2. Components of the resolving and stacking gels and their amounts for SDS-PAGE.

2.3.5. Two dimensional-polyacrylamide gel electrophoresis (2D-PAGE)

2D-PAGE involves the separation of proteins initially on the basis of their net charge by isoelectric focusing (IEF) followed by SDS-PAGE, which separates the proteins by their mass. IEF were performed using a 7cm immobilized drystrips (pH3-10, NL) (GE Healthcare) following the manufacturer's instructions. Protein samples were extracted from meicytes and quantified as described in section 2.3.2 and 2.3.3 respectively. Prior to each IEF, ~90µg of a desired protein sample was precipitated in 5 volumes of acetone containing 20mM DTT. The mixture was centrifuged at 6000 rpm for 2 minutes at 4°C. The supernatant was removed and the pellet air dried for 5 minutes

before resuspending in 125 μ l of rehydration buffer (see Appendix) in a sonicating water bath at room temperature for 2 hours. The resulting solution was then used to rehydrate an immobiline drystrip. The solution was evenly distributed along a strip holder. The immobiline strip was then placed, gel-side down, over the solution such that the solution was evenly distributed under the strip. Rehydration followed by IEF was performed using an Ettan IPGphor II IEF System as per Table 3. After IEF, the focussed strip was equilibrated by treatment with 10ml equilibration buffer (see Appendix) containing 100mg DTT in a rocking table for 25 minutes followed by incubation in 10ml equilibration buffer containing 250mg iodoacetamide in a rocking table for 25 minutes. The latter treatment was carried out in the dark since iodoacetamide is sensitive to light. Following equilibration, proteins in the strip were subjected to vertical SDS-PAGE using 3rd generation BioRad self-assembly kits. A 10% resolving gel was set up as described in 2.3.4. Instead of using a stacking gel, the 7cm immobiline drystrip strip was placed sideways on top of the resolving gel. A small well was cut out in one side of the resolving gel for loading a protein weight marker (PageRuler™ prestained protein ladder, Fermentas). SDS-PAGE was carried out as described in 2.3.4.

Step	pH interval	Voltage mode	Voltage (V)	Tme (h:min)	kVh
Rehydration	3-10, NL			20:00	
IEF	3-10, NL	1. Step and hold	300	0:30	0.2
		2. Gradient	1000	0:30	0.3
		3. Gradient	5000	1:30	4.5
		4 Step and hold	5000	0:12-0:36	3
		Total		2:42-3:06	6.0-8.0

Table 3. Conditions for rehydration and IEF for 2D-PAGE.

2.3.6. Coomassie staining

Protein gels were stained for 1 hour in Coomassie blue stain (0.1% Coomassie R250, 45% methanol, 45% Glacial Acetic acid, 9.9% MilliQ water). Gels were then washed using a de-staining solution (20% methanol, 7% acetic acid) until products were visible. Gels were dried and stored between cellophane sheets.

2.3.7. Western blotting

Following the resolution of proteins by SDS-PAGE or 2D-PAGE they were transferred to a Hybond-C Extra membrane (Amersham Biosciences) using a BioRad western transfer kit following manufacturer's instructions. The SDS-PAGE gel was placed next to the Hybond-C Extra membrane inside the transfer cassette. The cassette was then assembled inside a gel tank which was covered with 1x transfer buffer (see Appendix). An ice pack was added to the apparatus to prevent overheating of the buffer. Protein transfers were carried out at 400 mA for 1 hour. After transfers, the

membranes were blocked using milk block (5% milk, 0.1% Tween in 1X TBS) over night at 4 °C on a shaker.

2.3.8. Antibody labelling

After blocking nitrocellulose membranes following western blotting the membranes were incubated with a primary antibody (usually 1:1000 in milk block) for 2 hours whilst shaking gently at room temperature. Following incubation, the membranes were washed 3 times, for 10 minutes each, in 20ml of TBS wash solution (1x TBS with 0.1% Tween 20). The membranes were then incubated with a secondary antibody (1:10,000 in milk block) conjugated with either alkaline phosphatase (AP) or horse radish peroxidase (HRP) for 1 hour on a shaker at room temperature. The membranes were subsequently washed with 20ml of TBS wash solution 3 times for 10 minutes per wash prior to visualization.

2.3.9. Protein detection using enhanced chemiluminescence (ECL)

Western blotting membranes containing proteins were visualized using Amersham ECL Western blotting detection reagents and analysis system (GE Healthcare). Each membrane was treated with ECL reagents A and B according to the manufacturer's instructions. Blots were then exposed to photographic films (Amersham Hyperfilm ECL, GE Healthcare) and developed using an AGFA CURIX 60 Xograph.

2.4. Cytological procedures

2.4.1. Meiotic chromosome spreading

Arabidopsis inflorescences were removed from the plant and fixed in 3:1 fixative (3:1 ethanol:glacial acetic acid). The inflorescences were allowed to fix at room temperature for at least 2 days. Flower buds were removed from inflorescences and washed in 0.01 M citrate buffer (pH 4.5) three times, for five minutes each time. Buds were then digested in an enzyme mix (0.3% (w/v) pectolyase, 0.3% (w/v) cytohelicase, 0.3% (w/v) cellulase) and citrate buffer for 1.5 hours at 37°C. The digestion was halted by adding ice-cold water. A single bud was transferred to a clean slide with a small amount of buffer and macerated with a needle. 10µl of 60% acetic acid was added and the slide was put on a 45°C hotplate for 30 seconds. The slide was then taken off the hotplate and another 10µl of 60% acetic acid was added. Subsequently, 100µl of cold 3:1 fixative was added to the slide, around and on top of the material. The slide was washed with another 100µl of 3:1 fixative and dried. The cells were then stained with 10µl of 4',6-diamidino-2-phenylindole (DAPI) at 1µg/ml in Vectashield mounting medium (Vector laboratories) and subsequently visualized using fluorescence microscopy.

2.4.2. Preparation of fluorescence in situ hybridization (FISH) probes

The 5S and 45S probes were used to label rDNA in meiotic chromosomes during FISH. For preparation of the 5S rDNA probe, the plasmid pCT4.2 (Campbell et al.,

1992) containing the 5S rDNA gene from *A. thaliana* as a 500-bp insert cloned in pBlu was used. The 45S rDNA probe, on the other hand, was prepared using the plasmid pTa71 (Gerlach and Bedbrook, 1979), which consists of a 9 Kb *EcoRI* fragment of *Triticum aestivum* containing the 18S-5.8S-25S rRNA genes and spacer regions. For production of the probes, 3µg of plasmid DNA was mixed with 4µl of Biotin (BIO) or Digoxigenin (DIG) nick translation mix (Roche) and made up to 20µl with SDW water. The mixture was then incubated at 15°C for 90 minutes. The reaction was subsequently stopped by adding 1µl of 0.5M EDTA (pH 8.0) and heating the resulting mixture for 10 min in a water bath at 65°C.

2.4.3. Fluorescence in situ hybridization (FISH)

Metaphase I cells fixed on glass slides were washed in 2X SSC for 10 minutes at room temperature before being incubated with pepsin for 1.5 minutes at 37°C to remove unwanted proteins. The cells were then washed again using 2XSSC for 10 minutes at room temperature and treated with 4% paraformaldehyde in fume hood for 10 minutes. The cells were briefly washed with SDW before being treated with 70% ethanol for 2 minutes followed by a wash with 100% ethanol for 2 minutes. The cells were then air dried for 20 minutes. The probes 45S DIG and 5S BIO were added on top of the cells and a coverslip was placed on them. The edges of the coverslip on each slide were glued using rubber solution and each slide was heated at 70°C for 4 minutes on a hot plate. All slides were then incubated at 37°C overnight in a moist box to allow hybridization of probes. Subsequently, each slide was treated three times with 50% formamide containing 2X SSC, once with 2X SSC and once

with 4X SSC with 0.5% Tween20 for 5 minutes per treatment. The cells were then washed with 4X SCC at room temperature before adding anti-DIG FITC and AVIDIN-CYE3. Each slide was covered with parafilm and incubated at 37°C for 30 minutes. The cells were then subjected to three 5 minutes washes in dark using 4XSSC at room temperature, followed by a wash with SDW. Each slide was then treated with 70%, 85% and 100% ethanol for 2 minutes per treatment and allowed to air dry. The cells were then stained with DAPI/Vectashield and analysed using fluorescence microscopy.

2.4.4. Meiotic timecourse

Meiocytes were labelled by the incorporation of thymidine analog bromodeoxyuridine (BrdU) into nuclear DNA during meiotic S-phase. *Arabidopsis* stems containing inflorescence were cut to a length of ~5cm and transferred to 10mM BrdU from a labelling kit (Roche). Stems were immersed in BrdU for 2 hours to allow uptake via the transpiration stream. Following BrdU labelling, stems were transferred to water until desired time intervals. For analysis of BrdU incorporation, inflorescences were extracted from the stems and fixed in 3:1 ethanol: acetic acid. Chromosome spreads were prepared as described in 2.4.1 and treated with an anti-BrdU (mouse monoclonal) antibody (Roche) which also contains a mixture of nucleases. These nucleases generate single-stranded DNA fragments, which allow binding of the antibody to BrdU. The above immunolocalisation was carried out according to the manufacturer's instructions. Chromosome spreads were then counterstained with DAPI/Vectashield and analysed for BrdU staining using fluorescence microscopy. For

analysis, cells at each meiotic stage were classified as BrdU labelled or unlabelled (Armstrong et al, 2003).

2.4.5. Immunolocalization

Several (4-6) fresh *Arabidopsis* inflorescences were dissected under stereomicroscope on moist filter paper and buds less than ~300 µm in diameter were pooled as these were expected to contain meiocytes. Anthers were dissected out from these buds and placed in a glass slide containing 5µl of digestion mix (0.1g cytohelicase (Sigma), 0.0375g sucrose, 0.25g polyvinylpyrrolidone, in 25ml SDW). The anthers were tapped using a brass rod to disrupt tissues and the slide was then incubated at 37°C for 4 minutes in a moist box. Subsequently, 10µl of 1% lipsol was added to the meiocytes, which were then spread using a kneedle. The cells were then fixed using 4% paraformaldehyde, mixed and allowed to air dry for 2 hours in a fume cupboard. Fixed cells were incubated with primary antibody (usually 1:200) for 1 hour at 37°C in a moist box before washing twice with 1X PBS + 1% (v/v) triton X-100 (Sigma). The cells were then incubated with secondary antibody (1:50 for FITC and 1:200 for CY3/Texas Red) at 37°C for 30 minutes in a moist chamber followed by 3 washes with 1x PBS + 1% (v/v) triton X-100 (Sigma). The slides were then stained with DAPI/Vectashield and visualized using fluorescence microscopy.

2.4.6. Immunolocalization coupled with timecourse

BrdU pulse labelling was carried out as described in section 2.4.4. However, instead of fixing buds, they are used for the preparation of chromosome spreads for immunolocalisation studies. Slide preparation for immunolocalization was carried out similarly to that described in 2.4.5. Meiocytes were incubated with the primary antibody at 4°C overnight in a moist box. The primary antibody was subsequently detected using a suitable secondary antibody while the BrdU was detected using an anti-BrdU antibody (Roche), following the manufacturer's instructions. Cells were then stained using DAPI/Vectashield before being analysed using fluorescence microscopy.

2.4.7. Assessing pollen viability using Alexander's staining

Inflorescences were extracted and fixed using 70% ethanol for 3 hours. 5-7 anthers from each inflorescence were put on a slide and stained using 10µl of Alexander's stain (Alexander, 1969). Alexander's stain contains 10ml Ethanol (95%), 1 ml Malachite Green (1% in 95% ethanol), 5ml Fuchsin Acid (1% in water), 0.5ml Orange G (1% in water), 5g Phenol, 5g Chloral Hydrate, 2 ml Glacial acetic acid, 25 ml Glycerol, 50 ml distilled water. The anthers were squashed using a coverslip to allow pollen grains to be released from the anthers. The slides were incubated at 4°C for at least 16 hours to allow the stain to be absorbed by the pollen grains. Slides were analysed using a light microscope.

2.4.8. Fluorescence microscopy and image analysis

Fluorescence microscopy was carried out using a Nikon Eclipse E400 microscope and images were captured using a Hamamatsu ORCA-ER digital camera. Images were analysed using Cell P Soft Imaging System software (Olympus).

2.5. Transformation into *Arabidopsis*

The *AtASY3* cDNA was introduced in *Atasy3-1* mutant plants for a complementation study. *A. tumefaciens* (LBA 4404) containing pPF408 plasmid with *AtASY3* cDNA were transformed into *Arabidopsis* plants by the floral dip method (Clough and Bent, 1998). A 600ml bacterial culture was grown overnight at 28°C, shaking at 200 rpm in LB containing chloramphenicol (100µg/ml) and rifampicin (50µg/ml). The culture was grown to an OD₆₀₀ of 1.6 before being centrifuged 5000 rpm for 10minutes. The LB was then removed and the pellet re-suspended in 1200ml of 5% sucrose medium to make a final OD₆₀₀ of 0.8. 0.05% Silwet (500 µl/l) was added to the bacterial solution, which was then divided into three 400ml aliquots in beakers. *Arabidopsis* plants with 3-4 inflorescences containing non-flowering buds were dipped into the bacterial solution (2 plants per 400ml solution) for 2-5 seconds each with gentle agitating. Dipped plants were then grown in a moist box for 48 hours away from direct light inside a glasshouse. Subsequently, the plants were grown in normal conditions in the glasshouse until harvestation. Seeds from these plants were then grown under BASTA (DL-Phosphinothricin) (Duchefa Biochemie) selection either on MS plates (25

µg/ml) or on soil compost with the weedkiller, BASTA (0.1g/l) 3 times at 8–10 day intervals.

2.6. Genetic crossing of plants

Homozygous T-DNA insertion mutants were crossed with heterozygous plants to generate double mutants in which two of the desired genes were disrupted due to the presence of T-DNAs. For efficient crossing, homozygous plants with 4-6 inflorescences were selected as recipients while flowering heterozygous plants were used as donors. Siliques, flowers and buds which were either too small or mature were removed from each inflorescence leaving a nascent bud in each stem of recipient plants. Nascent buds were emasculated under a light microscope using forceps to remove all the immature anthers leaving the stigmata undamaged. Mature flowers containing pollen from the heterozygous plants were then used to pollinate the stigmata in the emasculated inflorescences under a binocular. Pollinated plants were then allowed to grow and siliques containing the hybrid seeds matured after 15-25 days from pollinated inflorescences. The siliques were harvested prior to their opening by cutting into a 1.5ml microfuge tube. The seeds from these siliques were stored for 2 days for maturation prior to sowing.

2.7. Statistical procedures

All statistical procedures described were carried out using Microsoft Office Excel.

CHAPTER 3

Investigation of the *Arabidopsis* RecQ helicase,

AtRECQ4B

3.1. Introduction

RECQ helicases are a conserved group of DNA helicases that are involved in the maintenance of genome integrity. RecQ helicase are known to unwind a variety of substrates including simple 3' -tailed duplexes, forked duplexes, four-way junctions, D-loops and guanine-rich genomic regions such as telomeres (Huber *et al.*, 2006, Mohaghegh *et al.*, 2001, van Brabant *et al.*, 2000). Defects in the human *RecQ* genes cause various rare genetic disorders. One of these disorders is Bloom's syndrome, which is caused by the disruption of the human RECQ helicase, BLM (Ellis *et al.*, 1995). Bloom's syndrome is associated with dwarfism, increased sister-chromatid exchange, sunlight sensitivity and a predisposition to most types of cancers (Mankouri and Hickson, 2007). In budding yeast, disruption of the BLM orthologue, SGS1 leads to increased DNA damage sensitivity and elevated recombination (Watt *et al.*, 1996). Furthermore, loss of SGS1 increases meiotic COs and causes transient accumulation of inter-homologue, inter-sister chromatid and multi-chromatid joint molecules during meiosis (Jessop *et al.*, 2006, Oh *et al.*, 2007, Oh *et al.*, 2008a). In *Arabidopsis*, out of the 7 *RecQ*-like genes identified so far, *AtRECQ4A* has been proposed to be the functional homologue of BLM and Sgs1 (Bagherieh-Najjar *et al.*, 2005, Hartung *et al.*, 2006, Hartung *et al.*, 2007). *AtRECQ4A* was found to suppress both the methyl methane sulfonate (MMS) hypersensitivity and hyper-recombination phenotype of budding yeast *sgs1* mutant (Bagherieh-Najjar *et al.*, 2003). Furthermore, *Atrecq4A* mutants exhibit an increased frequency of homologous COs in somatic cells suggesting that the *AtRECQ4A* acts as an anti-recombinase, similarly to yeast SGS1 (Hartung *et al.*, 2007). Additionally, *Arabidopsis* also contains the RecQ helicase, *AtRECQ4B* which arose from a recent

gene duplication event. AtRECQ4B is ~70% identical to AtRECQ4A in amino acid level (Hartung and Puchta, 2006). However, in contrast to *Atrecq4A*, *Atrecq4B* mutants are not sensitive to mutagen-induced DNA damage and exhibit impaired somatic homologous recombination. Hence, AtRECQ4B has been proposed to promote homologous recombination in somatic cells, antagonistic to its close relative AtRECQ4A (Hartung et al., 2007).

A previous study reported that there was no loss of fertility in the *Atrecq4A* mutant (Bagherieh-Najjar et al., 2005). However, a direct analysis of meiosis in the mutant was not performed during the study. Moreover, in an analysis of the *Brassica* meiotic proteome the *Brassica* homologues of AtRECQ4A and AtRECQ4B were found to be present in meiocytes suggesting putative roles for the proteins during meiosis (Sanchez-Moran et al., 2005; F.C.H.F. and K.O., unpublished). This observation along with the known meiotic role of yeast SGS1 led to the investigation of the two helicases during *Arabidopsis* meiosis. Analysis of *Atrecq4A* mutant revealed that pollen viability was decreased in the mutant resulting in a reduction in its fertility. However, there was no significant effect on meiotic COs in the mutant. Instead, AtRECQ4A was found to be required for the dissolution of recombination-dependent telomeric associations (J.H., K.O., F.C.H.F). Subsequently, AtRECQ4B was analysed to verify whether the helicase played a role during *Arabidopsis* meiosis. This chapter describes the expression analysis of *AtRECQ4A* (At1g10930) and *AtRECQ4B* (At1g60930) along with the molecular characterization of an *Atrecq4B* T-DNA

insertion mutant. The chapter also includes the cytological analysis of various meiotic stages in the mutant and in wild-type *Arabidopsis* (Col-0).

3.2. *AtRECQ4A* and *AtRECQ4B* expression is meiosis-specific

Reverse transcription (RT)-PCR was used to determine whether *AtRECQ4A* and *AtRECQ4B* are expressed during meiosis in wild-type *Arabidopsis* (Col-0). The primers, 4AF1 and 4AR1 were designed to check for *AtRECQ4A* expression while 4BF1 and 4BR1 were designed to analyse *AtRECQ4B* expression. Additionally, a set of 2 primers, GAPD-F1 and GAPD-R1 were used to check for the expression of the housekeeping gene, *AtGAPD*. *AtGAPD* expression was used as a control to equalize template RNA loading in the plants analysed. Subsequently, total RNA from wild-type bud tissues was extracted using RNeasy extraction kit (Qiagen). The RNA content was quantified using spectrophotometer to allow equalisation of template RNA in all samples that were subsequently analysed using RT-PCR. The RT-PCR reactions were carried out using SuperScript II reverse transcriptase (Invitrogen) following the manufacturer's protocol. The cDNAs generated by the RT-PCR reactions were subjected to PCR using the *AtRECQ4A*, *AtRECQ4B* and *GAPD*-specific primers mentioned above. The PCR products were then analysed via gel electrophoresis. This revealed that in wild-type, both *AtRECQ4A* and *AtRECQ4B* transcripts can be detected in the bud tissue suggesting that the helicases are expressed during *Arabidopsis* meiosis (Figure 4).

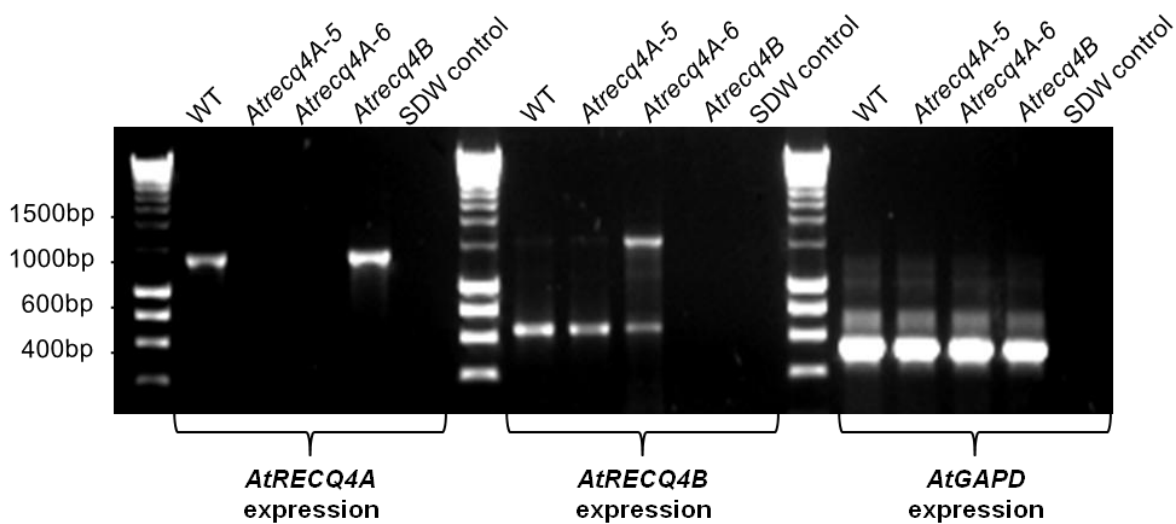


Figure 4. Expression analysis of *AtRECQ4A* and *AtRECQ4B* in flower buds.

AtRECQ4A is expressed in both WT and *Atrecq4B* mutant but not in the two *Atrecq4A* mutant lines, *Atrecq4A-5* and *Atrecq4A-6*. Similarly, *AtRECQ4B* is expressed in the WT and in the two *Atrecq4A* mutant lines but not in the *Atrecq4B* mutant. Similar *AtGAPD* expression from all tissues indicate approximately equal abundance of template mRNA in all samples.

3.3. Analysis of *AtRECQ4A* and *AtRECQ4B* expression in their corresponding mutant lines

To investigate whether *AtRECQ4B* has a role during *Arabidopsis* meiosis, a T-DNA insertion line (SALK_011357) of the gene was obtained from NASC. This line has already been described and its T-DNA insertion site was mapped in a previous study (Hartung et al., 2007). Seeds from this line were grown along with those of wild-type *Arabidopsis* (Col-0). Additionally, primers (RECQ4B-F1 and RECQ4B-R1) specific to either sides of the predicted T-DNA insertion site and another specific to the left-border region of the T-DNA (LBb1.3) were designed to check for zygosity of the T-DNA insertion in each plant. Subsequently, genomic DNA was extracted from leaves of mutant and wild-type plants and genotyped via PCRs using the primers above. The primers, RECQ4B-F1 and RECQ4B-R1 were used to amplify the wild-type genomic region while RECQ4B-F1 and LBb1.3 were used to detect the T-DNA. The PCRs allowed the identification of plants homozygous for the T-DNA insertion in *AtRECQ4B* in the mutant line. Hence these homozygous knockout plants are potentially deficient in *AtRECQ4B* expression.

Along with the *Atrecq4B* mutant line two *Atrecq4A* T-DNA insertion lines, *Atrecq4A-5* (SALK_069672) and *Atrecq4A-6* (SAIL_350_C06) were previously obtained from NASC for the analysis of the helicases. Homozygous knockout plants from two *Atrecq4A* mutant lines were identified earlier in our lab (J.H.). To verify the absence of *AtRECQ4B* and *AtRECQ4A* gene transcripts in *Atrecq4B* and the two *Atrecq4A* mutants respectively, an expression analysis of the two genes was performed using

RT-PCR. Total RNA was extracted from bud tissues of homozygous plants from each of these mutant lines. The RNA samples were then analysed via RT-PCR using the primers and methods similar to those used for *AtRECQ4A* and *AtRECQ4B* expression analysis in the wild-type (described in section 3.2). This revealed that the *AtRECQ4B* transcript was not detected in the *Atrecq4B* mutant (Figure 4), but was present in the two *Atrecq4A* mutant lines (Figure 4). Additionally, *AtRECQ4A* transcript was not detected in *Atrecq4A-5* and *Atrecq4A-6* mutant lines but was present in the *Atrecq4B* mutant (Figure 4). These observations confirm that the *Atrecq4B* and the two *Atrecq4A* mutant lines, *Atrecq4A-5* and *Atrecq4A-6* are completely defective in expression of their corresponding genes.

3.4. Analysis of *Atrecq4B* fertility

Analysis of *Atrecq4B* revealed that the mutant displayed normal vegetative growth similar to the wild-type. In addition, the *Atrecq4B* mutant did not exhibit any reduction in fertility compared to wild-type. The mean silique length in *Atrecq4B* was 15.51mm (n=50), which was not significantly different from 15.70mm (n=50) in the wild-type (P = 0.46, ANOVA). Moreover, the mean seed-set per silique in the mutant was 54.22 (n=50), which too was not significantly different from 56.64 (n=50) observed in the wild-type (P = 0.13, ANOVA). Additionally, pollen viability in the *Atrecq4B* mutant line was determined using Alexander's staining. This revealed that the ratio of viable:non-viable pollen in the mutant was 116:1 (n=345), which was similar to 129:1 (n=403) observed in the wild-type. This observation is consistent with the wild-type levels of

seed-set observed in the *Atrecq4B*. Altogether, the above results suggest that there is no reduction in fertility due to the disruption of *AtRECQ4B*.

3.5. Cytological analysis of wild-type and *Atrecq4B* meiotic stages

To verify whether loss of *AtRECQ4B* results in any meiotic defects DAPI-stained chromosome spreads of various meiotic stages from the mutant were compared to those from the wild-type.

In the wild-type, meiotic chromosomes become condensed and are clearly visible as fine thread-like structures at leptotene (Figure 5A). At zygotene, chromosomes often appear as a dense knot at one side of the nucleus and there is an aggregation of the pericentromeric heterochromatin into a variable number of clumps (Figure 5B). At pachytene, the homologous chromosomes are fully synapsed and are visible as much shorter but thicker strands with distinct densely stained centromeres (Figure 5C). At diplotene, homologous chromosomes de-synapse and form thin threads which appear to be more extended than those at zygotene (Figure 5D). During diakinesis COs are visible as chiasmata on bivalents (Figure 5E) and at metaphase I bivalents are aligned at the equatorial region of the cell (Figure 5F). At anaphase I, homologous chromosomes separate and move towards the two poles of the cell (Figure 5 G) leading to the formation of the dyad stage, where a set of chromosomes is present at each pole of the cell. This is followed by the second round of meiotic

division in which prophase II is substantially quicker than the first. Subsequently, fully condensed sister chromatids align at metaphase II (Figure 5H) followed by their separation in anaphase II leading to the formation of the tetrad stage where one member of each chromosome is present at each pole of the stage (Figure 5I).

Interestingly, analysis of the meiotic chromosome spreads from the *Atrecq4B* mutant revealed that its meiotic stages are indistinguishable from those of the wild-type. Meiotic chromosome condensation and pairing in *Atrecq4B* early prophase I nuclei appeared normal along with the synapsis of homologous chromosomes at pachytene (Figure 6A). In addition, normal metaphase I nuclei, each containing 5 bivalents, were observed in *Atrecq4B* (Figure 6B). Furthermore, all the *Atrecq4B* tetrads analysed were balanced with no signs of aneuploidy (Figure 6C). These observations confirm that there are no apparent meiotic defects in *Atrecq4B*.

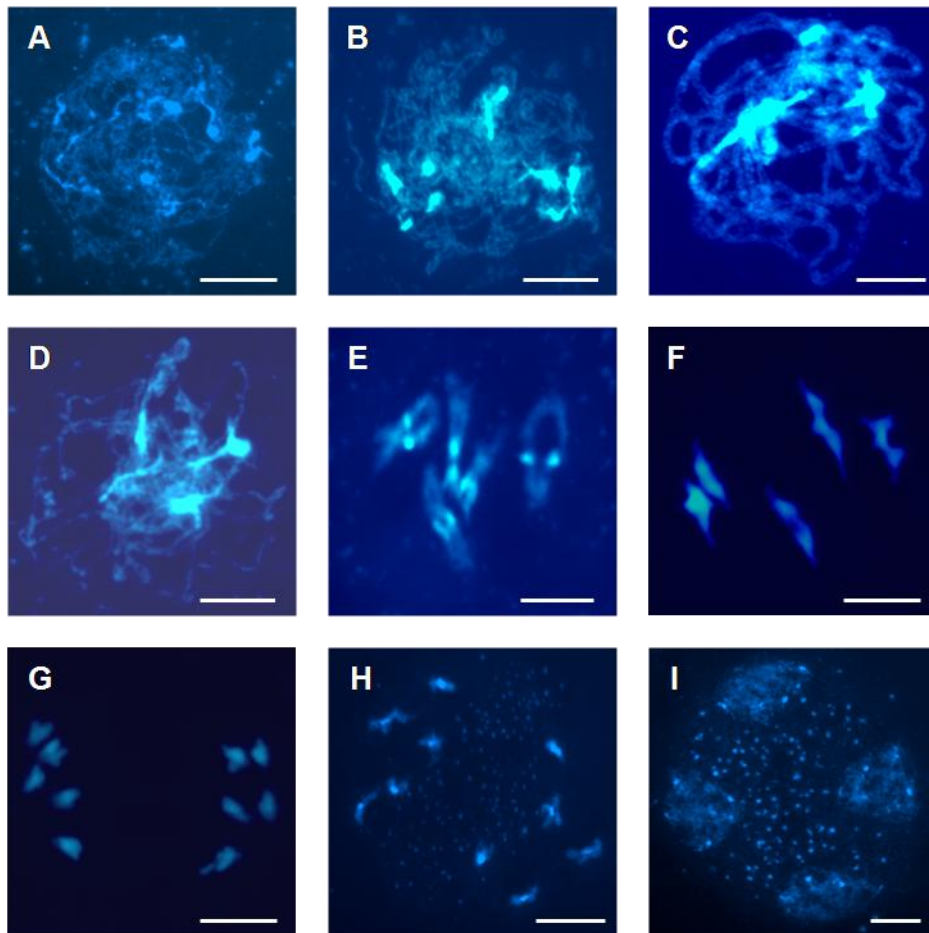


Figure 5. Meiotic atlas of WT *Arabidopsis*.

(A) Homologous chromosome pairing and synapsis initiates in leptotene. **(B)** Thicker chromosomes in zygotene signify more pairing. **(C)** Synapsis is completed by pachytene. **(D)** Chromosomes desynapse in diplotene **(E)** Chiasmata, which are physical connections between non-sister chromatids are visible in diakinesis **(F)** Bivalents align in metaphase I **(G)** Homologous chromosomes separate in anaphase I **(H)** Sister chromatids align at metaphase II before separating **(I)** Tetrad contains haploid sets of genetic information. Bar 10 μ m.

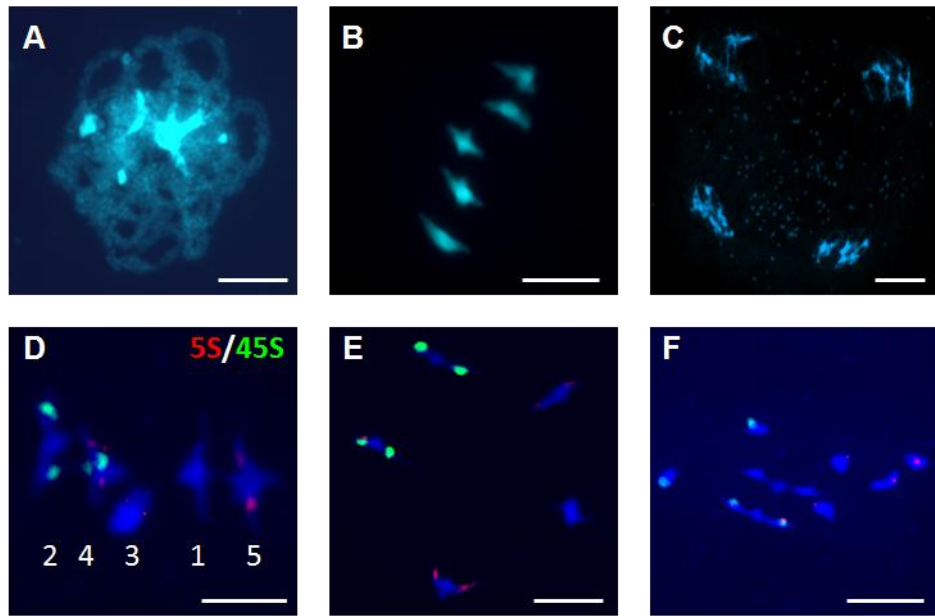


Figure 6. *Atrecq4B* mutant cytology.

(A) Homologue pairing and synapsis appear normal and complete by pachytene. **(B)** Bivalents are aligned at metaphase I. **(C)** Balanced tetrads containing haploid gametes are formed in the mutant **(D)** Analysis of WT metaphase I nuclei labelled using FISH with 5S (red) and 45S (green) rDNA probes revealed 8.29 chiasmata per WT nuclei ($n=50$). **(E)** *Atrecq4B* displays WT levels of chiasma frequency ($n=50$). **(F)** *Atrecq4B/Atmsh4* exhibit 1.08 chiasmata per nuclei ($n=66$). Bar 10 μ m.

3.6. AtRECQ4B is not essential for CO formation

A previous study implicated AtRECQ4B in playing a role in recombination in somatic cells. To verify whether the protein also played a role in meiotic recombination the chiasma frequency of *Atrecq4B* was compared to that of wild-type. Initially, chiasma frequency in wild-type meiocytes was determined by FISH analysis using 5S and 45S rDNA probes on 50 metaphase I nuclei. This revealed that each wild-type meiocyte possessed an overall mean chiasma frequency of 8.29 (n=50) (Figure 6D). Similar analysis of 50 *Atrecq4B* metaphase I nuclei revealed that each nucleus contained an overall mean chiasma frequency of 8.82, which was not statistically different from that of the wild-type ($P>0.1$, ANOVA) (Figure 6E). Although this finding suggests that loss of AtRECQ4B does not significantly affect meiotic CO formation, it does not reveal any modest changes to the chiasma frequency due to the loss of the protein. Hence, to clarify this issue an *Atrecq4B/Atmsh4* double mutant was constructed by crossing a homozygous *Atrecq4B* with a heterozygous *Atmsh4* plant followed by self-crossing their subsequent progeny. Chiasma frequency of the double mutant was then determined and compared to that of the *Atmsh4* single mutant. This revealed no statistical difference between the chiasma frequency of *Atrecq4B/Atmsh4* (1.08 per cell, n=64) and the *Atmsh4* single mutant (1.29 per cell, n=66) ($P>0.1$) (Figure 6F). This observation therefore confirms that AtRECQ4B is not essential for meiotic CO formation. This finding, in conjunction with the normal cytology of *Atrecq4B* mutant suggest that AtRECQ4B probably does not possess a meiotic role or that it functions redundantly with other protein(s) during *Arabidopsis* meiosis.

3.7. Discussion

3.7.1. *AtRECQ4A* and *AtRECQB4* are expressed during meiosis

RT-PCR analysis of *AtRECQ4A* and *AtRECQB4* expression revealed that both genes are transcribed in *Arabidopsis* flower buds. This is consistent with the previous reported expression pattern of these genes (Hartung et al., 2000). Furthermore, the finding is also consistent with proteomics studies that detected peptides corresponding to *AtRECQ4A* and *AtRECQB4* in an analysis of the meiotic proteome of *B. oleracea*, a close relative of *Arabidopsis* (Sanchez-Moran et al., 2005; F.C.H.F. and K.O., unpublished). Taken together, these suggest that both *AtRECQ4A* and *AtRECQ4B* are highly likely to be active during meiosis.

3.7.2. *Disruption of AtRECQ4B* does not lead to meiotic defects

Analysis of *AtRECQ4A* revealed that it is not essential for meiotic CO formation (J.H., K.O., F.C.H.F). Instead, *Atrecq4A* mutants displayed chromatin bridges at metaphase I which were dependent on meiotic recombination and telomere repeats, indicating that *AtRECQ4A* is required to remove connections between telomeres that arise during meiotic recombination. This suggests that *AtRECQ4A* may not play a meiotic similar role to its budding yeast homologue Sgs1 (J.H., K.O., F.C.H.F). To investigate a potential role of *AtRECQ4B* an *Atrecq4B* mutant line with a T-DNA insertion in the gene was obtained and the position of the T-DNA validated using molecular studies. Furthermore, RT-PCR analysis confirmed that the mutant did not express *AtRECQ4B*

during meiosis. Interestingly, this mutant did not exhibit any loss of fertility. This finding was inconsistent with a meiotic defect, and therefore, led to a thorough cytological comparison between the meiotic stages of *Atrecq4B* and the wild-type. This revealed that during wild-type meiosis, condensed homologous chromosomes pair and synapse during the leptotene and zygotene of prophase I. Homologous chromosomes appeared fully synapsed by pachytene and subsequently de-synapse at diplotene. At diakinesis, chromosomes further condense to form five bivalents, each of which contain a pair of homologous chromosomes linked via chiasmata. The five bivalents were found to be aligned at metaphase I before their segregation at anaphase I to form dyads. Subsequently, sister chromatids were found to be aligned at metaphase II followed by their separation at anaphase II to form tetrads, each containing four eventual pollen grains. These observations were consistent with previous reports of chromosome behaviour during meiosis in *A. thaliana* (Armstrong and Jones, 2003). Intriguing, cytological analysis of *Atrecq4B* revealed that all of its meiotic stages were similar to those of the wild-type. There was no indication of any defects in homologue pairing or synapsis. Additionally, recombination appeared normal with no evidence of any loss of chiasmata. Moreover, none of the meiotic stages in *Atrecq4B* displayed any evidence of chromatin bridges or chromosome fragmentation, which are a common phenotype of mutants of genes involved in maintaining genome integrity. These observations were consistent with the wild-type level of fertility observed in *Atrecq4B*. Altogether, these suggest that loss of AtRECQ4B does not lead to any meiotic defects in *A. thaliana*.

3.7.3. Loss of *AtRECQ4B* does not affect chiasma formation

Previous studies suggest that *AtRECQ4B* promotes homologous recombination in somatic cells (Hartung et al., 2007). To investigate whether the protein had a similar effect during meiotic recombination the chiasma frequency of *Atrecq4B* was analysed in detail. This revealed that there was no noticeable reduction in *Atrecq4B* chiasma frequency, which was statistically similar to that of the wild-type. Additionally, the chiasma frequency of *Atrecq4B/Atmsh4* double mutant was found to be statistically similar to that of *Atmsh4*, suggesting that there was no loss of neither MSH4-dependent nor MSH4-independent COs due to the loss of *AtRECQ4B*. This indicates that the protein is not essential of meiotic CO formation.

An interesting observation, however, emerged from immunolocalization studies of *AtRECQ4A*, performed by colleagues at our lab (J.H., K.O., F.C.H.F.). The researchers analysed localization of *AtRECQ4A* in wild-type, *Atrecq4A* and *Atrecq4B* using an anti-*AtRECQ4A* antibody that was raised against the *AtRECQ4A* N-terminus. This region displayed 51% identity with that of *AtRECQ4B*, thus allowing the possibility that the antibody might recognize both proteins. The analysis revealed that in wild-type meiocytes *AtRECQ4A/B* localized as numerous foci (mean of 103 per cell, n=5) on meiotic chromosome axes during early leptotene. These foci gradually decreased in number (mean of 77 per cell, n=5) at early zygotene. As prophase I progressed the *AtRECQ4A/B* foci further decreased in number such that at late zygotene only ~11 (n=5) large telomeric foci were detected. At pachytene, the number of these *AtRECQ4A/B* telomeric foci was found to be reduced to 4/5 (n=5) .

In *Atrecq4A-5* mutants the number of AtRECQ4A/B foci was substantially reduced to <10, most of which were telomeric. However, this was not the case in *Atrecq4B*, which displayed wild-type levels and pattern of AtRECQ4A/B foci. Interestingly, in an *Atrecq4A-5/Atrecq4B* double mutant the number of AtRECQ4A/B foci was further reduced to ~5 (n=10). Most of these were telomeric, similarly to those in *Atrecq4A-5*. This suggests that the anti-AtRECQ4A antibody may exhibit a small amount of cross-reaction with AtRECQ4B (J.H., K.O., F.C.H.F.). Intriguingly, this indicates that AtRECQ4B may indeed localize to meiotic chromosome axes and telomeres during early prophase I. This is consistent with the RT-PCR analysis suggesting the meiosis-specific expression of AtRECQ4B and the proteomics data which detected peptides of the AtRECQ4B homologue in *Brassica* meiotic proteome (Sanchez-Moran et al., 2005; F.C.H.F. and K.O., unpublished). Another important observation was the presence of some residual AtRECQ4A/B foci in the *Atrecq4A-5/Atrecq4B* double mutant. This indicates that the anti-AtRECQ4A antibody may also exhibit some cross-reaction with other member(s) of the AtRECQ family, suggesting the possibility of functional redundancy between the helicases (J.H., K.O., F.C.H.F.). Therefore, it seems highly likely that upon loss of AtRECQ4B another member of the AtRECQ family performs the former's meiotic role, which appears to exist based on evidence but still remains unknown.

CHAPTER 4

Molecular characterization of *ASY3* in *Arabidopsis thaliana* and *Brassica oleracea*

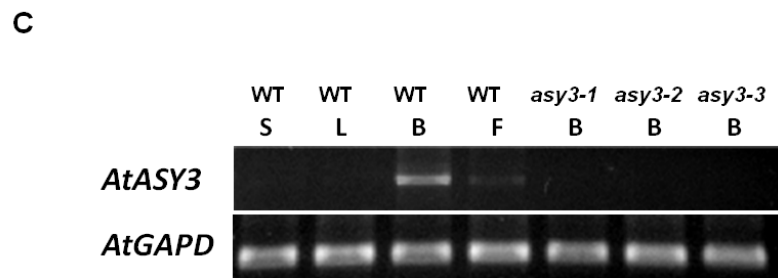
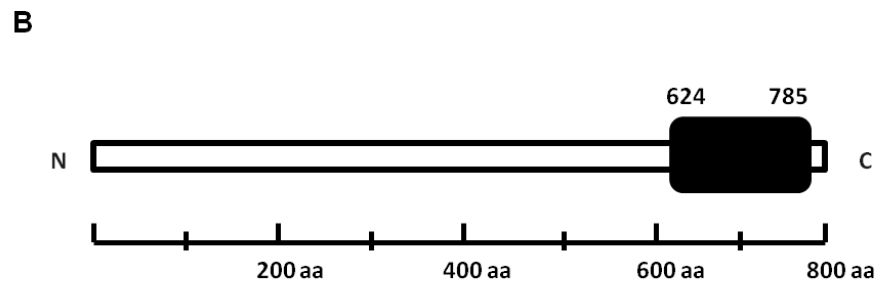
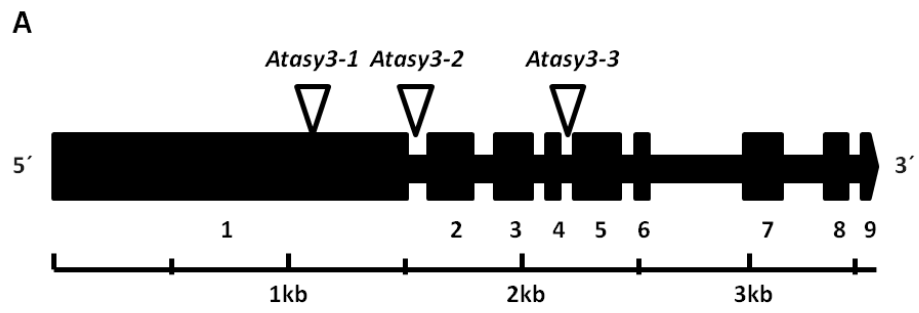
4.1. Introduction

An important feature of meiotic recombination is that it is tightly coupled with chromosome axis organization. In *Arabidopsis*, the axis protein AtASY1 has recently been shown to promote AtDMC1-mediated inter-homologue recombination (Sanchez-Moran *et al.*, 2007). Furthermore, *Arabidopsis* mutant plants lacking the SC component AtZYP1 display recombination between non-homologous chromosomes (Higgins *et al.*, 2005). These observations highlight the presence of a functional inter-relationship between axis components and the recombination machinery (discussed in chapter 1.6). However, understanding this inter-relationship has proved challenging in *Arabidopsis*. This is partly because chromosome axis and SC proteins display limited primary sequence conservation, which has made it difficult to identify their homologues in different species using solely *in silico* methods. In order to overcome this issue researchers in our lab have developed a proteomics-based approach to identify novel meiotic proteins by making an inventory of proteins present in meiocytes from *Arabidopsis* and its closely related species, *Brassica* (Sanchez-Moran *et al.*, 2005, Osman *et al.*, unpublished). The results from such a study along with homology searches led to the identification of a novel coiled-coil protein, ASYNAPTIC 3 (ASY3), required for normal meiosis in *Arabidopsis* and *Brassica*. This chapter describes the identification and cloning of ASY3 in *Arabidopsis* and *Brassica* along with the molecular characterization of three *Arabidopsis asy3* T-DNA insertion mutants. This chapter also describes the production of a recombination protein used to raise an antibody against ASY3, which was subsequently used for immunolocalization studies of ASY3.

4.2. Identification of *Arabidopsis* ASY3

Recently, a proteomics-based study was carried out in our lab with the aim of identifying novel proteins expressed in prophase I meiocytes from *Arabidopsis* and *Brassica*. The study involved co-immunoprecipitation (Co-IP) of prophase I proteins from *Brassica oleracea* meiocytes, extruded from staged anthers, using an antibody against a known meiotic axis protein such as AtASY1 followed by analysis using mass spectrometry (MS) (Osman et al., unpublished). Out of the many peptides detected by the MS analysis, four showed homology in BLAST (NCBI) searches to the predicted product of a previously uncharacterized *Arabidopsis* gene, At2g46980. Genome sequencing data from TAIR indicated that At2g46980 (referred to hereafter as AtASY3) encompasses a genomic region of 3562 base pairs (bp) containing 9 exons separated by 8 introns in *Arabidopsis* chromosome 2. Analysis using bioinformatics software revealed that AtASY3 is predicted to encode a ~88kDa protein, 793 amino acids (AAs) in length with an isoelectric point (pI) of 9.72. The AtASY3 protein is predicted to contain several sequence motifs including a putative nuclear localisation signal (NLS), a condensin-like domain and a DEAD-box helicase-like domain containing regions similar to P-loop NTPase, all of which are of potential functional significance. More interestingly, the C-terminal (residues 624 to 785) of AtASY3 protein is predicted to contain a coiled-coil domain, often found in meiotic axis/SC proteins (Figure 7A). Homology searches revealed that AtASY3 is 25.6% identical to the rice coiled coil meiotic chromosome axis protein PAIR3. Furthermore, AtASY3 also displayed weak homology (16.4% identity) to the budding yeast SC component Red1, which is also a coiled-coil protein (Figure 7D). These initial observations suggested that AtASY3 potentially possessed properties found in

meiotic axis proteins and thus led to further investigations to verify whether AtASY3 is involved in *Arabidopsis* meiosis.



D

```

Red1      MEGLEKKKIFGVCLKNDLAQTRNETKGIHYGLMTLETSKQLQEFLLHLLVIKREVIQNFELL 60
AtASY3    --MSDYRSFSGSNYH----PSSQSRKISIGVMADSQPKRN-----LVPDKDDGDIARV 47
          . : ** : . : : : * * : : . * :      ** : : : : :

Red1      FHIINVAVKITDSNLPDDIWHFILKLRFSSEINIDEDSKVLNLYLLETGIAMENPVSWKC 120
AtASY3    EKLKSAIVTELQANK--KEKSDLAARQNSAQVTVGHVTSFWR-----SPRSSHRKLG 98
          : : : : * . : : * : : : * * * : : . *      . . . .

Red1      LAVISSILSSVPQSKKIITNLIETEHAKKIGQLFDNIQDLQQGNFLVEILSNCFKKSASN 180
AtASY3    LESVLCKQTSSLSGSKGLNGLNGAHQT PARESFQNCPISSPQHSGLGELNGGRNDRVMDR 158
          * : . : * * . . * : : : * . : : * * . : * * : . . : . .

Red1      SKKVEKIPQLWQSRSKNKKFFENEFFPFSSKNGSLQTCQFLCENNFMSTLSFTGILRQVSY 240
AtASY3    SPERMEEPPSAVLQQKVASQREKMDKPKGKETNGTIDVLRSKLWEILGKASPAANNEDVNSE 218
          * : : * : * : * : * : * : * : * : * : * : * : * : *

Red1      SGSETLKNLRIFKKKDDENSYFIQCIYNKIYLWLDEKAPLEFERKKIRITKLNKNKIQIK 300
AtASY3    TPEVEKTNFKLSQDKGSNDPLIKPRHNSDSIETDSESPENATRRFVTRSLQRRVGA 277
          : . . * : : : * . . . . : * : * . : * : * : * : * : * : *

Red1      LRQPFHECVRITADKTAALLFNKTKGFQLEFEDEKLGGETFFHNVNIPKISEVQNFVLVDY 360
AtASY3    GVQKTKAGANLGRKCTEQVNSVFSFEELRG-KIGTAVNSSVMPKQGRRRKNTVVKCR 336
          * : . . . * : * . . * : . . * * : . . * : . . : * : *

Red1      IEEEPENEGEEEQIGRADEQKEDEEEESLDELSTPMVYPIKSSIPHNNHNEKVLVTPDR 420
AtASY3    KAHSRKKD--EADWSRKEASKSNTPPRSESTETGKRSSSSDKKSSSHDLHPQSKARKQKP 394
          . . : : * : : : : : . . . . * . . . * . . * : : : : . .

Red1      SVSIRSDWDLKSNTDEEGNVLADLKI SSTKETKRQTDYVHIDSEDQSPVVSQAQMRKMR 480
AtASY3    DISTREGDFHPSPEAEAAALPEMSQGLSKNGDKHERPSNIFREKSVPEPENEFQSPITFYK 454
          : * * . . . . : : * : : : * : : : * : : . . . : :

Red1      RESTKILEILRQEFKDKVQNKEDQSEQIQNPFVNTSSLVVGKSCLVNPKKPNIDQTVV 540
AtASY3    APISPPSPCCSPEASPLQPRNISPILDETEPIFSFG---TKKTSQGTGQASDTEKRLP 511
          : . . * . : : * . : : : * : . . * : . . : : : : :

Red1      GITELKSNSSIKKRDIN--ILDITFGQPPSKKQKQFHKKKQKQKLLNFKPIIDVPSQ 598
AtASY3    DFLEKKRDYSFRRESSPEPNEDLVLSDPSSDERDSDGSRDPSVVLGHNISPEERETANWT 571
          . : * * : * : : . . * : : : * . . . . : * : . : . : .

Red1      DKRNLRSNAPTKPKSIKVKSLRITDKKVIKESKSPETAEEKVDDQTVRSNDEQAQMSRATKE 658
AtASY3    NERSMLGFPSSVK---RNSNLKIGRVVLSPPSPLSKGIDKTDSEFQHCSEMEDDEDEGLG 627
          : * : . . . . * : * : * : * . . * * : . . * . : : : .

Red1      KCFPDVNEGKEITKDDAKVLSLESKNNETFVDSSVVEKHTPPDKDCNNCNIITDILESTTV 718
AtASY3    RAVALFAMALQNFERKLSAAEKSSSE---IIASVSEEIHLELENIKSHIITEAGKTSNL 684
          : . . . . : : * : * . . . : : * * * : : : . . * : : : :

Red1      IDLQSPHGLS-APGQNTFTNKLQEQIYSSINHFSNELVRKISIIINQELN--KKILKELSE 775
AtASY3    AKTKRKHAEIRLQEQEEMRMIHEKFKDDVSHHLEDFKSTIEELEANSQELKGSIKKQRT 744
          . : * . : * : . : * : : . . * . : : . * . : : . * : *

Red1      KYQKLFSELQDNFQNDTNEMLKFMGEIKDMMNLPEDQLVHAIRTRKFDNNKR 827
AtASY3    SHQKLIHFEGGIETKLDATKRIDSVNKSARGKMLQLKMIVAECLRDD--- 793
          : * * : : : : : : : : : : * : : : . . * * : : * :

```

Figure 7. Structure of *AtASY3* and its predicted product and *AtASY3* expression analysis.

(A) Map of the ~3.5kb *At2g46980* locus showing the exon/intron organization of *AtASY3*. The exons are represented by numbered black boxes. The triangles indicate the T-DNA insertion sites in *Atasy3-1*, *Atasy3-2* and *Atasy3-3*. (B) Diagrammatic representation of the 793aa *AtASY3* protein. The black box indicates the relative position of the putative coiled-coil domain. (C) Expression analysis of *AtASY3*. *AtASY3* is highly expressed in WT flower buds (B) and at a lower level in open flowers (F), however, there is no detectable expression in stem (S) and leaf (L) tissues. The *AtASY3* transcript cannot be detected in flower buds of *Atasy3-1*, *Atasy3-2* and *Atasy3-3* mutants. Expression of the housekeeping gene *AtGAPD* was analysed as a control. (D) ClustalW2 alignment of Red1 and *AtASY3* amino acid sequences. The two sequences show weak homology.

4.3. *AtASY3* is expressed in reproductive tissues

Reverse transcription (RT) PCR was used to determine the relative expression pattern of *AtASY3* in various tissues from wild-type *Arabidopsis* (Col-0). For this purpose a set of 2 primers, ASY3-EX-R1 and ASY3-EX-F1, encompassing all three T-DNA insertion sites was designed to check for *AtASY3* transcript. Another set of primers, GAPD-N and GAPD-C, was designed to check for the expression of the housekeeping gene, *GAPD*. *GAPD* is expressed equally in all plant tissues. Hence, analysis of its transcript from various plant tissues would act as a control enabling the comparison of the relative abundance of *AtASY3* transcripts from different tissues. To analyse *AtASY3* expression, total RNA from stem, leaf, bud and flower tissues from wild-type *Arabidopsis* were extracted using RNeasy extraction kit (Qiagen). The RNA content from each sample was quantified using spectrophotometer to allow equalisation of RNA in all samples. The RT-PCR reactions were carried out using SuperScript II reverse transcriptase (Invitrogen) following the manufacturer's protocol. The cDNAs generated by the RT-PCR reactions were subjected to PCR using the *AtASY3* and *GAPD*-specific primers mentioned above. Analysis of the products of this PCR via gel electrophoresis revealed that in wild-type, *AtASY3* transcripts can be detected in the reproductive tissues, bud and flower but not in the vegetative tissues, stem and leaf (Figure 7C). Further analysis revealed that the expression of *AtASY3* is notably higher in bud than in flower tissue. These findings suggest that *AtASY3* is expressed in meiotic tissues, which is consistent with a role for *AtASY3* during *Arabidopsis* meiosis.

4.4. Molecular characterization and analysis of *AtASY3* T-DNA insertion mutants

To investigate a potential meiotic role of *AtASY3* three *Arabidopsis* T-DNA insertion mutant lines of *AtASY3*, *Atasy3-1* (SALK_143676), *Atasy3-2* (SAIL_423_H01) and *Atasy3-3* (SALK_050971), were obtained from NASC. The seeds from these lines were grown along with the wild-type (Col-0) control. To check for zygosity of the T-DNA insertion, primers were designed on either sides of the T-DNA insertion site for each line. Genomic DNA was extracted from leaves of plants from each mutant line and the wild-type and genotyped via PCRs using primers specific to each T-DNA insertion. A set of 2 primers were used to verify wild-type *AtASY3* and another set to identify the T-DNA for each T-DNA insertion line. The primer sets ASY3-1-F1 and ASY3-1-R1 (for *Atasy3-1*), ASY3-2-F1 and ASY3-2-R1 (for *Atasy3-2*), ASY3-3-F1 and ASY3-3-R1 (for *Atasy3-3*) were used to amplify the wild-type genomic region. Additionally, the primer sets ASY3-1-R1 and LBb1.3 (for *Atasy3-1*), ASY3-2-R1 and LB3 (for *Atasy3-2*), ASY3-3-R1 and LBb1.3 (for *Atasy3-3*) were used to amplify the region where the T-DNA was inserted. The PCRs allowed the identification of plants homozygous for the T-DNA insertion in *AtASY3* in all three mutant lines. Hence, these homozygous knockout plants are potentially deficient in *AtASY3* expression. To determine the exact insertion site of each T-DNA, PCR products containing the partial T-DNA and *AtASY3* genomic sequence from a homozygous plant of each line were ligated to pDRIVE cloning vectors before being transformed into competent *E. coli* (DH5 α). Following verification of the products using boil preparations and restriction digestion using *EcoRI*, DNA was isolated using wizard preparation (Promega) and sequenced. The sequencing data was analysed using BLAST (NCBI)

and TAIR Seqviewer. This revealed that the T-DNA insertion site in *Atasy3-1* is located at the first exon (1188bp from start), in *Atasy3-2* is present in between first and second exon (1583bp from start) and in *Atasy3-3* is located in between fourth and fifth exon (2186bp from start) in the genomic sequence of *AtASY3* (Figure 7B).

To confirm the absence of *AtASY3* expression in the T-DNA insertion mutants *Atasy3-1*, *Atasy3-2* and *Atasy3-3*, total RNA was extracted from bud tissues of homozygous plants from each of these mutant lines. The RNA samples were then analysed via RT-PCR using the primers and methods similarly to those used for *AtASY3* expression analysis in the wild-type. This revealed that *AtASY3* transcript was not present in any of the *Atasy3* T-DNA insertion lines confirming that they were indeed knockout lines of *AtASY3* (Figure 7.C).

Analysis of homozygous *Atasy3-1*, *Atasy3-2* and *Atasy3-3* knockout mutants revealed that they displayed normal vegetative growth similar to wild-type Col-0. However, these mutants exhibit significantly reduced fertility compared to wild-type Col-0 (Figure 8AB). The mean silique length in *Atasy3-1*, *Atasy3-2* and *Atasy3-3* were 9.90mm, 10.2mm and 9.80mm respectively relative to 15.64mm in the wild-type (ANOVA, $P < 0.0001$; $n=50$) (Figure 8CD). The mean seed-set in *Atasy3-1*, *Atasy3-2* and *Atasy3-3* were 15.78, 15.96 and 15.70 respectively compared to 58.68 in the wild-type (ANOVA, $P < 0.0001$; $n=50$) (Figure 8.E). These results indicate a ~75% reduction in fertility in *Atasy3* mutants, consistent with a meiotic defect. In addition, pollen viability in *Atasy3* mutant lines was determined using Alexander's staining.

This revealed the presence of a large proportion of non-viable pollen in all three *Atasy3* T-DNA insertion lines (viable:non-viable ratio = ~1.8:1; n=1943) in contrast to wild-type (Col-0) (viable:non-viable ratio = 55:1; n=1973). These results are also suggestive of a potential meiotic defect in *Atasy3* mutant lines.

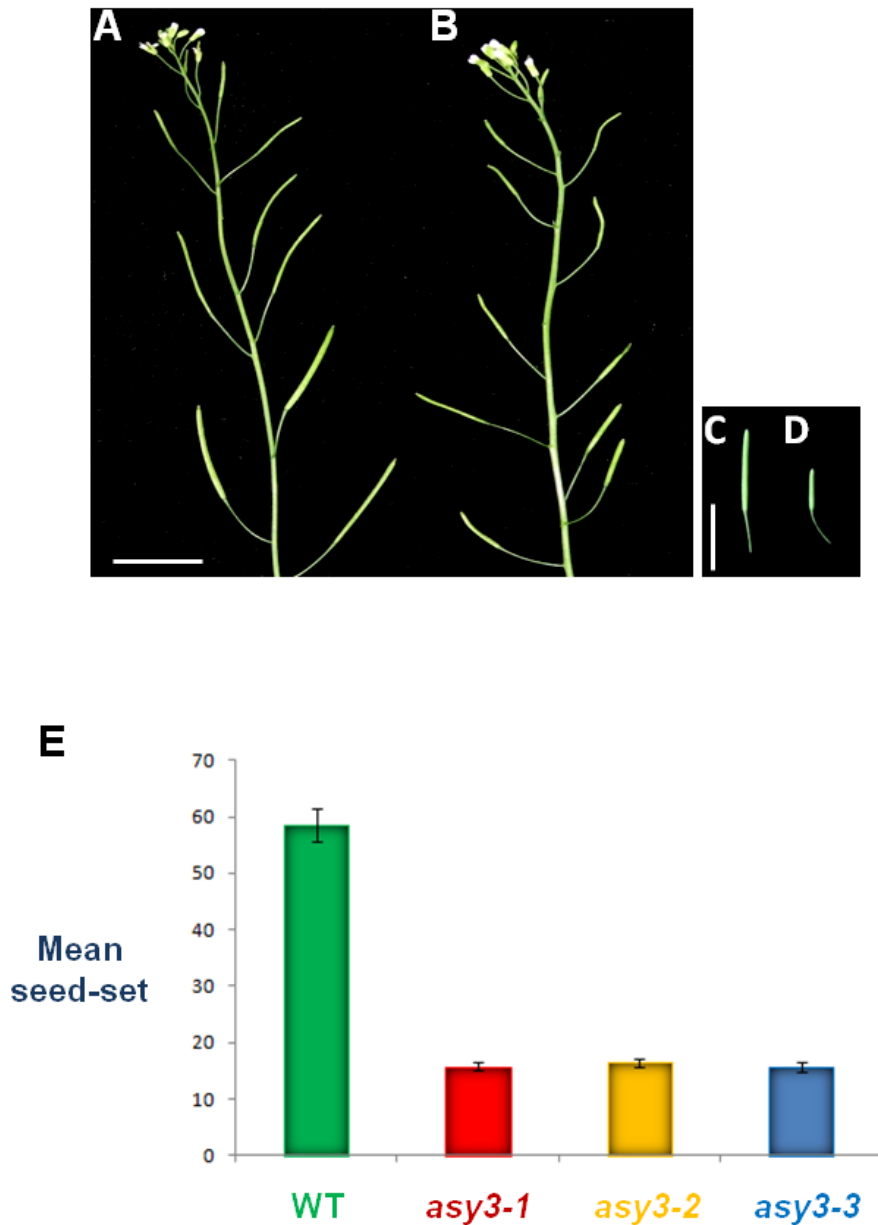


Figure 8. Comparison between WT and *Atasy3* fertility.

Reduced silique length in *Atasy3* (B, D) compared to wild-type (A, C). Bar 10mm. (E) Graph showing the variation in the mean seed-set between WT and the three *Atasy3* mutant lines. Fertility is ~75% reduced in *Atasy3* T-DNA insertion mutant lines compared to the WT.

4.5. Molecular characterization of *Brassica ASY3*

Proteomics studies involving CO-IP and MS analysis of proteins from *Brassica oleracea* meiocytes led to the identification of *Arabidopsis ASY3*, which encodes a meiosis-specific protein with a potential role during meiosis. It is common to find conservation between genes of *Brassica* and *Arabidopsis* since the two are closely related. Therefore, characterizing the *ASY3* gene in *B. oleracea* in addition to that in *Arabidopsis* would reveal if the two are conserved, and if so, would significantly aid in understanding the potential meiotic role of *ASY3*. To do so, the full length coding sequence of *B. oleracea ASY3* (*BoASY3*) needs to be compared with *AtASY3*. However, a limitation of using *B. oleracea* is the insufficient availability of its sequence data. Nevertheless, the *Brassica* genome has been completely sequenced for *B. rapa* via BAC sequencing using Sanger sequencing methods and de novo sequencing using second generation sequencers (*Brassica* database, BRAD). Analysis of *B. rapa* genome sequence using homology searches revealed the presence of a locus (Bra004486) similar to *AtASY3* in the line Chiifu 401. Further analysis revealed that the predicted product of this locus (hereafter referred to as *BrASY3*) was ~75% identical to *AtASY3* protein (Figure 9A). Hence this locus is ideal for designing primers which can subsequently be used to amplify and sequence full length *ASY3* from *Brassica oleracea*, which shares close phylogenetic relationship with *Brassica rapa*.

4.5.1. Determining *BoASY3* 3'-end nucleotide sequence using 3'-RACE

Homology analysis revealed that the 3' end of *BrASY3* display some variation to that of *AtASY3* at nucleotide level and hence was not suitable for designing primers for *BoASY3* amplification. Furthermore, the actual location of the termination codon in *BoASY3* cannot be predicted based on *BrASY3* nucleotide sequence since the length of coding sequences of conserved genes may vary from one species to another. Hence, to determine the unknown nucleotide sequence at the 3' end of *BoASY3*, its 3' end was amplified by 3' RACE. 3' RACE allows the amplification of nucleic acid sequences from an mRNA template between a defined internal site and the 3' end of the mRNA. The process involves 3 rounds of PCRs. During the first PCR cDNAs are generated from mRNA templates using reverse transcription and an oligo dT-adaptor primer, which consists of a short sequence of deoxy-thymine nucleotides and an adaptor sequence. The oligo dT-adaptor primer complements the natural poly(A) tail and adds the adaptor sequence to the 3' end of each cDNA. The second round of PCR involves the amplification of the 3' end of the desired cDNA using a gene specific primer (GSP) complementary to a known location and an anti-sense primer complementary to the oligo(dT)-adaptor sequence. The final round of PCR uses a nested GSP in conjunction with the primer complementary to the adaptor sequence to amplify the 3' end of the cDNA increasing specificity of the desired product. Hence, an oligo dT-adaptor primer (3RACE17AP) and an anti-sense primer complementary to the adaptor region (3RACEAP) were designed for the amplification of the 3' end of *BoASY3*. Additionally, a GSP (Bra486_3'RaceF1, 535bp from end) and a nested GSP (Bra486_3'RaceF2, 468bp from end) were also designed based on known conserved sequences at the 3' region of *BrASY3*. Total RNA was

extracted from *Brassica oleracea* buds and subjected to RT-PCR using Superscript II (Invitrogen) reverse transcriptase and 3RACE17AP. The resulting cDNA was subjected to PCR using Bra486_3-RaceF1 and 3RACEAP. The subsequent product was further amplified using Bra486_3-RaceF2 and 3RACEAP and analysed using gel electrophoresis. The analysis revealed the presence of a ~750bp product in high abundance (Figure 9B). The RACE-PCRs also generated 4 other products of varying sizes (two > 900bp, two < 400bp) and in very low abundance, possibly due to non-specific amplification. The ~750bp product was extracted from the electrophoresis gel using Qiaquick gel extraction kit (Qiagen), ligated to pDRIVE (Qiagen) expression vector and transformed into competent *E. coli* (DH5 α). Subsequently, the presence of the product was verified using boil preparation of plasmid DNA followed by its digestion using *EcoRI* restriction enzyme. Finally, the vector-product DNA was extracted using wizard preparation (Promega) and sequenced using M13 – Reverse primer. This revealed the previously unknown nucleotide sequence at the 3' region of *BoASY3* and the exact location of the termination codon in it. Homology analysis revealed that the 3' region of *BoASY3* displays high conservation with *BrASY3*, although the former contains more coding sequences with its stop codon located further downstream compared to the latter (Figure 9D). More importantly, the 3' of *BoASY3* is highly conserved to *AtASY3*, consistent with the conservation of the gene between the two species (Figure 9E). Furthermore, with the 3' nucleotide sequence of *BoASY3* now available, the rest of its coding sequence can be amplified and compared to *AtASY3*.

4.5.2. Cloning the full length coding sequence of *BoASY3*

Analysis of the predicted *BrASY3* mRNA sequence revealed that it shares 84% identity with that of *AtASY3* and hence is an ideal template for designing primers for *BoASY3* amplification. The length of the mRNA sequence of *BrASY3* is 2310bp and hence too large to be amplified error-free by PCR using *Taq* DNA polymerase. Therefore, 3 sets of primers, each with a forward and a reverse primer were designed to amplify their corresponding sections of DNA from the 5' region of *BoASY3* by PCR using *Taq* DNA polymerase. Each primer set was designed to overlap to allow the accurate alignment and ordering of their amplified products. The expected length of the products from the three primer sets, Bras4486_F3 and Bo486TAQR1, Bo486TAQF1 and Bo486TAQR2 and Bo486TAQF2 and Bo486TAQR3 were ~508bp, ~586bp and ~425bp respectively. Additionally, a fourth set of primers, consisting of Bras4486_F4 and Bras4486_R2 was designed to amplify a ~905bp region overlapping the ~425bp region and the already sequenced 3' region of *BoASY3*. The fourth set of primers was designed to amplify a longer section of *BoASY3* compared to the other sets particularly to avoid an extra PCR reaction to amplify the already sequenced 3'-end of *BoASY3*. Furthermore, the amplification of this relatively longer section would require PCR using the proofreading Pfu DNA polymerase for error-free amplification. Subsequently, three separate PCRs using *B. oleracia* bud cDNA and *Taq* DNA polymerase were carried out, each with a different set of primers designed for *BoASY3* amplification using *Taq* DNA polymerase. Similarly another PCR was carried out using bud cDNA, Pfu DNA polymerase and the primers from the fourth set. The PCR products from all reactions were then analysed using gel electrophoresis, which revealed that the primer sets were able to amplify their

corresponding regions of *BoASY3* (Figure 9C). All the PCR products were subsequently extracted from the electrophoresis gel using Qiaquick gel extraction kit (Qiagen). The products from the PCRs using Taq DNA polymerase were ligated to pDRIVE (Qiagen) expression vectors while the product from the PCR using Pfu DNA polymerase was ligated to pCR-Blunt (Invitrogen). The vectors were transformed into separate competent *E. coli* (DH5 α). Subsequently, the presence of the desired products was verified using boil preparation followed by their digestion using *EcoRI*. Each product with the corresponding amplified region of *BoASY3* was then extracted using wizard preparation (Promega) and sequenced using M13–Forward primer. Since all the amplified sections of *BoASY3* had overlapping regions BLAST (NCBI) searches were used to align and order each segment of sequenced DNA. The resulting nucleotide sequence was then conjoined with the known sequence of 3'-end of *BoASY3* to reveal the full length coding sequence of *BoASY3*. Homology analysis of the full length *BoASY3* coding sequence and its predicted product revealed that they are 95% and 93% identical respectively to those of *BrASY3*, suggesting a high level of conservation between the two genes. More interestingly, further analysis revealed that the full length coding sequence of *BoASY3* shares 85% identity with that of *AtASY3*. Furthermore, *BoASY3* is predicted to encode a protein that is 77% identical to *AtASY3* in amino acid sequence (Figure 9F). In addition, *BoASY3* is predicted to be ~86kDa in weight and 776 AA in length, therefore, of similar size and length to *AtASY3*. These results suggest that *AtASY3* is conserved at molecular level in *B. oleracea*.

A

```

AtASY3      MSDYRSFGSNYHPSSQSRKISIGVMADSQPKRNLPDKDDGDVIARVEKLSATVTELQA 60
BrASY3      MSEYRSFGSNFHPSSQSRKMSIGVMADSQPKRN--PDGD--AAIGRAEKLSAAATDLQL 56
          **:*****:*****:***** * * .*.*****:.*:**

AtASY3      NKKEK-SDLAAQRNSAQVTGHVTPWRSRSSHRLGTLSEVLCKQTSSLGSKGLNKG 119
BrASY3      NKKVTGDDVAAKQRSSATGTEHVTSPWRSRSSHRLGTLSEVLCKQTSSLGSKGLNKG 116
          *** .*.***** * *****:*****:*****:*****

AtASY3      LINGAHQTPARESFQNCPISSPQHSGLGELNGGRNDRVMDRSPERMEEPPSAVLQKVASQR 179
BrASY3      PNGAHQAPARDTFQDIPVSSPRHSDDEPISGRKGNEMDKSPERMQEPSSAVLPQKVASQR 176
          *****:***:.*: *.*:** * * .*.*****:***** *****

AtASY3      EKMDKPGKETNGTIDVLRSKLWEILGKASPANNEDVNSETPEVEKTNFKLSQDKGSNDP 239
BrASY3      EEKRGPETAKDGSTDVLRSKLWEILGKASPEYNEDVNSETPEVVKINSKLNQDKSSDNDP 236
          *: * . .:*****:***** ***** * * .*.*****:.*:**

AtASY3      LIKPRHNSDIETDSESPENATRRPVTRSLQRRVGAKGVQKTKAGANLGRKCTEQVNS 299
BrASY3      LTKPRHNSDIETDSESPVATRRPVTRSLQRRVGARGIQKRAKTGANLGGKSTEEVNN 296
          * *****:***** *****:*****:.*:.*:.*:***** *.*:**.

AtASY3      VFSFEGLRGKIGTAVNSSVMPKQGRRRKNIIVKCRKAHSRKKDEADWSRKEASKSNTP 359
BrASY3      VFTFEGRGRNGTAMNSTGVPKKQGRKKNTAVKCRKVQSRKDEADGILKETSCKSTP 356
          **:***:.*: *.*:**: *****:***.*****:.*:***** **.*:**.

AtASY3      PRSESTETGKRSSSDKKGSSHDLHPQSKARKQKPDISTREGDFHSPPEAAALPEMSQ 419
BrASY3      ARSESTRTGKRSSLSDRKSSLEFNQHTKAQNKQKPDVRTREEDFQPSPEAETAATPEMFR 416
          .*****:***** **.*:** :.: :.*:**:*****: * * .*.*****:.* ** * :

AtASY3      GLSKNGDKHERPSNIFREKSVPENEFQSPTFGYKAPISSPCCSPEASPLQPRNISPT 479
BrASY3      GLFKNGDEQKGPCEVLREKSVPEPDFQSPTFGYKAPISSPCLSPPEASPLHPQNISPA 476
          ** *.*:**: .*.:**:*****:*****:***** *****:.*:*****:

AtASY3      LDETETPIFSFGTKKTSQGTGQASDTEKRLPDFLEKRDYSFRRESSPEPNEDLVLSDP 539
BrASY3      FDEAETTIFSGTKKTPQGTKEASD--KRLHDFLEKKEDYSFGRESSAEPDEDLVLSDP 534
          :.*:.*.*****:.*.*:*** ** *.*:**.***** *****:.*:*****

AtASY3      SSDEKSDGSRSDSPVLGHNISPEERETANWITNERSMLGPPSSVKRNSNLKIGIRVVLSPP 599
BrASY3      SSDEKSDGSIEDSPALGHYNSPQAKETANGSNKSKPGFSSAKRNSNLKGNGRVTSS-- 592
          *****:***** *.*:** ** :.*:** :.*:** * * .*.***** *.* *

AtASY3      SPLSKGIDKDSFQHCSEMEDDEDEGLGRAVALFAMALQNFERKLSAAEKSSSEIIASV 659
BrASY3      --LSEGMHKTDSFQRFSEVDEDE--GLGRAVALFAVALQNFEKLSAAKKSSSEIIASV 648
          **:.*:.*:*****: *.*:** *****:*****:*****:*****

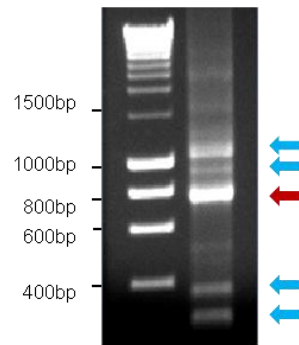
AtASY3      SEEIHLELENIKSHIITEAGKTSNLAKTKRKHAEIRLQEQEEMRMIHEKFKDDVSHHLE 719
BrASY3      SEEIHLELEIVKSHIITEAEKTSNVAKTKRKHAEIRLQEQEEMRMIHEKFKDDVGNHLE 708
          *****:***** *.*:** *****:*****:*****:*****:.*:**

AtASY3      DFKSTIEELEANQSELKGSIKKQRTSHQKLIHFEGGIETKLDATKRIDSVNKSARGKM 779
BrASY3      DFKSTIEGLEANHSELKGSIKKQRTSHQKLIHFEGGIETKLDNATKRINSVNEASPCSS 768
          ***** *.*:** *****:*****:*****:*****:.*:**: .

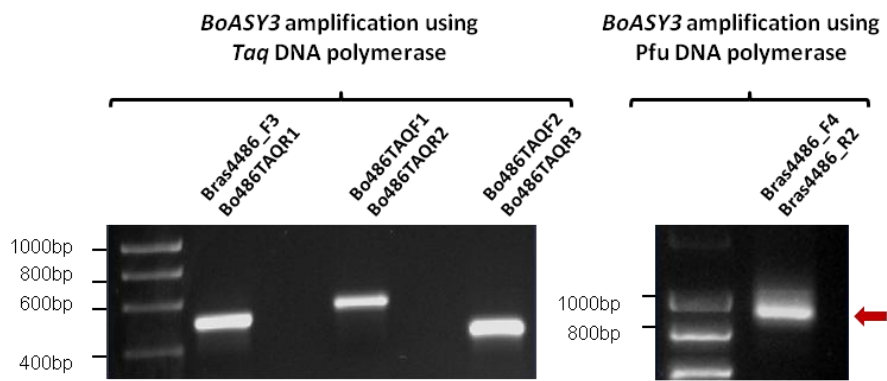
AtASY3      LQLKMIVAELRDD 793
BrASY3      A----- 769

```

B



C



D

```

BrAsy3      TCGAACCTTAAGGGCAATGGACGIGTTACCTCGTCTTTGTCCGAAAGGGATGCATAAAACT 1800
BoAsy3      -----

BrAsy3      GATTCCTTCCAGCGGTTTTTCAGAGGTGGATGAAGATGAAGGCTTGGGAAAGGGCTGTTGCA 1860
BoAsy3      -----CAGAGGTGGATGAAGATGAAGGCYTTGGGAAAGGGCTGTTGCA 41
                *****

BrAsy3      TTGTTTGCTGTGGCTCTTCAAAACTTCGAGAAAAAGCTGAAATCTGCAGCCAAAAAGAA 1920
BoAsy3      TTGTTTGCTGTGGCTCTTCAAAACTTTGAGAAAAAGCTGAAATCTGCAGCCAAAAAGAA 101
                *****

BrAsy3      TCTTCAGAAATTATAGCATCAGTCTCGGAGGAGATACATTTGGAGTTGGAGAAATGTGAAG 1980
BoAsy3      TCTTCAGAAATTATAGCATCAGTCTCGGAGGAGATACATTTGGAGTTGGAGAAATGTGAAG 161
                *****

BrAsy3      TCTCACATCATAACAGAAGCGGAAAAGACGAGTAACGTAGCCAAAACCTAAGAGAAAGCAT 2040
BoAsy3      TCTCACATCATAACAGAAGCGGAAAAGACGAGTAACGTAGCCAAAACCTAAGAGAAAGCAT 221
                *****

BrAsy3      GCTGAAACAAGATTACAAGGCAACAAGAGAAAATGGAATGATCCATGAAAAGTTTAA 2100
BoAsy3      GCTGAAACAAGATTACAAGGCAACAAGAGAAAATGGAATGATCCATGAAAAGTTTAA 281
                *****

BrAsy3      GATGATGTCGGGAACCATCTTGAAGATTTCAAGAGTACTATTGAAGGGCTTGAAGCAAAC 2160
BoAsy3      GATGATGTCGGGAACCATCTTGAAGATTTCAAGAGTACTATTGAAGGGCTTGAAGCAAAC 341
                *****

BrAsy3      CACTCAGAGTTGAAAGGAAGCATAAAGAAACAAAGAACATCACACCAAAGCTCATTGCG 2220
BoAsy3      CACTCAGAGTTGAAAGGAAGCATAAAGAAACAAAGAACATCGCACCAAAGCTCATTGCG 401
                *****

BrAsy3      CATTTTGAAAGAGGCATCGAGACAAAACCTGGACAATGCGACCAAGAGAAATCAACTCTGTC 2280
BoAsy3      CATTTTGAAAGAGGCATCGAAACAAAACCTGGACAATGCGACCAAAAGAAATCAACTCTGTC 461
                *****

BrAsy3      AACGAG--GCAAGCCCTTG--TICTAGCGCTTAA----- 2310
BoAsy3      AACGAGTCTGCGAGAGGAAAGATGCTGCGAGTGAAGATGATTGTGGCAGAAATGTTTGAAG 521
                *****  **.*. :. * *. .*** **

BrAsy3      -----
BoAsy3      GATGATGTGTGTTAG 536

```

E

```

AtAsy3      CCTTTGTCAAAAGGGATCGATAAAAAGTATTTCCTCCAGCATTGTTTCAGAGATGGATGAG 1860
BoAsy3      -----CAGAGGTG----- 8
                ****,*

AtAsy3      GATGAAGATGAAGGCTTGGGAAGGGCTGTTGCATTGTTTCGCTAIGGCITTCAAAACITTT 1920
BoAsy3      GATGAAGATGAAGGCTTGGGAAGGGCTGTTGCATTGTTTCGCTAIGGCITTCAAAACITTT 68
                *****

AtAsy3      GAGAGAAAAGCTGAAATCTGCAGCTGAAAAGAGTCCTCAGAAATATAGCATCAGTCTCC 1980
BoAsy3      GAGAAAAGCTGAAATCTGCAGCCAAAAGAGTCTTCAGAAATATAGCATCAGTCTCG 128
                ****,*

AtAsy3      GAGGAGATACATCTGGAGTTGGAGAATATCAAGTCCCATATCATAACAGAAGCGGGAAAG 2040
BoAsy3      GAGGAGATACATTTGGAGTTGGAGAATGTGAAGTCTCACATCATAACAGAAGCGGAAAAG 188
                *****

AtAsy3      ACAAGTAACCTAGCCAAAAGCTAAGAGAAAGCATGCCGAAACAAGATTACAAGAGCAAGAA 2100
BoAsy3      ACGAGTAACCTAGCCAAAAGCTAAGAGAAAGCATGCTGAAACAAGATTACAAGAGCAACAA 248
                **,*

AtAsy3      GAGAAAATGAGAATGATCCATGAAAAGTTCAAGGACGATGTCAGCCATCATCTTGAAGAT 2160
BoAsy3      GAGAAAATGAGAATGATCCATGAAAAGTTTAAAGGATGATGTCGGGAACCATCTTGAAGAT 308
                *****

AtAsy3      TTTAAGAGTACTATCGAAGGCTTGAAGCAAACCGATCAGAGCTGAAAGGAAGCATAAAG 2220
BoAsy3      TTCAGAGTACTATTTGAAGGGCTTGAAGCAAACCGATCAGAGTGAAGGAAGCATAAAG 368
                **

AtAsy3      AAGCAAAGAACATCACCCAAAAGCTCATTGCACATTTTGAAGGAGGCATCGAGACAAA 2280
BoAsy3      AAACAAAGAACATCGCACAAAAGCTCATTGCACATTTTGAAGGAGGCATCGAAACAAA 428
                **,*

AtAsy3      CTGGACGATGCGACCAAAAAGAACTGATTCTGTAAACAAGTCTGCGAGAGGAAAGATGCTG 2340
BoAsy3      CTGGACAATGCGACCAAAAAGAACTGATTCTGTAAACAAGTCTGCGAGAGGAAAGATGCTG 488
                *****

AtAsy3      CAGCTGAAGATGATTGTCGAGAAATGTTTGAAGGATGAT-TGA----- 2382
BoAsy3      CAGCTGAAGATGATTGTCGAGAAATGTTTGAAGGATGATGTTGTTAG 536
                *****

```



Figure 9. (A,D,E,F) ClustalW2 alignment of various sequences, (B) 3' RACE PCR products and (C) Amplification of *BoASY3*.

(A) The amino acid sequence of *BrASY3* displays ~75% identity to that of *AtASY3*. (B) 3' RACE PCR products. The reaction generated the expected ~750bp product (red arrow) along with four non-specific products (blue arrows). (C) Amplification of *BoASY3*. Overlapping sequential regions of *BoASY3* were amplified by three PCRs using *Taq* DNA polymerase and one PCR using *Pfu* DNA polymerase. (D) *BoASY3* C-terminal nucleotide sequence displays high conservation with *BrASY3*, although the former contains more coding sequences and its stop codon is located further downstream compared to the latter (E) The 3' of *BoASY3* is highly similar to *AtASY3* (F) *BoASY3* is 77% identical to *AtASY3* in amino acid sequence.

4.6. Production of an anti-ASY3 antibody

4.6.1. Cloning the AtASY3 C-terminal region for recombinant protein production

The availability of an antibody that detects AtASY3 would allow immunolocalization studies for understanding the functional role of the protein. Since, AtASY3 has been found to be 77% identical to BoASY3 the anti-ASY3 antibody may also be useful for studying functional similarities between the two. Database searches revealed that AtASY3 shares sequence identity with rice axis protein, PAIR3 (25.6%) and budding yeast axis component, RED1 (16.4%). Interestingly, the coiled-coil region (a feature of meiotic axis proteins) at the C-terminal of AtASY3 displays the most conservation with PAIR3 and Red1. Hence, the C-terminal of AtASY3 was selected for generating a recombinant protein that would be used for the production of an anti-ASY3 antibody. The primers, RED1F1 and RED1R1 were designed to amplify a 702bp region from the wild-type (Col-0) bud cDNA corresponding to the last 234 residues of the AtASY3 C-terminal (Figure 7A). RED1F1 and RED1R1 were designed to contain *NdeI* and *XhoI* restriction sites respectively, to allow cloning of the amplified product into an expression vector in the correct orientation. The *NdeI* restriction site was specifically chosen for amplification of the 5'-end of the desired fragment as it contains the ATG start codon. RNA was extracted from wild-type inflorescences and cDNA was generated by RT-PCR using Superscript II (Invitrogen). The cDNA was amplified by PCR using the primers RED1F1 and RED1R1 and its product run on an electrophoresis gel (Figure 10A). Subsequently, the PCR product was extracted from

the gel and ligated to pDRIVE before being transformed into competent *E. coli* (DH5 α). Following verification of the product using boil preparations and restriction digestion using *EcoRI*, DNA was isolated using wizard preparation (Promega) and sequenced. The sequencing results confirmed that the correct sequence was amplified and was in frame for subsequent expression. Hence, the fragment was isolated using *NdeI/XhoI* double digestion and gel extraction, sub-cloned into pET21b expression vector (Novogen) and transformed into competent *E. coli* (DH5 α). The presence of the insert was again verified using boil preparations and restriction digestion using *EcoRI*. Finally, plasmid DNA was isolated using wizard preparation (Promega) and transformed into competent *E. coli* (BL21) (DE3) for subsequent expression of the *AtASY3* C-terminal fragment (hereafter referred to as *AtASY3-C*). Computational analysis using BCM Search Launcher program (<http://searchlauncher.bcm.tmc.edu>) revealed that the expected product of the *AtASY3-C* is a ~27kDa protein. However, the actual weight of the final product is expected to be slightly higher due to the addition of a histidine-tag from the pET21b vector.

4.6.2. Production of the recombinant protein for anti-ASY3 antibody preparation

Prior to a larger scale production of the *AtASY3-C* test induction experiments were carried out for the verification of *AtASY3-C* expression. For this purpose, 4 different bacterial cultures (each 10ml) were grown, each from a separate colony of *E. coli* BL21 (DE3) containing pET21b-*AtASY3-C*. Samples from each of the 4 cultures were

induced for the expression of the recombinant protein using IPTG (final concentration of 1mM), an artificial inducer of the *lac* operon in pET21b. Control experiments were also set up in parallel where no IPTG was added to samples from each of the 4 cultures. After incubation with or without IPTG, proteins were isolated from both induced and non-induced cultures using BugBuster (Novagen). Proteins were separated into a soluble and an insoluble fraction and resolved using SDS-PAGE. The proteins were subsequently detected using coomassie blue staining. This revealed that the AtASY3-C recombinant protein (~27kDa) was present in the insoluble fraction but undetectable in the soluble fraction (Figure 10BC.). Further analysis of the insoluble fraction revealed that AtASY3-C was expressed in both the induced and non-induced samples, although its expression was several fold higher in each of the induced samples relative to their corresponding non-induced samples (Figure 10B). The expression of AtASY3-C in non-induced samples was probably due to the leaky baseline expression by the T7 polymerase in *E. coli* BL21 (DE3). Nevertheless, the results clearly suggest that AtASY3-C is generated by the pET21b-AtASY3-C expression system, which can now be used for a larger scale production of the recombinant protein, needed for anti-ASY3 antibody production.

For the large scale production of recombinant AtASY3-C protein a 200ml culture was grown from a single colony of *E. coli* BL21 (DE3) clone 1 from the test induction. Protein expression was induced using IPTG and the subsequent proteins were extracted using sonication. The insoluble fraction containing proteins including AtASY3-C was separated and various amounts (10µl, 5µl, 2.5µl, 1µl, 0.5µl) of it were

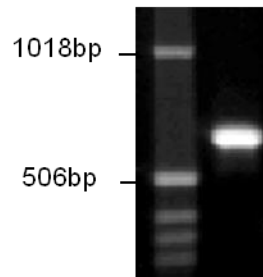
loaded into a SDS-PAGE gel. Additionally varying amounts of BSA of known concentrations (10, 5, 2.5, 1.25mg/ml) were also loaded into the gel for the quantification of AtASY3-C in the samples. All the samples were resolved using SDS-PAGE and subsequently detected using coomassie blue staining. The result showed that *AtASY3-C* was successfully expressed to produce the *AtASY3-C* recombinant protein (Figure 10D). In addition, comparison of band intensities of *AtASY3-C* to those from known BSA concentrations in conjunction with BIORAD assay allowed the quantification of the amount of *AtASY3-C*. This revealed that the concentration of *AtASY3-C* produced from the large scale production was ~3mg/ml. The *AtASY3-C* protein sample was then diluted to 1mg/ml and sent to BioGenes (Germany) for the production of the anti-ASY3 antibody in rabbit.

4.6.3. Validation of anti-ASY3 antiserum

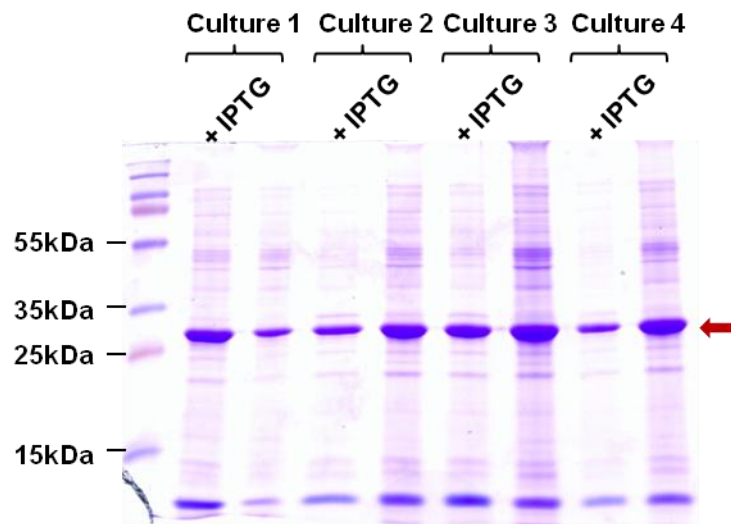
At BioGenes (Germany), two rabbits numbered 5073 and 5074 were inoculated with *AtASY3-C* for the production of anti-ASY3 antibody. Subsequently, the pre-immune sera and the anti-sera containing the anti-ASY3 antibody from each of the two rabbits were collected and sent to our lab. However, whether the antisera can detect the recombinant *AtASY3-C* needed to be verified before use. To do so, two different amounts (1µl and 0.5µl) of the recombinant *AtASY3-C* protein were loaded into one half of a SDS-PAGE gel for their subsequent detection by western blotting using each of the two antisera. As a control, similar amounts of the same protein were also loaded on the other half of the same gel to check for any detection by the pre-immune anti-sera from the two rabbits. A second gel was also set up similarly but

only for detection of the presence of AtASY3-C recombinant protein via coomassie bluestaining. Once the proteins were resolved by SDS-PAGE, those from the first gel were electroblotted to a nitrocellulose membrane (GE Healthcare) for probing while the ones from the second gel were detected using coomassie blue staining. The nitrocellulose membrane was separated into two halves and each probed using either the pre-immune serum from rabbit 5073 or 5074 (1:3000). Subsequently, the membranes were probed using anti-rabbit secondary conjugated to horseradish peroxidase (HRP) (1:10,000) and visualized using ECL. No bands were detected at various exposures confirming that the pre-immune serum from either rabbit is incapable of detecting recombinant AtASY3-C. The nitrocellulose membranes were then washed, blocked using milk and re-probed using anti-sera from the two rabbits. The membrane initially analysed using pre-immune serum from rabbit 5073 was probed with anti-sera from 5073 (1:3000). Similarly, the other half of the membrane initially analysed using pre-immune serum from rabbit 5074 was probed with anti-sera obtained from 5074 (1:3000). The membranes were then probed using anti-rabbit secondary conjugated to HRP (1:10,000) and visualized using ECL. This revealed that the anti-serum from rabbit 5074 is able to detect AtASY3-C recombinant protein very clearly in all the lanes in which the protein was loaded into (Figure 10E). However, the anti-serum from rabbit 5073 does not detect the recombinant AtASY3-C adequately. Although there is some detection of the proteins in both the 1 μ l and 0.5 μ l lane, they are several fold less compared to the detection by the antiserum from rabbit 5074 (Figure 10E). Nevertheless, these validation studies revealed that the antiserum from rabbit 5074 contains the anti-ASY3 antibody, which can now be used for further studies of AtASY3.

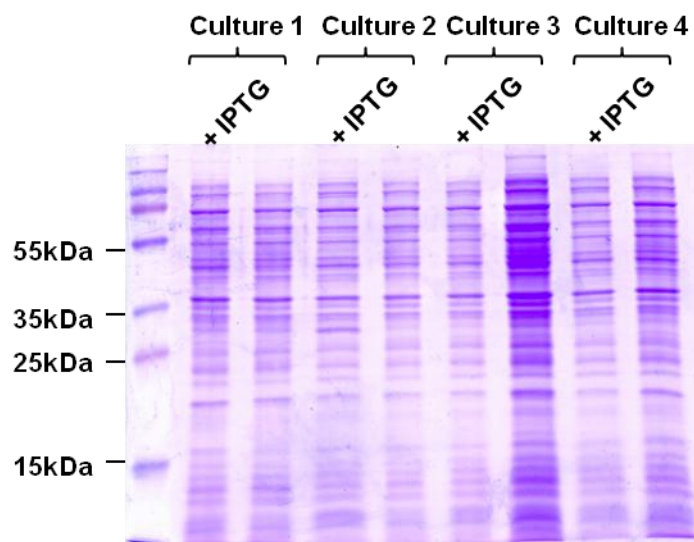
A



B



C



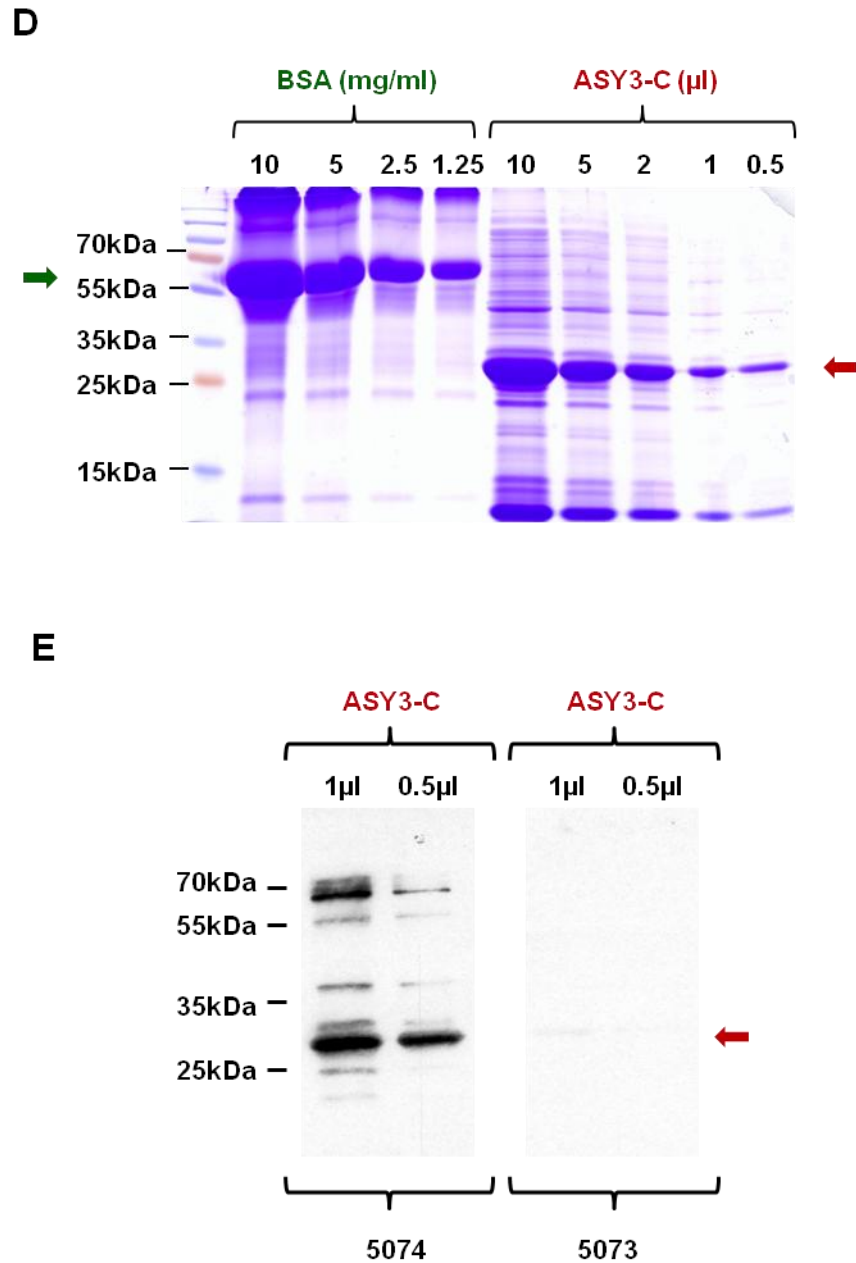


Figure 10. Cloning and detection of AtASY3-C recombinant protein and validation of anti-ASY3 antibody.

(A) A 702bp region of *AtASY3* C-terminal was amplified by PCR. (B) Coomassie blue staining of SDS-PAGE gel revealed that AtASY3-C (red arrow) was present in the insoluble fraction of the protein samples (C) AtASY3-C was absent in the soluble fractions (D) Coomassie stained SDS-PAGE gel showing various amounts of AtASY3-C after large-scale production for antibody preparation. Known concentrations of BSA allow estimation of protein concentrations in the samples. (E) Western blotting analysis revealed that the anti-serum from rabbit 5074 can efficiently detect AtASY3-C (red arrow) while that from rabbit 5073 does not detect the recombinant protein adequately.

4.7. Discussion

4.7.1. ASY3 is a putative meiotic axis protein in *Arabidopsis* and *Brassica*

Analysis of *B. oleracea* meiotic proteome led to the identification of a novel protein, AtASY3, with a putative meiotic role in *Arabidopsis*. Analysis of the protein revealed that it is weakly predicted to contain a putative NLS, a condensin-like domain and a DEAD-box helicase-like domain containing regions similar to P-loop NTPase. NLS allows protein to be imported into the nucleus while the condensin-like domain may provide structural properties to the protein. Furthermore, DEAD-box family of proteins are involved in chromatin remodelling during diverse cellular processes suggesting that AtASY3 may possess similar functional capabilities. (Linder and Jankowsky, 2011). More importantly, however, AtASY3 is predicted to contain a coiled-coil domain towards the C-terminal. Coiled-coil domains are known to provide structural stability and are involved in protein-protein interactions (Mason and Arndt, 2004). Interestingly, this structural feature is found in other meiotic proteins, such as RED1 in budding yeast, OsPAIR3 in rice and SCP3 in mammals, which are all components of the AE of the meiotic SC and so far reported to have no close homologues in other species. In addition to the similar coiled-coil regions AtASY3 was found to exhibit 16.4% and 25.6% identity to RED1 and OsPAIR3 respectively at sequence level. This is consistent with previous reports which highlight that meiotic axis/SC proteins exhibit little conservation in primary sequence level but shares certain structural properties (Higgins et al., 2005). These observations make AtASY3 an ideal candidate as a meiotic axis protein in *Arabidopsis*.

Additionally, homology analysis of AtASY3 revealed that it shares 75% sequence identity with the putative product of a locus in *B. rapa*. This prompted the cloning and sequencing of ASY3 from *B. oleracea*. Comparison of BoASY3 and AtASY3 revealed that the two were 85% identical in nucleotide level and 77% identical in amino acid level. Furthermore, BoASY3 was found to present in *B. oleracea* meiotic proteome (Sanchez-Moran et al., 2005, Osman et al., unpublished). These findings suggest that ASY3 is conserved between *Brassica* and *Arabidopsis*, which is not surprising as the two species are closely related and thought to have diverged only 14-18 million years ago (BRAD database).

4.7.2. AtASY3 is expressed in Arabidopsis meiocytes

Analysis of AtASY3 expression from a range of wild-type *Arabidopsis* tissues revealed that AtASY3 is expressed in flower buds. Since buds contain anthers with PMCs in them it is highly likely that AtASY3 may be involved during meiosis. Additionally, AtASY3 expression, although relatively reduced, was also detected in flowers. Flower contains the ovary where female gametogenesis occurs. Hence, it is likely that AtASY3 is also involved in female meiosis. Moreover, in *Arabidopsis*, female gametogenesis is relatively delayed compared to male meiosis to avoid self-fertilization. This may account for the comparatively lower expression of AtASY3 detected in flower by RT-PCR at that instance. Nevertheless, the expression analysis revealed no detection of AtASY3 in wild-type stem and leaf tissue thereby ruling out a

role of *AtASY3* in vegetative tissues. The finding that *AtASY3* is expressed in reproductive tissues is consistent with a role for it during meiosis.

4.7.3. *Atasy3* mutants display reduced fertility

To further analyse *AtASY3* the T-DNA insertion lines *Atasy3-1*, *Atasy3-2* and *Atasy3-3*, were obtained and the presence of their T-DNA verified. Subsequent RT-PCR analysis failed to detect *AtASY3* expression in flower buds from any of the mutant lines confirming that the T-DNA insertion successfully mutated *AtASY3* in all three mutant lines. Further analysis of *Atasy3* mutants revealed that their mean seed-set was reduced ~75% compared to the wild-type. Moreover, all three mutant lines contained a substantial proportion of non-viable pollen. These observations confirm that fertility is significantly reduced in all *Atasy3* mutants. Reduced fertility is often an indication of a meiotic defect and has been reported in previous studies of various *Arabidopsis* meiotic mutants (reviewed in Osman et al., 2011). Based on this, it is highly probable that the reduced fertility of *Atasy3* mutants may be a direct consequence of defects in their meiosis.

4.7.4. Anti-ASY3 antibody is capable of detecting recombinant ASY3

The anti-ASY3 antibody was produced primarily for immunolocalization studies of the protein. Although *AtASY3* showed limited identity to OsPAIR3 (25.6%) and Red1 (16.4%) at overall sequence level the proteins displayed relatively high conservation in their C-terminal which contained the coiled-coil domain. Hence, the C-terminal

region of *AtASY3* was cloned and expressed in *E. coli* for producing the recombinant protein *AtASY3-C*, which was subsequently used in generating the anti-ASY3 antibody in two different rabbits. In western analysis, the anti-serum from rabbit 5074 was able to detect *AtASY3-C* recombinant protein very clearly. However, the anti-serum from rabbit 5073 only weakly detected *AtASY3-C*. This may be because the inoculum failed to generate an appropriate level of immune response in the rabbit or vice versa. Nevertheless, the pre-immune serum from both rabbits taken before their inoculation with *AtASY3-C* was incapable of detecting *AtASY3-C*. Altogether, these observations suggest that the anti-serum from rabbit 5074 contains the anti-ASY3 antibody which is specific to *AtASY3* and therefore can be used for immunolocalization studies of *AtASY3*.

CHAPTER 5

Cytology and immunolocalization of ASY3

5.1. Introduction

Proteomic studies and homology analysis led to the identification of a novel coiled-coil protein, AtASY3 in *Arabidopsis*. Molecular characterization of AtASY3 revealed that the protein is meiosis-specific and is conserved in *Brassica*. Analysis of three *Atasy3* mutant lines revealed that all three lines exhibit reduced fertility, an indication of probable defects in their meiosis. This chapter describes the cytological investigation of *Atasy3* mutants carried out to verify and analyse the putative meiotic defects in them. Additionally, an anti-ASY3 antibody has been raised for immunolocalization studies of AtASY3. This chapter also illustrates the wild-type localization of AtASY3 and BoASY3 along with the immunolocalization of various meiotic proteins in *Atasy3* mutant. Furthermore, this chapter describes the cytological analysis of various genetic crosses of *Atasy3* which aid in understanding the meiotic role of AtASY3.

5.2. Cytological analysis of *Atasy3* mutants

To confirm that the reduction in fertility of *Atasy3* mutants was due to the disruption of AtASY3 gene DAPI-stained chromosome spread preparations from PMCs of all three *Atasy3* T-DNA insertion mutant lines were analysed using fluorescence microscopy.

Analysis of *Atasy3-1* revealed that chromosome behaviour in its early meiotic stages, leptotene and zygotene, were indistinguishable from those of the wild-type (Col-0) (Figure:11AB). However, normal pachytene nuclei were not observed in the *Atasy3-1*

mutant. Although there were no apparent defects in axis formation, it was clear that homologous chromosomes failed to synapse in *Atasy3-1*, in contrast to the wild-type which exhibit complete chromosome synapsis at pachytene (Figure:11C). Furthermore, at late diplotene/diakinesis it was apparent that a portion of the homologous chromosomes were not linked by any chiasmata in *Atasy3-1* (Figure:11DE). This was confirmed by the presence of univalents at metaphase I in the mutant, in stark contrast to wild-type metaphase I where five bivalents are observed (Figure:11F). In wild-type meiosis, the bivalents segregate normally at anaphase I followed by the segregation of sister chromatids at anaphase II which generates four haploid gametes. In comparison, the loss of COs and the presence of univalents in metaphase I in *Atasy3-1* lead to mis-segregation in both meiotic divisions resulting in the formation of aneuploid tetrads (Figure:11GHI). Cytological analysis of the meiotic stages of *Atasy3-2* and *Atasy3-3* revealed that the two mutant lines are cytologically indistinguishable from *Atasy3-1* (Figure 12A-F, G-L). Hence, these observations confirm that all three *Atasy3* T-DNA insertion lines undergo defective meiosis which leads to reduction in their fertility.

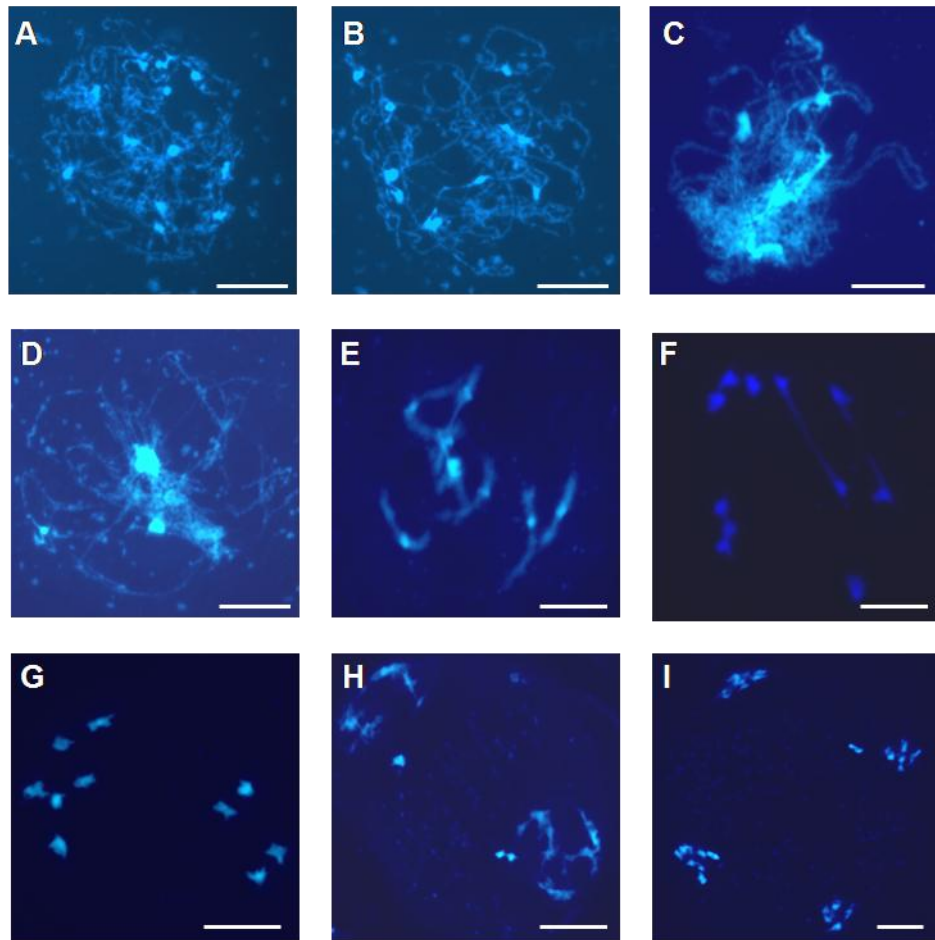


Figure 11. Representative meiotic stages from *Atasy3-1* PMCs.

Early prophase I stages, **(A)** leptotene and **(B)** zygotene in *Atasy3-1* are indistinguishable from those of wild-type, however, normal **(C)** pachytene was not observed in the mutant. Homologous chromosomes fail to undergo full synapsis in *Atasy3-1*. Chromosomes condense further in **(D)** diplotene and **(E)** diakinesis, where it is apparent that some chromosomes are not connected by chiasma. Both bivalents and univalents are present at **(F)** metaphase I. The lack of normal levels of COs in *Atasy3-1* lead to chromosome mis-segregation at **(G)** anaphase I leading to the formation of unbalanced **(H)** dyad and **(I)** tetrad. Bar 10 μ m.

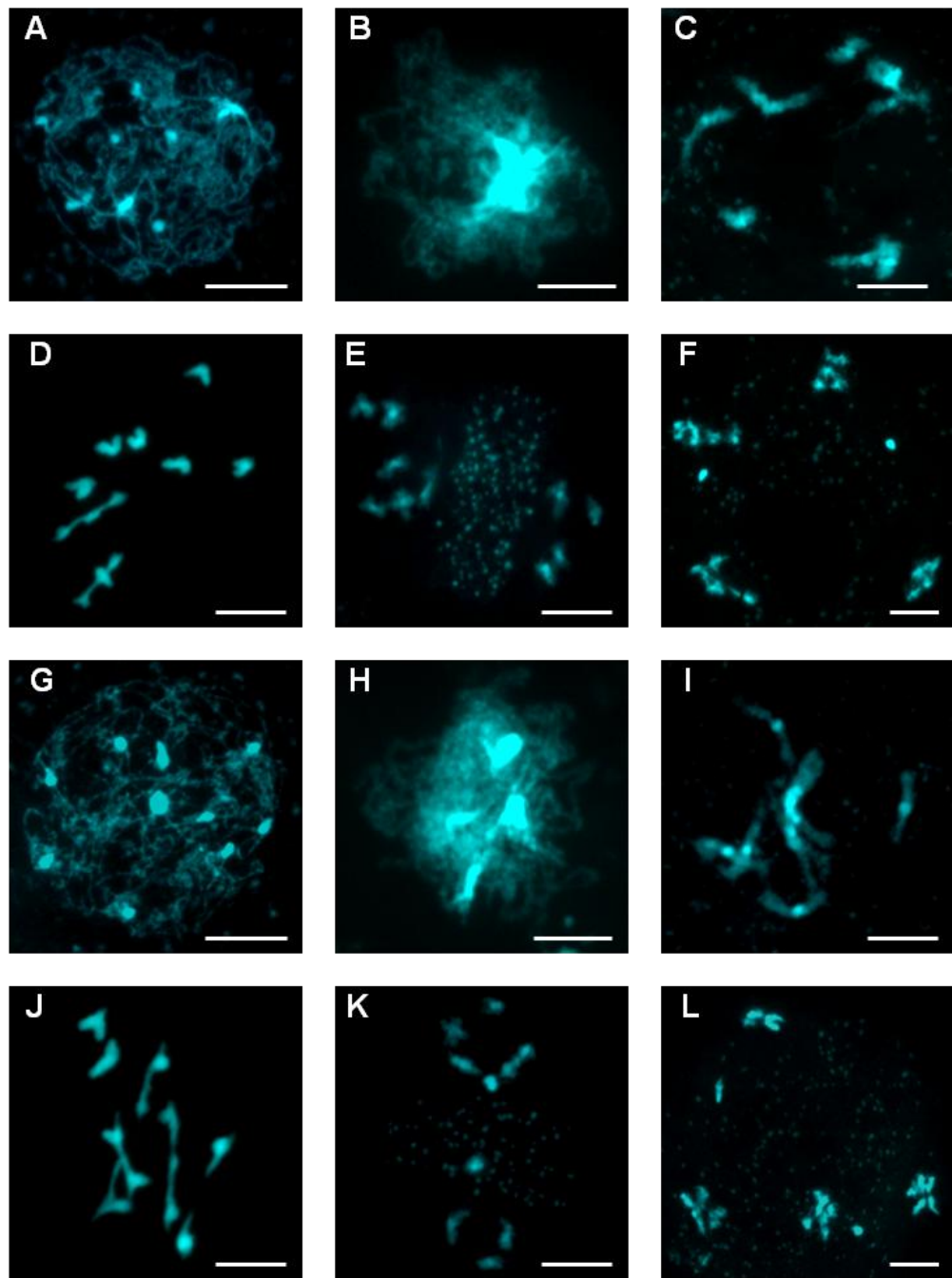


Figure 12. Representative meiotic stages of *Atasy3-2* (A-F) and *Atasy3-3* (G-L). Leptotene (A,G); pachytene (B,H); diakinesis (C,I); metaphase (D,J); dyad (E,K) tetrad (F,L). All stages are indistinguishable from their corresponding stages in *Atasy3-1*. Bar 10 μ m.

5.3. Verification of *Atasy3* mutant phenotype

5.3.1. Allelism test

To confirm that meiotic phenotype observed in *Atasy3* mutants was due to the disruption of the *AtASY3* gene an allelism test was carried out by crossing homozygous *Atasy3-1* and heterozygous *Atasy3-2* lines. As expected, approximately half the progeny were genotyped as homozygous *Atasy3-1/Atasy3-2* hetero-allelic knockouts which possessed a T-DNA in each allele of *AtASY3* obtained from either *Atasy3-1* or *Atasy3-2*. Cytological analysis of meiotic chromosome spreads from homozygous *Atasy3-1/Atasy3-2* revealed that chromosomes fail to synapse at prophase I in the double mutant (Figure 13Ai). Furthermore, univalents are formed at metaphase I which leads to the formation of unbalanced tetrads in the double mutant, similarly to homozygous *Atasy3-1* and *Atasy3-2* single mutant (Figure 13Aiii). Hence, the meiotic defects in *Atasy3-1/Atasy3-2* are indistinguishable from those of its parental lines. These observations therefore suggest that disruption of *AtASY3* leads to the aberrant meiotic phenotype observed in *Atasy3* mutants.

5.3.2. Complementation test

A complementation test was also carried out to confirm that the meiotic phenotype of *Atasy3-1* mutant was due to the knockout of *AtASY3*. In the complementation test, a wild-type copy of *AtASY3* cDNA was cloned and expressed in *Atasy3-1* and subsequent transformed lines were analysed for the recovery of wild-type phenotype.

The presence of wild-type features in transformed plants would indicate that the mutant *Atasy3* gene was complemented by the wild-type *AtASY3* cDNA and hence the former is responsible for the defective meiotic phenotype observed in *Atasy3* mutant.

5.3.2.1. Cloning *AtASY3* cDNA for complementation of *Atasy3* mutants

For the complementation test a modified pBluescript II plasmid containing the wild-type (Col-0) *AtASY3* cDNA with both 5' and 3' untranslated regions (UTRs) was obtained from RIKEN BRC (Japan). The plasmid was transformed into *E. coli* (DH5 α) and the presence of the cDNA verified using boil preparation and restriction digestion using *XhoI* and *BamHI*. Plasmid DNA was then extracted using wizard preparation (Promega) and sequenced for ensuring the integrity of the *AtASY3* cDNA nucleotide sequence. Since the *AtASY3* cDNA with the UTRs was ~3kb in length it was divided into 5 parts and each part sequenced by a separate primer designed using the *AtASY3* cDNA nucleotide sequence (resource number: pda19140) from RIKEN BRC database (<http://www.brc.riken.jp/lab/epd/catalog/cdnaclone.html>). The T7 promoter primer along with the primers, RED1_cDNA_F1, RED1_cDNA_F2, RED1_cDNA_F3 and RED1_cDNA_F4 were used to sequence overlapping regions from the 5' to the 3' end of *AtASY3* cDNA. The resulting nucleotide sequences were then conjoined in the correct order to obtain the full length nucleotide sequence of *AtASY3* cDNA. Analysis of the *AtASY3* cDNA nucleotide sequence revealed that it was identical to that from the RIKEN BRC database and hence can be used for complementation of the *Atasy3* mutant.

The *AtASY3* cDNA along with its 5' and 3' UTRs was amplified by PCR using Pfu DNA polymerase and the primers RED1_cDNA_FWD1 and RED1_cDNA_REV1 which had the restriction sites of *XhoI* and *SpeI* respectively incorporated in them. Subsequent gel electrophoresis revealed that, as expected, the PCR amplified a ~3kb product which was then extracted from the gel using QiaQuick gel extraction kit (Qiagen) (Figure 13B). The extracted product was ligated to pZERO, transformed into *E. coli* (DH5 α) and verified using boil preparation and double digestion using *XhoI* and *SpeI* restriction enzymes. Plasmid DNA containing the amplified product was then isolated using wizard preparation (Promega) and the two ends of the product sequenced using M13 reverse and forward primers. The results confirmed that the sequences analysed were from the 5' and 3' UTRs of *AtASY3* cDNA and contained the *XhoI* and *SpeI* restriction sites respectively. Subsequently, the *AtASY3* cDNA with the UTRs was isolated using *XhoI/SpeI* double digestion and gel extraction and sub-cloned into the expression vector, pPF408. The pPF408 plasmid contains a DMC1 promoter which is ideal for meiosis-specific expression of a desired product in *Arabidopsis*. The pPF408-*AtASY3* cDNA was then transformed into competent *E. coli* (DH5 α) and subsequently verified using boil preparations and *XhoI/SpeI* double restriction digestion. The plasmid DNA was subsequently isolated using wizard preparation (Promega) and transformed into *Agrobacterium tumefaciens* (LBA4404). Finally, the presence of the *AtASY3* cDNA was verified in various *Agrobacterium* colonies by colony PCR using the primers ASY3-1-F1 and ASY3-1-R1 and a selected colony was used to grow a bacterial culture for the subsequent transformation into *Atasy3-1* mutants.

5.3.2.2. Transformation of AtASY3 cDNA into *Atasy3* mutants and analysis of subsequent transformants

AtASY3 cDNA containing both 5' and 3' UTRs were transformed into *Arabidopsis Atasy3-1* mutants via the floral dipping method described by Clough and Bent, 1998. Flowering *Atasy3-1* mutant plants were dipped into the *Agrobacterium* culture containing pPF408-*AtASY3* cDNA. As a control an *Atasy3-1* mutant was dipped into an *Agrobacterium* culture containing only the pPF408 plasmid. The dipped *Atasy3-1* plants were then allowed to mature and produce seeds which were later harvested. Plants were grown from the harvested seeds on MS media containing BASTA for selection of transformants. Since pPF408 plasmid contains the BASTA resistance gene only transformed plants are able to survive on the selective media. Eventually, transformants which grew on the MS media which were later transferred and grown in pots containing soil compost.

The transformants were genotyped to verify their zygosity for *Atasy3* mutation using a set of 2 primers, one in exon 1 and the other in intron 1, designed to amplify solely genomic *AtASY3*. Genomic DNA from transgenic plants was amplified by PCR using the primers Comp_Geno_676-LP and Comp_Geno_676-RP while the presence of the T-DNA was verified using Comp_Geno_676-RP and LbB1.3. These experiments revealed that all the transformants were homozygous for the *Atasy3* mutation. Furthermore, the presence of the transgene was verified by PCR using the primers, ASY3-EX-C-LP (in exon 9) and ASY3-EX-C-RP (in exon 5) which were designed to amplify a shorter product from the transgene and a longer product from genomic

AtASY3. The analysis revealed that the shorter PCR product, therefore the transgene, was present in all the transgenics whose parental line was transformed with pPF408-*AtASY3* cDNA but not in the wild-type (Col-0) or the control transformant whose parental line was transformed with only pPF408.

The transformants were then analysed for the restoration of wild-type phenotype. Analysis of the transgenic plants revealed that seed count was increased in all plants compared to the *Atasy3-1* mutant and that the transgenics displayed varying levels of recovery of wild-type fertility (Table 4). Analysis of a transformant which displayed siliques of wild-type sizes (Figure 13Ciii) revealed that it had a mean seed set of 41.27 compared to 46.13 in the wild-type (Figure 13Ci), thus exhibiting ~90% level of wild-type fertility. In addition, the transformant displayed ~66% more fertility than *Atasy3-1* mutant which was grown in parallel and exhibited a mean seed set of 14.13 (Figure 13Cii). Furthermore, the control transformant whose parental line was transformed with only pPF408 exhibited a mean seed set of 14.9 which was not statistically different from *Atasy3-1* mutant ($p=0.4$, ANOVA), indicating that there was no increase in fertility in the absence of *AtASY3* cDNA. These results are consistent with the potential complementation of the mutant *Atasy3* gene in the transformant that displayed ~90% of wild-type fertility. To confirm the complementation of the mutant *Atasy3* gene chromosome spreads of various meiotic stages from the transformant were analysed using fluorescence microscopy. This revealed that homologous chromosomes were properly synapsed in pachytene (Figure 13Civ), in contrast to the *Atasy3-1* mutant which is asynaptic. Additionally, five bivalents were

observed along with the absence of univalents at metaphase I in the transformant (Figure 13Cv), unlike in *Atasy3-1* where univalents were found in metaphase I. The univalents in *Atasy3-1* lead to mis-segregation during meiotic divisions resulting in the formation of aneuploid tetrads in the mutant. In contrast, balanced tetrads were observed in chromosome spreads from the transformant suggesting chromosomes segregate normally in it, similarly to wild-type (Figure 13Cvi). These observations suggest that normal meiosis was restored in transgenics whose parental *Atasy3-1* mutant line was transformed with *AtASY3* cDNA. Therefore, the aberrant meiotic phenotype observed in *Atasy3-1* mutant is indeed due to the disruption of the *AtASY3* gene.

Percentage of fertility (seed-set)	Number of <i>Atasy3</i> ^{DMC1-ASY3} transformants
21-40 %	12
41-60 %	8
61-80 %	16
81-100 %	4

Table 4. Number of transgenic plants and the percentage of their fertility (mean seed-set) relative to the wild-type.

Percentage of fertility of transgenics was calculated by measuring their mean seed-set and comparing them to that of the wild-type. Transgenic plants exhibited varying range of fertility (mean seed-set).

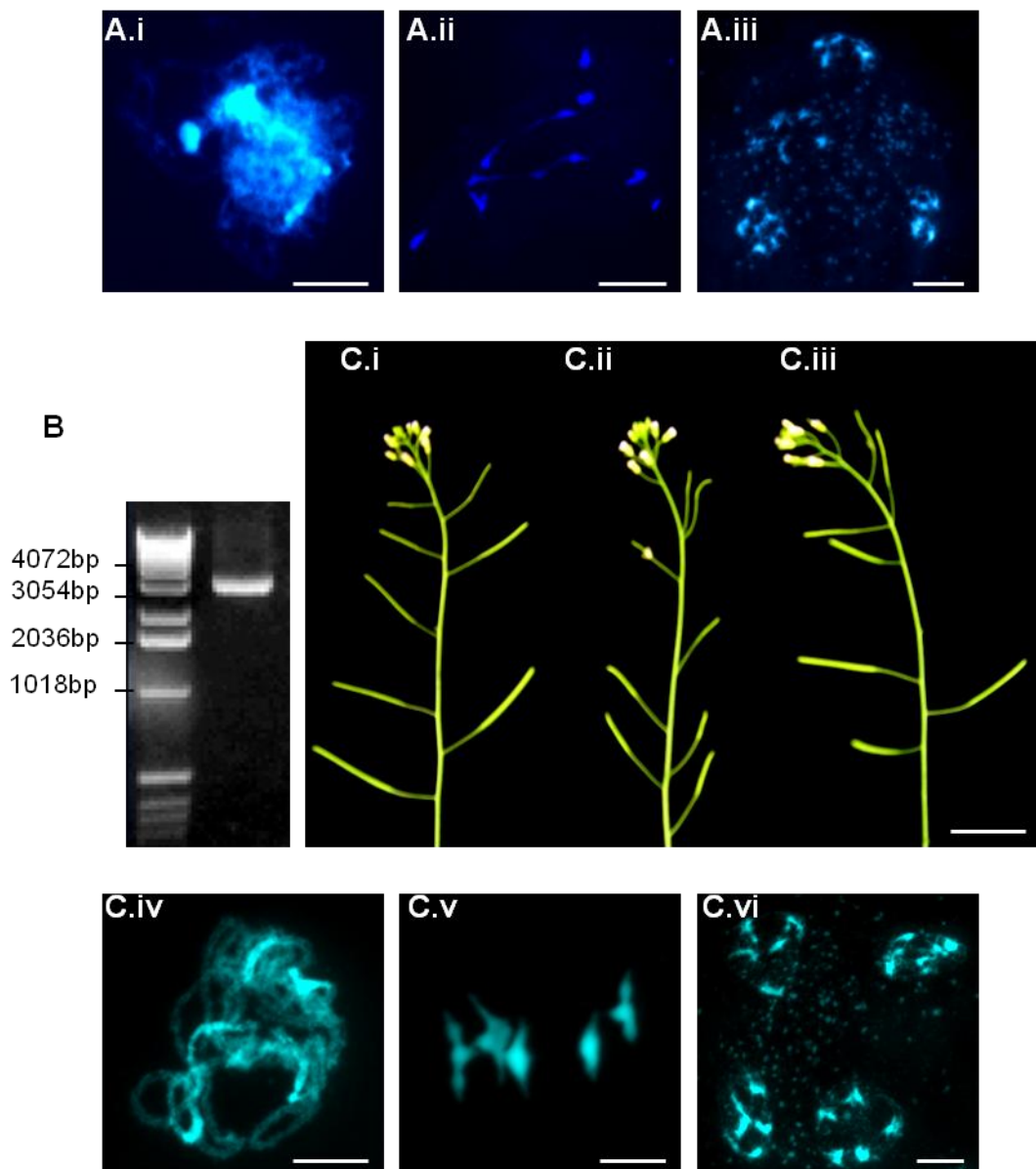


Figure 13. (A) Allelism and (B, C) complementation analysis.

(Ai) *Atasy3-1/Atasy3-2* exhibits (Ai) asynapsis in pachytene (Aii) loss of normal levels of COs and univalents in metaphase I. These lead to missegregation at meiotic divisions resulting in the formation of (Aiii) unbalanced tetrads. Bar 10 μ m. (B) PCR amplification of ~3kb *AtASY3* cDNA. (Ciii) Fertility in an *Atasy3* complementation line was restored to normal levels observed in WT (Ci) in contrast to *Atasy3* (Cii). Bar 10mm. Cytological analysis confirmed that normal meiosis was restored in the *Atasy3* complementation line. Homologous chromosomes underwent normal synapses in (Civ) pachytene. A full complement of five bivalents was observed in (Cv) metaphase I. These underwent normal segregation leading to the formation of balanced (Cvi) tetrads. Bar 10 μ m.

5.4. AtASY3 localizes to meiotic chromosome axes in early prophase I

The localization and distribution of AtASY3 on wild-type meiocytes were studied by immunolocalization using the anti-ASY3 antibody that was produced and found to be capable of detecting the recombinant AtASY3-C peptide in a western blot analysis. As a control, an immunolocalization study was performed on DAPI-stained wild-type (Col-0) chromosome spreads initially using the pre-immune serum from the rabbit which produced the anti-ASY3 antibody. This revealed that the pre-immune serum did not detect any signal suggesting that it did not contain any substance that was capable of detecting AtASY3. Immunolocalization studies were then carried out on DAPI-stained wild-type chromosome spreads using the antiserum which contained the anti-AtASY3 antibody in conjunction with antibodies that recognize the axis-associated protein, AtASY1 and the SC TF component, AtZYP1. The chromosome spreads were then visualized by fluorescence microscopy (Figure 14). The analysis revealed that AtASY3 foci were first detected on chromatin at late G2 phase concomitantly with AtASY1 localization. Although AtASY1 localizes as numerous foci on chromatin at G2, AtASY3 is predominantly nucleolar at this stage with relatively fewer foci associated with chromatin (Figure 14A). However, at early leptotene when AtASY1 signal appears to become axis-associated, the nucleolar association of AtASY3 disappears and the protein localizes as numerous foci on the chromosome axes (Figure 14B). Subsequently, at early zygotene, when AtASY1 is visible as a continuous linear signal, numerous punctuate foci and short stretches of linear AtASY3 signal can be observed (Figure 14C). By late zygotene, when AtZYP1 has polymerized into short stretches, some AtASY3 stretches are found to partially co-

localize with the AtZYP1 stretches. As prophase I progresses, AtASY3 gradually polymerizes such that at pachytene when AtZYP1 is visible as a continuous signal indicating a fully formed SC, AtASY3 also forms a continuous signal that partially co-localizes with AtZYP1 (Figure 14D). The AtASY3 signal was not observed in nuclei of later meiotic stages suggesting that the protein only persists till pachytene. These observations indicate that AtASY3 localizes to meiotic chromosome axes in early prophase I and remains axis/SC-associated till pachytene in wild-type meiocytes. To ensure specificity of the anti-ASY3, the antibody was used to perform an immunolocalization study on DAPI-stained prophase I chromosome spreads from *Atasy3-1*. This revealed that the antibody was unable to detect any AtASY3 in the mutant confirming that it was indeed specific to AtASY3 (Figure 14E).

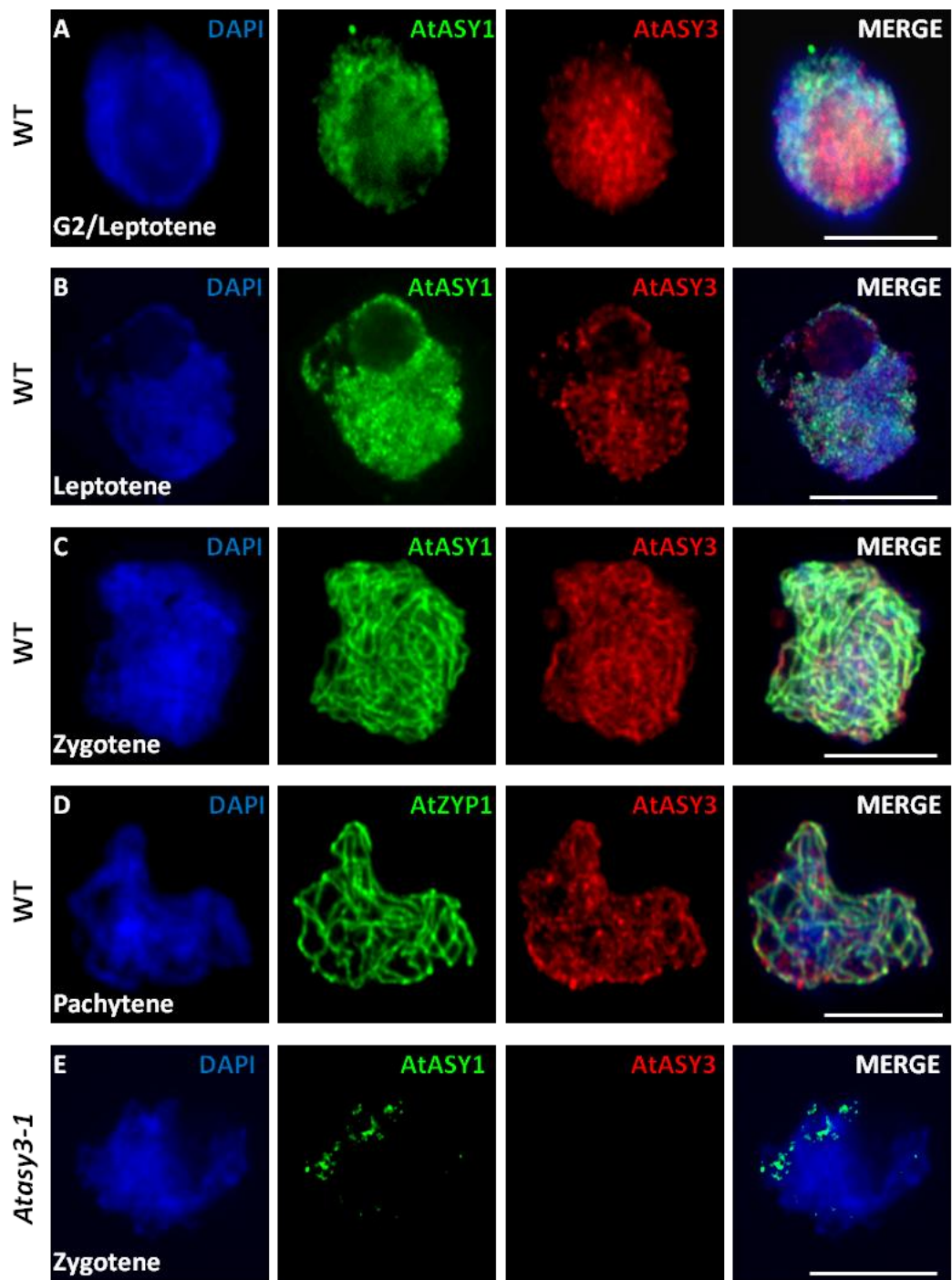


Figure 14. Immunolocalization of AtASY3 in WT.

(A) In late G2/early leptotene AtASY3 is predominantly nucleolar. (B) AtASY3 localizes in early leptotene as numerous foci which co-localize with AtASY1. (C) AtASY3 foci gradually polymerize as prophase I progresses. (D) Linear stretches of AtASY3 co-localize with AtZYP1. (E) AtASY3 signal is not observed in *Atasy3-1* mutant. Bar 10 μ m.

5.5. BoASY3 localizes to meiotic chromosome axes similarly to AtASY3

Since AtASY3 shares substantial sequence homology with BoASY3 it was probable that the anti-ASY3 antibody could detect BoASY3 in immunolocalization studies. If so, the antibody could be used to analyse BoASY3 localization and compare it with that of AtASY3. For this purpose, immunolocalization was performed initially on DAPI-stained chromosome spreads of *B. oleracea* using the pre-immune serum from the rabbit which produced the anti-ASY3 antibody. As expected the pre-immune serum could not detect BoASY3 (Figure 15D). Subsequently, to detect and analyse BoASY3 localization immunolocalization was performed on DAPI-stained chromosome spreads of *Brassica oleracea* using the anti-ASY3 antibody in conjunction with anti-ASY1 antibody. The analysis revealed that in leptotene BoASY3 localizes as numerous foci, most of which co-localize with the axis-associated foci and short stretches of BoASY1 (Figure 15A). At zygotene, numerous short stretches and foci of BoASY3 are observed which partially co-localize with the continuous linear signal of BoASY1 (Figure 15B). At late zygotene/early pachytene, just before BoASY1 dissociation when the protein produces a diffuse linear axis-associated signal BoASY3 is observed to form a continuous linear signal which co-localizes with BoASY1 (Figure 15C). These observations suggest that BoASY3 localizes to the meiotic chromosome axes during prophase I in *Brassica*. This phenotype is reminiscent to that of AtASY3 suggesting that the two share similar localization patterns and may be functionally homologous to each other.

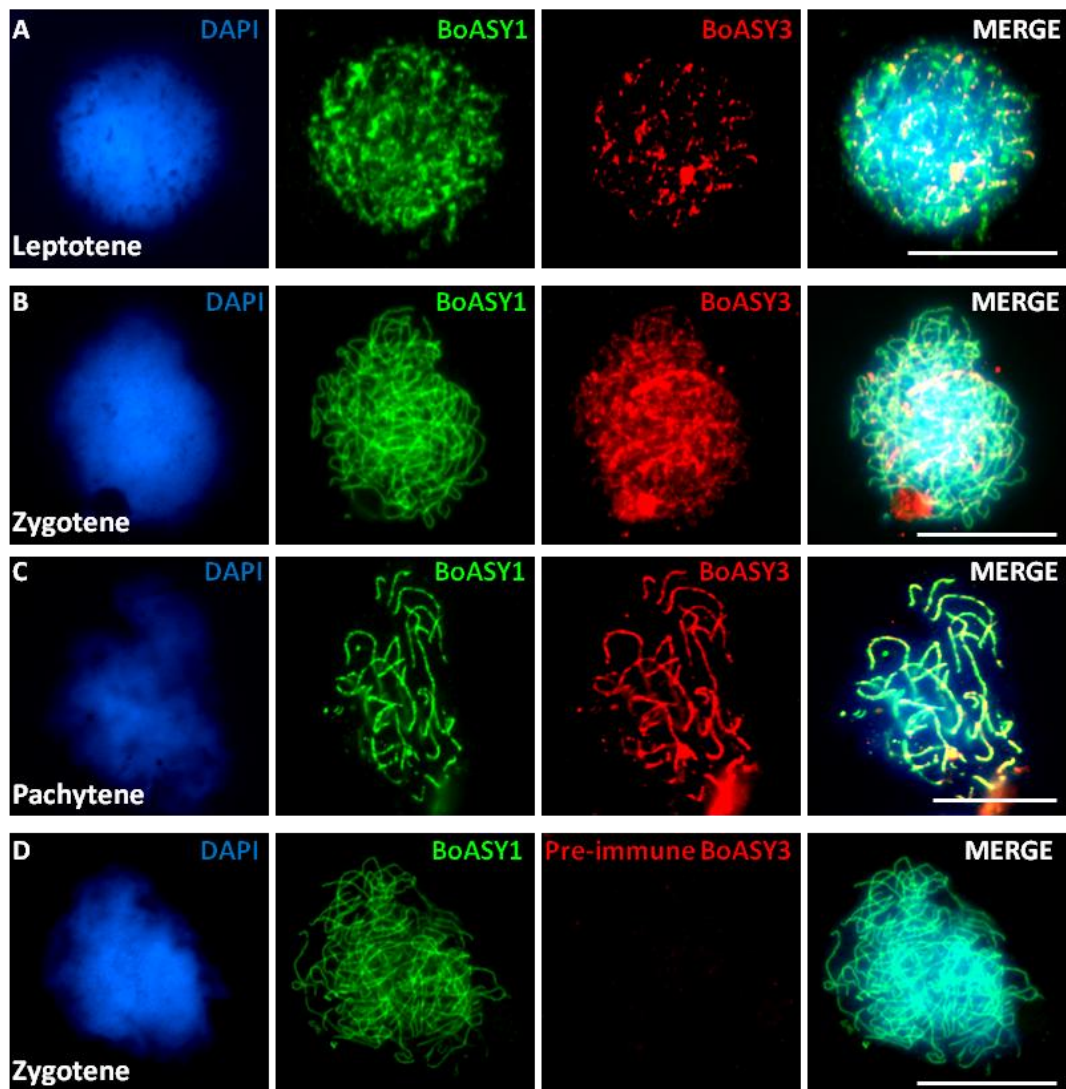


Figure 15. Immunolocalization of BoASY3 using anti-ASY3 antibody.

Brassica BoASY3 localises to meiotic chromosomes as numerous axis-associated foci in leptotene and gradually polymerizes, as prophase I progresses, to a continuous linear signal which co-localizes with the axis-associated signal of BoASY1 by late zygotene/early pachytene. The localisation of BoASY3 is reminiscent to AtASY3. BoASY3 was not detected using pre-immune anti-AtASY1 antiserum. Bar 10 μ m.

5.6. Analysis of meiotic chromosome axis and SC proteins in *Atasy3-1* mutant

Analysis of AtASY3 revealed that it is a meiotic chromosome axis protein and its absence leads to asynapsis during *Arabidopsis* meiosis. Hence the effect of the loss of AtASY3 on other axis components was investigated using immunocytological studies of the *Atasy3-1* mutant, whose meiotic defects are indistinguishable from the other two *Atasy3* mutant lines.

5.6.1. Meiotic cohesin components AtSMC3 and AtSYN1 localize normally in *Atasy3-1*

The localization of the meiotic cohesin proteins AtSMC3 and AtSYN1 were analysed by immunolocalization studies. In wild-type (Col-0), both AtSMC3 and AtSYN1 are first detected as numerous foci in early leptotene. As leptotene and zygotene progresses, both AtSMC3 and AtSYN1 foci linearize to form corresponding stretches which display partial co-localization. By pachytene both AtSMC3 and AtSYN1 signals appear as linear, continuous and co-localized with each other along the entire length of the chromosomes (Figure 16 A, C). Analysis of *Atasy3-1* chromosome spreads revealed that the localization of both AtSMC3 and AtSYN1 were indistinguishable from the wild-type. Both cohesin proteins were detected as linear continuous signals which were found to be axis-associated (Figure 16 B, D). The results confirm that loss of AtASY3 does not disrupt global sister chromatid cohesion in *Atasy3-1*. In contrast, analysis of AtASY3 localization using the anti-ASY3 antibody in *Atsyn1* mutant revealed that AtASY3 localization is completely disrupted in the mutant,

suggesting that localization of AtASY3 is dependent on AtSYN1 (Figure 16E). To investigate whether AtASY3 functions following AtSYN1 an *Atasy3-1/Atsyn1* double mutant was generated and chromosome spreads of its meiocytes were analysed using DAPI staining followed by fluorescence microscopy. This revealed that the double mutant exhibited extensive chromosome fragmentation throughout its meiosis (Figure 17G) and failed to form any chiasmata, consistent with the previously reported phenotype of the *Atsyn1* mutant (Bai *et al.*, 1999, Cai, 2003). The suppression of the meiotic defects of *Atasy3-1* by the fragmentation phenotype of *Atsyn1* in the *Atasy3-1/Atsyn1* double mutant suggest that AtASY3 localization and function is dependent on AtSYN1, and therefore the meiotic cohesin complex.

5.6.2. AtASY1 localization is disrupted in *Atasy3-1*

In wild-type meiocytes, the meiotic chromosome axis protein AtASY1 localizes to chromatin during late G2 as numerous foci. By early leptotene the AtASY1 foci forms axis-associated stretches which progressively polymerizes to a linear continuous signal along the entire length of chromosomes by late leptotene/early zygotene (Figure 16F). At pachytene, AtASY1 is depleted along the meiotic axis and its signal disappears soon afterwards. In contrast, analysis of *Atasy3-1* meiotic chromosome spreads revealed that normal AtASY1 localization is disrupted in the mutant. Immunocytological analysis of *Atasy3-1* revealed that initially at leptotene AtASY1 localizes as numerous chromatin-associated foci and short stretches which later become axis-associated similarly to wild-type. However, as prophase I progressed, instead of polymerizing to a linear signal AtASY1 was detected as discrete foci which

were evenly distributed on the chromosomes (Figure 16G). Further analysis revealed that the number of AtASY1 foci in each *Atasy3-1* meiocyte varied considerably from 42 to 132 with an overall mean of 74 per nucleus (n=20).

In wild-type, AtASY1 association with meiotic chromosome axes has been shown to be independent of AtSPO11-mediated DSB formation (Sanchez-Moran et al., 2007). To investigate whether the AtASY1 foci on *Atasy3-1* were DSB dependent an *Atasy3-1/Atspo11-1-4* double mutant was constructed by crossing a homozygous *Atasy3* with a plant heterozygous for *AtSPO11* gene followed by self-crossing their subsequent offspring. Chromosome spreads from *Atasy3-1/Atspo11-1-4* double mutant were then analysed by immunolocalization using the anti-ASY1 antibody. This revealed that the axis-associated AtASY1 foci remained on the double mutant suggesting that localization of the AtASY1 foci in *Atasy3-1* is independent of AtSPO11-mediated DSB formation, similarly to those in the wild-type (Figure 16H).

Since normal localization of AtASY1 was found to be dependent on AtASY3, localization of AtASY3 was analysed in the *Atasy1* mutant to investigate whether their localization relationship was reciprocal. Immunolocalization on DAPI-stained chromosome spreads from *Atasy1* using anti-ASY3 antibody revealed that localization of AtASY3 was indistinguishable from that in the wild-type (Figure16I). Therefore, although normal AtASY1 localization requires AtASY3, localization of the AtASY3 does not require AtASY1.

5.6.3. *AtZYP1* fails to polymerize in *Atasy3-1*

To investigate the defects in chromosome synapsis in *Atasy3-1* in more detail, localization of the SC TF component *AtZYP1* was analysed in the mutant and compared to that in wild-type. In wild-type meiocytes, *AtZYP1* localizes on chromatin as numerous foci at leptotene. At zygotene, numerous axis-associated *AtZYP1* foci and short stretches are observed. By pachytene, *AtZYP1* polymerizes to form the linear central region of the SC which produces a continuous signal along the entire length of homologous chromosomes and signals the completion of their synapsis (Figure 16J). In contrast, immunolocalization studies of *AtZYP1* localization in *Atasy3-1* revealed that the SC TF component fails to localize normally in the mutant. Although early localization of *AtZYP1* appeared normal, rather than polymerizing to form a continuous linear signal between the homologues as in wild-type, the protein formed discrete foci and short stretches which failed to polymerize into a continuously linear signal in *Atasy3-1* (Figure 16K). Further analysis revealed that the *AtZYP1* foci and short stretches in the mutant were often abnormally thick and distorted in appearance. Therefore, the analysis reveals that lack of *AtZYP1* polymerization in *Atasy3-1* forms the basis of the synaptic defects observed in the mutant.

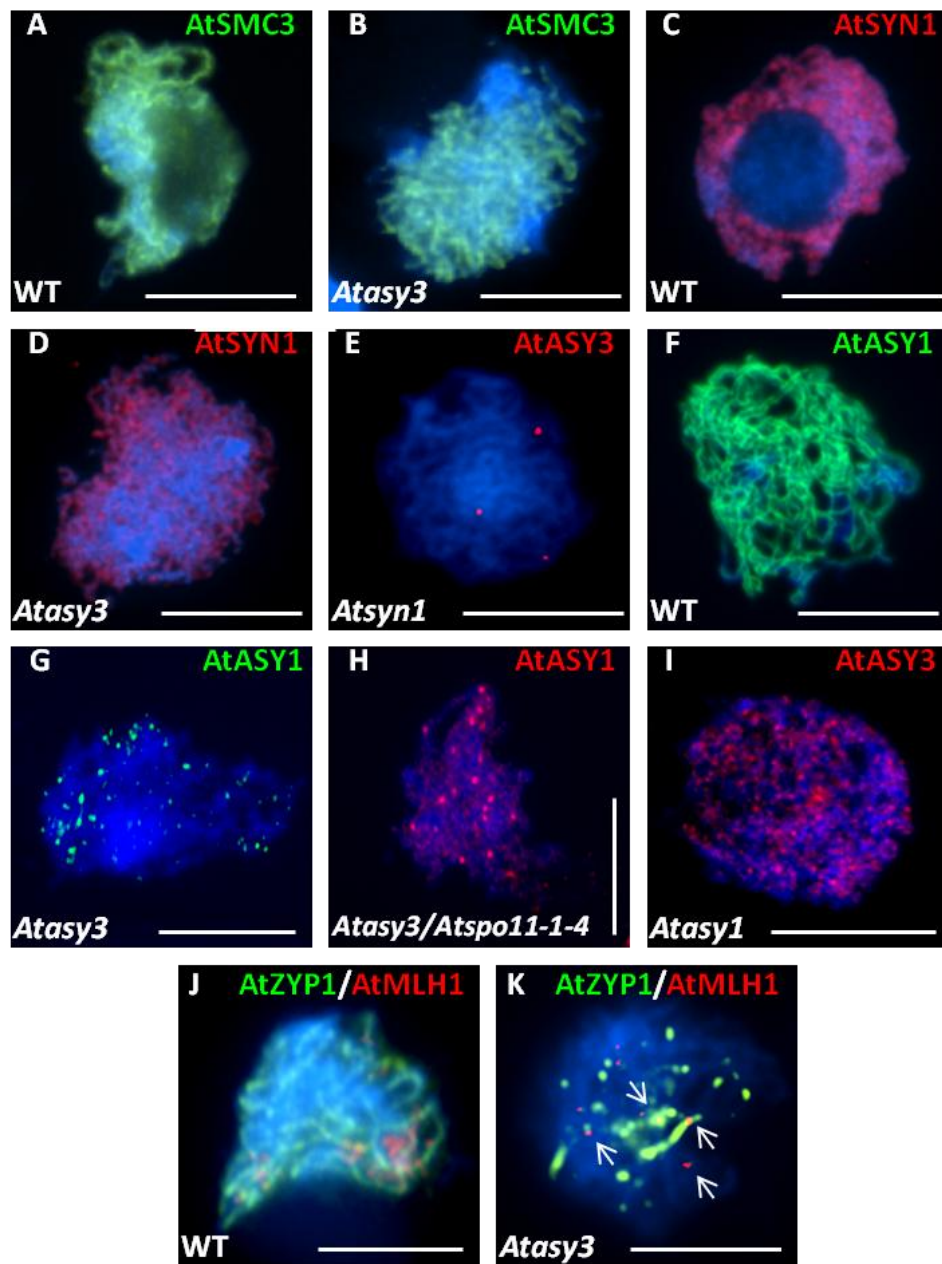


Figure 16. Immunolocalization of axis and SC proteins in *Atasy3-1*.

During WT leptotene both (A) AtSMC3 (green) and (C) AtSYN1 (red) localise as a continuous signal along meiotic chromosome axes. Similar loading patterns were observed for the two proteins (B, D respectively) in *Atasy3-1*. (E) AtASY3 fails to localize in *Atsyn1* mutant. (F) In WT, AtASY1 polymerizes along the entire length of meiotic chromosome axes in leptotene. (G) In contrast, AtASY1 fails to polymerize in *Atasy3-1*, instead the protein forms numerous discrete foci (~74, n=5) along the lengths of chromosomes. (H) The aberrant AtASY1 foci persist in *Atasy3-1/Atspo11-1-4*. (I) AtASY3 can localize normally in *Atasy1* mutant. (J) During WT pachytene, AtZYP1 polymerizes into a continuous signal, which co-localizes with AtMLH1. (K) In *Atasy3-1*, AtZYP1 fails to polymerize and forms discrete foci and/or short stretches, some of which co-localize with the remaining AtMLH1 foci (white arrows). Bar 10µm.

5.7. Chiasma frequency is significantly reduced in *Atasy3* mutants

Cytological analysis of diakinesis and metaphase I from *Atasy3* mutant lines revealed that a portion of the homologous chromosomes failed to form chiasmata in the mutants. To quantify the reduction in COs 50 *Atasy3-1* metaphase I nuclei were analysed by FISH using 5S and 45S rDNA probes. This revealed that the number of chiasmata varied between 0-6 per nuclei with each meiocyte possessing a mean chiasma frequency of 3.34 (Figure 17B). Furthermore, FISH analysis of *Atasy3-2* and *Atasy3-3* metaphase I nuclei revealed that they possessed a mean chiasma frequency of 3.17 (n=50) and 3.32 (n=50) respectively, which are not statistically different from that of *Atasy3-1* ($p \gg 0.05$ for both, ANOVA). These observations are in stark contrast with wild-type (Col-0) in which each meiocyte contain 8-12 chiasmata with an overall mean chiasma frequency of 9.76 (n=50) (Figure 17A). These results, therefore, suggest a ~65% reduction in chiasma frequency in *Atasy3* mutants compared to the wild-type. Analysis of the distribution of the residual chiasmata in *Atasy3* mutants revealed that 74.80% of the chiasmata were located at the distal regions of chromosomes. The distal localization of *Atasy3* chiasmata is similar to that observed in wild-type, in which 73.80% of the chiasmata are found in the distal regions of chromosomes (n=50).

To investigate whether the residual COs in *Atasy3-1* are DSB-dependent DAPI-stained chromosome spreads from an *Atasy3-1/Atspo11-1-4* double mutant were analysed using fluorescence microscopy. The analysis revealed that the double mutant failed to form any chiasmata and contained only univalents at metaphase I

(Figure 17H) in contrast to wild-type which has 5 bivalents containing 8-10 chiasmata per metaphase I nucleus. This observation confirms that the residual chiasmata formed in *Atasy3-1* are dependent on AtSPO11-mediated formation of DSBs.

Additionally, an *Atasy3-1/Atmsh4* double mutant was constructed to analyse whether the loss of AtASY3 is responsible for a reduction in MSH4-dependent or MSH4-independent COs. Chiasma frequency of *Atasy3-1/Atmsh4* double mutant was then analysed using FISH to determine whether loss of AtASY3 resulted in any further reduction in chiasmata over that observed in *Atmsh4*. Out of the 30 *Atasy3-1/Atmsh4* metaphase I nuclei analysed none were found to have any COs (Figure 17D). In contrast, FISH analysis of 30 metaphase I nuclei from *Atmsh4* grown in parallel revealed that the mutant exhibited a mean chiasma frequency of 1.10 (Figure 17C). Therefore, the loss of AtASY3 results in a further reduction of COs over the MSH4-dependent COs that are lost in *Atmsh4*. This observation suggests that AtASY3 is required for the formation of both MSH4-dependent and MSH4-independent COs.

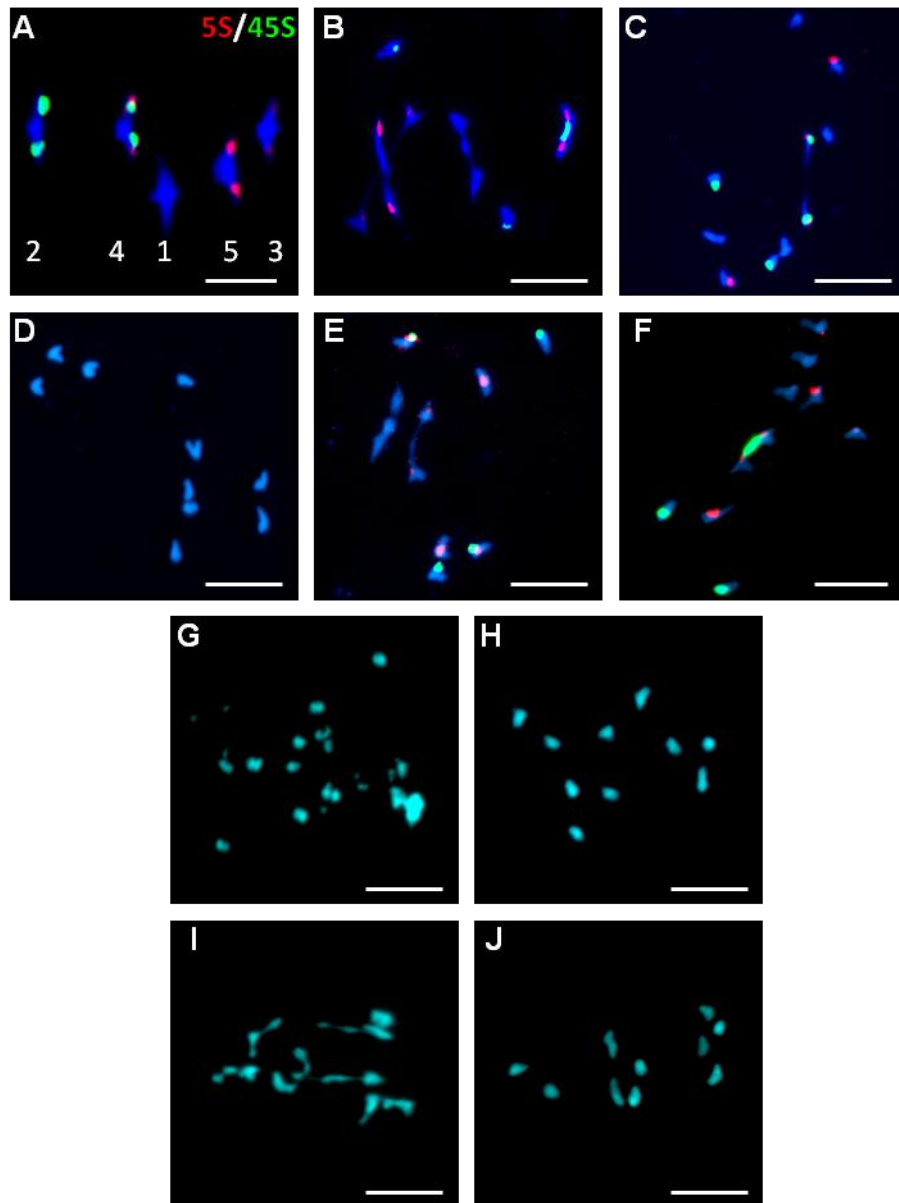


Figure 17. Cytological and FISH analysis of WT, *Atasy3-1* and various other mutants.

Analyses of metaphase I nuclei revealed that (A) WT exhibits a mean chiasma frequency of 9.76 (n=50). (B) In contrast, the mean chiasma frequency in *Atasy3-1* was significantly reduced to 3.34. (C) *Atmsh4* displays a mean chiasma frequency of 1.10 (n=50). (D) Whereas, *Atasy3-1/Atmsh4* failed to form any COs (n=30). (E) *Atasy3-1/Atasy1* exhibits a mean chiasma frequency of 1.78, which is statistically similar to that of (F) *Atasy1* but significantly reduced from that of (B) *Atasy3-1*. (G) *Atasy3-1/Atsyn1* and (I) *Atasy3-1/Atrad51* exhibit extensive chromosome fragmentation. (H) *Atasy3-1/Atspo11-1-4* and (J) *Atasy3-1/Atdmc1* failed to form chiasmata. Bar 10µm.

5.8. Analysis of recombination proteins in *Atasy3-1* mutant

To analyse the basis of the reduction of COs in *Atasy3-1* the localization of various recombination proteins were analysed by fluorescence immunolocalization using their corresponding antibodies.

5.8.1. DSB formation is reduced in *Atasy3-1*

The meiosis-specific histone variant H2AX is phosphorylated to generate γ H2AX soon after DSB formation (Rogakou et al., 1998). In wild-type meiocytes, γ H2AX forms numerous foci on chromatin encompassing DSBs in early prophase I. Therefore, γ H2AX foci may be used as an indicator for meiotic DSBs. Hence to investigate whether the loss of AtASY3 affects DSB formation the distribution of γ H2AX in *Atasy3-1* was compared to that in wild-type, assuming that H2AX was phosphorylated at all DSBs and the turn-over rate of DSBs were identical in both wild-type and *Atasy3-1*. Immunostaining analysis of γ H2AX on DAPI-stained chromosome spreads from *Atasy3-1* revealed that the mean number of γ H2AX foci per leptotene nuclei was 115 (n=5) (Figure 18B). This number was in stark contrast to the wild-type, which possessed on average 162 (n=5) γ H2AX foci per nuclei (Figure 18A). This observation suggests that DSB formation is significantly reduced in *Atasy3-1* ($P < 0.01$).

5.8.2. Number of foci of strand exchange proteins is reduced in *Atasy3-1*

Immunolocalization studies in wild-type meiocytes revealed that both strand exchange proteins AtRAD51 and AtDMC1 localize to meiotic chromosomes as numerous foci in early leptotene. Similarly, in *Atasy3-1* meiocytes, the two proteins localize as numerous foci in early prophase I although their numbers are significantly reduced. Immunostaining analysis revealed that the number of AtRAD51 foci was reduced from 142 in the wild-type (n=5) (Figure 18C) to 96 in *Atasy3-1* (n=5) ($P<0.05$) (Figure 18D). In addition, the number of AtDMC1 foci was reduced from 146 in the wild-type (n=5) (Figure 18E) to 110 in *Atasy3-1* (n=5) ($P<0.05$) (Figure 18F). These observations are consistent with the reduction in the number of γ H2AX in *Atasy3-1*.

To further investigate the relationship between AtASY3 and the two strand exchange proteins an *Atasy3-1/Atrad51* and an *Atasy3-1/Atdmc1* double mutant was generated by genetic crossing. Cytological analysis of the *Atasy3-1/Atrad51* meiotic chromosome spreads revealed that the double mutant fails to form any chiasmata and exhibits extensive chromosome fragmentation at metaphase I (Figure 17I). This phenotype is similar to that reported for the *Atrad51* single mutant and suggests that the double mutant fails to repair DSBs (Li, 2004). In contrast, cytological analysis of chromosome spreads from *Atasy3-1/Atdmc1* meiocytes revealed that although the double mutant did not exhibit any chromosome fragmentation, it only contained univalents at metaphase I (Figure 17J). This suggests that although DSBs are repaired the double mutant failed to form any COs, a phenotype reminiscent of the

Atdmc1 single mutant. Interestingly, the suppression of the meiotic defects of *Atasy3-1* in both *Atasy3-1/Atrad51* and *Atasy3-1/Atdmc1* double mutants suggest that AtASY3 plays a role in meiotic recombination downstream of the two strand exchange proteins.

5.8.3. Localization of AtMSH4 and AtMLH1 is reduced in *Atasy3-1*

The *Arabidopsis* MutS homologue AtMSH4 is required for the formation of normal levels of interference sensitive COs. Previously, AtMSH4 has been reported to localize on meiotic chromosome as numerous foci during leptotene. The number of AtMSH4 foci gradually decreases as prophase I progresses such that at pachytene only 9-10 foci are present on synapsed homologous chromosomes in each meiocyte. These remaining AtMSH4 foci were found to co-localize with AtZYP1 during wild-type pachytene (Higgins et al., 2008b). Immunostaining analysis of AtMSH4 localization in wild-type meiocytes revealed that a mean of 145 (n=5) foci were initially present per nucleus during leptotene (Figure 18G). As reported previously, the number of AtMSH4 foci per nucleus gradually decreased to 9-10, which were found to co-localize with AtZYP1 during pachytene. Immunolocalization studies on *Atasy3-1* chromosome spreads revealed a notable difference in the number of AtMSH4 foci during their initial localization in the mutant compared to that in the wild-type. Although numerous AtMSH4 foci were able to localize to chromosomes during leptotene their number was considerably reduced to a mean of 112 (n=5) per meiocyte in the *Atasy3-1* mutant (Figure 18H). As prophase I progressed the number of AtMSH4 foci in the mutant decreased gradually, similarly to wild-type. However, at

pachytene, instead of the 9-10 foci found in each wild-type nucleus only 0-4 AtMSH4 foci were observed that co-localized with the distorted AtZYP1 foci and stretches in each *Atasy3-1* meiocyte.

In addition, the localization of the MutL homologue, AtMLH1, thought to mark the sites of COs was also analysed in the *Atasy3-1* mutant and compared to that in the wild-type. It has been previously reported that approximately 8-12 AtMLH1 foci co-localize with AtZYP1 in each wild-type pachytene nucleus (Jackson *et al.*, 2006). In agreement, immunolocalization studies of wild-type chromosome spreads revealed that the mean number of AtMLH1 foci per pachytene nucleus was 10.20 (n=5) (Figure 18I). In contrast, similar analysis of *Atasy3-1* pachytene nuclei revealed that the mean number of AtMLH1 foci was significantly reduced to 3.1 per nucleus ($P < 0.01$ n=5) (Figure 18J). This number is consistent with the observed chiasma frequency of 3.34 in *Atasy3-1*. Furthermore, the residual AtMLH1 foci in *Atasy3-1* were found to co-localize with the aberrant AtZYP1 foci and short stretches observed in the mutant. Hence, it is likely that these AtMLH1 foci mark the sites for subsequent COs that are formed in *Atasy3-1* mutant. Interestingly, the reduction in AtMLH1 numbers revealed an important observation regarding the loss of recombination in the mutant. Earlier studies of recombination proteins in *Atasy3-1* revealed a coordinated reduction in the number of γ H2AX, AtRAD51, AtDMC1 and early AtMSH4 foci, reflecting a reduction of DSBs to ~70% of wild-type level in the mutant. However, the mean number of AtMLH1 foci and chiasmata in *Atasy3-1* were found to be 3.1 and 3.34 respectively, indicating an overall CO formation of only ~35% of wild-

type levels in the mutant. This suggests that there is an additional defect or defects during meiotic recombination in addition to the reduction in DSB formation in *Atasy3-1*.

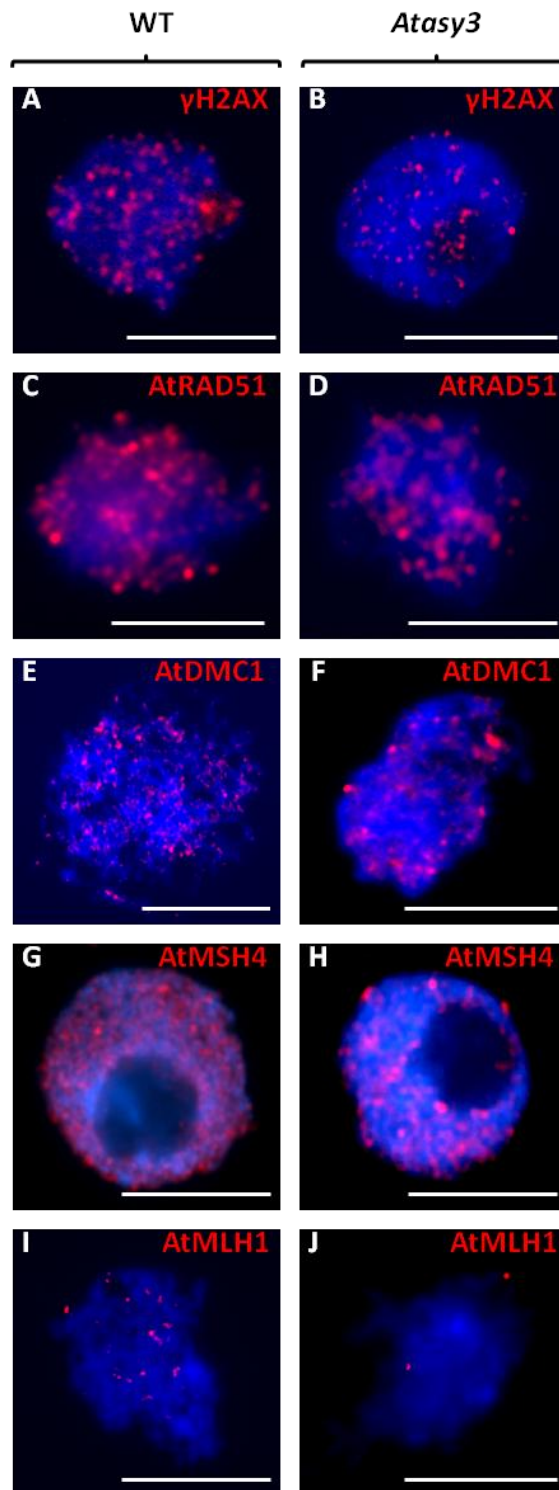


Figure 18. Immunolocalization of various recombination proteins in WT and *Atasy3-1*. Analysis revealed ~30% reduction in the number of γ H2AX, AtRAD51 and AtDMC1 in *Atasy3-1* (**B**, **D**, **F** respectively) compared to WT (**A**, **C**, **E** respectively). These figures indicate a ~30% reduction in the number of DSBs in *Atasy3-1*. (**G**) In WT, the mean number of initial AtMSH4 foci was 145. (**H**) This was reduced to 112 in *Atasy3-1*. (**I**) The mean number of MLH1 foci in WT was 10.20. (**J**) in contrast, this was reduced to 3.10 in *Atasy3-1*. N=5 for all studies. Bar = 10 μ m.

5.9. The residual AtASY1 foci stabilizes AtDMC1 in *Atasy3-1*

A previous study reported that stabilization of the strand exchange protein, AtDMC1 on meiotic chromosome axes requires the axis-associated protein, AtASY1 (Sanchez-Moran et al., 2007). The authors compared the localization of AtDMC1 in both *Atasy1* and wild-type using BrdU pulse labelling of PMCs coupled with immunolocalization. This revealed that in wild-type meiocytes, numerous AtDMC1 foci localized to meiotic chromosomes ~12h post pulse labelling at S-phase and a substantial portion of them persisted till ~30h post labelling. In contrast, although initial AtDMC1 loading in *Atasy1* was indistinguishable from that in wild-type, its number was considerably reduced by 24h post pulse-labelling. Furthermore, at 30h post pulse-labelling only a small proportion of the *Atasy1* meiocytes analysed contained only few AtDMC1 foci while all wild-type meiocytes were found to possess substantially higher number of AtDMC1 foci. These observations suggest that AtDMC1 is destabilized in the absence of AtASY1 (Sanchez-Moran et al., 2007). In *Atasy3*, normal localization and levels of AtASY1 was not observed. Hence the localization of AtDMC1 was analysed in the mutant for comparison with those in *Atasy1* and wild-type to verify whether *Atasy3* exhibits a similar scenario to *Atasy1* with regards to AtDMC1 loading. PMCs from the two mutants and the wild-type were subjected to BrdU pulse-labelling at S-phase followed by immunolocalization using anti-DMC1 and anti-BrdU antibodies and subsequently visualized using fluorescence microscopy. This revealed that in wild-type, *Atasy1* and *Atasy3-1* the maximum number of AtDMC1 foci accumulated on meiotic chromosomes ~12h post pulse-labelling at S-phase (Figure 19A). However, at 24h post BrdU pulse labelling AtDMC1 foci was entirely absent in *Atasy1* meiocytes (Figure 19A). In stark contrast,

there was no reduction in the number of AtDMC1 foci in *Atasy3-1* similarly to the wild-type (Figure 19A). Furthermore, at 30h post pulse-labelling a substantial number of AtDMC1 foci persisted on *Atasy3-1* and wild-type meiotic chromosomes while none was observed in *Atasy1* meiocytes (Figure 19A). These observations suggest that the rapid loss of AtDMC1 observed in *Atasy1* does not occur in *Atasy3-1*. The rapid loss of AtDMC1 in *Atasy1* represent a swift turnover of the protein presumably due to the loss of some AtASY1-mediated normal barrier to progression which allows recombination to proceed but causes some DSBs to be repaired via inter-sister interactions rather than inter-homologue recombination. Interestingly, the observation that the initial rate of AtDMC1 loading is normal and most of its foci persist throughout early prophase I in *Atasy3-1* suggest that the slight reduction in AtDMC1, observed earlier during immunolocalization studies in the mutant, may be due to a loss in overall DSBs rather than a swift turnover of the protein. This, therefore, suggests that although slightly reduced in number the remaining AtDMC1 foci are stabilized in *Atasy3-1*, most likely by the residual AtASY1 domains in the mutant.

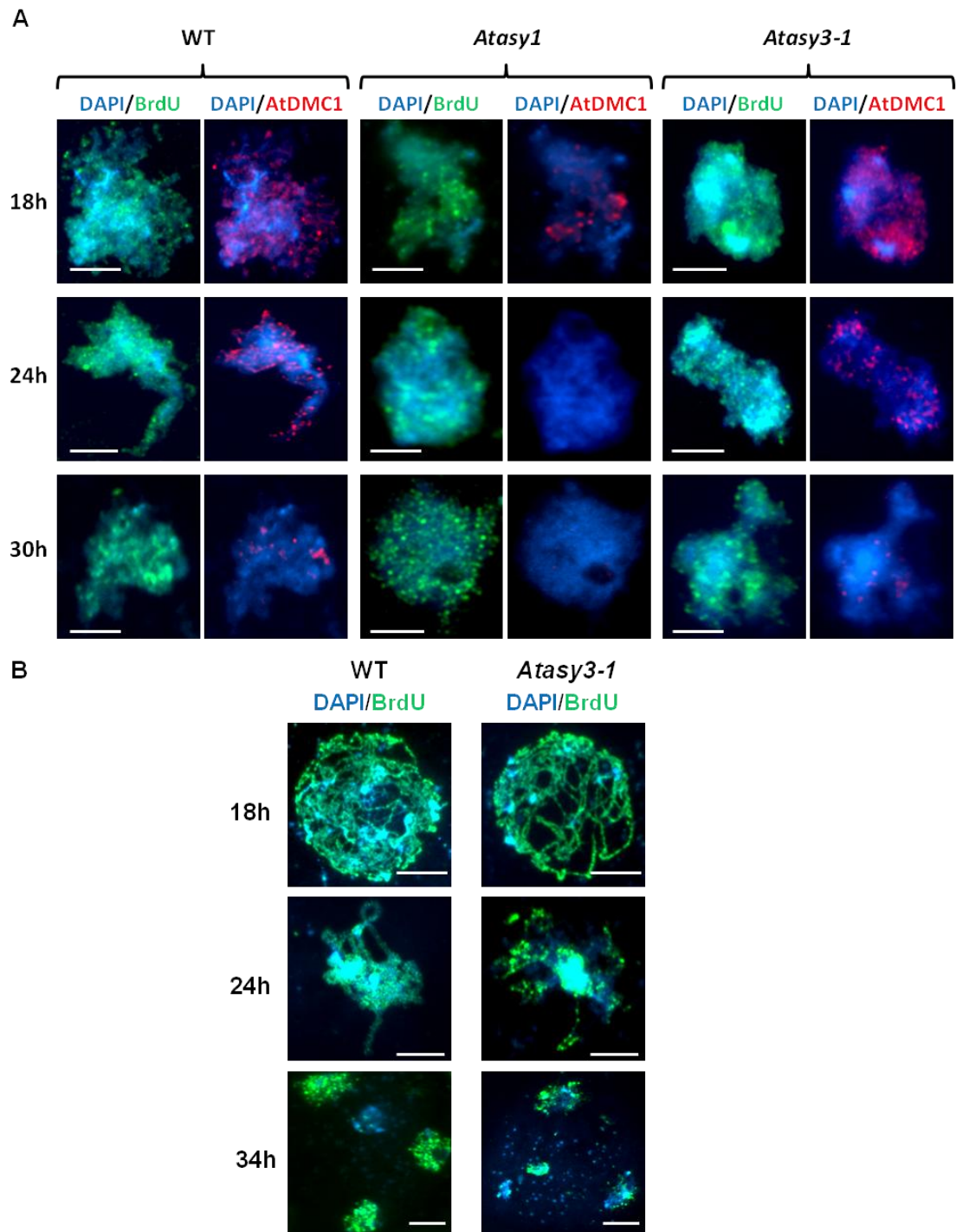


Figure 19. Time-course analysis of AtDMC1 localization in WT, *Atasy1* and *Atasy3* and of meiotic progression in *Atasy3-1*.

(A) Time-course analysis of AtDMC1 localization in WT, *Atasy1* and *Atasy3*. AtDMC1 foci in *Atasy3-1* persist in high numbers at least up to 24h post BrdU pulse labeling at S phase before gradually decreasing in abundance by 30h. This observation was similar to that in WT but in stark contrast to that of *Atasy1*, where AtDMC1 foci are destabilized soon after loading by ~18h. **(B) Time-course analysis of meiotic progression in *Atasy3-1*.** In WT, leptotene was labeled with BrdU 24h post pulse labeling, pachytene by 24h and tetrad by 34h post labeling. Similar observations were made for *Atasy3-1*. Bar 10µm.

5.10. AtASY1 is epistatic to AtASY3 with regard to CO formation

To study the relationship between AtASY3 and AtASY1 further an *Atasy3-1/Atasy1* double mutant was constructed and its chiasma frequency compared to those of *Atasy3-1* and *Atasy1* single mutants. FISH analysis using 5S and 45S rDNA probes on DAPI-stained metaphase I chromosome spread preparations from the double mutant revealed that it possessed a mean chiasma frequency of 1.78 (n=50) (Figure 17E). This was a significant reduction from the mean chiasma frequency of 3.34 (n=50) observed in the *Atasy3-1* single mutant ($P < 10^{-7}$, ANOVA) (Figure 17B). However, the mean chiasma frequency observed in the double mutant was not significantly different from that in *Atasy1* single mutant, which possessed an overall mean chiasma frequency of 1.88 (n=50; $P = 0.68$, ANOVA) (Figure 17F). These observations suggest that AtASY1 is epistatic to AtASY3 with regard to CO formation. Interestingly, the findings also suggest that the higher CO frequency in *Atasy3-1* compared to *Atasy3-1/Atasy1* double mutant may be due to the residual AtASY1 foci that remain in the single mutant.

5.11. Loss of AtASY3 does not affect progression of meiosis

In *Arabidopsis*, the normal duration of meiosis is ~34h in the wild-type (Col-0) (Armstrong et al., 2003, Sanchez-Moran et al., 2007). Previous studies of *Arabidopsis* meiotic mutants reported delays in meiosis due to defects in recombination (Higgins, 2004, Higgins et al., 2005, Jackson et al., 2006). To

investigate whether the loss of COs in *Atasy3-1* results in a delay during its meiosis, PMCs from the mutant were analysed along with those from the wild-type using BrdU pulse-labelling at S-phase followed by detection using anti-BrdU antibody and DAPI staining. This revealed that in wild-type, most pachytene chromosomes were found to be stained with BrdU at 24h post labelling suggesting that homologue synapsis was complete at this time period, consistent with previous reports (Armstrong et al., 2003, Higgins, 2004) (Figure 19B). Similar observations were made in the PMCs from *Atasy3-1* indicating that prophase I progressed normally in the mutant (Figure 19B). Additionally, wild-type tetrads were found to be BrdU-stained at 34h post labelling suggesting that meiosis was complete at this time period. This observation too was consistent with previous reports (Figure 19B) (Armstrong *et al.*, 2003, Higgins, 2004). Similarly to the wild-type, tetrads were also observed to be stained with BrdU at 34h post pulse labelling in the *Atasy3-1* mutant (Figure 19B). This suggests that loss of AtASY3 does not cause any delay in meiotic progression in *Atasy3-1*. This finding is not surprising as there is no evidence of chromosome fragmentation and hence, no apparent defect in the underlying DSB-repair process in the mutant. Furthermore, although there is a coordinated reduction in the number of various recombination proteins due to the loss of DSBs and/or synapsis, they were still found to localize presumably to recombination intermediates during early prophase I in *Atasy3-1*. Therefore, it is conceivable that, regardless of the consequences of the loss of AtASY3, the recombination machinery repairs DSBs which fail to undergo inter-homologue recombination, possibly via inter-sister interactions, thereby ensuring the timely processing of DSBs across recombination checkpoints in *Atasy3-1*.

5.12. Discussion

5.12.1. Loss of *AtASY3* results in asynapsis and other meiotic defects

Cytological analysis of the T-DNA insertion line *Atasy3-1* revealed that normal pachytene nuclei were not observed in the mutant line. Unlike in wild-type where homologous chromosomes were fully synapsed in pachytene they failed to synapse in *Atasy3-1*. This asynaptic phenotype of *Atasy3-1* was confirmed by immunolocalization studies of SC TF component AtZYP1. Instead of polymerizing to continuous linear signal as found in the wild-type AtZYP1 formed abnormal discrete foci or on occasion short stretches. These failed to polymerize into a continuous linear signal confirming that normal SC formation was disrupted in *Atasy3-1*. The disruption of the SC in *Atasy3-1* is further supported by EM studies of silver-stained chromosome spread preparations of meiocytes from the mutant, performed by our collaborators (M.P. and N.C.). Their analysis revealed that in contrast to the fully synapsed homologous chromosomes found in the wild-type *Atasy3-1* nuclei were diffuse and chromosome axes could not be clearly detected using similar spreading conditions. A subsequent modification in their technique then allowed the visualization of *Atasy3-1* nuclei where more extensive regions of the axis were visible. This revealed extensive disarrangement of chromosome axes in the mutant. Although in some cases there was some detectable alignment of axes the spacing between them appeared variable (M.P. and N.C., personal communication). Interestingly, the EM study of *Atasy3-1* meiocytes suggests that despite the asynapsis chromosome axes are still formed in the mutant. However, the observation

that the mutant nuclei appear diffuse indicates that there is likely an underlying structural defect in the axes that causes chromosome fragmentation during the spread preparations. Alternatively, it is also possible that axis formation remains incomplete in *Atasy3-1*. Nonetheless, the observation suggests that there may be abnormalities in the meiotic chromosome axes in *Atasy3-1*.

In addition to asynapsis, cytological analysis revealed that *Atasy3-1* fails to form normal levels of chiasmata between homologous chromosomes. Additionally, the mutant also contains univalents at metaphase I. These lead to mis-segregation at both meiotic divisions and results in the formation of aneuploid gametes. Similar phenotypes were also observed in meiocytes from the two other T-DNA insertion lines, *Atasy3-2* and *Atasy3-3*. Furthermore, the fact that these meiotic phenotypes were due to a mutation in *AtASY3* was confirmed by an allelism test as well as a complementation test. Taken together, these findings confirm that loss of *AtASY3* does indeed lead to defects during *Arabidopsis* meiosis.

5.12.2. *ASY3* is a meiotic chromosome axis protein in *Arabidopsis* and *Brassica*

AtASY3 localization was studied by immunolocalization using the anti-*ASY3* antibody, which has been produced and found to detect the C-terminal of the protein in western analysis. Preliminary immunolocalization studies using the antibody revealed that it was capable of detecting the *AtASY3* signal in wild-type meiocytes. Furthermore, no signal was detected in similar studies of meiotic chromosome

spreads from *Atasy3* mutants. In addition to confirming the RT-PCR analysis which indicated that the *Atasy3* mutants lack *AtASY3* transcript the above findings also highlight the successful production of an antibody capable of specifically detecting *AtASY3* in *Arabidopsis*. Subsequent immunolocalization studies of wild-type meiocytes using the anti-ASY3 antibody revealed that initially at G2 the *AtASY3* is predominantly nucleolar. This mirrors the initial localization pattern of certain meiotic proteins, such as *AtDMC1* and *AtRAD51*, which has also been observed to localize to the nucleolus during G2 (Klimyuk and Jones, 1997, Li, 2004). The significance of the nucleolar localization of meiotic proteins is not known but it is plausible that the nucleolus may serve as a storage area for the proteins prior to their actual localization during meiosis (Carmo-Fonseca et al., 2000). At early leptotene *AtASY3* was found to localize as numerous axis-associated foci which progressively polymerize to short stretches as prophase I progressed. At this stage all the *AtASY3* signals were found co-localized with the linear *AtASY1* signal, which marks the meiotic chromosome axes. Furthermore, by pachytene when *AtZYP1* is visible as a continuous signal indicating a fully formed SC, *AtASY3* formed a continuous signal that partially co-localizes with *AtZYP1*. These observations clearly indicate that *AtASY3* is meiotic chromosome axis protein. Furthermore, this is consistent with the finding that loss of *AtASY3* results in asynapsis in *Atasy3*.

Previously, homology analysis revealed that *AtASY3* is conserved in *B. oleracea* at primary sequence level. This prompted the analysis of localization patterns between the homologues during meiosis. Immunolocalization studies on *B. oleracea* prophase

I meiocytes using anti-ASY3 revealed that BoASY3 localization during early prophase I was indistinguishable from that of AtASY3. This indicates that like AtASY3, BoASY3 also localizes to meiotic chromosome axes and the two share stark resemblances in localization patterns during meiosis. Therefore it is highly likely that in addition to being similar in sequence level the two proteins are also functional homologues of each other.

5.12.3. Normal AtASY1 localization is dependent on AtASY3

Previous immunolocalization studies revealed that during wild-type meiosis the axis protein AtASY1 localizes as numerous foci at late G2 and progressively polymerizes into a continuous axis-associated linear signal by late leptotene (Armstrong et al., 2002). This pattern of AtASY1 localization was also observed during the analysis of wild-type meiocytes in this study. In contrast, although AtASY1 was found to initially localize as numerous axis-associated foci at early prophase I it failed to form a linear continuous signal as prophase I progressed in *Atasy3-1*. Instead, AtASY1 was found to form several discrete foci in the mutant, indicating a clear deviation from its normal loading pattern in the wild-type. More recently, a detailed analysis of the linear AtASY1 signal observed in wild-type meiocytes during early prophase I was carried out using deconvolution software in our lab. The findings suggest that AtASY1 is distributed along the axes as a series of hyper-abundant domains separated by stretches of lower abundance. These AtASY1 domains appeared evenly spaced and their numbers were found to be quite consistent (mean number per nucleus = 160, n=10) (J.H., F.C.H.F., personal communication). The domain-like organization of

AtASY1 is supported by EM studies of the protein in the plant *Crepis capillaris*. Immunogold labelling of AtASY1 on *C. capillaris* revealed that the gold particles formed discrete axis-associated clusters rather than a continuous linear signal (S. A., F.C.H.F., personal communication). Furthermore, this pattern of AtASY1 localization is highly reminiscent to that of its homologue in budding yeast, HOP1 which has been proposed to form domains of alternating hyper-abundance and lower abundance at early prophase I (Borner et al., 2008, Joshi et al., 2009). Although these latest observations suggest an underlying domain-like organization of AtASY1 in the wild-type itself, the localization pattern of the protein was still found to be aberrant in *Atasy3-1* compared to the wild-type. The most notable difference was that the mean number of AtASY1 foci in the mutant (74 per nucleus) was far fewer than the AtASY1 domains in the wild-type (160 per nucleus). Furthermore, the number of AtASY1 foci in *Atasy3-1* varied considerably from 42 to 132 in the meiocytes analysed, whereas, the AtASY1 domains in the wild-type were consistent in their numbers. Therefore, it is clear that loss of AtASY3 results in abnormal localization of AtASY1 during meiosis.

A previous study reported that in budding yeast the AtASY1 homologue HOP1 fails to localize to meiotic chromosome axes in the absence of the axis protein RED1 (Smith and Roeder, 1997). However, recent analysis of HOP1 revealed that although localization of normal levels of the protein requires RED1, some HOP1 is able to load onto DSBs sites independently of RED1 (Woltering et al., 2000). This relationship is similar to that observed between AtASY1 and AtASY3. Furthermore, while normal

AtASY1 localization was dependent on AtASY3, this relationship was not found to be reciprocal. This scenario too was also similar to budding yeast, where Hop1 localization requires RED1 but not vice versa. These observations indicate that AtASY1 and AtASY3 share similarities to yeast axis proteins Hop1 and Red1 in terms of their loading patterns during meiosis.

5.12.4. *AtASY1* localization in *Atasy3-1* is DSB-independent

Recent analyses using deconvolution software suggests that AtASY1 localizes as hyper-abundant domains along the axes during early prophase I. These domains were found to correlate both spatially and numerically with γ H2AX and AtDMC1 suggesting that they encompass DSB sites (J.H. and F.C.H.F., personal communication). This is in accord with a previous report proposing that AtASY1 promotes inter-homologue recombination during meiosis (Sanchez-Moran et al., 2007). However, AtASY1 is able to localize normally in *Atspo11-1-4* mutant indicating that its localization during prophase I is DSB-independent (Sanchez-Moran et al., 2007). This suggests that AtASY1 localization and recruitment of recombination machinery to the axes may not be inter-dependent events. Interestingly, the residual axis-associated AtASY1 foci observed in *Atasy3-1* mutant were also found in the *Atasy3-1/Atspo11-1-4* double mutant, which lack DSB formation. This suggests that, similarly to *Atspo11-1-4*, the formation of the AtASY1 foci in *Atasy3-1* is DSB-independent. However, it is unclear whether the AtASY1 domains in *Atasy3-1* and *Atspo11-1-4* are identical to those of the wild-type. If so, it would suggest that in wild-type AtASY1 is recruited to predetermined sites which encompass DSB hotspot,

possibly to promote inter-homologue recombination by establishing a bias favouring it. Alternatively, it is also possible that AtASY1 recruitment is influenced by DSB formation or the pre-DNA break recombination complex. Nevertheless, this would support the current accepted proposal in budding yeast that inter-homologue bias is established prior the break formation and that the bias is enforced afterwards during the transition of the nascent DSB to a joint molecule recombination intermediate (Schwacha and Kleckner, 1997). Hence, a more detailed analysis of the AtASY1 foci in *Atasy3-1* is required to clarify this avenue.

5.12.5. DSBs appear reduced in *Atasy3-1*

In *Arabidopsis*, the level of DSBs may be estimated by quantifying the number of the DSB marker, γ H2AX and/or the strand exchange proteins, AtRAD51 and AtDMC1 present in meiocytes during early prophase I (Sanchez-Moran et al., 2007). In wild-type prophase I meiocytes, the mean number of γ H2AX, AtRAD51 and AtDMC1 foci per nucleus were found to be 162, 142 and 146 respectively. In contrast, their numbers dropped to 115, 96 and 110 per meiocyte respectively in the *Atasy3-1* mutant. These figures indicate ~30% reduction in the number of γ H2AX, AtRAD51 and AtDMC1, and therefore, in the number of DSBs in *Atasy3-1*. However, since this method of DSB quantification is indirect it is arguable that not all the DSBs are detected in the mutant. Furthermore, due to the dynamic nature of meiotic recombination it is possible that all γ H2AX foci were not detected in *Atasy3-1*. Additionally, the statistical analysis which supported the variation in γ H2AX numbers between wild-type and *Atasy3-1* was based on observations from a small number of

cells (n=5), which may not provide a concrete evidence towards a decrease in γ H2AX numbers in the mutant. Nevertheless, as both the DSB marker and the strand exchange proteins show similar reduction in their numbers in *Atasy3-1* it can be surmised that their numbers reflect a true reduction in DSBs in the mutant.

An important aspect of meiotic recombination is its close coupling with the chromosome axes development. Hence the recombination machinery is found to be associated with the chromosome axes (Blat et al., 2002, Carpenter, 1975, Kleckner, 2006). However, there remains some obscurity to the issue of whether the recruitment of the recombination machinery precedes DSB formation or vice versa. Recent studies in budding yeast suggest that the DSB machinery becomes tethered to the chromosome axes prior to break formation (Panizza et al., 2011). This process has been found to require the axis proteins RED1 and HOP1 as mutants lacking either protein exhibit defects in DSB formation (Kim et al., 2010). Loss of normal levels of DSBs in *AtASY3*-deficient plants suggests that the protein may play a similar role during *Arabidopsis* meiosis. Therefore, it is plausible that *AtASY3* may be involved in organizing the chromosome axes such that it favours formation of normal levels of meiotic DSBs. This is supported by the observation that *Atasy3-1* mutant exhibits defects in axis formation during meiosis. However, it is also possible that loss of *AtASY3* results in a change in chromatin conformation that causes a subsequent reduction in DSB formation. Interestingly, the correlated reduction in the numbers of γ H2AX and the recombination proteins in *Atasy3-1* suggest that DSB formation occurs in context of the axis, lending support to the findings in budding yeast.

Whereas, if the recombination machinery was recruited to the axes following DSB formation then defects in the axes would not lead to a reduction in γ H2AX, which is not the case in *Atasy3-1*.

Interestingly, in a recent analysis the number of γ H2AX foci in *Atasy1* early prophase I meiocyte was found to be 129.5 (n=10), compared to 160.8 (n=5) in the wild-type (P=0.12). This suggests that albeit a small reduction there is no significant reduction in γ H2AX, and hence, DSB formation in *Atasy1* mutant (J.H. and F.C.H.F., personal communication). Therefore, while lack of AtASY3 leads to significant reduction in the number of meiotic DSBs, loss of AtASY1 does not have much effect on DSB formation. This observation is consistent with a previous study of AtASY1 (Sanchez-Moran et al., 2007). It is possible that the variation in DSB levels between *Atasy1* and *Atasy3-1* mutants may be due to the differences in the state of their meiotic axes. While axis formation was disrupted in *Atasy3-1*, the *Atasy1* mutant possess a clearly defined axes, although with some minor discontinuities (Pradillo et al., 2007). This therefore further highlights the importance the meiotic axes may play in ensuring the formation of normal levels of DSBs. However, it is worth noting that although loss of AtASY1 does not lead to a significant loss of DSBs in *Arabidopsis*, disruption of its homologues, HOP1 and HORMAD, result in severe losses of DSBs in budding yeast and mouse respectively (Daniel et al., 2011, Schwacha and Kleckner, 1994). The basis of this difference is currently unknown but may represent an underlying difference in the control of DSB formation between the organisms.

5.12.6. *AtASY3* is required for normal levels of CO formation

Investigation of three *Atasy3* T-DNA insertion lines revealed that chiasma frequency was reduced to ~34% of the wild-type level in all the lines analysed. Furthermore, analysis of *Atasy3-1/Atmsh4* revealed that the double mutant failed to form any COs, indicating that loss of *AtASY3* results in a loss of both interference-sensitive MSH4-dependent and interference-insensitive MSH4-independent COs. This finding suggests that *AtASY3* plays an important role early in the meiotic recombination pathway. Interestingly, reduction in chiasma frequency is also a phenotype of budding yeast and rice axis proteins, *RED1* and *OsPAIR3* respectively (Rockmill and Roeder, 1990, Schwacha and Kleckner, 1997, Yuan et al., 2009). In budding yeast *RED1* is proposed to impose a bias such that meiotic DSBs are repaired using the homologue rather than the sister as a template. It is suggested that *RED1* achieves this function by constraining the loading of the sister chromatid cohesion mediator, *REC8* at DSB sites. Loss of the protein is thought to alleviate the constraint on *REC8* loading thus shifting the bias towards inter-sister repair for meiotic DSBs (Kim et al., 2010). It is conceivable that loss of *AtASY3* results in a similar scenario during *Arabidopsis* meiosis. Intriguingly, the reduction in COs in *Atasy3-1* was found to be proportionally greater than that expected from the loss of DSBs in the mutant. Assuming that the ratio of COs to NCOs was maintained in the *Atasy3-1*, a ~30% reduction in DSBs should result in decrease of the mean chiasma frequency to 6-7 in the mutant. Instead, the mean chiasma frequency was found to be 3.34 indicating an additional loss of meiotic COs in *Atasy3-1*. Furthermore, there was no evidence of chromosome fragmentation suggesting that there was no overall DSB repair defect in the mutant. These observations indicate that there is a loss of inter-homologue bias

and that a higher proportion of meiotic DSBs were repaired using the sister chromatid as a template in *Atasy3-1*. This, therefore, suggests that AtASY3 may play a similar role to RED1 during meiotic CO formation in *Arabidopsis*. Alternatively, it is also possible that loss of AtASY3 may cause all or some recombination intermediates to be processed in such a way that result in the formation of NCOs rather than COs. Hence, further research is necessary to distinguish between the two possibilities.

Analysis of the distribution of the residual chiasmata in *Atasy3-1* revealed that ~75% of the chiasmata were located at the distal/sub-telomeric regions of homologous chromosomes. This observation is consistent with a previous report which suggest that prior to meiosis in *Arabidopsis* telomeres cluster while remaining associated with the nucleolus thereby bringing telomeres of homologous chromosomes into close proximity which may aide in subsequent pairing and genetic exchange between them (Armstrong et al., 2001). Similarly, a previous study also reported that virtually all the residual chiasmata in the *Atasy1* mutant were found to be in distal regions of homologous chromosomes, highlighting the importance of telomere clustering prior to meiosis in *Arabidopsis* (Ross et al., 1997).

5.12.7. Residual AtASY1 mediate AtDMC1-dependent inter-homologue recombination in Atasy3-1

Previous studies suggest that loss of AtASY1 leads to the destabilization of AtDMC1 during early prophase I resulting in the loss of inter-homologue recombination in *Atasy1* mutant (Sanchez-Moran et al., 2007). Analysis of *Atasy3-1* revealed that

AtASY1 fails to localize normally and its number is significantly reduced in the mutant compared to the wild-type. To investigate whether this leads to a similar scenario to that in *Atasy1* AtDMC1 localization during prophase I was compared between the two mutants and the wild-type. The study revealed that although there was a loss of AtDMC1 foci soon after their initial loading in *Atasy1* this was not the case in *Atasy3-1*, in which AtDMC1 persisted throughout early prophase I similarly to that in the wild-type. Interestingly, although the number of AtASY1 was reduced in *Atasy3-1* they were still found to localize as discrete foci to meiotic chromosome axes in the mutant. This suggests that the remaining AtASY1 is sufficient to stabilize AtDMC1 in the mutant. Consistent with this, analysis using deconvolution software suggests that virtually all the AtASY1 foci in *Atasy3-1* were found to co-localize with AtDMC1 and γ H2AX (J.H., F.C.H.F., personal communication).

To further analyse the impact of the remaining AtASY1 in *Atasy3-1* the chiasma frequency was analysed in an *Atasy3-1/Atasy1* double mutant. This revealed that the mean chiasma frequency was significantly reduced from 3.34 in *Atasy3-1* to 1.78 in the double mutant. This number, however, was not significantly different from the mean chiasma frequency of 1.88 in the *Atasy1* single mutant. This suggests that AtASY1 is epistatic to AtASY3 in terms of CO formation, although this relationship is reversed in terms of protein loading. Interestingly, a similar scenario is observed in budding yeast with regards to DSB formation and RED1 and HOP1 loading during meiosis (Rockmill and Roeder, 1990, Smith and Roeder, 1997). Although Hop1 localization is greatly reduced in the absence of RED1, the relationship is not

reciprocal. Additionally, *hop1* mutant which lacks HOP1 entirely exhibits a stronger defect in DSB formation than *red1*, which possess reduced HOP1 (Rockmill and Roeder, 1990, Smith and Roeder, 1997). Similarly, assuming that immunolocalization detects all the axis-associated AtASY1 foci in *Atasy3-1*, the observation that *Atasy3-1* exhibits relatively lower recombination defects than *Atasy3-1/Atasy1* suggests that higher number of COs in *Atasy3-1* is most likely due to the residual AtASY1 in the single mutant. Nevertheless, these remaining AtASY1 foci are still insufficient to promote wild-type levels of COs in *Atasy3-1*.

An interesting observation that emerged from the analysis of the residual AtASY1 in *Atasy3-1* was that the mean number of γ H2AX foci was greater than that of the AtASY1 domains and that these additional γ H2AX foci did not co-localise with AtASY1 domains in the mutant (J.H, F.C.H.F). If the loss of DSBs and AtASY1 domains in *Atasy3-1* occurred randomly it would lead to the formation of similar proportion of γ H2AX and AtASY1 foci that are not associated with each other, since DSB formation and AtASY1 localization are not inter-dependent processes. However, this was not observed in *Atasy3-1*, suggesting that some DSBs may occur outside of AtASY1 domains. One possibility for the lack of co-localization between some γ H2AX and AtASY1 foci could be that although the AtASY1 domains in *Atasy3-1* actually correspond to the position of the domains observed in wild-type, they are substantially smaller in size. Therefore, although these domains spatially associate with recombination complexes including γ H2AX they no longer appear co-localized during immunolocalization. Alternatively, some DSBs may occur in regions of lower

AtASY1 abundance which are found between the AtASY1 hyper-abundant domains. Interestingly, previous studies in budding yeast suggest that some meiotic DSBs are formed at random sites outside of DSB hotspots (Schwacha and Kleckner, 1997). Assuming that AtASY1 domains coincide with DSB hotspots, this may also be the case in *Arabidopsis*.

5.12.8. SC nucleation is sufficient to prevent ectopic recombination during meiosis

In addition to its structural role budding yeast ZIP1, along with other ZMM proteins, is also required for the formation of interference-sensitive COs during meiosis (Borner et al., 2004). In *Arabidopsis*, loss of the budding yeast ZIP1 homologue, AtZYP1 results in a slight reduction in chiasma frequency to ~80% of the wild-type level. However, the remaining COs has been reported to occur between ectopic chromosome regions, which are most likely to be duplicated sequences that amount to ~60% of the *Arabidopsis* genome. These COs result in the formation of univalents, multivalents, homologous bivalents and more importantly, non-homologous bivalents during metaphase I suggesting that CO control is compromised in *Atzyp1* (Higgins et al., 2005). Analysis of *Atasy3-1* revealed that SC formation and synapsis was extensively disrupted in the mutant. This was confirmed by immunolocalization which revealed that unlike in the wild-type AtZYP1 fails to polymerize into a continuous signal at early prophase I in the mutant. Instead, AtZYP1 formed discrete, abnormally thick and deformed foci and occasional short stretches during early prophase I in *Atasy3-1*. It is possible that some of these may represent an accumulation of

polycomplexes, nucleating at sites where AtZYP1 polymerization initiated but subsequently failed to continue. Interestingly, although *Atasy3-1* was essentially asynaptic there was no evidence of any ectopic recombination in the mutant. Although, COs were reduced in *Atasy3-1*, the remaining COs were always found to occur between homologous chromosomes and there was no evidence of multivalent formation. Earlier, immunolocalization studies revealed that the number of AtMLH1 foci was reduced to 3.1 in *Atasy3-1*, consistent with the reduction in its chiasma frequency. Nevertheless, all the remaining AtMLH1 foci, which are thought to mark CO sites (Jackson et al., 2006), were found to be invariably associated with the AtZYP1 foci and/or short stretches. These observations indicate that instead of extensive SC polymerization, the presence of AtZYP1 at sites of recombination is sufficient to prevent non-homologous interactions during *Arabidopsis* meiosis. Additionally, this finding confirms that in addition to its role in SC formation, AtZYP1 is also essential for maintaining CO fidelity during *Arabidopsis* meiosis. This is consistent with previous finding that AtZYP1 localizes as numerous foci early in leptotene well before SC formation during zygotene, suggesting it may play a role in CO formation in addition to SC formation (Higgins et al., 2005).

CHAPTER 6

Analysis of Arabidopsis asy1-T295A mutants

6.1. Introduction

In budding yeast, the AE proteins HOP1, RED1 and MEK1 are essential for establishing a bias towards inter-homologue recombination rather than inter-sister interactions during meiotic recombination (Niu et al., 2005). In addition to these the protein kinase MEC1 has also been implicated in partner choice during meiotic recombination. Budding yeast *mec1* mutant exhibits elevated levels of ectopic recombination (Grushcow et al., 1999). Furthermore, there is an accumulation of MEC1 in addition to HOP1, RED1 and MEK1 in the *dmc1* mutant which fails to form meiotic inter-homologue associations and arrest at late prophase I (Hochwagen and Amon, 2006). Additionally, *dmc1 mec1* double mutant proceeds through meiosis without repairing DSBs suggesting that MEC1 might be regulating a common process related to meiotic inter-homologue bias (Lydall et al., 1996, Weinert and Hartwell, 1988). MEC1 functions in conjunction with TEL1, similarly like their mammalian homologues ATR and ATM respectively (Mallory and Petes, 2000). Like their mammalian counterparts, MEC1 and TEL1 are serine/threonine kinases that preferentially phosphorylate their substrates on serine (S) or threonine (T) residues that precede glutamine (Q) residues, otherwise known as S/TQ motifs (Mallory and Petes, 2000, Traven and Heierhorst, 2005). Targets of ATM/ATR family proteins usually contain S/TQ cluster domains (SCDs) in which three S/TQ motifs are found within a region of 100 amino acid residues (Traven and Heierhorst, 2005). Interestingly, a recent study in budding yeast reported that HOP1 contains eight S/TQ motifs, three of which (S298, S311 and T318) form an SCD that acts as a target site for MEC1/TEL1 phosphorylation (Carballo et al., 2008). The study revealed that mutation of the S/TQ motifs within the HOP1 SCD in a *dmc1* mutant

resulted in repair of DSBs via RAD51-dependent pathway. This suggests that Mec1/Tel1-mediated phosphorylation of HOP1 SCD is required for preventing DMC1-independent repair of meiotic DSBs. Furthermore, the study also included a more detailed analysis of the effect of mutating each S/TQ motif within the HOP1 SCD individually. This revealed that mutation of T at residue 318 to Alanine (A) conferred a *hop1* mutant phenotype and resulted in the most severe reduction in spore viability compared to that resulting from the mutation of the other two S/TQ motifs within the SCD (Carballo et al., 2008).

Intriguingly, a previous homology analysis of HOP1 and its *Arabidopsis* counterpart AtASY1, conducted in our lab, revealed that the T318 S/TQ motif within the SCD in HOP1 was conserved in AtASY1 (residue T295). Furthermore, the T295 [S/T]Q motif of AtASY1 was present within 30 residues of two similar motifs, thus defining a putative SCD. These observations led to the construction of *Atasy1-T295A* mutants to verify whether the T295 residue in AtASY1 is important for normal functioning of the protein (E.C., F.C.H.F.). Colleagues in our lab used Site Directed Mutagenesis kit (Stratagene) to induce a point mutation that resulted in the conversion of T to A at residue 295 in AtASY1. The resulting *AtASY1^{T295A}* was cloned into pEarleyGate100 vector, which possessed a 35S promoter, using the Gateway recombination system. The plasmid was then transformed into *Atasy1* (SALK_144182) via *Agrobacterium* for subsequent expression of the transgene (E.C., F.C.H.F.). A preliminary immunostaining analysis of the resulting transgenic plants using anti-ASY1 antibody revealed that the antibody signal was detected in the transformants indicating the successful

expression of the transgene in them (A.M.,F.C.H.F.). However, the intensity of the signals varied between transformants reflecting the varying levels of expression of the transgene. Out of all the transformants analysed, early prophase I meiocytes from the transgenic line 511.54.1 displayed relatively higher levels of anti-ASY1 staining suggesting good expression of the transgene, *AtASY1*^{T295A} (A.M.,F.C.H.F.). Therefore this line was selected for carrying out a more detailed analysis of *Atasy1-T295A*. This chapter describes the molecular characterization and cytological analysis of the *Atasy1-T295A*. Additionally, this chapter also describes the analysis of AtASY1 protein expression pattern in *Atasy1-T295A*.

6.2. Molecular characterization of *Atasy1-T295A*

Atasy1-T295A (511.54.1) plants were grown on MS media containing the herbicide BASTA for selection of transformants. Since the pEarleyGate100 plasmid contains the BASTA resistance gene only transformed plants were able to survive on the selective media. Eventually, 9 transformants that survived the selection were transferred and grown in pots containing soil compost.

The transformants were initially genotyped to verify their zygosity for the *Atasy1* mutation. Genomic DNA from transgenic plants was amplified by PCR using the primers ASY1RP-EX1 and ASY1LP-EX5 while the T-DNA was detected using ASY1RP-EX1 and LbB1.3. The PCRs revealed that all the transformants were

homozygous for the *Atasy1* mutation. To determine the exact insertion site of the T-DNA in *Atasy1-T295A*, PCR product containing the partial T-DNA and *AtASY1* genomic sequence from a homozygous plant was ligated to pDRIVE cloning vector before being transformed into competent *E. coli* (DH5 α). Following verification of the product using boil preparations and restriction digestion using *EcoRI*, DNA was isolated using wizard preparation (Promega) and sequenced. The sequencing data was analysed using BLAST (NCBI) and TAIR Seqviewer. This revealed that the T-DNA insertion site in *Atasy1-T295A* was located at the third exon (521bp from start) in the genomic *AtASY1*, consistent with previous reports.

Subsequently, the presence of the transgene in *Atasy1-T295A* was verified by PCR using the primers, TRANS-ID-F1 and TRANS-ID-R1. These primers were designed such that half of each primer was specific to the end of one exon while its other half was specific to the beginning of the subsequent exon. This ensured the amplification of the transgene and not genomic *AtASY1*. PCR analysis of the transformants using these primers confirmed that the transgene was present in all the transgenics analysed. Additionally, the primers TRANS-ID-F1 and TRANS-ID-R1 were designed to be specific to sequences on either side of the 'GCA' codon in the transgene that coded for A instead of T at residue 295 in *AtASY1*. Hence, their amplified product should contain a point mutation replacing the nucleotide A with G at position 883 in the coding sequence of *AtASY1*. To verify if this point mutation was present in the transgene a PCR-amplified product of the primers was ligated to pDRIVE and transformed into competent *E. coli* (DH5 α). Following verification of the product using

boil preparations and restriction digestion using *EcoRI*, DNA was isolated using wizard preparation (Promega) and sequenced. Homology analysis of the sequencing data with *AtASY1* coding sequence using BLAST (ClustalW) revealed that the point mutation, resulting in the replacement of the nucleotide A with G at position 883, was indeed present in the nucleotide sequence of the transgene (Figure 20A). Moreover, analysis of the nucleotide sequence of the transgene in *Atasy1-T295A* using BCM Search Launcher (<http://searchlauncher.bcm.tmc.edu>) revealed that this point mutation leads to the replacement of T with and A at residue 295 in its predicted product (Figure 20B). These findings confirm that the transgene in *Atasy1-T295A* encodes a putative protein (hereafter referred to as *AtASY1*^{T295A}) in which the T295 [S/T]Q motif has been mutated to A.

A

```

AtAsy1      CATCTCGTGTTAACGCTAAAGGTC AAGAGCGTGCTTGATCCTTGTGAAGATGAAAATGAC 720
AtAsy1-TA  -----CGCTAAAGGTC AAGAGCGTGCTTGATCCTTGTGAAGATGAAAATGAC 47
          *****

AtAsy1      GACATGCAAGATGATGGTAAGAGTATAGGACCTGATTCTGTACATGATGACCAGCCTTCT 780
AtAsy1-TA  GACATGCAAGATGATGGTAAGAGTATAGGACCTGATTCTGTACATGATGACCAGCCTTCT 107
          *****

AtAsy1      GATTGAGATAGCGAGATCAGTCAAACACAAGAAAAATCAATTCATTGTGGCGCCAGTAGAG 840
AtAsy1-TA  GATTGAGATAGCGAGATCAGTCAAACACAAGAAAAATCAATTCATTGTGGCGCCAGTAGAG 167
          *****

AtAsy1      AACCAAGATGACGATGATGGAGAGGTTGATGAAGATGACAAACACAGGATCCGGCTGAG 900
AtAsy1-TA  AACCAAGATGACGATGATGGAGAGGTTGATGAAGATGACAAACACAGGATCCGGCTGAR 227
          *****

AtAsy1      AATGAACAGCAGTTAGCAAGGGTGAAGGACTGGATCAACTCCCCTGACCTTGATACTCTG 960
AtAsy1-TA  AATGAACAGCAGTTAGCAAGGGTGAAGGACTGGATCAACTCCCCTGACCTTGATACTCTG 287
          *****

AtAsy1      GAGCTCACAGATATTTCTTGCAAACCTCCCAAGATACTCAATAGTCTTACTGAAAGAAATC 1020
AtAsy1-TA  GAGCTCACAGATATTTCTTGCAAACCTCCCAAGATACTCAATAGTCTTACTGAAAGAAATC 347
          *****

AtAsy1      ATGGATCAGCTCGTGACAGAGGTTGTTCTTTGAAAACGGGGAAGGACATGTACATTAAA 1080
AtAsy1-TA  ATGGATCAGCTCGTGACAGAGGTTGTTCTTTGAAAACGGGGAAGGACATGTACATTAAA 407
          *****

AtAsy1      AAGAGAGACAAGACACCAGAGAGCGAATTACCTTTGTGAAAGAGGAAGCCGATGGTCAA 1140
AtAsy1-TA  AAGAGAGACAAGACACCAGAGAG----- 430
          *****

```

B

```

AtASY1      DDVTPPDYEPFFFRGCTEDEAQVWTKNPLRMEIGNVNSKHLVLT LKVKSVLDPCEDEND 240
AtASY1-T295A -----LKV KSVLDPCEDEND 15
          *****

AtASY1      DMQDDGKSI GPDSVHDDQPSDSSEI SQTQENQFIVAPVEKQDDDDGEVDEDDNTQDPAE 300
AtASY1-T295A DMQDDGKSI GPDSVHDDQPSDSSEI SQTQENQFIVAPVEKQDDDDGEVDEDDNAQDPAX 75
          *****

AtASY1      NEQQLARVKDWINSRHLDTILELTDILANFPDISIVLSEEIMDQLVTEGVL SKTGKDMYIK 360
AtASY1-T295A NEQQLARVKDWINSRHLDTILELTDILANFPDISIVLSEEIMDQLVTEGVL SKTGKDMYIK 135
          *****

AtASY1      KRDKTPESEFTFVKEEADGQISPGKSVAPEDYLYMKALYHSLPMKHVITIKLHMLDGEA 420
AtASY1-T295A KRDKTPE----- 142
          *****

```

Figure 20. Analysis of the nucleotide and amino acid sequence of the transgene in *Atasy1T295A*.

(A) The point mutation, resulting in the replacement of A with G at position 883 (red arrow) was present in the transgene. **(B)** The putative product of the transgene is predicted to contain A instead of T at residue 295 (red arrow).

6.3. Analysis of *Atasy1-T295A*

Analysis of *Atasy1-T295A* transgenic plants revealed that the transformants displayed normal vegetative growth. However, comparison of silique lengths from the transformants (511.54.1-511.54.9) revealed that their mean silique lengths varied between 6.4mm - 8.1mm (n=10 for each), all of which were significantly reduced from the mean silique length of 13.3mm in the wild-type (n=10) ($P < 0.0001$, ANOVA) (Table 5). Furthermore, analysis of seed sets from the transformants (511.54.1-511.54.9) revealed that their mean seed set varied between 5.3 - 8.3 (n=10 for each), all of which were also significantly reduced from the mean seed set of 49.50 in the wild-type (n=10) ($P < 0.0001$, ANOVA) (Table 6). Additionally, the mean silique sizes and seed sets of *Atasy1-T295A* transgenic plants were all highly similar to the *Atasy1*, which exhibit a mean silique length of 6.7mm (n=10) and seed set of 7.3 (n=10) (Table 5,6). These observations suggest that *Atasy1-T295A* transgenic exhibit severely reduced fertility, consistent with a meiotic defect.

Silique number (n)	Silique length (mm)										
	<i>Atasy1-T295A</i> (line 511.54.1.)									<i>Atasy1</i>	WT (Col-0)
	1	2	3	4	5	6	7	8	9		
1	9	7	6	9	9	8	8	6	7	6	14
2	8	8	7	9	7	9	8	6	6	8	13
3	8	8	6	9	8	7	7	9	7	7	15
4	7	8	6	8	8	8	8	8	7	7	14
5	7	9	6	6	8	8	8	7	6	6	13
6	6	7	7	8	9	7	9	8	6	7	14
7	9	9	6	6	8	7	10	11	6	7	14
8	8	7	7	7	6	8	7	6	6	7	12
9	7	8	6	7	7	9	7	8	7	7	13
10	7	7	7	7	7	7	9	9	6	5	11
MEAN	7.6	7.8	6.4	7.6	7.7	7.8	8.1	7.8	6.4	6.7	13.3

Table 5. Comparison of lengths of siliques from WT, *Atasy1* and *Atasy1-T295A* mutants.

Silique number (n)	Seeds per silique										
	<i>Atasy1-T295A</i> (line 511.54.1.)									<i>Atasy1</i>	WT (Col-0)
	1	2	3	4	5	6	7	8	9		
1	11	7	5	9	11	6	9	6	5	6	54
2	9	6	6	9	6	12	8	5	5	8	52
3	10	8	4	9	9	6	6	11	6	6	56
4	8	8	5	11	7	9	8	7	7	7	53
5	6	8	4	5	7	7	8	7	4	8	42
6	5	6	5	8	11	6	8	11	4	7	52
7	8	8	5	4	8	7	11	12	5	7	60
8	11	7	5	9	6	8	9	5	6	8	42
9	7	7	4	5	7	10	5	9	6	7	38
10	8	6	6	5	6	6	9	10	5	9	46
MEAN	8.3	7.1	4.9	7.4	7.8	7.7	8.1	8.3	5.3	7.3	49.5

Table 6. Comparison of mean seed-sets of WT, *Atasy1* and *Atasy1-T295A* mutants.

6.4. Cytological analysis of *Atasy1-T295A*

To verify whether the reduction in fertility of *Atasy1-T295A* was due to defective meiosis DAPI-stained chromosome spread preparations from PMCs of *Atasy1-T295A* were analysed using fluorescence microscopy. This revealed that although the early prophase I stages, leptotene and zygotene, were indistinguishable from those of the wild-type normal pachytene nuclei was not observed in *Atasy1-T295A*. In contrast to wild-type, which exhibit complete chromosome synapsis at pachytene homologous chromosomes failed to synapse in *Atasy1-T295A* (Figure 21A). Furthermore, at late diakinesis it was apparent that a portion of the homologous chromosomes were not linked by any chiasmata in *Atasy1-T295A* (Figure 21B). This was confirmed by the presence of univalents at metaphase I in the transformant (Figure 21C), unlike the wild-type metaphase I where five bivalents are present instead. The absence of normal level of COs in *Atasy1-T295A* leads to mis-segregation in both of its meiotic divisions resulting in the subsequent formation of aneuploid gametes in the transformed line (Figure 21D). These observations confirm that *Atasy1-T295A* exhibit severe defects during meiosis. Interestingly, the meiotic defects in *Atasy1-T295A* are reminiscent of the *Atasy1* mutant. Hence, these findings indicate that the product of the transgene, AtASY1^{T295A} is dysfunctional suggesting that replacing the T with an A at residue 295 of AtASY1 severely affects the meiotic function of the protein.

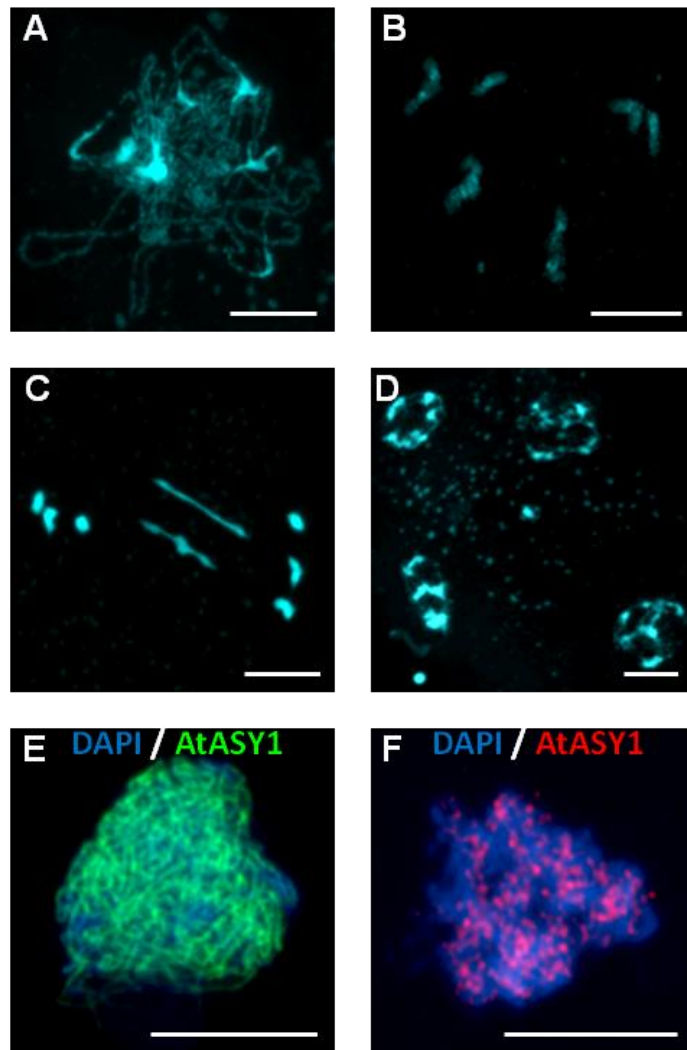


Figure 21. Cytology of *Atasy1T295A* and *AtASY1* localisation in the mutant.

(A) Homologous chromosomes fail to undergo synapsis in pachytene. (B) Loss of COs are apparent in diakinesis (C) Univalents are present in metaphase I. (D) These result in the formation of unbalanced tetrads. **E**) In WT, *AtASY1* polymerizes into a continuous signal in early prophase I. **F**) In contrast, *AtASY1* fails to polymerize, instead forms discrete foci in *Atasy1T295A*. Bar 10 μ m.

6.5. Normal AtASY1 localization may be disrupted *Atasy1-T295A*

Previous immuno-staining analysis revealed that anti-ASY1 antibody signal was detected in *Atasy1-T295A* suggesting that AtASY1^{T295A} was present during meiosis. Interestingly, a more detailed immuno-staining analysis of AtASY1^{T295A} localization revealed that AtASY1^{T295A} localized as numerous thick abnormal foci of varying shape and size during early prophase I in *Atasy1-T295A* (Figure 21F). Moreover, the continuous linear signal of AtASY1, as observed in early wild-type prophase I (Figure 21E), was not detected in any of the meiocytes analysed. These observations indicate that AtASY1^{T295A} localization to meiotic chromosomes during early prophase I is aberrant and not similar to AtASY1 localization in the wild-type. Furthermore, although a proportion of AtASY1^{T295A} appears to localize to chromosomes during meiosis, it is apparent that the protein is devoid of normal AtASY1 functions resulting in defects during meiosis in *Atasy1-T295A*.

6.6. Analysis of AtASY1^{T295A} protein expression in *Atasy1-T295A*

The analysis of *Atasy1-T295A* so far indicates that the transgenic line fails to undergo normal meiosis even though the product of the transgene, AtASY1^{T295A}, may be present in it. Hence, to confirm the presence of AtASY1^{T295A} in *Atasy1-T295A* proteins from early prophase I meiocytes of the transformant were extracted, probed with anti-ASY1 antibody and compared to AtASY1 expression in the wild-type.

6.6.1. Detection of AtASY1 in wild-type and *Atasy1* mutant

The presence of AtASY1 in protein samples from wild-type (Col-0) meiocytes was analysed by western blotting using a GST-tagged anti-ASY1 antibody raised in rat (No. 44). As a control, a similar analysis was also performed on meiotic proteins from *Atasy1* mutant. Proteins were extracted from wild-type and *Atasy1* meiotic buds using Quick Protein Extraction protocol (K.O.). The concentrations of proteins in the samples prepared were verified by BIORAD assay and equal amount (~40µg) of each sample was loaded into a SDS-PAGE gel for the subsequent detection of AtASY1. Additionally, ~10µg of each protein sample was also loaded into a separate SDS-PAGE gel for the subsequent expression analysis of the housekeeping protein Tubulin, which would ensure similar loading of the wild-type and mutant samples. Once the proteins in both gels were resolved by SDS-PAGE they were electroblotted to two different nitrocellulose membranes (GE Healthcare). The membrane with ~40µg of each sample was probed using anti-ASY1 antibody (1:1000) followed by an anti-rat secondary antibody (1:10,000). The other membrane with ~10µg of each sample was probed using a mouse anti-Tubulin antibody (Sigma) (1:5000) followed by an anti-mouse secondary antibody (1:10,000). Both the membranes were then visualized using ECL. Analysis of Tubulin expression ensured that approximately equal amounts of the wild-type and *Atasy1* samples were loaded into all the gels (Figure 22A). Additionally, analysis of AtASY1 expression revealed that the protein (~67kDa) can be clearly detected in the protein sample from wild-type meiocytes (Figure 22A). Furthermore, AtASY1 was undetectable in the protein sample from *Atasy1* mutant confirming that the mutant is deficient of the protein (Figure 22A). Interestingly, a product of shorter size (~62kDa) was detected in the

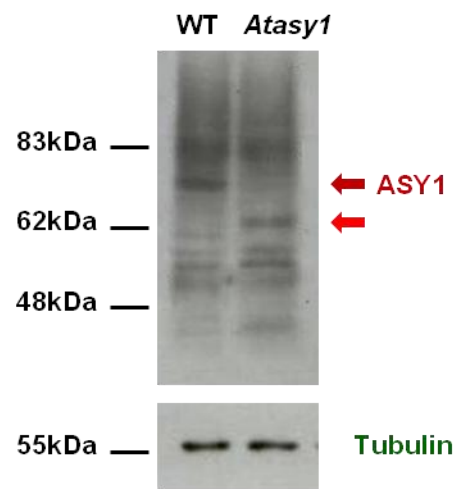
sample from the *Atasy1* mutant. This product was not present in the sample from the wild-type.

6.6.2. Detection of AtASY1^{T295A} in *Atasy1-T295A*

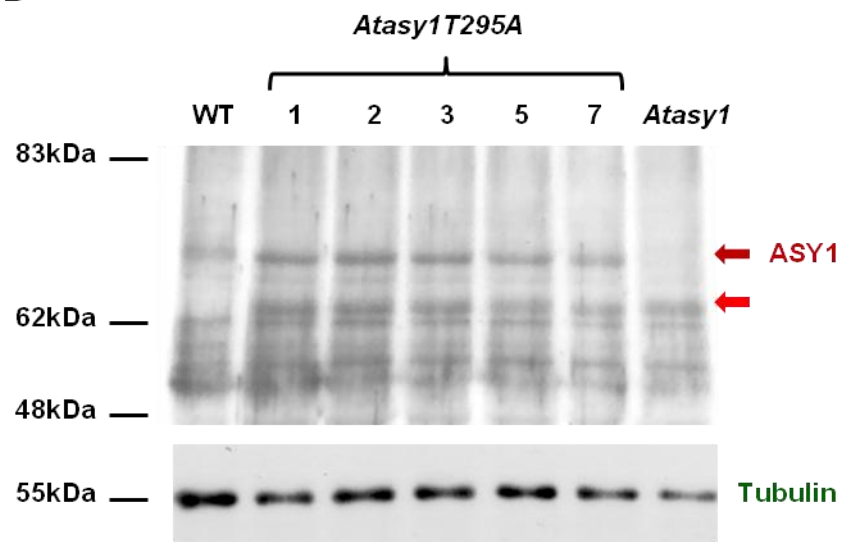
To determine whether AtASY1^{T295A} is expressed in the *Atasy1-T295A*, meiotic proteins were extracted from 5 different plants (511.54.1, 2, 3, 5 and 7) using Quick Protein Extraction protocol (K.O.). Each sample was quantified using BIORAD assay and subsequently ~20µg of each sample along with that of wild-type and *Atasy1* was loaded into a SDS-PAGE gel for the subsequent detection of AtASY1^{T295A}. Additionally, ~10µg of each protein sample was also loaded into a separate SDS-PAGE gel for the subsequent expression analysis of Tubulin. Once the proteins in both gels were resolved by SDS-PAGE they were electro-blotted into two different nitrocellulose membranes (GE Healthcare). The membrane with ~20µg of each sample was probed using anti-ASY1 antibody (1:1000) followed by an anti-rat secondary antibody (1:10,000). The other membrane with ~10µg of each sample was probed using a mouse anti-Tubulin antibody (Sigma) (1:5000) followed by an anti-mouse secondary antibody (1:10,000). Both the membranes were then visualized using ECL. Analysis of Tubulin expression ensured that approximately equal amounts of all the samples were loaded into all the gels (Figure 22B). Analysis of AtASY1 expression revealed that the protein can be detected in the protein sample from wild-type meiocytes (Figure 22B). More interestingly, the anti-ASY1 antibody is able to detect a product of similar size to AtASY1 in all the samples from the transgenic plants (Figure 22B). Additionally, this product was not detected in the

protein sample from *Atasy1* mutant (Figure 22B). Altogether, these findings suggest that AtASY1^{T295A} is expressed in *Atasy1-T295A*. Nevertheless, *Atasy1-T295A* still fails to undergo normal meiosis suggesting that replacement of T to A at residue 295 in AtASY1 renders the protein dysfunctional. Hence the S/TQ motif T295 of AtASY1 is essential for normal function of the protein during *Arabidopsis* meiosis. Further analysis suggests that the intensity of the anti-ASY1 signal is substantially higher in the samples from *Atasy1-T295A* mutants than in that of the wild-type indicating a difference in expression level between genomic *AtASY1* and the transgene *AtASY1^{T295A}*. Intriguingly, the shorter product (~62kDa) detected by anti-ASY1 in the sample from the *Atasy1* mutant was also observed in all the samples from *Atasy1-T295A*. However, this product was not observed in the sample from the wild-type suggesting that it is solely specific to *Atasy1* mutants.

A



B



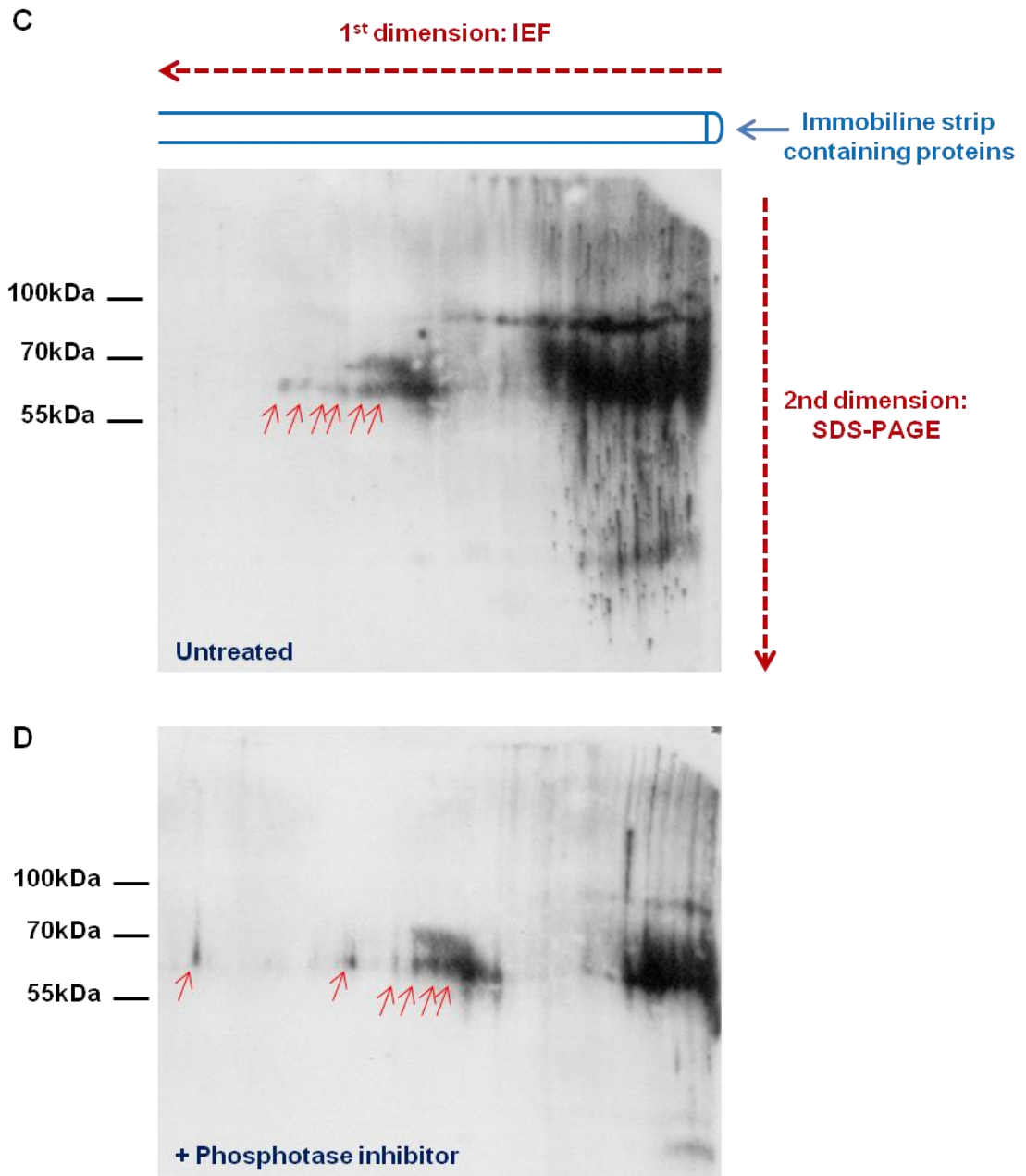


Figure 22. Western blotting analysis of ASY1 in extracts from WT, *Atasy1*, *Atasy1T295A* and *Brassica*.

(A) AtASY1 (dark red arrow) is detectable in extract from WT but not in that from *Atasy1*. A shorter product (light red arrow) is detectable in *Atasy1* but not in the WT. **(B)** AtASY1 (dark red arrow) is detectable in extracts from five *Atasy1T295* mutants confirming that the protein is present in the mutants. The shorter product (light red arrow) is also present in the *Atasy1T295* mutants **(C)** Western blotting analysis using anti-ASY1 antibody of 2D-PAGE resolved *B. oleracea* meiotic proteins showed at least 6 dot-like signals which are of similar sizes to BoASY1. **(D)** Similar analysis of *B. oleracea* extracts treated with phosphatase inhibitor revealed a variation in the distribution of the 6 dot-like putative BoASY1 signals, suggesting that the treatment may have resulted in changes in the phosphorylation states of BoASY1.

6.7. Preliminary analysis of ASY1 phosphorylation using 2D gel electrophoresis

Analysis of *Atasy1-T295A* suggests that AtASY1 may be a substrate for phosphorylation, which is essential for normal functioning of the protein. This finding prompted the detection of the phosphorylated states of the protein. Phosphorylated isoforms of proteins can be detected using two dimensional-polyacrylamide gel electrophoresis (2D-PAGE). During 2D-PAGE, proteins are first separated on the basis of their net charge by isoelectric focusing (IEF) followed by SDS-PAGE which separates the proteins by their mass. Therefore, this method is ideal for further investigation of the effect of phosphorylation on AtASY1. However, extracting large volumes of meiotic proteins from *Arabidopsis* is somewhat strenuous. Hence, the effect of phosphorylation was instead studied on the homologue of AtASY1, BoASY1 from *Brassica oleracea* (Armstrong et al., 2002), from which large volumes of meiotic proteins can be easily extracted. Early prophase I meiotocytes from *Brassica oleracea* were verified using aceto-orcein staining and light microscopy before the subsequent extraction of their proteins using Quick Protein Extraction protocol (K.O.). A sample from the extraction was treated with HALT phosphatase inhibitor (ThermoScientific) to preserve the phosphorylated states of proteins while another sample was left untreated. The protein samples were then quantified using BIORAD assay and ~90µg each sample was used for rehydration of two different 7cm immobilized drystrips (pH3-10,NL) (GE Healthcare). Rehydration of the strips followed by IEF and the subsequent equilibration of the proteins in the two samples were carried out as per manufacturer's instructions. Once the strips were focused and the proteins separated by their isoelectric point, each strip was placed sideways on top of a

separate 10% SDS-PAGE gel. As a control, ~40µg of *Brassica oleracea* meiotic proteins treated with phosphatase inhibitor was loaded into the SDS-PAGE gel with the strip containing proteins treated with the phosphatase inhibitor. Similarly, ~40µg of the untreated sample was loaded into the SDS-PAGE gel with the strip containing untreated proteins. The second dimension, SDS-PAGE, then separated the proteins by their mass. Once the proteins in both gels were resolved they were electro-blotted into two different nitrocellulose membranes (GE Healthcare). Each membrane was then probed using anti-ASY1 antibody (1:1000) followed by an anti-rat secondary antibody (1:10,000) and subsequently visualized using ECL. Analysis of the blots revealed that no proteins including AtASY1 could be detected in the control samples that were subjected to only one dimensional gel electrophoresis (Figure 22 C, D). However, discrete dot-like protein signals were observed in the blots from both the phosphatase inhibitor-treated and untreated samples that were subjected to 2D-PAGE. Further analysis of the blot of untreated sample revealed the presence of a cluster of 4 distinct dots next to at least 2 dot-like signals of anti-ASY1 antibody, all of which were approximately 60kDa in size. The sizes of each of these signals were roughly consistent with the size of BoASY1 (Figure 24C). In addition, analysis of the blot of the sample treated with phosphatase inhibitor revealed the presence of at least 6 dot-like signals each weighing ~60kDa in size also (Figure 24D). It is plausible that each of these signals may represent a different phosphorylated isoform for BoASY1, however, there is not enough clear evidence in the blots to confirm this observation.

Interestingly, the distribution of the ~60kDa dot-like anti-ASY1 antibody signals between the blots from the two samples was notably different from one another. In the blot from the untreated sample all the dot-like signals were spaced adjacent to each other in a cluster. In contrast, in the blot of the treated sample two of the dot-like signals were spaced apart from the cluster of the remaining 4 signals. Moreover, these two signals were spaced far away from each other. Hence, it is apparent that the treatment with phosphatase inhibitor has a direct effect on the phosphorylation state of proteins extracted from meiocytes. Therefore, this treatment may preserve phosphorylated forms of ASY1 and can be used in future studies of the effect of phosphorylation on the protein.

6.8. Discussion

6.8.1. Mutation of T to A at residue 295 of AtASY1 leads to meiotic defects

In a previous study, the *AtASY1-T295A* transgene encoding AtASY1 in which the T residue at position 295 was mutated to A was transformed into *Atasy1* mutant plants in order to investigate the significance of this residue (E.C., F.C.H.F.). The resulting transformants displayed varying levels of AtASY1 signal when analysed by immunolocalization using anti-ASY1 antibody (A.M., F.C.H.F.). The probable cause of this variation may be due to the differences in the regulation of *AtASY1-T295A*

transgene expression between the transgenics. The transgenic line (*Atasy1-T295A*, line 511.54.1) that exhibited the highest AtASY1 signal in immunolocalization studies was analysed in further detail. Molecular characterization of 9 progenies of *Atasy1-T295A* confirmed that these were homozygous knockouts of *Atasy1*. Furthermore, similar methods also validated the presence of the transgene and the point mutation in all *Atasy1-T295A* mutants. Analysis of *Atasy1-T295A* mutants revealed that fertility was significantly reduced in them compared to the wild-type, which possessed on average 49.50 seeds per silique. While most *Atasy1-T295A* transformants displayed a mean seed-set of 7/8 seeds per silique, two were found to contain a mean of ~5 seeds per silique. This variation is likely due to the small amount of the sample size. Nevertheless, compared to the wild-type all *Atasy1-T295A* mutant plants displayed reduced mean seed sets, which intriguingly, were similar to that of the *Atasy1* mutant (Caryl et al., 2000). Reduction in fertility is considered to be an indication of meiotic defect. Consistent with this subsequent cytological analysis revealed that *Atasy1-T295A* failed to undergo synapsis. Furthermore, *Atasy1-T295A* failed to form normal levels of chiasmata during meiosis. This results in mis-segregation during meiotic divisions resulting in the formation of aneuploid gametes. The above meiotic defects were reminiscent to those of *Atasy1*. More importantly, they suggest that even though *AtASY1-T295A* transgene is supposedly expressed *Atasy1-T295A* mutant failed to undergo normal synapsis and recombination, indicating that the mutation of T295 in AtASY1 leads meiotic defects that are similar to those exhibited by *Atasy1*.

6.8.2. Residue T295 may be essential for the normal AtASY1 localization

In wild-type meiocytes, AtASY1 was found to localize onto meiotic chromosome axes as numerous foci at leptotene. By zygotene AtASY1 formed a linear axis-associated signal. This observation was consistent with previous reports (Armstrong et al., 2002). Prior immunolocalization studies confirmed that the anti-ASY1 antibody is able to detect a signal at the chromosome axes during early prophase I in *Atasy1-T295A* mutant. This signal is likely to be AtASY1^{T295A}, the product of *AtASY1-T295A* transgene (A.M., F.C.H.F.). Further analysis of AtASY1^{T295A} revealed that instead of forming a linear signal like AtASY1 in wild-type meiocytes, it formed numerous thick and abnormal foci during early prophase I in *Atasy1-T295A*. This suggests that mutation of T295 may disrupt the normal localization of AtASY1 during meiosis. Since protein targeting to axes appears normal, it is conceivable that the mutation might cause a conformational change in AtASY1^{T295A} which disrupts its normal spatial association with the axes or its ability to polymerize normally along the axes. Alternatively, it is also possible that the mutation might reduce protein stability. This is consistent with previous reports in budding yeast where HOP1 stability is dependent on phosphorylation at the STQ motif T181 (Carballo et al., 2008). Given that the AtASY1^{T295A} foci appear abnormally thick and aberrant, the former possibility is likely to be the case in *Atasy1-T295A*. Interestingly, recent studies in wild-type meiocytes using deconvolution software suggests that instead of forming a linear signal AtASY1 is distributed along the axes as a series of evenly spaced hyper-abundant domains (mean number per cell = 160) which are separated by stretches of lower abundance (J.H., F.C.H.F.). This raises the question whether the AtASY1^{T295A} foci in *Atasy1-T295A* are in fact similar to the AtASY1 domains in wild-type. Since the AtASY1^{T295A}

foci in *Atasy1-T295A* were not analysed via deconvolution software and their numbers were not quantified there is not sufficient data at the moment to validate this. Nevertheless, it is apparent that some AtASY1^{T295A} domains may not be maintained in *Atasy1-T295A*.

6.8.3. *AtASY1T295A* is unable to promote normal levels of inter-homologue recombination in *Atasy1-T295A*

Western blotting analysis using an ASY1 antibody was able to detect the ~67kDa AtASY1 in protein extracts from *Arabidopsis* meiotocytes. This was not the case for *Atasy1* confirming that the mutant was deficient in AtASY1. However, a shorter product of ~62kDa was detected in the sample from the *Atasy1* mutant which was not present in that from the wild-type. It is conceivable that this shorter product may be a truncated or degraded non-functional version of AtASY1. It is also possible that this could be a result of expression from an unknown promoter in the T-DNA in *Atasy1*. Alternatively, it may also be that this product is present in the wild-type, but in such low level that it was undetectable in the ECL exposure times used during this experiment. If the latter is the case then this may indicate that AtASY1 is regulated as its absence may trigger a higher expression of this shorter product. Nevertheless, the data suggests that full-length AtASY1 is only detectable in the wild-type and not in the *Atasy1*. With this in context, the focus was shifted to verifying the presence of AtASY1^{T295A} in the five *Atasy1-T295A* mutant plants using similar methods as above. This revealed that in all five *Atasy1-T295A* mutants the anti-ASY1 antibody was able to detect AtASY1^{T295A}, which was indistinguishable in size from AtASY1 in the wild-

type. Moreover, the antibody was unable to detect AtASY1 in *Atasy1*, suggesting that AtASY1^{T295A} is indeed present in *Atasy1-T295A* mutants. This finding is consistent with immunolocalization studies of AtASY1^{T295A} in *Atasy1-T295A*. Furthermore, this finding confirms that the meiotic defects observed in *Atasy1-T295A* were not due to the absence of AtASY1. Instead, the data indicates that AtASY1^{T295A} which bears a mutation in T295 to A cannot perform the normal functions of AtASY1. AtASY1 has previously shown to promote AtDMC1-mediated inter-homologue recombination (Sanchez-Moran et al., 2007). Therefore, it appears that T295 is essential for the above function of AtASY1. This is consistent with the loss of chiasmata in *Atasy1-T295A*. Moreover, T295 is predicted to be a target site for serine/threonine kinase-mediated phosphorylation of AtASY1. Hence, it is plausible that phosphorylation of AtASY1 at T295 may be essential for ensuring normal levels of CO formation between homologous chromosomes during meiosis.

A notable observation during the above western blotting analysis was that the intensity of the anti-ASY1 signal was substantially higher in the samples from *Atasy1-T295A* mutants compared that of the wild-type. This is likely due to the difference in expression level between the transgene *AtASY1^{T295A}* and genomic *AtASY1*. The probable cause of this variation may be due to the expression of the transgene via the 35S promoter in pEarleyGate100 plasmid. This expression is unregulated and occurred in both meiotic and somatic tissues in flower buds which were used for protein extraction, unlike genomic *AtASY1* expression, which is meiosis specific (Armstrong et al., 2002) and may be regulated by co-factors.

Intriguingly, the shorter product (~62kDa) detected by anti-ASY1 in the sample from the *Atasy1* mutant was also observed in all the samples from *Atasy1-T295A*. Although AtASY1^{T295A}, which is capable of localizing to meiotic chromosomes, is present in *Atasy1-T295A* the shorter product still persists in the mutant. This may suggest that the shorter product possibly originates from the T-DNA in the *Atasy1*. In accord, this product was not observed in the sample from the wild-type suggesting that it is specific to mutants with a T-DNA in *AtASY1*. Nevertheless, the actual source of this shorter product still remains to be determined.

6.8.4. Preliminary analysis suggests that BoASY1, homologue of AtASY1, may be a likely substrate for phosphorylation

Western blotting analysis revealed that T295 is essential for normal AtASY1 function. As T295 is a predicted target site for phosphorylation, studies were performed to verify whether this was the case. Since western blotting studies revealed no AtASY1 band shift, which is generally an indication of phosphorylated form of a protein, a 2D-PAGE was used to detect phosphorylated AtASY1. However, due to the impracticality associated with extracting large volumes of proteins from *Arabidopsis* meiocytes the study was performed using meiocytes from its close relative, *B. oleracea*. *Brassica* meiotic protein samples were either untreated or treated with phosphatase inhibitor to preserve phosphorylated states of proteins before being subjected to 2D-PAGE. During the second dimension an untreated and treated sample were added next to their corresponding previous samples as a control to

detect BoASY1 and use it as a reference when analysing the phosphorylated forms of proteins. Analysis of the western blots following 2D-PAGE, however, revealed no detection of BoASY1 in the control samples. This was probably due to leakage of the control protein samples after loading into their corresponding wells. The leakage may have been caused by the defective formation of their wells which were at the edge of each vertical gel. The controls too were probably not appropriate as they were only subjected to one dimension separation whereas the treated and untreated were subjected to two dimensions of resolution. Nonetheless, had they worked they could have been used to compare phosphorylated forms of proteins in relation to BoASY1 migration. Interestingly, as anticipated discrete dot-like signals, ~60kDA is size, were observed in the blots from both the phosphatase inhibitor-treated and untreated samples. These are likely to be phosphorylated forms of BoASY1 as they are of similar size to the protein. This in turn would suggest that AtASY1, homologue of BoASY1, may also be phosphorylate during *Arabidopsis* meiosis. In light of the observations in *Atasy1-T295A* this seems a likely possibility. However, this claim remains inconclusive due to the absence of appropriate controls and comprehensive data.

Additionally, although there appears to be at least 6 dot-like signals at ~60kDA in each blot this number was by no means concrete as there was substantial background in the blots making it difficult to extrapolate the signals. Nevertheless, there appears to be a difference in distribution of these signals in the two blots. In the blot from the untreated sample all the dot-like signals were spaced adjacent to each

other in a cluster. In contrast, in the blot of the treated sample two of the dot-like signals were spaced apart from the cluster of the remaining signals. This may suggest that some phosphorylated forms of AtASY1 which may be lost in the untreated sample may be preserved when treated with phosphatase inhibitor. Although the above data indicates a notable variation between the two treatments one cannot rule out the possibility that the dot-like signals were due to cross-reaction of the anti-ASY1 antibody or that they were entirely an artefact of the preparation technologies involved, given that BoASY1 was undetectable in the control samples. Hence, although informative, the 2D-PAGE data remains inconclusive and requires a more comprehensive repetition.

CHAPTER 7

General Discussion

7.1. Introduction

Meiosis plays a central role during sexual reproduction in nearly all eukaryotic organisms. Among the major genetic events that occur during meiosis are paternal and maternal homologous chromosome synapsis and recombination, which leads to CO formation between them and subsequently generates genetic diversity. However, the mechanisms that regulate homologous chromosome synapsis and CO formation still remain poorly understood. Hence, this project was aimed at studying such mechanisms in order to gain further insight into the control of chromosome synapsis and recombination during meiosis in *Arabidopsis*. The main findings of this project and future perspectives are described in this chapter.

7.2. AtRECQ4B is not essential for normal meiosis

Previous studies indicate that AtRECQ4A is homologue of the mammalian BLM and budding yeast SGS1 helicase (Bagherieh-Najjar et al., 2005, Hartung et al., 2007). Loss of AtRECQ4A leads to an increased frequency of homologous COs in somatic cells suggesting that AtRECQ4A, like BLM and SGS1, acts as an anti-recombinase (Hartung et al., 2007). *AtRECQ4A* has been proposed to have undergone a recent gene duplication, giving rise to *AtRECQ4B* whose product was predicted to be ~70% identical to that of *AtRECQ4A* (Hartung and Puchta, 2006). In contrast to AtRECQ4A, AtRECQ4B has been proposed to promote homologous recombination in somatic

cells (Hartung et al., 2007). Interestingly, a recent analysis of the *Brassica* meiotic proteome revealed that *Brassica* homologues of AtRECQ4A and AtRECQ4B were present in meiocytes, suggesting putative roles for the proteins during meiosis (Sanchez-Moran et al., 2005; F.C.H.F. and K.O., unpublished).

Expression analysis of *AtRECQ4A* and *AtRECQ4B* revealed that both genes were indeed expressed in flower buds during meiosis. However, a subsequent detailed analysis, performed by colleagues, suggested that AtRECQ4A was not essential for normal levels of meiotic CO formation. *Atrecq4A* mutants exhibited normal levels of meiotic COs but displayed chromatin bridges at metaphase I which were dependent on meiotic recombination and telomere repeats. Therefore, the protein was proposed to be required for the dissolution of inter-chromosomal connections that arise during meiotic recombination (J.H., K.O., F.C.H.F.). This raised the question whether AtREC4QB, the close relative of AtRECQ4A, performed the SGS1-like functions during meiosis or whether it maintained its recombinase activity also during meiosis. To investigate such possibilities an *Atrecq4B* mutant was obtained and analysed. Surprisingly, the mutant displayed no reductions in seed-set or pollen viability, two hallmark features of mutants with meiotic defects. Subsequent cytological analysis revealed that all the meiotic stages in *Atrecq4B* were similar to that of the wild-type. Homologous chromosome pairing, synapsis and meiotic CO formation all appeared normal with no indication of any chromatin bridges and any loss of chiasmata at metaphase I, confirming the absence of any meiotic defects in the mutant. Since previous reports suggest that AtRECQ4B promote CO formation in somatic cells,

such a role of the protein was also investigated during meiosis. Analysis of chiasma frequency of *Atrecq4B* revealed no significant difference from that of the wild-type. Furthermore, a more detailed analysis of the chiasma frequency of an *Atrecq4B/Atmsh4* double mutant revealed no statistical difference in chiasma frequency between the double and *Atmsh4* single mutant. This indicated that loss of AtRECQ4B did not have any impact on MSH4-dependent or MSH4-independent COs, suggesting that the protein is not crucial for normal *Arabidopsis* meiosis.

However, analysis of AtRECQ4A localization during prophase I suggests that AtRECQ4B may be of some functional significance during meiosis (J.H., K.O., F.C.H.F). AtRECQ4A localization was analysed using an antibody that was found to detect the protein predominantly but evidence suggests that it may also display some cross-reactivity in detecting AtRECQ family members. In wild-type, AtRECQ4A/B foci were found to localize to meiotic chromosome axes as numerous foci at leptotene. At pachytene the number of these foci per cell was reduced to only ~5, which were mostly telomeric. In the *Atrecq4A-5* mutant AtRECQ4A/B foci failed to localize as numerous foci, instead formed <10, mostly telomeric foci at early prophase I. Interestingly, in an *Atrecq4A-5/Atrecq4B* double mutant the number of AtRECQ4A/B foci was further reduced to ~5 per nucleus, suggesting that there was an additional loss of foci in the absence of AtRECQ4B (J.H., K.O., F.C.H.F). This suggests that some AtRECQ4B may localize to chromosome axes during meiosis, consistent with the RT-PCR analysis suggesting the meiosis-specific expression of AtRECQ4B and the proteomics data which detected peptides of the AtRECQ4B homologue in

Brassica meiotic proteome (Sanchez-Moran et al., 2005; F.C.H.F. and K.O., unpublished). The above findings are consistent with a role for AtRECQ4B during meiosis. Furthermore, the presence of some residual AtRECQ4A/B foci in the *Atrecq4A-5/Atrecq4B* double mutant indicates that the anti-AtRECQ4A antibody may also exhibit cross-reaction with other member(s) of the AtRECQ family. This suggests that there may be functional redundancy between members of the AtRECQ helicase family (J.H., K.O., F.C.H.F).

Recent studies suggest that meiotic recombination intermediates that cannot be resolved as COs by the normal Holliday junction resolvase are removed by dissolution via a hemicatenane intermediate. In *Arabidopsis* this is performed by the RTR protein complex that is comprised of AtRMI1, AtTOP3 α and a RECQ helicase (Chelysheva et al., 2008, Hartung et al., 2008). It has been proposed that AtRECQ4A may perform the helicase activity of the RTR complex. However, AtRECQ4A was not found to be involved in meiotic progression leading to the suggestion that it was either not involved in such mechanism or it functions redundantly with another helicase(s) (Chelysheva et al., 2008, Hartung et al., 2008). Additionally, recent analysis of AtRECQ4A suggests that it is only involved in resolving inter-chromosomal telomeric connections during meiotic recombination (J.H., K.O., F.C.H.F). Nevertheless, immunolocalization studies showed that AtRECQ4A localizes to meiotic chromosome axes during early prophase I in the wild-type. Moreover, 63% of the AtRECQ4A foci were found to co-localize with AtMSH4 at zygotene. Additionally, some of the residual AtRECQ4A foci were found co-localized

with the late recombination protein and CO marker, AtMLH1 (J.H., K.O., F.C.H.F). These observations suggest that AtRECQ4A is associated with recombination intermediates during early prophase I leading the researchers to suggest that the protein might be involved in the RTR complex but its role can be substituted by another member of the AtRECQ helicase family (J.H., K.O., F.C.H.F). Taking into account that AtRECQ4B is present during meiosis and that some of it may localize to meiotic chromosome axes during early prophase I it is probable that AtRECQ4B may also be involved in maintaining genome integrity, however, similarly to AtRECQ4A it too possibly functions redundantly with other helicases during *Arabidopsis* meiosis.

7.3. AtASY3, a novel meiotic axes component, is required for synapsis and CO formation during meiosis

7.3.1. ASY3 is a novel component of meiotic chromosome axes

Analysis of the *Brassica* meiotic proteome followed by homology searches led to the identification of a novel gene, *AtASY3*, in *Arabidopsis*. RT-PCR analysis of *AtASY3* revealed that the gene is expressed specifically during meiosis. Analysis of three *Atasy3* T-DNA insertion mutant lines revealed that all of them displayed reduced fertility, consistent with a meiotic defect. Cytological analysis of these mutants revealed that they were all defective in homologous chromosome synapsis. This was verified by immunolocalization studies, which revealed that the SC TF component

failed to polymerize during early prophase I, confirming that normal synapsis was disrupted in the mutant. Furthermore, EM study of *Atasy3-1* early prophase I meiocytes, performed by collaborators, suggests that normal axis formation was disrupted in the mutant (M.P, N.C.). In addition, *Atasy3* mutants displayed a reduction in chiasmata and the formation of univalents at metaphase I. These led to mis-segregation at both meiotic divisions resulting in the formation of aneuploid gametes and the subsequent loss of fertility in the mutants. That disruption of *AtASY3* leads to the above phenotypes was verified using an allelism test, where homozygous *Atasy3-1/Atasy3-2* double mutant exhibited the same meiotic defects as its parental lines. Additionally, a complementation analysis, where transforming the *AtASY3* cDNA into *Atasy3-1* rescued nearly wild-type levels of fertility, supports the above findings.

AtASY3 is predicted to encode a ~88kDA protein, 793 AA in length, whose C-terminal contains a putative coiled coil domain, a feature found in other meiotic axis proteins. The C-terminal of *AtASY3* was used to generate a recombinant protein which was subsequently used to produce an antibody that could detect *AtASY3*. Immunolocalization studies using anti-ASY3 antibody revealed that in wild-type meiocytes *AtASY3* localizes to meiotic chromosome axes in late G2/early leptotene as numerous foci, which gradually polymerize to form a continuous signal by late leptotene. Analysis using deconvolution software suggests that *AtASY3* co-localizes with the axis-associated hyper-abundant domains of *AtASY1* at this stage (J.H., F.C.H.F., personal communication). Furthermore, the linear *AtASY3* signal mostly co-

localizes with the continuous signal of the SC TF component AtZYP1. These observations indicate that AtASY3 localizes to meiotic chromosome axes in *Arabidopsis*.

Interestingly, homology analysis suggested that AtASY3 was conserved in *Brassica*, with BoASY3 exhibiting 77% sequence identity with AtASY3. Immunolocalization studies of *B. oleracea* meiocytes using anti-ASY3 antibody revealed that the antibody was able to detect BoASY3, which was found to display a similar loading pattern to AtASY3 during early prophase I. Furthermore, BoASY3 also co-localized with the axis-associated BoASY1 during early prophase I. These findings indicate that AtASY3 is conserved, both in sequence level and in functions, in *Brassica*.

7.3.2. AtASY3 is required for normal levels of meiotic DSB and CO formation

Immunolocalization analysis of the DSB marker γ H2AX was carried out in order to analyse the status of meiotic DSB formation in *Atasy3-1*. This revealed that there was ~30% reduction in the number of γ H2AX foci in the mutant suggesting that although DSBs were able to form in the mutant their numbers were moderately reduced to ~70% of the wild-type level. This finding is supported by a similar reduction in the number of early recombination proteins, AtRAD51, AtDMC1 and AtMSH4 in *Atasy3-1*.

Cytological analysis of *Atasy3* mutants revealed that some of its chromosomes were not linked by any COs during metaphase I. FISH studies of *Atasy3* metaphase I nuclei revealed that the mean chiasma frequency was 3.34 in the mutant. This was a ~65% reduction compared to the chiasma frequency in wild-type. Furthermore, analysis of *Atasy3-1/Atmsh4* revealed that the double mutant failed to form any chiasmata. This suggests that AtASY3 is required for the formation of both interference sensitive and insensitive COs.

7.3.4. AtASY3 is required for normal AtASY1 localization

A recent analysis of AtASY1 using deconvolution software suggests that instead of linearizing the protein forms evenly distributed axis-associated hyper-abundant domains (mean number of 160 per nucleus) during early prophase I. These were found to co-localize with AtASY3 at the chromosome axes during early prophase I. (J.H., F.C.H.F.). Analysis of *Atasy3-1* revealed that this localization of AtASY1 was disrupted in the absence of AtASY3. Although AtASY1 was able to form axis-associated domains in *Atasy3-1*, their mean number was significantly reduced to 74 per nucleus. Moreover, these were unevenly distributed and distorted in appearance. These suggest that normal AtASY1 localization is dependent on AtASY3.

Previous studies reported that loss of AtASY1 destabilizes AtDMC1 soon after its loading during early prophase I resulting in a loss of inter-homologue recombination (Sanchez-Moran et al., 2007). In *Atasy3-1* the overall number of AtDMC1 was

moderately reduced to ~70% of the wild-type level. Nevertheless, timecourse studies using BrdU pulse labelling coupled with immunolocalization revealed that the residual AtDMC1 foci in *Atasy3-1* remained localized to meiotic chromosomes throughout early prophase I. This suggest that the reduction of AtDMC1 foci in the mutant is more likely due to the loss of overall DSBs and the loading of the residual AtDMC1 is stabilized in *Atasy3-1*. This may be attributable to the remaining AtASY1 domains in *Atasy3-1*. Consistent with this, the remaining AtASY1 domains were virtually always found to be co-localized with AtDMC1 and γ H2AX (J.H, F.C.H.F). However, these were not sufficient to maintain normal levels of inter-homologue recombination in the *Atasy3-1*.

In accord with the above findings, AtASY1 was found to be epistatic to AtASY3 in terms of CO formation. In FISH studies, the *Atasy3-1* single mutant was found to exhibit a reduction in its mean chiasma frequency from 9-10 in the wild-type to 3.34. This was significantly less severe than that of *Atasy3-1/Atasy1* that displayed a mean chiasma frequency of 1.78, which was not significantly different from 1.88 in the *Atasy1* single mutant. Interestingly, this inter-relationship was found to resemble that of Hop1 and Red1 in budding yeast with regards to DSB formation. Previous studies reported that *hop1* mutant that lacks HOP1 entirely exhibits a stronger defect in DSB formation than *red1*, which possess reduced HOP1 (Rockmill and Roeder, 1990, Smith and Roeder, 1997). Assuming that such an inter-relationship is maintained in *Arabidopsis*, the higher number of chiasmata in *Atasy3* compared to *Atasy1* is likely due to the remaining AtASY1 domains in the former.

7.3.5. ASY3 interacts with ASY1 in Arabidopsis and Brassica

Analysis of AtASY3 revealed that the protein is responsible for normal localization of AtASY1 onto meiotic chromosome axes. Furthermore, the two proteins were found to co-localize during early prophase I, suggesting the possibility of physical interaction between them. This led researchers in our lab to investigate a possible interaction between AtASY3 and AtASY1 *in planta* by a Co-IP experiment using anti-ASY1 antibody. However, extracting sufficient amount of meiotic proteins from *Arabidopsis* was impractical due to the small size of its anthers. Hence, the researchers carried out the Co-IP using meiocytes from *B. oleracea* instead (K.O. and F.C.H.F., personal communication). This was a suitable alternative since BoASY1 has been reported to share 83% identity in amino acid sequence with AtASY1 and the anti-ASY1 antibody has been found to detect BoASY1 (Armstrong et al., 2002). Furthermore, analysis of AtASY3 revealed that it was 77% identical to BoASY3, which too was found to localize to meiotic chromosome axes similarly to the former in immunolocalization studies. The Co-IP was anticipated to separate the anti-ASY1 antibody bound to BoASY1 and any other recombination protein or proteins which formed a complex with the protein during meiosis. Following Co-IP, the resulting proteins were analysed using MS of tryptic peptides followed by homology searches against a combined *Brassica* database which also included full length amino acid sequences of BoASY1 and BoASY3. This revealed that BoASY1 was identified as the top hit with 40 unique peptides corresponding to 397 out of the 599 amino acids (65% coverage) of the protein. Furthermore, BoASY3 was identified as the second hit with 28 peptides corresponding to 297 out of the 776 amino acids (38% coverage) of the protein. Additionally, neither of the two proteins were found in the control sample. This led the

researchers to suggest that BoASY3 and BoASY1 are able to interact *in planta* and may be components of a meiotic complex (K.O., E.R., K.M., F.C.H.F., personal communication). Since, BoASY3 and BoASY1 are conserved in *Arabidopsis*, it is highly likely that AtASY3 and AtASY1 also interacts with each other, similarly to their *B. oleracea* counterparts.

The above findings prompted other researchers in our lab to determine whether AtASY3 and AtASY1 can directly interact with each other in a yeast two hybrid assay. For this purpose the researchers cloned full length *AtASY3* and *AtASY1* cDNAs as in-frame fusions with the GAL4 activator domain (AD) and the GAL4 DNA binding domain (DBD) respectively into two separate yeast two hybrid plasmids which were subsequently co-transformed into yeast. Additionally, control co-transformations were also carried out where either of the two constructs was replaced by an empty vector. The principal behind this yeast two hybrid assay was that only if AtASY3 and AtASY1 physically interacted with one another, the DBD and AD would be brought close together to reconstitute a functionally active factor that would activate expression of particular genes on the plasmids required for the yeast to grow on the corresponding selective media. The researchers found that under high stringency selection (-Leu/-Trp/-His/-Ade) yeast that expressed either one of the two genes were unable to grow on the selective media. However, under the same selection yeast was able to grow only when both *AtASY3* and *AtASY1* were co-expressed. This suggest that AtASY3 and AtASY1 are able to interact with each other directly, affirming the findings of the above Co-IP experiment (C.L., F.C.H.F., personal communication).

Additionally, the researchers carried out further similar assays in which several truncated regions of AtASY3 were fused with the AD instead of the full length AtASY3. This revealed that yeast that contained AtASY1 and residues 623-793 of AtASY3, and no other truncated forms of AtASY3, were able to grow on under high stringency selection (-Leu/-Trp/-His/-Ade). Interestingly, the researchers noted that this region of AtASY3 corresponded to the predicted coiled-coiled domain of the protein. This finding, therefore, suggests that the interaction between AtASY3 and AtASY1 is mediated via the coiled-coiled domain in AtASY3 (C.L., F.C.H.F., personal communication).

7.3.6. AtASY3 shares functional similarities with RED1

In budding yeast, the coiled coil protein RED1 forms the AE component of the meiotic SC and has been proposed to play an important role, together with HOP1, in mediating inter-homologue recombination during meiosis (Niu et al., 2005, Smith and Roeder, 1997). A previous study suggests that the mammalian protein, SYCP might be a structural analogue of RED1 as the former is predicted to possess a coiled coil domain and has been shown to localize to the LE of the mammalian SC (de los Santos and Hollingsworth, 1999). However, a functional orthologue of RED1 has yet to be identified in a multi-cellular organism. Analysis of AtASY3 suggests that the protein is also predicted to contain a coiled coil domain and shares 16.4% identity with RED1 in amino acid sequence. More importantly, AtASY3 has been found to share functional similarities with RED1. In budding yeast loss of RED1 disrupts the normal localization of the HORMA domain protein, HOP1 (Smith and Roeder, 1997).

Similarly, disruption of AtASY3 results in aberrant localization of the HORMA domain protein, AtASY1 during *Arabidopsis* meiosis. Additionally, Red1 has been shown to interact with HOP1 in Co-IP experiments and yeast two hybrid assays (Woltering et al., 2000). Yeast two hybrid data suggests that this interaction is dependent on the 290 amino acids at the C-terminal of RED1. This region has been predicted to encode the coiled coil domain of RED1 (Woltering et al., 2000). Similarly, Co-IP experiments using *Brassica* meiocytes and anti-ASY1 antibody followed by MS analysis, performed by colleagues and collaborators, suggest a possible interaction between BoASY3 and BoASY1, the homologues of AtASY3 and AtASY1 respectively (K.O., E.R., K.M., F.C.H.F.). Furthermore, a direct interaction between AtASY3 and AtASY1 has been confirmed by yeast two hybrid assays, performed by colleagues in our lab. The analysis also revealed that the C-terminal of AtASY3, that is predicted to contain the coiled-coil domain, is essential for the interaction between the two proteins (C.L., F.C.H.F.). These findings highlight the striking similarities between AtASY3 and Red1 with regards to their inter-relationship with their corresponding HORMA domain proteins. Additionally, previous studies suggest that RED1 is required for normal levels of DSB formation during meiosis in budding yeast (Xu et al., 1997). Interestingly, *Atasy3-1* mutant exhibits a ~30% decrease in meiotic DSBs, although the reduction was not as pronounced as that in *red1* mutant, where a ~70% reduction in meiotic DSB formation has been reported (Xu et al., 1997). This suggests that, like RED1, AtASY3 is required for normal levels of meiotic DSB formation during meiosis.

Interestingly, AtASY3 was also found to exhibit 25.6% identity in amino acid sequence with OsPAIR3 in rice. Like AtASY3 and RED1, OsPAIR3 is predicted to contain a coiled-coil domain and has been shown to localize to the meiotic chromosome axes in rice (Wang et al., 2011, Yuan et al., 2009). Furthermore, localization of the rice HORMA domain protein OsPAIR2 has been found to be dependent on OsPAIR3 (Wang et al., 2010a). This inter-relationship is similar to that of AtASY3 and RED1 and their corresponding HORMA proteins. However, a direct interaction between OsPAIR3 and OsPAIR2 has not been shown yet. Nevertheless, *Ospair3* mutants display similar phenotypes to *Atasy3-1*. Taken together, these observations suggest that like AtASY3, OsPAIR3 may also be a functional homologue of RED1.

7.3.7. Putative roles of the axis protein AtASY3 in CO formation

An important aspect of meiotic recombination is its close coupling with chromosome axes/SC (reviewed in Kleckner, 2006). Recently, several studies have focussed on the significance of this close association. These revealed that in addition to their structural roles, some meiotic axes/SC components are also involved in CO formation. In budding yeast, the axis proteins RED1 and HOP1 have been shown to be involved in DSB formation. It is proposed that the proteins are required to tether the DSB machinery to chromosome axes prior to DSB formation (Kim et al., 2010, Panizza et al., 2011). In accord with this, *red1* mutants exhibit defect in DSB formation (Schwacha and Kleckner, 1997, Xu et al., 1997). Similarly, *Atasy3-1* mutants were found to exhibit ~30% reduction in DSB formation and abnormalities in

axis formation. Furthermore, analysis of AtASY3 suggests that it is likely to be a functional homologue of RED1. Hence, it is probable that AtASY3 functions similarly to RED1 and may be involved in organizing the meiotic axes such that it promotes normal level of DSB formation.

In addition to its role in DSB formation, the axis protein RED1 has been proposed to form a complex with HOP1 and the kinase MEK1 in order to promote inter-homologue recombination in budding yeast (Niu et al., 2005). It has been proposed that soon after DSB formation HOP1 is phosphorylated which causes it to dimerize and activate MEK1. MEK1 is then thought to phosphorylate one or more substrate(s) in the vicinity of the DSB which subsequently activates RED1 (Niu et al., 2005). It has been proposed that RED1 constrains the loading of the sister chromatid cohesion mediator, REC8 at DSB sites such that DSBs are repaired via inter-homologue interactions rather than inter-sister interactions (Kim et al., 2010). This is consistent with a reduction in chiasmata in the *red1* mutant (Rockmill and Roeder, 1990, Schwacha and Kleckner, 1997). Similarly, *Atasy3* mutant also exhibits a reduction in chiasma formation which, intriguingly, was greater in proportion than expected. Assuming that the ratio of COs to NCOs are maintained a ~30% reduction in meiotic DSBs, by simple extrapolation, should result in a ~30% decrease in the chiasma frequency of *Atasy3*. However, this was not the case as the mutant exhibits ~65% reduction in mean chiasma frequency from 9.76 in the wild-type to 3.34. This indicates that there is an additional loss of inter-homologue recombination and that a greater proportion of meiotic DSBs are repaired probably via inter-sister interactions

in *Atasy3*. This finding suggests that AtASY3 may be involved in mediating inter-homologue recombination during *Arabidopsis* meiosis. Interestingly, in *Arabidopsis*, AtASY1 has recently been shown to play a key role in mediating inter-homologue recombination (Sanchez-Moran et al., 2007). Furthermore, our colleagues have been able to show an interaction between BoASY3 and BoASY1, homologues of AtASY3 and AtASY1 respectively, *in planta* (K.O., E.R, K.M, F.C.H.F) as well as a direct interaction between AtASY3 and AtASY1 (C.L., F.C.H.F). Therefore, it is highly likely that AtASY3 interacts with AtASY1, early in the recombination pathway, to form a bias that promotes CO formation via inter-homologue recombination rather than inter-sister interactions, probably using similar mechanisms to their yeast counterparts RED1 and HOP1 respectively.

7.3.8. Future perspectives

Post-translational modifications, particularly sumoylation and phosphorylation, are known to be essential for normal functioning of chromosome axis/SC proteins during meiosis.

7.3.8.1. Putative interaction of SUMO with AtASY3

The post-translational modification of SMT3, a small ubiquitin-like modifier (SUMO), has been shown to control SC assembly in budding yeast. In budding yeast, the SC initiation protein ZIP3 acts as an E3 ligase which causes SMT3 to form conjugates along the two AEs. These SMT3 conjugates interact with the C-terminal globular

domains of the SC TF component, ZIP1 to drive SC assembly between homologous chromosomes during early prophase I (Cheng et al., 2006). Recently, sumoylation of the budding yeast AE component, RED1 has also been proposed to be important for SC assembly. This modification was found to be dependent on the lysine residues in the RED1 C-terminal (Eichinger and Jentsch, 2010). In addition to being SUMO modified RED1 was also found to bind the 9-1-1 meiotic checkpoint complex (DDC1/MEC3/RAD17) (Eichinger and Jentsch, 2010). These two physical interactions have been proposed to ensure timely SC formation during meiosis. However, only a small proportion of RED1 was found to be covalently modified by SUMO during meiosis. Furthermore, *red1^{KR}* mutants that expressed sumoylation defective RED1 were also found to be capable of forming normal meiotic SC, similarly to the wild-type, suggesting that sumoylation of RED1 was not necessary of SC assembly but only its timely formation (Eichinger and Jentsch, 2010). Interestingly, a recent study suggests that interaction between RED1 and SUMO chains instead play an important role in SC assembly (Lin et al., 2010). Red1 has previously been shown to directly interact with SMT3 in a yeast two hybrid screen (Ito et al., 2001). A more recent study identified two putative SMT3-interacting motifs, SIM1 (ILESTTVID) and SIM2 (ISII), in the RED1 C-terminal, which has been shown to strongly interact with SMT3 chains in yeast two hybrid assays (Lin et al., 2010). A detailed analysis revealed that SIM2 was better than SIM1 in binding Smt3 chains. Consistent with this, *V5-red1^{I758R}* mutants with a mutation in SIM2 were found to exhibit almost no spore viability similarly to the asynaptic *red1* null mutant, while *V5-red1^{2R}* with a mutation in SIM1 were found to exhibit much less severe defect in spore viability. Interestingly, RED1 stability, chromosomal targeting, phosphorylation,

oligomerization and interaction with HOP1 were all found to be unaffected in both *V5-red1^{1758R}* and *V5-red1^{2R}* mutants. These observations suggest that the meiotic defects in *V5-red1^{1758R}* and *V5-red1^{2R}* were due to a disruption in the interaction of RED1 with SUMO chains (Lin et al., 2010). Additionally, the study found that only the C-terminal, containing the two SIM domains, of RED1 was able to directly interact with the globular domain at the ZIP1 C-terminal, which is known to bind Smt3 chains. This led the authors to propose that RED1 and ZIP1 non-covalently sandwich SUMO chains to mediate SC assembly during meiosis (Lin et al., 2010). Another important finding of the study was that HOP1 was not phosphorylated in *V5-red1^{1758R}* and *V5-red1^{3R}* (where both SIM1 and SIM2 were mutated), similarly to *red1* null mutant. This suggested that HOP1 phosphorylation, which is known to be dependent on the kinases MEC1 and TEL1, does not occur in the absence of RED1-SUMO chain interaction (Lin et al., 2010). HOP1 phosphorylation has been shown to be required for the activation of MEK1, whose kinase activity is essential for forming a bias towards inter-homologue recombination rather than inter-sister repair of DSBs during meiotic recombination (Carballo et al., 2008, Niu et al., 2007, Niu et al., 2005). The above findings, therefore, indicate that the establishment of this bias is essentially dependent on interaction of RED1 with SUMO chains. This is consistent with the finding that both *red1^{1758R}* and *V5-red1^{3R}* exhibit nearly no viable spores similarly to *red1* null mutant (Lin et al., 2010).

Analysis of *Arabidopsis* AtASY3 revealed that it is a functional homologue of RED1. *Atasy3-1* mutants fail to form normal SC during early prophase I. Immunolocalization

studies indicate that instead of linearizing into a continuous signal at pachytene the budding yeast ZIP1 homologue, AtZYP1 forms distorted foci and short stretches. This suggests that although SC nucleation occurs it fails to extend properly in the mutant. Assuming that, like budding yeast, AtZYP1-SUMO chain-AtASY3 interaction is necessary for normal SC assembly the above finding would suggest that any remaining AtZYP1-SUMO chain interaction in *Atasy3* mutant is insufficient to mediate normal SC assembly in the absence of AtASY3. Alternatively, the loss of AtASY3 may disrupt the proper alignment of homologue axes which may in turn prevent normal SC elongation along the AEs. Hence, further work is necessary to determine whether AtASY3 or AtZYP1 can interact with SUMO proteins and whether the two can interact with each other, although this may be particularly difficult as AtZYP1 is encoded in two adjacent genes on the same chromosome and a disruption of either only leads to a mild effect on fertility.

AtASY3 was also found to interact with AtASY1, similarly to their budding yeast homologues RED1 and HOP1 respectively, to promote a bias towards inter-homologue rather than inter-sister recombination. In budding yeast this process involved the activation of MEK1 via the RED1-SUMO chain-ZIP1 dependent phosphorylation of HOP1 (Carballo et al., 2008, Lin et al., 2010, Niu et al., 2005). Although a homologue of MEK1 has not yet been identified in *Arabidopsis* there is considerable evidence suggesting that AtASY1 phosphorylation is essential for normal levels of CO formation (described in Chapter 6). So far, it is unknown whether AtASY1 phosphorylation is dependent on AtASY3. However, given the extensive

similarities in the inter-relationship between AtASY1 and AtASY3 and their yeast counterparts it may be the case in *Arabidopsis*, although this needs to be verified through future studies. A notable observation was the lack of conservation of the RED1 lysine residues and SIM domains in the AtASY3 amino acid sequence, questioning the possibility of any potential SUMO interactions. Apart from showing a direct interaction one way of shedding more light into this may be by the detection of SUMO chains on chromosome axis/SC during early prophase I. This may be carried out via dual-immunolocalization using antibodies against SUMO and axis/SC proteins. However, given that SUMO modifications may be required for normal functioning of other meiotic proteins there may be some cross reactivity during immunolocalization. Nevertheless, it is worth analysing the effect of SUMO-mediated modifications on AtASY3 in further detail.

7.8.3.2. Putative phosphorylation of AtASY3

Recent studies in budding yeast indicate that RED1 binds to SUMO chains to promote MEC1/TEL1-mediated phosphorylation of HOP1, which leads to the activation of MEK1 and the subsequent prevention of DMC1-independent repair of meiotic DSBs (Carballo et al., 2008, Lin et al., 2010, Niu et al., 2005). Furthermore, RED1 has been shown to directly interact with MEC3 and DDC1, two of the three components of the 9-1-1 meiotic checkpoint complex (Eichinger and Jentsch, 2010). It has been suggested that essential components of the MEC1/TEL1 DNA damage checkpoint pathway and the 9-1-1 complex promote MEK1-dependent phosphorylation of RED1 (Hong and Roeder, 2002). This is consistent with previous

studies which reported that RED1 is a phosphoprotein, which is phosphorylated by MEK1 and dephosphorylated by protein phosphatase type I (GLC7) (Bailis and Roeder, 1998, 2000, de los Santos and Hollingsworth, 1999). It has been proposed that MEK1-phosphorylated RED1 prevents exit from pachytene until meiotic recombination is complete, when RED1 is dephosphorylated by GLC7 (Roeder and Bailis, 2000). This proposal highlights the importance of RED1 phosphorylation during meiosis. However, the amino acid residues responsible for this modification was not mapped or verified during these earlier studies. Subsequent research suggests that RED1 is not a target of MEK1-dependent phosphorylation, instead, it acts upstream of the kinase (Hochwagen and Amon, 2006, Wan et al., 2004). It has been proposed that RED1 is phosphorylated by an unknown kinase and that the subsequent phosphorylated RED1 interacts with MEK1 to recruit the kinase to DSB sites. MEK1 is then thought to be activated to promote DMC1-independent repair of DSBs (Wan et al., 2004). Nevertheless, this proposal also emphasizes the importance of RED1 phosphorylation during meiosis. More recent studies, however, indicate that phosphorylation of RED1 may not be important for normal meiosis (Lai et al., 2011). Western blotting timecourse analysis of meiotic proteins separated by SDS-PAGE revealed that both phosphorylated and non-phosphorylated RED1 were detected in *spo11Δ* and *mek1Δ* diploid mutants, indicating that RED1 phosphorylation was neither recombination specific nor MEK1-dependent. Additionally, RED1 was found to be phosphorylated in *rad24Δtel1Δ* (deficient in MEC1/TEL1 function) suggesting that RED1 phosphorylation is independent of MEC1/TEL1 activity. Furthermore, the studies suggest that RED1 de-phosphorylation was also not required for pachytene exit during meiosis (Lai et al., 2011). RED1 was

found to be a substrate for CDC28 protein kinase. RED1 is predicted to contain seven S/T-P or S-X-K-K motifs which form putative target sites for CDC28 kinase. Importantly, *V5-red1^{7A}* mutant, in which all the seven CDC28 target sites were mutated, displayed hypo-phosphorylated RED1 but similar spore viability as the wild-type indicating that phosphorylation at these sites are not necessary for normal RED1 functions during meiosis (Lai et al., 2011). Interestingly, although reduced in amount RED1 phosphorylation was not entirely absent in *V5-red1^{7A}*, suggesting the presence of a CDC28-independent pathway for RED1 phosphorylation. Subsequent studies revealed that *V5-red1^{1758R}* mutant, which is defective in RED1-SUMO interactions, also displayed hypo-phosphorylated RED1. Furthermore, *V5-red1^{1758,7A}* synthetic mutant were found to generate few viable spores suggesting that RED1 phosphorylation in *V5-red1^{1758R}* was CDC28-dependent while that in *V5-red1^{7A}* was CDC28-independent (Lai et al., 2011). Although a kinase for the latter pathway was not identified the researchers mapped four putative sites for CDC28-independent phosphorylation in RED1. When each of these were mutated there was loss of RED1 phosphorylation in *V5-red1^{7A}* background, however, there was no loss of any spore viability compared to the wild-type. Taken together, the above findings led the researchers to conclude that although RED1 is phosphorylated, this modification is not essential for normal meiosis (Lai et al., 2011). Intriguingly, CDC28-independent RED1 phosphorylation was found to be dependent on HOP1 and RED1-SUMO interactions (Lai et al., 2011). Similarly, HOP1 phosphorylation was found to be dependent on RED1 and RED1-SUMO interactions in a previous study (Lin et al., 2010). These observations suggest that HOP1-RED1-SUMO interaction may mediate

RED1 and HOP1 phosphorylation for the genetic events during meiosis (Lai et al., 2011).

AtASY3 was shown to interact with AtASY1, similarly like their budding yeast counterparts RED1 and HOP1, to mediate inter-homologue recombination in *Arabidopsis*. It is highly likely that the mechanisms and therefore the post-translational modifications underlying this process are similar to that in budding yeast. Consistent with this, recent data suggests that phosphorylation of AtASY1 is essential for normal levels of inter-homologue recombination (detailed in Chapter 6). Since RED1 is a phosphoprotein and its phosphorylation may be important for normal meiosis it is highly likely that this too may be the case for AtASY3, given the functional similarities between the two. Although phosphorylation of AtASY3 was not verified during this study one way validating this would be to detect AtASY3 in protein extracts from *Arabidopsis* meiocytes by western blotting using the anti-ASY3 antibody. Assuming that anti-ASY3 antibody would be able to detect AtASY3 in protein extracts from plant tissues, if AtASY3 is phosphorylated, this might be detected via band shifts if they are noticeable. An alternative option for detecting AtASY3 phosphorylation may be the identification on phosphorylation target sites on the protein. Based on the little amino acid sequence homology, which is often the case for meiotic axis proteins from different organisms, there appears to be no clear conservation of target sites which are similar to those responsible for CDC28-independent phosphorylation of RED1 in budding yeast. Nevertheless, out of the seven S/T-P sites responsible for CDC28-dependent phosphorylation of RED1 only

two (S550 and S631) appears to be conserved in AtASY3. The significance of these, if any, may be determined via targeted mutations in future studies. Other putative phosphorylation sites include S/TQ motifs which are known potential targets of serine/threonine kinases. Targets of serine/threonine kinases usually contain SCDs in which three S/TQ motifs are found within a region of 100 amino acid residues (Traven and Heierhorst, 2005). Although homology searches indicate that AtASY3 contains six putative S/TQ motifs they do not form any SCD and hence are unlikely to be phosphorylation target sites. Intriguingly, three of the putative S/TQ motifs (S15, S28 and S177) in AtASY3 are conserved in its *Brassica* homologue BoASY3, suggesting that they may potentially be of some functional significance. Hence it may be worth analysing these sites in more detail via site directed mutagenesis studies. It may also be possible to identify a putative *Arabidopsis* protein kinase that may be involved in phosphorylating AtASY3 via means of sequence or functional homology analysis. However, due to the functional redundancy between kinases the process may prove somewhat difficult. Nevertheless, analysing phosphorylation of AtASY3 remains vastly important for understanding its effect on the control of the protein, given that this avenue is subject to immense debate at the moment.

7.4. AtASY1 phosphorylation is essential for mediating inter-homologue recombination

7.4.1. Atasy1-T295 mutants exhibit defective meiosis

In budding yeast, the axis proteins HOP1 along with RED1 and MEK1 are essential for establishing a bias that promotes inter-homologue recombination rather than inter-sister repair of DSBs during meiosis (Niu et al., 2005). This process is thought to be dependent on post-translational modifications of the above proteins (Carballo et al., 2008, de los Santos and Hollingsworth, 1999, Wan et al., 2004). One in particular is the phosphorylation of HOP1. Recent studies indicate that HOP1 is a target of the serine/threonine kinase, MEC1/TEL1. HOP1 is predicted to contain eight S/TQ motifs, three of which (S298, S311 and T318) form an SCD that acts as a target site for MEC/TEL1 phosphorylation. Studies revealed that mutation of T at residue 318 to A conferred a *hop1* mutant phenotype and resulted in the most severe reduction in spore viability (Carballo et al., 2008). Interestingly, a previous analysis in our lab found that HOP1 T318 is conserved at residue T295 in the *Arabidopsis* meiosis axis protein, AtASY1. This led to the construction of an *AtASY1-T295A* transgene that encoded AtASY1 in which the T residue at position 295 was mutated to A. This transgene was transformed via a vector into *Atasy1* mutant plants in order to investigate whether T295 was of similar significance to HOP1 T318 (E.C., F.C.H.F.). A later study identified a line, *Atasy1-T295A*, from the resulting transformants that exhibited the highest AtASY1 signal in immunolocalization studies (A.M., F.C.H.F.). Subsequent molecular characterization of *Atasy1-T295A* confirmed the presence of T-DNA, the transgene and the point mutation in the mutant. Analysis of the *Atasy1-*

T295A revealed that although the mutant displayed normal vegetative growth it possessed significantly reduced fertility compared to the wild-type. The reduction in seed-set was found to be similar to the levels observed in *Atasy1* mutant. Moreover, this reduction in fertility is consistent with a meiotic defect. Cytological analysis of *Atasy1-T295A* revealed that the mutant failed to undergo synapsis. Furthermore, *Atasy1-T295A* failed to form normal levels of chiasmata during meiosis. This results in mis-segregation during meiotic divisions resulting in the formation of aneuploid gametes. The above meiotic defects were reminiscent to those of *Atasy1* (Caryl et al., 2000). More importantly, they suggest that even though *AtASY1-T295A* transgene is expressed in *Atasy1-T295A*, they failed to undergo normal synapsis and recombination, indicating that the mutation of T295 in AtASY1 leads meiotic defects, which are similar to those of *Atasy1*.

7.4.2. AtASY1 T295 is essential for normal levels of inter-homologue recombination

Previous immunolocalization studies detected an axis-associated signal using anti-ASY1 antibody in *Atasy1-T295A* mutant. This signal is likely to be AtASY1^{T295A}, suggesting that the *AtASY1-T295A* transgene is expressed in the mutant. Interestingly, analysis of AtASY1^{T295A} revealed that the protein formed numerous thick aberrant foci on meiotic chromosome axes during early prophase I in *Atasy1-T295A*. This was in contrast to previous studies which reported that AtASY1 forms a distinct linear axis-associated signal in prophase I (Armstrong et al., 2002). However, recent studies in wild-type meiocytes using deconvolution software suggests that

instead of forming a linear signal AtASY1 is distributed along the meiotic axes as a series of hyper-abundant domains that are separated by stretches of lower abundance (J.H., F.C.H.F.). Hence, it is likely that AtASY1^{T295} foci in *Atasy1-T295A* are essentially similar to the ASY1 domains in wild-type, although it is apparent that some of these domains are lost in *Atasy1-T295A*. Nevertheless, the immunolocalization studies suggest that AtASY1^{T295A} is able to localize to meiotic chromosomes in *Atasy1-T295A*.

To validate the presence of AtASY1^{T295A}, meiotic proteins were extracted from 5 *Atasy1-T295A* plants, an *Atasy1* mutant and a wild-type. These were subjected to SDS-PAGE followed by western blotting using anti-ASY1 antibody. This revealed that the antibody was able to detect a band corresponding to AtASY1 in the protein sample from the wild-type but not in that of *Atasy1* mutant. More interestingly, the antibody was also able to detect a similar band in samples from all 5 *Atasy1-T295A* plants confirming that AtASY1^{T295A} is indeed present in *Atasy1-T295A* mutants. This finding is consistent with previous immunolocalization studies of AtASY1^{T295A}. Taken together, these observations indicate that AtASY1^{T295A}, which bears a mutation in T295 to A, can localize to chromosome axes during meiosis, however, it is unable to perform the normal functions of AtASY1. AtASY1 has previously been shown to promote AtDMC1-mediated inter-homologue recombination (Sanchez-Moran et al., 2007). Therefore, it appears that T295 is essential for the above function of AtASY1. This is consistent with the loss of chiasmata in *Atasy1-T295A*. Moreover, T295 is predicted to be a target site for serine/threonine kinase-mediated phosphorylation of

AtASY1. Hence, it is likely that phosphorylation of AtASY1 at T295 may be essential for ensuring normal levels of CO formation between homologous chromosomes during meiosis. Interestingly, there was no evidence of chromosome fragmentation in *Atasy1-T295A*, suggesting that DSBs are repaired via AtDMC1-independent pathway. This suggests AtASY1 phosphorylation is likely to function by inhibiting inter-sister interactions rather than promoting inter-homologue recombination. This is in accord with the proposed mode of action of AtASY1 (Sanchez-Moran et al., 2007). Additionally this is also consistent with the observation that phosphorylation of HOP1, the homologue of AtASY1, is essential for establishing a bias towards inter-homologue recombination rather than inter-sister interactions in budding yeast (Carballo et al., 2008).

7.4.3. Further work

Analysis of *Atasy1-T295A* suggests that AtASY1 is subjected to phosphorylation. However, no phosphorylated forms were noticeable in western blots of *Arabidopsis* meiotic proteins using anti-ASY1 antibody. Hence, to detect phosphorylated ASY1 a 2D-PAGE, which separates proteins based on their pI and molecular weight, was performed followed by western blotting using anti-ASY1 antibody. Due to the difficulty in extracting large amounts of proteins from *Arabidopsis* meiocytes the study was performed using meiocytes from its close relative, *B. oleracea*. Although the study lacked an appropriate control the anti-ASY1 antibody, which has previously been shown to detect BoASY1 (Armstrong et al., 2002), was able to detect several dot-like signals which were consistent in size with BoASY1. Hence, based on the sizes of

these signals they may correspond to several phosphorylated forms of BoASY1. This finding suggests that AtASY1, homologue of BoASY1, is also phosphorylated during *Arabidopsis* meiosis. However, the 2D-PAGE data was inconclusive, as the anti-ASY1 antibody failed to detect BoASY1 in the control samples. Furthermore, the blots displayed extensive background which made it difficult to quantify the number of dot-like signals in them. Hence, repeating this study may lead to more conclusive data regarding AtASY1 phosphorylation. Moreover, using a longer immobiline strip with less pH variation may significantly improve the resolution of signals in future studies. During the 2D-PAGE analysis a sample of *Brassica* meiotic protein extracts were treated with phosphatase inhibitor while another was left untreated. Comparison of their subsequent blots indicated a notable difference in the distribution of signals between the two blots. In the blot from the untreated sample all the dot-like signals were spaced adjacent to each other in a cluster. In contrast, in the blot of the treated sample two of the dot-like signals were spaced apart from the cluster of the remaining signals. This may suggest that some phosphorylated forms of AtASY1 which may be lost in the untreated sample may be preserved when treated with phosphatase inhibitor. Therefore, it may be worth repeating this experiment, but with the addition of a further treatment with a phosphatase. Phosphatases are known to cleave phosphate groups, hence it would allow a better comparison between phosphorylated and non-phosphorylated forms of AtASY1.

Another aspect worth analysing in further detail is the localization of AtASY1^{T295A} during prophase I using deconvolution software. Analysis of AtASY1^{T295A} localization

in relation to other axis and recombination proteins may help to understand the spatial relationship between them and provide a better understanding of the basis of the defects in CO formation in *Atasy1-T295A*. Since, CO formation is reduced in *Atasy1-T295A* it is conceivable that some of these may be due to a reduction in DSB formation in *Atasy1-T295A*. This is consistent with the loss of normal levels of DSB formation in budding yeast mutants that are defective in HOP1, the homologue of AtASY1 (Schwacha and Kleckner, 1994). However, this is unlikely as *Atasy1* mutants display almost normal levels of DSB formation (J.H., F.C.H.F.).

Further analysis of AtASY1 may also be focussed on determining the significance of the remaining S/TQ motifs in AtASY1. In AtASY1 the residues S266 and T268 together with T295 form an SCD, the target site of serine/threonine kinases. Analysing the effects of mutating these sites may aide in understanding their significance. Furthermore, AtASY1 is predicted to contain four more S/TQ sites, three of which (S566, S569 and S593) are predicted to form an SCD. It is worth determining the importance of this second SCD and the sites within it. It may also be important to identify the kinase(s) responsible for AtASY1 phosphorylation. Since Hop1 has been shown to be a substrate for phosphorylation by MEC1/TEL1 (Carballo et al., 2008), it is likely that their mammalian counterparts ATR/ATM may be responsible for phosphorylating AtASY1. However, this needs to be verified, possibly via comparing the defects in *Atasy1-T295A* with those in *Atatr/Atatm* double mutant. Additionally, phosphorylation of budding yeast HOP1 was found to be dependent on RED1 and vice versa (Lai et al., 2011, Lin et al., 2010). Recent data

indicates that their *Arabidopsis* homologues, AtASY1 and AtASY3 exhibit close inter-relationship during meiosis. Therefore, future work may also focus on the impact, if any, of AtASY1 phosphorylation on AtASY3 and vice versa, if the latter is found to be phosphorylated.

7.5. Final word

The studies in this project provide further insight into the role of chromosome axis/SC proteins in the control of meiotic CO formation. Additionally, they highlight the fact that although meiotic axis/SC components between different species share limited primary sequence homology they display a close functional relationship that is conserved between species.

REFERENCES

- Agarwal, S. and Roeder, G.S.** (2000) Zip3 provides a link between recombination enzymes and synaptonemal complex proteins. *Cell*, **102**: (2): 245-255.
- Albini, S.M. and Jones, G.H.** (1984) Synaptonemal complex-associated centromeres and recombination nodules in plant meiocytes prepared by an improved surface-spreading technique. *Exp Cell Res*, **155**: (2): 588-592.
- Alexander, M.P.** (1969) Differential staining of aborted and nonaborted pollen. *Stain Technol*, **44**: (3): 117-122.
- Armstrong, S.J., Caryl, A.P., Jones, G.H. and Franklin, F.C.** (2002) Asy1, a protein required for meiotic chromosome synapsis, localizes to axis-associated chromatin in Arabidopsis and Brassica. *J Cell Sci*, **115**: (Pt 18): 3645-3655.
- Armstrong, S.J., Franklin, F.C. and Jones, G.H.** (2001) Nucleolus-associated telomere clustering and pairing precede meiotic chromosome synapsis in Arabidopsis thaliana. *J Cell Sci*, **114**: (Pt 23): 4207-4217.
- Armstrong, S.J., Franklin, F.C.H. and Jones, G.H.** (2003) A meiotic time-course for Arabidopsis thaliana. *Sexual Plant Reproduction*, **16**: (3): 141-149.
- Armstrong, S.J. and Jones, G.H.** (2003) Meiotic cytology and chromosome behaviour in wild-type Arabidopsis thaliana. *J Exp Bot*, **54**: (380): 1-10.
- Arumugam, P., Gruber, S., Tanaka, K., Haering, C.H., Mechtler, K. and Nasmyth, K.** (2003) ATP hydrolysis is required for cohesin's association with chromosomes. *Curr Biol*, **13**: (22): 1941-1953.
- Bagherieh-Najjar, M.B., de Vries, O.M., Hille, J. and Dijkwel, P.P.** (2005) Arabidopsis RecQ14A suppresses homologous recombination and modulates DNA damage responses. *Plant J*, **43**: (6): 789-798.
- Bagherieh-Najjar, M.B., de Vries, O.M., Kroon, J.T., Wright, E.L., Elborough, K.M., Hille, J. and Dijkwel, P.P.** (2003) Arabidopsis RecQsim, a plant-specific member of the RecQ helicase family, can suppress the MMS hypersensitivity of the yeast *sgs1* mutant. *Plant Mol Biol*, **52**: (2): 273-284.
- Bai, X., Peirson, B.N., Dong, F., Xue, C. and Makaroff, C.A.** (1999) Isolation and characterization of SYN1, a RAD21-like gene essential for meiosis in Arabidopsis. *Plant Cell*, **11**: (3): 417-430.
- Bailis, J.M. and Roeder, G.S.** (1998) Synaptonemal complex morphogenesis and sister-chromatid cohesion require Mek1-dependent phosphorylation of a meiotic chromosomal protein. *Genes Dev*, **12**: (22): 3551-3563.
- Bailis, J.M. and Roeder, G.S.** (2000) Pachytene exit controlled by reversal of Mek1-dependent phosphorylation. *Cell*, **101**: (2): 211-221.
- Baker, S.M., Plug, A.W., Prolla, T.A., Bronner, C.E., Harris, A.C., Yao, X., Christie, D.M., Monell, C., Arnheim, N., Bradley, A., Ashley, T. and Liskay, R.M.** (1996) Involvement of mouse Mlh1 in DNA mismatch repair and meiotic crossing over. *Nat Genet*, **13**: (3): 336-342.
- Barlow, A.L. and Hulten, M.A.** (1998) Crossing over analysis at pachytene in man. *Eur J Hum Genet*, **6**: (4): 350-358.
- Bass, H.W., Riera-Lizarazu, O., Ananiev, E.V., Bordoli, S.J., Rines, H.W., Phillips, R.L., Sedat, J.W., Agard, D.A. and Cande, W.Z.** (2000) Evidence for the coincident initiation of homolog pairing and synapsis during the telomere-clustering (bouquet) stage of meiotic prophase. *J Cell Sci*, **113** (Pt 6): 1033-1042.
- Baudat, F., Buard, J., Grey, C., Fledel-Alon, A., Ober, C., Przeworski, M., Coop, G. and de Massy, B.** (2009) PRDM9 Is a Major Determinant of Meiotic Recombination Hotspots in Humans and Mice. *Science*, **327**: (5967): 836-840.
- Baudat, F. and de Massy, B.** (2007) Regulating double-stranded DNA break repair towards crossover or non-crossover during mammalian meiosis. *Chromosome Res*, **15**: (5): 565-577.

- Bishop, D.K.** (1994) RecA homologs Dmc1 and Rad51 interact to form multiple nuclear complexes prior to meiotic chromosome synapsis. *Cell*, **79**: (6): 1081-1092.
- Bishop, D.K.** (2006) Multiple mechanisms of meiotic recombination. *Cell*, **127**: (6): 1095-1097.
- Bishop, D.K., Park, D., Xu, L. and Kleckner, N.** (1992) DMC1: a meiosis-specific yeast homolog of *E. coli* recA required for recombination, synaptonemal complex formation, and cell cycle progression. *Cell*, **69**: (3): 439-456.
- Bishop, D.K. and Zickler, D.** (2004) Early decision; meiotic crossover interference prior to stable strand exchange and synapsis. *Cell*, **117**: (1): 9-15.
- Blat, Y., Protacio, R.U., Hunter, N. and Kleckner, N.** (2002) Physical and functional interactions among basic chromosome organizational features govern early steps of meiotic chiasma formation. *Cell*, **111**: (6): 791-802.
- Bleuyard, J.-Y., Gallego, M. and White, C.** (2004a) Meiotic defects in the Arabidopsis rad50 mutant point to conservation of the MRX complex function in early stages of meiotic recombination. *Chromosoma*, **113**: (4).
- Bleuyard, J.-Y., Gallego, M.E., Savigny, F. and White, C.I.** (2004b) Differing requirements for the Arabidopsis Rad51 paralogs in meiosis and DNA repair. *The Plant Journal*, **41**: (4): 533-545.
- Bleuyard, J.Y. and White, C.I.** (2004) The Arabidopsis homologue of Xrcc3 plays an essential role in meiosis. *EMBO J*, **23**: (2): 439-449.
- Boddy, M.N., Gaillard, P.H., McDonald, W.H., Shanahan, P., Yates, J.R., 3rd and Russell, P.** (2001) Mus81-Eme1 are essential components of a Holliday junction resolvase. *Cell*, **107**: (4): 537-548.
- Borde, V., Robine, N., Lin, W., Bonfils, S., Geli, V. and Nicolas, A.** (2009) Histone H3 lysine 4 trimethylation marks meiotic recombination initiation sites. *EMBO J*, **28**: (2): 99-111.
- Borner, G.V., Barot, A. and Kleckner, N.** (2008) Yeast Pch2 promotes domainal axis organization, timely recombination progression, and arrest of defective recombinosomes during meiosis. *Proc Natl Acad Sci U S A*, **105**: (9): 3327-3332.
- Borner, G.V., Kleckner, N. and Hunter, N.** (2004) Crossover/noncrossover differentiation, synaptonemal complex formation, and regulatory surveillance at the leptotene/zygotene transition of meiosis. *Cell*, **117**: (1): 29-45.
- Buard, J., Barthes, P., Grey, C. and de Massy, B.** (2009) Distinct histone modifications define initiation and repair of meiotic recombination in the mouse. *EMBO J*, **28**: (17): 2616-2624.
- Busygina, V., Sehorn, M.G., Shi, I.Y., Tsubouchi, H., Roeder, G.S. and Sung, P.** (2008) Hed1 regulates Rad51-mediated recombination via a novel mechanism. *Genes & Development*, **22**: (6): 786-795.
- Cai, X.** (2003) The Arabidopsis SYN1 cohesin protein is required for sister chromatid arm cohesion and homologous chromosome pairing. *Journal of Cell Science*, **116**: (14): 2999-3007.
- Campell, B.R., Song, Y., Posch, T.E., Cullis, C.A. and Town, C.D.** (1992) Sequence and organization of 5S ribosomal RNA-encoding genes of Arabidopsis thaliana. *Gene*, **112**: (2): 225-228.
- Carballo, J.A., Johnson, A.L., Sedgwick, S.G. and Cha, R.S.** (2008) Phosphorylation of the Axial Element Protein Hop1 by Mec1/Tel1 Ensures Meiotic Interhomolog Recombination. *Cell*, **132**: (5): 758-770.
- Carmo-Fonseca, M., Mendes-Soares, L. and Campos, I.** (2000) To be or not to be in the nucleolus. *Nat Cell Biol*, **2**: (6): E107-112.
- Carpenter, A.T.** (1975) Electron microscopy of meiosis in *Drosophila melanogaster* females: II. The recombination nodule--a recombination-associated structure at pachytene? *Proc Natl Acad Sci U S A*, **72**: (8): 3186-3189.
- Caryl, A.P., Armstrong, S.J., Jones, G.H. and Franklin, F.C.** (2000) A homologue of the yeast HOP1 gene is inactivated in the Arabidopsis meiotic mutant *asy1*. *Chromosoma*, **109**: (1-2): 62-71.

- Chang, M., Bellaoui, M., Zhang, C., Desai, R., Morozov, P., Delgado-Cruzata, L., Rothstein, R., Freyer, G.A., Boone, C. and Brown, G.W.** (2005) RMI1/NCE4, a suppressor of genome instability, encodes a member of the RecQ helicase/Topo III complex. *EMBO J*, **24**: (11): 2024-2033.
- Chelysheva, L.** (2005) AtREC8 and AtSCC3 are essential to the monopolar orientation of the kinetochores during meiosis. *Journal of Cell Science*, **118**: (20): 4621-4632.
- Chelysheva, L., Gendrot, G., Vezon, D., Doutriaux, M.P., Mercier, R. and Grelon, M.** (2007) Zip4/Spo22 is required for class I CO formation but not for synapsis completion in *Arabidopsis thaliana*. *PLoS Genet*, **3**: (5): e83.
- Chelysheva, L., Vezon, D., Belcram, K., Gendrot, G. and Grelon, M.** (2008) The *Arabidopsis* BLAP75/Rmi1 Homologue Plays Crucial Roles in Meiotic Double-Strand Break Repair. *PLoS Genetics*, **4**: (12): e1000309.
- Chen, C., Zhang, W., Timofejeva, L., Gerardin, Y. and Ma, H.** (2005) The *Arabidopsis* ROCK-N-ROLLERS gene encodes a homolog of the yeast ATP-dependent DNA helicase MER3 and is required for normal meiotic crossover formation. *The Plant Journal*, **43**: (3): 321-334.
- Chen, Z., Higgins, J.D., Hui, J.T.L., Li, J., Franklin, F.C.H. and Berger, F.** (2011) Retinoblastoma protein is essential for early meiotic events in *Arabidopsis*. *The EMBO Journal*, **30**: (4): 744-755.
- Cheng, C.H., Lo, Y.H., Liang, S.S., Ti, S.C., Lin, F.M., Yeh, C.H., Huang, H.Y. and Wang, T.F.** (2006) SUMO modifications control assembly of synaptonemal complex and polycomplex in meiosis of *Saccharomyces cerevisiae*. *Genes Dev*, **20**: (15): 2067-2081.
- Chi, P., San Filippo, J., Sehorn, M.G., Petukhova, G.V. and Sung, P.** (2007) Bipartite stimulatory action of the Hop2-Mnd1 complex on the Rad51 recombinase. *Genes & Development*, **21**: (14): 1747-1757.
- Chikashige, Y., Tsutsumi, C., Yamane, M., Okamasa, K., Haraguchi, T. and Hiraoka, Y.** (2006) Meiotic Proteins Bqt1 and Bqt2 Tether Telomeres to Form the Bouquet Arrangement of Chromosomes. *Cell*, **125**: (1): 59-69.
- Chua, P.R. and Roeder, G.S.** (1998) Zip2, a meiosis-specific protein required for the initiation of chromosome synapsis. *Cell*, **93**: (3): 349-359.
- Cloud, V., Chan, Y.L., Grubb, J., Budke, B. and Bishop, D.K.** (2012) Rad51 is an accessory factor for Dmc1-mediated joint molecule formation during meiosis. *Science*, **337**: (6099): 1222-1225.
- Clough, S.J. and Bent, A.F.** (1998) Floral dip: a simplified method for *Agrobacterium*-mediated transformation of *Arabidopsis thaliana*. *Plant J*, **16**: (6): 735-743.
- Cole, F., Keeney, S. and Jasin, M.** (2010) Evolutionary conservation of meiotic DSB proteins: more than just Spo11. *Genes & Development*, **24**: (12): 1201-1207.
- Connelly, J.C. and Leach, D.R.** (2002) Tethering on the brink: the evolutionarily conserved Mre11-Rad50 complex. *Trends Biochem Sci*, **27**: (8): 410-418.
- Conrad, M.N., Lee, C.Y., Chao, G., Shinohara, M., Kosaka, H., Shinohara, A., Conchello, J.A. and Dresser, M.E.** (2008) Rapid telomere movement in meiotic prophase is promoted by NDJ1, MPS3, and CSM4 and is modulated by recombination. *Cell*, **133**: (7): 1175-1187.
- Conrad, M.N., Lee, C.Y., Wilkerson, J.L. and Dresser, M.E.** (2007) MPS3 mediates meiotic bouquet formation in *Saccharomyces cerevisiae*. *Proc Natl Acad Sci U S A*, **104**: (21): 8863-8868.
- Copenhaver, G.P., Housworth, E.A. and Stahl, F.W.** (2002) Crossover interference in *Arabidopsis*. *Genetics*, **160**: (4): 1631-1639.
- Couteau, F., Belzile, F., Horlow, C., Grandjean, O., Vezon, D. and Doutriaux, M.P.** (1999) Random chromosome segregation without meiotic arrest in both male and female meiocytes of a *dmc1* mutant of *Arabidopsis*. *Plant Cell*, **11**: (9): 1623-1634.
- Crismani, W., Girard, C., Froger, N., Pradillo, M., Santos, J.L., Chelysheva, L., Copenhaver, G.P., Horlow, C. and Mercier, R.** (2012) FANCM limits meiotic crossovers. *Science*, **336**: (6088): 1588-1590.

- Cromie, G.A., Hyppa, R.W., Taylor, A.F., Zakharyevich, K., Hunter, N. and Smith, G.R.** (2006) Single Holliday junctions are intermediates of meiotic recombination. *Cell*, **127**: (6): 1167-1178.
- Daniel, K., Lange, J., Hached, K., Fu, J., Anastassiadis, K., Roig, I., Cooke, H.J., Stewart, A.F., Wassmann, K., Jasin, M., Keeney, S. and Toth, A.** (2011) Meiotic homologue alignment and its quality surveillance are controlled by mouse *HORMAD1*. *Nat Cell Biol*, **13**: (5): 599-610.
- Daoudal-Cotterell, S., Gallego, M.E. and White, C.I.** (2002) The plant Rad50-Mre11 protein complex. *FEBS Lett*, **516**: (1-3): 164-166.
- de los Santos, T. and Hollingsworth, N.M.** (1999) Red1p, a MEK1-dependent phosphoprotein that physically interacts with Hop1p during meiosis in yeast. *J Biol Chem*, **274**: (3): 1783-1790.
- de los Santos, T., Hunter, N., Lee, C., Larkin, B., Loidl, J. and Hollingsworth, N.M.** (2003) The Mus81/Mms4 endonuclease acts independently of double-Holliday junction resolution to promote a distinct subset of crossovers during meiosis in budding yeast. *Genetics*, **164**: (1): 81-94.
- De Muyt, A., Pereira, L., Vezon, D., Chelysheva, L., Gendrot, G., Chambon, A., Laine-Choinard, S., Pelletier, G., Mercier, R., Nogue, F. and Grelon, M.** (2009) A high throughput genetic screen identifies new early meiotic recombination functions in *Arabidopsis thaliana*. *PLoS Genet*, **5**: (9): e1000654.
- De Muyt, A., Vezon, D., Gendrot, G., Gallois, J.L., Stevens, R. and Grelon, M.** (2007) AtPRD1 is required for meiotic double strand break formation in *Arabidopsis thaliana*. *EMBO J*, **26**: (18): 4126-4137.
- De Muyt, A., Jessop, L., Kolar, E., Sourirajan, A., Chen, J., Dayani, Y. and Lichten, M.** (2012) BLM Helicase Ortholog Sgs1 Is a Central Regulator of Meiotic Recombination Intermediate Metabolism. *Molecular Cell*, **46**: (1): 43-53.
- Dion, É., Li, L., Jean, M. and Belzile, F.** (2007) An *Arabidopsis* MLH1 mutant exhibits reproductive defects and reveals a dual role for this gene in mitotic recombination. *The Plant Journal*, **51**: (3): 431-440.
- Dray, E., Siaud, N., Dubois, E. and Doutriaux, M.P.** (2006) Interaction between *Arabidopsis* Brca2 and Its Partners Rad51, Dmc1, and Dss1. *Plant Physiology*, **140**: (3): 1059-1069.
- Eichinger, C.S. and Jentsch, S.** (2010) Synaptonemal complex formation and meiotic checkpoint signaling are linked to the lateral element protein Red1. *Proc Natl Acad Sci U S A*, **107**: (25): 11370-11375.
- Eijpe, M., Offenbergh, H., Jessberger, R., Revenkova, E. and Heyting, C.** (2003) Meiotic cohesin REC8 marks the axial elements of rat synaptonemal complexes before cohesins SMC1beta and SMC3. *J Cell Biol*, **160**: (5): 657-670.
- Ellis, N.A., Groden, J., Ye, T.Z., Straughen, J., Lennon, D.J., Ciocci, S., Proytcheva, M. and German, J.** (1995) The Bloom's syndrome gene product is homologous to RecQ helicases. *Cell*, **83**: (4): 655-666.
- Fernandez-Capetillo, O., Mahadevaiah, S.K., Celeste, A., Romanienko, P.J., Camerini-Otero, R.D., Bonner, W.M., Manova, K., Burgoyne, P. and Nussenzweig, A.** (2003) H2AX is required for chromatin remodeling and inactivation of sex chromosomes in male mouse meiosis. *Dev Cell*, **4**: (4): 497-508.
- Franklin, F.C., Higgins, J.D., Sanchez-Moran, E., Armstrong, S.J., Osman, K.E., Jackson, N. and Jones, G.H.** (2006) Control of meiotic recombination in *Arabidopsis*: role of the MutL and MutS homologues. *Biochem Soc Trans*, **34**: (Pt 4): 542-544.
- Fraune, J., Schramm, S., Alsheimer, M. and Benavente, R.** (2012) The mammalian synaptonemal complex: Protein components, assembly and role in meiotic recombination. *Experimental Cell Research*.
- Fricke, W.M. and Brill, S.J.** (2003) Slx1-Slx4 is a second structure-specific endonuclease functionally redundant with Sgs1-Top3. *Genes Dev*, **17**: (14): 1768-1778.

- Fung, J.C., Rockmill, B., Odell, M. and Roeder, G.S.** (2004) Imposition of crossover interference through the nonrandom distribution of synapsis initiation complexes. *Cell*, **116**: (6): 795-802.
- Gerlach, W.L. and Bedbrook, J.R.** (1979) Cloning and characterization of ribosomal RNA genes from wheat and barley. *Nucleic Acids Res*, **7**: (7): 1869-1885.
- Gilbertson, L.A. and Stahl, F.W.** (1996) A test of the double-strand break repair model for meiotic recombination in *Saccharomyces cerevisiae*. *Genetics*, **144**: (1): 27-41.
- Golubovskaya, I.N., Harper, L.C., Pawlowski, W.P., Schichnes, D. and Cande, W.Z.** (2002) The *pam1* gene is required for meiotic bouquet formation and efficient homologous synapsis in maize (*Zea mays* L.). *Genetics*, **162**: (4): 1979-1993.
- Graumann, K., Runions, J. and Evans, D.E.** (2010) Characterization of SUN-domain proteins at the higher plant nuclear envelope. *The Plant Journal*, **61**: (1): 134-144.
- Grelon, M., Vezon, D., Gendrot, G. and Pelletier, G.** (2001) AtSPO11-1 is necessary for efficient meiotic recombination in plants. *EMBO J*, **20**: (3): 589-600.
- Grey, C., Barthes, P., Chauveau-Le Friec, G., Langa, F., Baudat, F. and de Massy, B.** (2011) Mouse PRDM9 DNA-binding specificity determines sites of histone H3 lysine 4 trimethylation for initiation of meiotic recombination. *PLoS Biol*, **9**: (10): e1001176.
- Grey, C., Baudat, F. and de Massy, B.** (2009) Genome-wide control of the distribution of meiotic recombination. *PLoS Biol*, **7**: (2): e35.
- Gruber, S., Haering, C.H. and Nasmyth, K.** (2003) Chromosomal cohesin forms a ring. *Cell*, **112**: (6): 765-777.
- Grushcow, J.M., Holzen, T.M., Park, K.J., Weinert, T., Lichten, M. and Bishop, D.K.** (1999) *Saccharomyces cerevisiae* checkpoint genes MEC1, RAD17 and RAD24 are required for normal meiotic recombination partner choice. *Genetics*, **153**: (2): 607-620.
- Guacci, V., Hogan, E. and Koshland, D.** (1994) Chromosome condensation and sister chromatid pairing in budding yeast. *J Cell Biol*, **125**: (3): 517-530.
- Guacci, V., Koshland, D. and Strunnikov, A.** (1997) A direct link between sister chromatid cohesion and chromosome condensation revealed through the analysis of MCD1 in *S. cerevisiae*. *Cell*, **91**: (1): 47-57.
- Haber, J.E. and Heyer, W.D.** (2001) The fuss about Mus81. *Cell*, **107**: (5): 551-554.
- Haering, C.H., Lowe, J., Hochwagen, A. and Nasmyth, K.** (2002) Molecular architecture of SMC proteins and the yeast cohesin complex. *Mol Cell*, **9**: (4): 773-788.
- Haering, C.H., Schoffnegger, D., Nishino, T., Helmhart, W., Nasmyth, K. and Lowe, J.** (2004) Structure and stability of cohesin's SMC1-kleisin interaction. *Mol Cell*, **15**: (6): 951-964.
- Harper, L., Golubovskaya, I. and Cande, W.Z.** (2004) A bouquet of chromosomes. *J Cell Sci*, **117**: (Pt 18): 4025-4032.
- Hartung, F., Plchova, H. and Puchta, H.** (2000) Molecular characterisation of RecQ homologues in *Arabidopsis thaliana*. *Nucleic Acids Res*, **28**: (21): 4275-4282.
- Hartung, F. and Puchta, H.** (2001) Molecular characterization of homologues of both subunits A (SPO11) and B of the archaebacterial topoisomerase 6 in plants. *Gene*, **271**: (1): 81-86.
- Hartung, F. and Puchta, H.** (2006) The RecQ gene family in plants. *J Plant Physiol*, **163**: (3): 287-296.
- Hartung, F., Suer, S., Bergmann, T. and Puchta, H.** (2006) The role of AtMUS81 in DNA repair and its genetic interaction with the helicase AtRecQ4A. *Nucleic Acids Research*, **34**: (16): 4438-4448.
- Hartung, F., Suer, S., Knoll, A., Wurz-Wildersinn, R. and Puchta, H.** (2008) Topoisomerase 3 α and RMI1 suppress somatic crossovers and are essential for resolution of meiotic recombination intermediates in *Arabidopsis thaliana*. *PLoS Genet*, **4**: (12): e1000285.

- Hartung, F., Suer, S. and Puchta, H.** (2007) Two closely related RecQ helicases have antagonistic roles in homologous recombination and DNA repair in *Arabidopsis thaliana*. *Proceedings of the National Academy of Sciences*, **104**: (47): 18836-18841.
- Hayashi, K., Yoshida, K. and Matsui, Y.** (2005) A histone H3 methyltransferase controls epigenetic events required for meiotic prophase. *Nature*, **438**: (7066): 374-378.
- Higgins, J.D.** (2004) The *Arabidopsis* MutS homolog AtMSH4 functions at an early step in recombination: evidence for two classes of recombination in *Arabidopsis*. *Genes & Development*, **18**: (20): 2557-2570.
- Higgins, J.D., Buckling, E.F., Franklin, F.C.H. and Jones, G.H.** (2008a) Expression and functional analysis of AtMUS81 in *Arabidopsis* meiosis reveals a role in the second pathway of crossing-over. *The Plant Journal*, **54**: (1): 152-162.
- Higgins, J.D., Perry, R.M., Barakate, A., Ramsay, L., Waugh, R., Halpin, C., Armstrong, S.J. and Franklin, F.C.H.** (2012) Spatiotemporal Asymmetry of the Meiotic Program Underlies the Predominantly Distal Distribution of Meiotic Crossovers in Barley. *The Plant Cell*.
- Higgins, J.D., Sanchez-Moran, E., Armstrong, S.J., Jones, G.H. and Franklin, F.C.** (2005) The *Arabidopsis* synaptonemal complex protein ZYP1 is required for chromosome synapsis and normal fidelity of crossing over. *Genes & Development*, **19**: (20): 2488-2500.
- Higgins, J.D., Vignard, J., Mercier, R., Pugh, A.G., Franklin, F.C.H. and Jones, G.H.** (2008b) AtMSH5 partners AtMSH4 in the class I meiotic crossover pathway in *Arabidopsis thaliana*, but is not required for synapsis. *The Plant Journal*, **55**: (1): 28-39.
- Hiraoka, Y. and Dernburg, A.F.** (2009) The SUN Rises on Meiotic Chromosome Dynamics. *Developmental Cell*, **17**: (5): 598-605.
- Hochwagen, A. and Amon, A.** (2006) Checking your breaks: surveillance mechanisms of meiotic recombination. *Curr Biol*, **16**: (6): R217-228.
- Hollingsworth, N.M.** (2004) The Mus81 solution to resolution: generating meiotic crossovers without Holliday junctions. *Genes & Development*, **18**: (2): 117-125.
- Hollingsworth, N.M., Goetsch, L. and Byers, B.** (1990) The HOP1 gene encodes a meiosis-specific component of yeast chromosomes. *Cell*, **61**: (1): 73-84.
- Hong, E.J. and Roeder, G.S.** (2002) A role for Ddc1 in signaling meiotic double-strand breaks at the pachytene checkpoint. *Genes Dev*, **16**: (3): 363-376.
- Huber, M.D., Duquette, M.L., Shiels, J.C. and Maizels, N.** (2006) A conserved G4 DNA binding domain in RecQ family helicases. *J Mol Biol*, **358**: (4): 1071-1080.
- Hunter, N. and Borts, R.H.** (1997) Mlh1 is unique among mismatch repair proteins in its ability to promote crossing-over during meiosis. *Genes Dev*, **11**: (12): 1573-1582.
- Hunter, N. and Kleckner, N.** (2001) The single-end invasion: an asymmetric intermediate at the double-strand break to double-holliday junction transition of meiotic recombination. *Cell*, **106**: (1): 59-70.
- Ip, S.C.Y., Rass, U., Blanco, M.G., Flynn, H.R., Skehel, J.M. and West, S.C.** (2008) Identification of Holliday junction resolvases from humans and yeast. *Nature*, **456**: (7220): 357-361.
- Ito, T., Chiba, T., Ozawa, R., Yoshida, M., Hattori, M. and Sakaki, Y.** (2001) A comprehensive two-hybrid analysis to explore the yeast protein interactome. *Proc Natl Acad Sci U S A*, **98**: (8): 4569-4574.
- Jackson, N., Sanchez-Moran, E., Buckling, E., Armstrong, S.J., Jones, G.H. and Franklin, F.C.** (2006) Reduced meiotic crossovers and delayed prophase I progression in AtMLH3-deficient *Arabidopsis*. *EMBO J*, **25**: (6): 1315-1323.
- Jensen, R.B., Carreira, A. and Kowalczykowski, S.C.** (2010) Purified human BRCA2 stimulates RAD51-mediated recombination. *Nature*, **467**: (7316): 678-683.
- Jessop, L., Rockmill, B., Roeder, G.S. and Lichten, M.** (2006) Meiotic chromosome synapsis-promoting proteins antagonize the anti-crossover activity of sgs1. *PLoS Genet*, **2**: (9): e155.

- Jones, G.H.** (1984) The control of chiasma distribution. *Symp Soc Exp Biol*, **38**: 293-320.
- Jones, G.H., Armstrong, S.J., Caryl, A.P. and Franklin, F.C.** (2003) Meiotic chromosome synapsis and recombination in *Arabidopsis thaliana*; an integration of cytological and molecular approaches. *Chromosome Res*, **11**: (3): 205-215.
- Jones, G.H. and Franklin, F.C.** (2006) Meiotic crossing-over: obligation and interference. *Cell*, **126**: (2): 246-248.
- Joshi, N., Barot, A., Jamison, C. and Borner, G.V.** (2009) Pch2 links chromosome axis remodeling at future crossover sites and crossover distribution during yeast meiosis. *PLoS Genet*, **5**: (7): e1000557.
- Kankel, M.W., Ramsey, D.E., Stokes, T.L., Flowers, S.K., Haag, J.R., Jeddloh, J.A., Riddle, N.C., Verbsky, M.L. and Richards, E.J.** (2003) *Arabidopsis* MET1 cytosine methyltransferase mutants. *Genetics*, **163**: (3): 1109-1122.
- Kauppi, L., Jeffreys, A.J. and Keeney, S.** (2004) Where the crossovers are: recombination distributions in mammals. *Nature Reviews Genetics*, **5**: (6): 413-424.
- Keeney, S., Giroux, C.N. and Kleckner, N.** (1997) Meiosis-specific DNA double-strand breaks are catalyzed by Spo11, a member of a widely conserved protein family. *Cell*, **88**: (3): 375-384.
- Kerzendorfer, C.** (2006) The *Arabidopsis thaliana* MND1 homologue plays a key role in meiotic homologous pairing, synapsis and recombination. *Journal of Cell Science*, **119**: (12): 2486-2496.
- Kim, J.S., Krasieva, T.B., LaMorte, V., Taylor, A.M. and Yokomori, K.** (2002) Specific recruitment of human cohesin to laser-induced DNA damage. *J Biol Chem*, **277**: (47): 45149-45153.
- Kim, K.P., Weiner, B.M., Zhang, L., Jordan, A., Dekker, J. and Kleckner, N.** (2010) Sister cohesion and structural axis components mediate homolog bias of meiotic recombination. *Cell*, **143**: (6): 924-937.
- Kleckner, N.** (2004) A mechanical basis for chromosome function. *Proceedings of the National Academy of Sciences*, **101**: (34): 12592-12597.
- Kleckner, N.** (2006) Chiasma formation: chromatin/axis interplay and the role(s) of the synaptonemal complex. *Chromosoma*, **115**: (3): 175-194.
- Klein, F., Mahr, P., Galova, M., Buonomo, S.B., Michaelis, C., Nairz, K. and Nasmyth, K.** (1999) A central role for cohesins in sister chromatid cohesion, formation of axial elements, and recombination during yeast meiosis. *Cell*, **98**: (1): 91-103.
- Klimyuk, V.I. and Jones, J.D.** (1997) AtDMC1, the *Arabidopsis* homologue of the yeast DMC1 gene: characterization, transposon-induced allelic variation and meiosis-associated expression. *Plant J*, **11**: (1): 1-14.
- Koszul, R. and Kleckner, N.** (2009) Dynamic chromosome movements during meiosis: a way to eliminate unwanted connections? *Trends in Cell Biology*, **19**: (12): 716-724.
- Kurzbauer, M.T., Uanschou, C., Chen, D. and Schlogelhofer, P.** (2012) The recombinases DMC1 and RAD51 are functionally and spatially separated during meiosis in *Arabidopsis*. *Plant Cell*, **24**: (5): 2058-2070.
- Lai, Y.J., Lin, F.M., Chuang, M.J., Shen, H.J. and Wang, T.F.** (2011) Genetic requirements and meiotic function of phosphorylation of the yeast axial element protein Red1. *Mol Cell Biol*, **31**: (5): 912-923.
- Lam, W.S.** (2005) Characterization of *Arabidopsis thaliana* SMC1 and SMC3: evidence that AtSMC3 may function beyond chromosome cohesion. *Journal of Cell Science*, **118**: (14): 3037-3048.
- Lee, C.Y., Conrad, M.N. and Dresser, M.E.** (2012) Meiotic chromosome pairing is promoted by telomere-led chromosome movements independent of bouquet formation. *PLoS Genet*, **8**: (5): e1002730.

- Lee, J., Iwai, T., Yokota, T. and Yamashita, M.** (2003) Temporally and spatially selective loss of Rec8 protein from meiotic chromosomes during mammalian meiosis. *J Cell Sci*, **116**: (Pt 13): 2781-2790.
- Li, W.** (2004) The Arabidopsis AtRAD51 gene is dispensable for vegetative development but required for meiosis. *Proceedings of the National Academy of Sciences*, **101**: (29): 10596-10601.
- Li, W.** (2005) The AtRAD51C Gene Is Required for Normal Meiotic Chromosome Synapsis and Double-Stranded Break Repair in Arabidopsis. *Plant Physiology*, **138**: (2): 965-976.
- Lin, F.M., Lai, Y.J., Shen, H.J., Cheng, Y.H. and Wang, T.F.** (2010) Yeast axial-element protein, Red1, binds SUMO chains to promote meiotic interhomologue recombination and chromosome synapsis. *EMBO J*, **29**: (3): 586-596.
- Linder, P. and Jankowsky, E.** (2011) From unwinding to clamping - the DEAD box RNA helicase family. *Nat Rev Mol Cell Biol*, **12**: (8): 505-516.
- Lipkin, S.M., Moens, P.B., Wang, V., Lenzi, M., Shanmugarajah, D., Gilgeous, A., Thomas, J., Cheng, J., Touchman, J.W., Green, E.D., Schwartzberg, P., Collins, F.S. and Cohen, P.E.** (2002) Meiotic arrest and aneuploidy in MLH3-deficient mice. *Nat Genet*, **31**: (4): 385-390.
- Liu Cm, C.M., McElver, J., Tzafrir, I., Joosen, R., Wittich, P., Patton, D., Van Lammeren, A.A. and Meinke, D.** (2002) Condensin and cohesin knockouts in Arabidopsis exhibit a titan seed phenotype. *Plant J*, **29**: (4): 405-415.
- Loidl, J., Klein, F. and Scherthan, H.** (1994) Homologous pairing is reduced but not abolished in asynaptic mutants of yeast. *J Cell Biol*, **125**: (6): 1191-1200.
- Longworth, M.S., Herr, A., Ji, J.Y. and Dyson, N.J.** (2008) RBF1 promotes chromatin condensation through a conserved interaction with the Condensin II protein dCAP-D3. *Genes Dev*, **22**: (8): 1011-1024.
- Lorenz, A., Estreicher, A., Kohli, J. and Loidl, J.** (2006) Meiotic recombination proteins localize to linear elements in *Schizosaccharomyces pombe*. *Chromosoma*, **115**: (4): 330-340.
- Lorenz, A., West, S.C. and Whitby, M.C.** (2009) The human Holliday junction resolvase GEN1 rescues the meiotic phenotype of a *Schizosaccharomyces pombe* mus81 mutant. *Nucleic Acids Research*, **38**: (6): 1866-1873.
- Losada, A. and Hirano, T.** (2005) Dynamic molecular linkers of the genome: the first decade of SMC proteins. *Genes Dev*, **19**: (11): 1269-1287.
- Lukaszewski, A.J.** (1997) The development and meiotic behavior of asymmetrical isochromosomes in wheat. *Genetics*, **145**: (4): 1155-1160.
- Lydall, D., Nikolsky, Y., Bishop, D.K. and Weinert, T.** (1996) A meiotic recombination checkpoint controlled by mitotic checkpoint genes. *Nature*, **383**: (6603): 840-843.
- Macaisne, N., Novatchkova, M., Peirera, L., Vezon, D., Jolivet, S., Froger, N., Chelysheva, L., Grelon, M. and Mercier, R.** (2008) SHOC1, an XPF Endonuclease-Related Protein, Is Essential for the Formation of Class I Meiotic Crossovers. *Current Biology*, **18**: (18): 1432-1437.
- MacQueen, A.J., Phillips, C.M., Bhalla, N., Weiser, P., Villeneuve, A.M. and Dernburg, A.F.** (2005) Chromosome Sites Play Dual Roles to Establish Homologous Synapsis during Meiosis in *C. elegans*. *Cell*, **123**: (6): 1037-1050.
- Mallory, J.C. and Petes, T.D.** (2000) Protein kinase activity of Tel1p and Mec1p, two *Saccharomyces cerevisiae* proteins related to the human ATM protein kinase. *Proc Natl Acad Sci U S A*, **97**: (25): 13749-13754.
- Mankouri, H.W. and Hickson, I.D.** (2007) The RecQ helicase-topoisomerase III-Rmi1 complex: a DNA structure-specific 'dissolvasome'? *Trends Biochem Sci*, **32**: (12): 538-546.
- Martini, E., Borde, V., Legendre, M., Audic, S., Regnault, B., Soubigou, G., Dujon, B. and Llorente, B.** (2011) Genome-wide analysis of heteroduplex DNA in mismatch repair-deficient yeast cells reveals novel properties of meiotic recombination pathways. *PLoS Genet*, **7**: (9): e1002305.

- Martini, E., Diaz, R.L., Hunter, N. and Keeney, S.** (2006) Crossover Homeostasis in Yeast Meiosis. *Cell*, **126**: (2): 285-295.
- Mason, J.M. and Arndt, K.M.** (2004) Coiled Coil Domains: Stability, Specificity, and Biological Implications. *ChemBioChem*, **5**: (2): 170-176.
- Mazina, O.M., Mazin, A.V., Nakagawa, T., Kolodner, R.D. and Kowalczykowski, S.C.** (2004) *Saccharomyces cerevisiae* Mer3 helicase stimulates 3'-5' heteroduplex extension by Rad51; implications for crossover control in meiotic recombination. *Cell*, **117**: (1): 47-56.
- Melamed-Bessudo, C. and Levy, A.A.** (2012) Deficiency in DNA methylation increases meiotic crossover rates in euchromatic but not in heterochromatic regions in Arabidopsis. *Proc Natl Acad Sci U S A*, **109**: (16): E981-988.
- Mercier, R., Jolivet, S., Vezon, D., Huppe, E., Chelysheva, L., Giovanni, M., Nogué, F., Doutriaux, M.-P., Horlow, C., Grelon, M. and Mézard, C.** (2005) Two Meiotic Crossover Classes Cohabit in Arabidopsis. *Current Biology*, **15**: (8): 692-701.
- Merker, J.D., Dominska, M., Greenwell, P.W., Rinella, E., Bouck, D.C., Shibata, Y., Strahl, B.D., Mieczkowski, P. and Petes, T.D.** (2008) The histone methylase Set2p and the histone deacetylase Rpd3p repress meiotic recombination at the HIS4 meiotic recombination hotspot in *Saccharomyces cerevisiae*. *DNA Repair (Amst)*, **7**: (8): 1298-1308.
- Michaelis, C., Ciosk, R. and Nasmyth, K.** (1997) Cohesins: chromosomal proteins that prevent premature separation of sister chromatids. *Cell*, **91**: (1): 35-45.
- Mieczkowski, P.A., Dominska, M., Buck, M.J., Lieb, J.D. and Petes, T.D.** (2007) Loss of a histone deacetylase dramatically alters the genomic distribution of Spo11p-catalyzed DNA breaks in *Saccharomyces cerevisiae*. *Proc Natl Acad Sci U S A*, **104**: (10): 3955-3960.
- Mimitou, E.P. and Symington, L.S.** (2009) DNA end resection: Many nucleases make light work. *DNA Repair*, **8**: (9): 983-995.
- Mohaghegh, P., Karow, J.K., Brosh, R.M., Jr., Bohr, V.A. and Hickson, I.D.** (2001) The Bloom's and Werner's syndrome proteins are DNA structure-specific helicases. *Nucleic Acids Res*, **29**: (13): 2843-2849.
- Mullen, J.R., Nallaseth, F.S., Lan, Y.Q., Slagle, C.E. and Brill, S.J.** (2005) Yeast Rmi1/Nce4 controls genome stability as a subunit of the Sgs1-Top3 complex. *Mol Cell Biol*, **25**: (11): 4476-4487.
- Munoz, I.M., Hain, K., Declais, A.C., Gardiner, M., Toh, G.W., Sanchez-Pulido, L., Heuckmann, J.M., Toth, R., Macartney, T., Eppink, B., Kanaar, R., Ponting, C.P., Lilley, D.M. and Rouse, J.** (2009) Coordination of structure-specific nucleases by human SLX4/BTBD12 is required for DNA repair. *Mol Cell*, **35**: (1): 116-127.
- Nakagawa, T.** (2001) The MER3 Helicase Involved in Meiotic Crossing Over Is Stimulated by Single-stranded DNA-binding Proteins and Unwinds DNA in the 3' to 5' Direction. *Journal of Biological Chemistry*, **276**: (34): 31487-31493.
- Nasmyth, K. and Haering, C.H.** (2005) The Structure and Function of Smc and Kleisin Complexes. *Annual Review of Biochemistry*, **74**: (1): 595-648.
- Nishant, K.T., Plys, A.J. and Alani, E.** (2008) A Mutation in the Putative MLH3 Endonuclease Domain Confers a Defect in Both Mismatch Repair and Meiosis in *Saccharomyces cerevisiae*. *Genetics*, **179**: (2): 747-755.
- Niu, H., Li, X., Job, E., Park, C., Moazed, D., Gygi, S.P. and Hollingsworth, N.M.** (2007) Mek1 kinase is regulated to suppress double-strand break repair between sister chromatids during budding yeast meiosis. *Mol Cell Biol*, **27**: (15): 5456-5467.
- Niu, H., Wan, L., Baumgartner, B., Schaefer, D., Loidl, J. and Hollingsworth, N.M.** (2005) Partner choice during meiosis is regulated by Hop1-promoted dimerization of Mek1. *Mol Biol Cell*, **16**: (12): 5804-5818.
- Nonomura, K.I., Nakano, M., Murata, K., Miyoshi, K., Eiguchi, M., Miyao, A., Hirochika, H. and Kurata, N.** (2004) An insertional mutation in the rice PAIR2 gene, the ortholog of Arabidopsis ASY1 ,

results in a defect in homologous chromosome pairing during meiosis. *Molecular Genetics and Genomics*, **271**: (2): 121-129.

Oh, S.D., Lao, J.P., Hwang, P.Y., Taylor, A.F., Smith, G.R. and Hunter, N. (2007) BLM ortholog, Sgs1, prevents aberrant crossing-over by suppressing formation of multichromatid joint molecules. *Cell*, **130**: (2): 259-272.

Oh, S.D., Lao, J.P., Taylor, A.F., Smith, G.R. and Hunter, N. (2008a) RecQ Helicase, Sgs1, and XPF Family Endonuclease, Mus81-Mms4, Resolve Aberrant Joint Molecules during Meiotic Recombination. *Molecular Cell*, **31**: (3): 324-336.

Oh, S.D., Lao, J.P., Taylor, A.F., Smith, G.R. and Hunter, N. (2008b) RecQ helicase, Sgs1, and XPF family endonuclease, Mus81-Mms4, resolve aberrant joint molecules during meiotic recombination. *Mol Cell*, **31**: (3): 324-336.

Osakabe, K., Yoshioka, T., Ichikawa, H. and Toki, S. (2002) Molecular cloning and characterization of RAD51-like genes from *Arabidopsis thaliana*. *Plant Mol Biol*, **50**: (1): 71-81.

Osman, K., Higgins, J.D., Sanchez-Moran, E., Armstrong, S.J. and Franklin, F.C.H. (2011) Pathways to meiotic recombination in *Arabidopsis thaliana*. *New Phytologist*, **190**: (3): 523-544.

Osman, K., Sanchez-Moran, E., Mann, S.C., Jones, G.H. and Franklin, F.C. (2009) Replication protein A (AtRPA1a) is required for class I crossover formation but is dispensable for meiotic DNA break repair. *EMBO J*, **28**: (4): 394-404.

Panizza, S., Mendoza, M.A., Berlinger, M., Huang, L., Nicolas, A., Shirahige, K. and Klein, F. (2011) Spo11-accessory proteins link double-strand break sites to the chromosome axis in early meiotic recombination. *Cell*, **146**: (3): 372-383.

Panoli, A.P., Ravi, M., Sebastian, J., Nishal, B., Reddy, T.V., Marimuthu, M.P., Subbiah, V., Vijaybhaskar, V. and Siddiqi, I. (2006) AtMND1 is required for homologous pairing during meiosis in *Arabidopsis*. *BMC Mol Biol*, **7**: 24.

Parvanov, E.D., Petkov, P.M. and Paigen, K. (2010) Prdm9 controls activation of mammalian recombination hotspots. *Science*, **327**: (5967): 835.

Perrella, G., Consiglio, M.F., Aiese-Cigliano, R., Cremona, G., Sanchez-Moran, E., Barra, L., Errico, A., Bressan, R.A., Franklin, F.C. and Conicella, C. (2010) Histone hyperacetylation affects meiotic recombination and chromosome segregation in *Arabidopsis*. *Plant J*, **62**: (5): 796-806.

Pradillo, M., Lopez, E., Romero, C., Sanchez-Moran, E., Cunado, N. and Santos, J.L. (2007) An analysis of univalent segregation in meiotic mutants of *Arabidopsis thaliana*: a possible role for synaptonemal complex. *Genetics*, **175**: (2): 505-511.

Prieto, I., Suja, J.A., Pezzi, N., Kremer, L., Martinez, A.C., Rufas, J.S. and Barbero, J.L. (2001) Mammalian STAG3 is a cohesin specific to sister chromatid arms in meiosis I. *Nat Cell Biol*, **3**: (8): 761-766.

Puizina, J. (2004) Mre11 Deficiency in *Arabidopsis* Is Associated with Chromosomal Instability in Somatic Cells and Spo11-Dependent Genome Fragmentation during Meiosis. *The Plant Cell Online*, **16**: (8): 1968-1978.

Raynard, S., Zhao, W., Bussen, W., Lu, L., Ding, Y.Y., Busygina, V., Meetei, A.R. and Sung, P. (2008) Functional role of BLAP75 in BLM-topoisomerase IIIalpha-dependent holliday junction processing. *J Biol Chem*, **283**: (23): 15701-15708.

Revenkova, E., Eijpe, M., Heyting, C., Gross, B. and Jessberger, R. (2001) Novel meiosis-specific isoform of mammalian SMC1. *Mol Cell Biol*, **21**: (20): 6984-6998.

Riha, K. and Shippen, D.E. (2003) Telomere structure, function and maintenance in *Arabidopsis*. *Chromosome Res*, **11**: (3): 263-275.

Riley, R., Chapman, V. and Kimber, G. (1959) Genetic control of chromosome pairing in intergeneric hybrids with wheat. *Nature*, **183**: (4670): 1244-1246.

- Rockmill, B. and Roeder, G.S.** (1988) RED1: a yeast gene required for the segregation of chromosomes during the reductional division of meiosis. *Proc Natl Acad Sci U S A*, **85**: (16): 6057-6061.
- Rockmill, B. and Roeder, G.S.** (1990) Meiosis in asynaptic yeast. *Genetics*, **126**: (3): 563-574.
- Roeder, G.S. and Bailis, J.M.** (2000) The pachytene checkpoint. *Trends Genet*, **16**: (9): 395-403.
- Rogakou, E.P., Pilch, D.R., Orr, A.H., Ivanova, V.S. and Bonner, W.M.** (1998) DNA double-stranded breaks induce histone H2AX phosphorylation on serine 139. *J Biol Chem*, **273**: (10): 5858-5868.
- Ross-Macdonald, P. and Roeder, G.S.** (1994) Mutation of a meiosis-specific MutS homolog decreases crossing over but not mismatch correction. *Cell*, **79**: (6): 1069-1080.
- Ross, K.J., Fransz, P., Armstrong, S.J., Vizir, I., Mulligan, B., Franklin, F.C. and Jones, G.H.** (1997) Cytological characterization of four meiotic mutants of Arabidopsis isolated from T-DNA-transformed lines. *Chromosome Res*, **5**: (8): 551-559.
- San Filippo, J., Sung, P. and Klein, H.** (2008) Mechanism of Eukaryotic Homologous Recombination. *Annual Review of Biochemistry*, **77**: (1): 229-257.
- Sancar, A., Lindsey-Boltz, L.A., Ünsal-Kaçmaz, K. and Linn, S.** (2004) Molecular mechanisms of mammalian DNA repair and the DNA damage checkpoints. *Annual Review of Biochemistry*, **73**: (1): 39-85.
- Sanchez-Moran, E., Mercier, R., Higgins, J.D., Armstrong, S.J., Jones, G.H. and Franklin, F.C.** (2005) A strategy to investigate the plant meiotic proteome. *Cytogenet Genome Res*, **109**: (1-3): 181-189.
- Sanchez-Moran, E., Santos, J.L., Jones, G.H. and Franklin, F.C.H.** (2007) ASY1 mediates AtDMC1-dependent interhomolog recombination during meiosis in Arabidopsis. *Genes Dev*, **21**: (17): 2220-2233.
- Scherthan, H.** (2001) A bouquet makes ends meet. *Nat Rev Mol Cell Biol*, **2**: (8): 621-627.
- Schommer, C., Beven, A., Lawrenson, T., Shaw, P. and Sablowski, R.** (2003) AHP2 is required for bivalent formation and for segregation of homologous chromosomes in Arabidopsis meiosis. *Plant J*, **36**: (1): 1-11.
- Schwacha, A. and Kleckner, N.** (1994) Identification of joint molecules that form frequently between homologs but rarely between sister chromatids during yeast meiosis. *Cell*, **76**: (1): 51-63.
- Schwacha, A. and Kleckner, N.** (1997) Interhomolog bias during meiotic recombination: meiotic functions promote a highly differentiated interhomolog-only pathway. *Cell*, **90**: (6): 1123-1135.
- Schwartz, E.K. and Heyer, W.D.** (2011) Processing of joint molecule intermediates by structure-selective endonucleases during homologous recombination in eukaryotes. *Chromosoma*, **120**: (2): 109-127.
- Segurel, L., Leffler, E.M. and Przeworski, M.** (2011) The case of the fickle fingers: how the PRDM9 zinc finger protein specifies meiotic recombination hotspots in humans. *PLoS Biol*, **9**: (12): e1001211.
- Sheehan, M.J. and Pawlowski, W.P.** (2009) Live imaging of rapid chromosome movements in meiotic prophase I in maize. *Proceedings of the National Academy of Sciences*, **106**: (49): 20989-20994.
- Shinohara, A., Ogawa, H. and Ogawa, T.** (1992) Rad51 protein involved in repair and recombination in *S. cerevisiae* is a RecA-like protein. *Cell*, **69**: (3): 457-470.
- Shinohara, M., Oh, S.D., Hunter, N. and Shinohara, A.** (2008) Crossover assurance and crossover interference are distinctly regulated by the ZMM proteins during yeast meiosis. *Nature Genetics*, **40**: (3): 299-309.
- Shinohara, M., Sakai, K., Shinohara, A. and Bishop, D.K.** (2003) Crossover interference in *Saccharomyces cerevisiae* requires a TID1/RDH54- and DMC1-dependent pathway. *Genetics*, **163**: (4): 1273-1286.

- Shinohara, M., Shita-Yamaguchi, E., Buerstedde, J.M., Shinagawa, H., Ogawa, H. and Shinohara, A.** (1997) Characterization of the roles of the *Saccharomyces cerevisiae* RAD54 gene and a homologue of RAD54, RDH54/TID1, in mitosis and meiosis. *Genetics*, **147**: (4): 1545-1556.
- Shroff, R., Arbel-Eden, A., Pilch, D., Ira, G., Bonner, W.M., Petrini, J.H., Haber, J.E. and Lichten, M.** (2004) Distribution and dynamics of chromatin modification induced by a defined DNA double-strand break. *Curr Biol*, **14**: (19): 1703-1711.
- Shultz, R.W., Tatineni, V.M., Hanley-Bowdoin, L. and Thompson, W.F.** (2007) Genome-Wide Analysis of the Core DNA Replication Machinery in the Higher Plants Arabidopsis and Rice. *Plant Physiology*, **144**: (4): 1697-1714.
- Siaud, N., Dray, E., Gy, I., Gerard, E., Takvorian, N. and Doutriaux, M.P.** (2004) Brca2 is involved in meiosis in Arabidopsis thaliana as suggested by its interaction with Dmc1. *EMBO J*, **23**: (6): 1392-1401.
- Sjogren, C. and Nasmyth, K.** (2001) Sister chromatid cohesion is required for postreplicative double-strand break repair in *Saccharomyces cerevisiae*. *Curr Biol*, **11**: (12): 991-995.
- Smith, A.V. and Roeder, G.S.** (1997) The yeast Red1 protein localizes to the cores of meiotic chromosomes. *J Cell Biol*, **136**: (5): 957-967.
- Smith, G.R., Boddy, M.N., Shanahan, P. and Russell, P.** (2003) Fission yeast Mus81.Eme1 Holliday junction resolvase is required for meiotic crossing over but not for gene conversion. *Genetics*, **165**: (4): 2289-2293.
- Snowden, T., Acharya, S., Butz, C., Berardini, M. and Fishel, R.** (2004) hMSH4-hMSH5 Recognizes Holliday Junctions and Forms a Meiosis-Specific Sliding Clamp that Embraces Homologous Chromosomes. *Molecular Cell*, **15**: (3): 437-451.
- Soustelle, C., Vedel, M., Kolodner, R. and Nicolas, A.** (2002) Replication protein A is required for meiotic recombination in *Saccharomyces cerevisiae*. *Genetics*, **161**: (2): 535-547.
- Stacey, N.J., Kuromori, T., Azumi, Y., Roberts, G., Breuer, C., Wada, T., Maxwell, A., Roberts, K. and Sugimoto-Shirasu, K.** (2006) Arabidopsis SPO11-2 functions with SPO11-1 in meiotic recombination. *The Plant Journal*, **48**: (2): 206-216.
- Stahl, F.W.** (2004) Does Crossover Interference Count in *Saccharomyces cerevisiae*? *Genetics*, **168**: (1): 35-48.
- Storlazzi, A., Tesse, S., Gargano, S., James, F., Kleckner, N. and Zickler, D.** (2003) Meiotic double-strand breaks at the interface of chromosome movement, chromosome remodeling, and reductional division. *Genes Dev*, **17**: (21): 2675-2687.
- Storlazzi, A., Xu, L., Schwacha, A. and Kleckner, N.** (1996) Synaptonemal complex (SC) component Zip1 plays a role in meiotic recombination independent of SC polymerization along the chromosomes. *Proc Natl Acad Sci U S A*, **93**: (17): 9043-9048.
- Strom, L., Lindroos, H.B., Shirahige, K. and Sjogren, C.** (2004) Postreplicative recruitment of cohesin to double-strand breaks is required for DNA repair. *Mol Cell*, **16**: (6): 1003-1015.
- Sturtevant, A.H.** (1915) CASTLE AND WRIGHT ON CROSSING OVER IN RATS. *Science*, **42**: (1080): 342.
- Sugiyama, T., Kantake, N., Wu, Y. and Kowalczykowski, S.C.** (2006) Rad52-mediated DNA annealing after Rad51-mediated DNA strand exchange promotes second ssDNA capture. *EMBO J*, **25**: (23): 5539-5548.
- Sung, P.** (1997) Yeast Rad55 and Rad57 proteins form a heterodimer that functions with replication protein A to promote DNA strand exchange by Rad51 recombinase. *Genes & Development*, **11**: (9): 1111-1121.
- Svendsen, J.M., Smogorzewska, A., Sowa, M.E., O'Connell, B.C., Gygi, S.P., Elledge, S.J. and Harper, J.W.** (2009) Mammalian BTBD12/SLX4 assembles a Holliday junction resolvase and is required for DNA repair. *Cell*, **138**: (1): 63-77.

- Sym, M., Engebrecht, J.A. and Roeder, G.S.** (1993) ZIP1 is a synaptonemal complex protein required for meiotic chromosome synapsis. *Cell*, **72**: (3): 365-378.
- Symington, L.S.** (2002) Role of RAD52 Epistasis Group Genes in Homologous Recombination and Double-Strand Break Repair. *Microbiology and Molecular Biology Reviews*, **66**: (4): 630-670.
- Tay, Y.D. and Wu, L.** (2010) Overlapping Roles for Yen1 and Mus81 in Cellular Holliday Junction Processing. *Journal of Biological Chemistry*, **285**: (15): 11427-11432.
- Terasawa, M., Ogawa, H., Tsukamoto, Y., Shinohara, M., Shirahige, K., Kleckner, N. and Ogawa, T.** (2007) Meiotic recombination-related DNA synthesis and its implications for cross-over and non-cross-over recombinant formation. *Proceedings of the National Academy of Sciences*, **104**: (14): 5965-5970.
- Tesse, S., Storlazzi, A., Kleckner, N., Gargano, S. and Zickler, D.** (2003) Localization and roles of Ski8p protein in *Sordaria* meiosis and delineation of three mechanistically distinct steps of meiotic homolog juxtaposition. *Proc Natl Acad Sci U S A*, **100**: (22): 12865-12870.
- Thorslund, T., Esashi, F. and West, S.C.** (2007) Interactions between human BRCA2 protein and the meiosis-specific recombinase DMC1. *EMBO J*, **26**: (12): 2915-2922.
- Traven, A. and Heierhorst, J.** (2005) SQ/TQ cluster domains: concentrated ATM/ATR kinase phosphorylation site regions in DNA-damage-response proteins. *Bioessays*, **27**: (4): 397-407.
- Trelles-Sticken, E., Dresser, M.E. and Scherthan, H.** (2000) Meiotic telomere protein Ndj1p is required for meiosis-specific telomere distribution, bouquet formation and efficient homologue pairing. *J Cell Biol*, **151**: (1): 95-106.
- Tsubouchi, H. and Roeder, G.S.** (2002) The Mnd1 Protein Forms a Complex with Hop2 To Promote Homologous Chromosome Pairing and Meiotic Double-Strand Break Repair. *Molecular and Cellular Biology*, **22**: (9): 3078-3088.
- Tsubouchi, T., Zhao, H. and Roeder, G.S.** (2006) The Meiosis-Specific Zip4 Protein Regulates Crossover Distribution by Promoting Synaptonemal Complex Formation Together with Zip2. *Developmental Cell*, **10**: (6): 809-819.
- Uanschou, C., Siwiec, T., Pedrosa-Harand, A., Kerzendorfer, C., Sanchez-Moran, E., Novatchkova, M., Akimcheva, S., Woglar, A., Klein, F. and Schlogelhofer, P.** (2007) A novel plant gene essential for meiosis is related to the human CtlP and the yeast COM1/SAE2 gene. *EMBO J*, **26**: (24): 5061-5070.
- Uhlmann, F.** (2004) The mechanism of sister chromatid cohesion. *Experimental Cell Research*, **296**: (1): 80-85.
- Uhlmann, F. and Nasmyth, K.** (1998) Cohesion between sister chromatids must be established during DNA replication. *Curr Biol*, **8**: (20): 1095-1101.
- van Brabant, A.J., Ye, T., Sanz, M., German, I.J., Ellis, N.A. and Holloman, W.K.** (2000) Binding and melting of D-loops by the Bloom syndrome helicase. *Biochemistry*, **39**: (47): 14617-14625.
- Vazquez, J., Belmont, A.S. and Sedat, J.W.** (2002) The dynamics of homologous chromosome pairing during male *Drosophila* meiosis. *Curr Biol*, **12**: (17): 1473-1483.
- Vignard, J., Siwiec, T., Chelysheva, L., Vrielynck, N., Gonord, F., Armstrong, S.J., Schlogelhofer, P. and Mercier, R.** (2007) The interplay of RecA-related proteins and the MND1-HOP2 complex during meiosis in *Arabidopsis thaliana*. *PLoS Genet*, **3**: (10): 1894-1906.
- von Wettstein, D., Rasmussen, S.W. and Holm, P.B.** (1984) The synaptonemal complex in genetic segregation. *Annu Rev Genet*, **18**: 331-413.
- Wan, L., de los Santos, T., Zhang, C., Shokat, K. and Hollingsworth, N.M.** (2004) Mek1 kinase activity functions downstream of RED1 in the regulation of meiotic double strand break repair in budding yeast. *Mol Biol Cell*, **15**: (1): 11-23.
- Wang, K., Wang, M., Tang, D., Shen, Y., Qin, B., Li, M. and Cheng, Z.** (2010a) PAIR3, an axis-associated protein, is essential for the recruitment of recombination elements onto meiotic chromosomes in rice. *Molecular Biology of the Cell*, **22**: (1): 12-19.

- Wang, K., Wang, M., Tang, D., Shen, Y., Qin, B., Li, M. and Cheng, Z.** (2011) PAIR3, an axis-associated protein, is essential for the recruitment of recombination elements onto meiotic chromosomes in rice. *Mol Biol Cell*, **22**: (1): 12-19.
- Wang, M., Wang, K., Tang, D., Wei, C., Li, M., Shen, Y., Chi, Z., Gu, M. and Cheng, Z.** (2010b) The central element protein ZEP1 of the synaptonemal complex regulates the number of crossovers during meiosis in rice. *Plant Cell*, **22**: (2): 417-430.
- Wang, T.F., Kleckner, N. and Hunter, N.** (1999) Functional specificity of MutL homologs in yeast: evidence for three Mlh1-based heterocomplexes with distinct roles during meiosis in recombination and mismatch correction. *Proc Natl Acad Sci U S A*, **96**: (24): 13914-13919.
- Wang, X. and Haber, J.E.** (2004) Role of Saccharomyces Single-Stranded DNA-Binding Protein RPA in the Strand Invasion Step of Double-Strand Break Repair. *PLoS Biology*, **2**: (1): e21.
- Waterworth, W.M., Altun, C., Armstrong, S.J., Roberts, N., Dean, P.J., Young, K., Weil, C.F., Bray, C.M. and West, C.E.** (2007) NBS1 is involved in DNA repair and plays a synergistic role with ATM in mediating meiotic homologous recombination in plants. *The Plant Journal*, **52**: (1): 41-52.
- Watt, P.M., Hickson, I.D., Borts, R.H. and Louis, E.J.** (1996) SGS1, a homologue of the Bloom's and Werner's syndrome genes, is required for maintenance of genome stability in Saccharomyces cerevisiae. *Genetics*, **144**: (3): 935-945.
- Weinert, T.A. and Hartwell, L.H.** (1988) The RAD9 gene controls the cell cycle response to DNA damage in Saccharomyces cerevisiae. *Science*, **241**: (4863): 317-322.
- White, C.I.** (2008) News from Arabidopsis on the meiotic roles of Blap75/Rmi1 and Top3alpha. *PLoS Genet*, **4**: (12): e1000306.
- Wijeratne, A.J.** (2005) The Arabidopsis thaliana PARTING DANCERS Gene Encoding a Novel Protein Is Required for Normal Meiotic Homologous Recombination. *Molecular Biology of the Cell*, **17**: (3): 1331-1343.
- Wojtasz, L., Daniel, K., Roig, I., Bolcun-Filas, E., Xu, H., Boonsanay, V., Eckmann, C.R., Cooke, H.J., Jasin, M., Keeney, S., McKay, M.J. and Toth, A.** (2009) Mouse HORMAD1 and HORMAD2, Two Conserved Meiotic Chromosomal Proteins, Are Depleted from Synapsed Chromosome Axes with the Help of TRIP13 AAA-ATPase. *PLoS Genetics*, **5**: (10): e1000702.
- Wold, M.S.** (1997) Replication protein A: a heterotrimeric, single-stranded DNA-binding protein required for eukaryotic DNA metabolism. *Annu Rev Biochem*, **66**: 61-92.
- Woltering, D., Baumgartner, B., Bagchi, S., Larkin, B., Loidl, J., de los Santos, T. and Hollingsworth, N.M.** (2000) Meiotic segregation, synapsis, and recombination checkpoint functions require physical interaction between the chromosomal proteins Red1p and Hop1p. *Mol Cell Biol*, **20**: (18): 6646-6658.
- Woods, L.M., Hodges, C.A., Baart, E., Baker, S.M., Liskay, M. and Hunt, P.A.** (1999) Chromosomal influence on meiotic spindle assembly: abnormal meiosis I in female Mlh1 mutant mice. *J Cell Biol*, **145**: (7): 1395-1406.
- Xu, L., Weiner, B.M. and Kleckner, N.** (1997) Meiotic cells monitor the status of the interhomolog recombination complex. *Genes Dev*, **11**: (1): 106-118.
- Yamada, T., Mizuno, K., Hirota, K., Kon, N., Wahls, W.P., Hartsuiker, E., Murofushi, H., Shibata, T. and Ohta, K.** (2004) Roles of histone acetylation and chromatin remodeling factor in a meiotic recombination hotspot. *EMBO J*, **23**: (8): 1792-1803.
- Yelina, N.E., Choi, K., Chelysheva, L., Macaulay, M., de Snoo, B., Wijnker, E., Miller, N., Drouaud, J., Grelon, M., Copenhaver, G.P., Mezard, C., Kelly, K.A. and Henderson, I.R.** (2012) Epigenetic remodeling of meiotic crossover frequency in Arabidopsis thaliana DNA methyltransferase mutants. *PLoS Genet*, **8**: (8): e1002844.
- Youds, J.L., Mets, D.G., McIlwraith, M.J., Martin, J.S., Ward, J.D., NJ, O.N., Rose, A.M., West, S.C., Meyer, B.J. and Boulton, S.J.** (2010) RTEL-1 enforces meiotic crossover interference and homeostasis. *Science*, **327**: (5970): 1254-1258.

- Yuan, L., Liu, J.G., Zhao, J., Brundell, E., Daneholt, B. and Hoog, C.** (2000) The murine SCP3 gene is required for synaptonemal complex assembly, chromosome synapsis, and male fertility. *Mol Cell*, **5**: (1): 73-83.
- Yuan, W., Li, X., Chang, Y., Wen, R., Chen, G., Zhang, Q. and Wu, C.** (2009) Mutation of the rice gene PAIR3 results in lack of bivalent formation in meiosis. *Plant J*, **59**: (2): 303-315.
- Zakharyevich, K., Ma, Y., Tang, S., Hwang, P.Y., Boiteux, S. and Hunter, N.** (2010) Temporally and biochemically distinct activities of Exo1 during meiosis: double-strand break resection and resolution of double Holliday junctions. *Mol Cell*, **40**: (6): 1001-1015.
- Zakharyevich, K., Tang, S., Ma, Y. and Hunter, N.** (2012) Delineation of Joint Molecule Resolution Pathways in Meiosis Identifies a Crossover-Specific Resolvase. *Cell*, **149**: (2): 334-347.
- Zalevsky, J., MacQueen, A.J., Duffy, J.B., Kempthues, K.J. and Villeneuve, A.M.** (1999) Crossing over during *Caenorhabditis elegans* meiosis requires a conserved MutS-based pathway that is partially dispensable in budding yeast. *Genetics*, **153**: (3): 1271-1283.
- Zhang, C., Song, Y., Cheng, Z.-h., Wang, Y.-x., Zhu, J., Ma, H., Xu, L. and Yang, Z.-N.** (2012) The *Arabidopsis thaliana* DSB FORMATION (AtDFO) Gene is Required for Meiotic Double Strand Break Formation. *The Plant Journal*, no-no.
- Zhang, X., Henriques, R., Lin, S.S., Niu, Q.W. and Chua, N.H.** (2006) Agrobacterium-mediated transformation of *Arabidopsis thaliana* using the floral dip method. *Nat Protoc*, **1**: (2): 641-646.
- Zickler, D. and Kleckner, N.** (1998) The leptotene-zygotene transition of meiosis. *Annu Rev Genet*, **32**: 619-697.
- Zickler, D. and Kleckner, N.** (1999) Meiotic chromosomes: integrating structure and function. *Annu Rev Genet*, **33**: 603-754.

APPENDIX

9.1. GENERAL BUFFERS AND SOLUTIONS

CYTOLOGY

1x PBS

Phosphate Buffer Saline (Sigma) 1 tablet per 100ml SDW
(pH 7)

Citrate Buffer

Citric acid	0.1 M
Sodium citrate	0.1 M

Diluted 1:10 with SDW (pH 5.4)

20x SSC

NaCl	3 M
Trisodium citrate	300 mM

pH 7 using HCl

Alexander Stain

Ethanol 95%	10 ml
Malachite green (1% in 95% Ethanol)	1 ml
Fuchsin acid (1% in water)	5 ml
Orange G (1% in water)	0.5 ml
Phenol	5g
Chloral hydrate	5g
Glacial acetic acid	2 ml
Glycerol	25 ml
Distilled water	50 ml

NUCLEIC ACID MANIPULATIONS

DNA Loading Buffer

Bromophenol blue	50µl
SDW	138µl

LB Medium

1-1bacto-tryptone	10g
1-1 bacto-yeast extract	5g
NaCl	10g

5x TBE

Tris	0.445 M
Boric acid	0.445 M
EDTA	0.01 M

LB Agar

1-1bacto-tryptone	10g
1-1 bacto-yeast extract	5g
NaCl	10g
Bacto-agar	15g

DNA Extraction Buffer

KCl	0.25 M
EDTA	10 mM
Tris-HCl	100 mM

Media was prepared in SDW and sterilised by autoclaving at 15 psi C for 20 min.

Dilution Buffer

3x BSA in water

PROTEIN MANIPULATIONS

5x Protein Loading Buffer (PLB)

Tris-HCl (pH 6.8)	12.5%(v/v)
SDS	2%(w/v)
Glycerol	10%(v/v)
B-Mercaptoethanol	5%(v/v)
Bromophenol blue	0.001%(w/v)

Lysis Buffer

Tris HCl	50 mM
NaCl	100 mM
EDTA	1 mM
pH 8	

1x Reservoir Buffer

Tris	25 mM
Glycine	192 mM
SDS	0.1 %(w/v)
pH 8.3	

Denaturing Buffer

NaH ₂ PO ₄	100 mM
Tris HCl	10 mM
Urea pH 8	8 M

Western Transfer Buffer

Methanol	20 %(v/v)
Sodium hydrogen carbonate	0.01 M
Sodium carbonate	3.0mM

Coomassie Blue Stain

Coomassie Blue	1%
SDW	45 %(v/v)
Methanol	45 %(v/v)
Glacial acetic acid	10%

Milk Block

PBS	1x
Milk powder	5% (w/v)

Destain

Methanol	30 %(v/v)
Glacial acetic acid	10 %(v/v)

Elution Buffer

Tris HCl	50 mM
NaCl	300 mM
Urea	8 M
Varying concentrations of Imidazol, pH 8	

Rehydration Buffer

Urea	8 M
CHAPS	2%
Bromophenol Blue	Few grains

IP Buffer

Tris HCl (pH 7.5)	20 mM
NaCl	150 mM
Glycerol	10%
EDTA	2 mM

Equilibration Buffer

Tris HCl (pH 8.8)	50 mM
Urea	6 M
Glycerol	30%
SDS	2%
Bromophenol Blue	Few grains

9.2. List of primers

	Other name	Sequence (5' - 3')	T _m (°C)	Purpose
T7 promoter		TAATACGACTCACTATAGGG		Sequencing
M13 forward		TGACCGGCAGCAAATG		
M13 reverse		AACAGCTATGACCATG		
Oligo dt 24		TTTTTTTTTTTTTTTTTTTTTTTTTTTT	42.2	RT-PCR
GAPD-N	GAPD-N	CTTGAAGGGTGGTGCCAAGAAGG	64.2	<i>GAPD</i> expression
GAPD-C	GAPD-C	CCTGTTGTCGCCAACGAAGTCAG	64.2	

LB3	Sail Lb3	TTCATAACCAATCTCGATACAC	54.7	Genotyping
LBb1.3	Salk LBb1.3	ATTTTGCCGATTTTCGGAAC	52.4	
Wisc LB		AACGTCCGCAATGTGTTAAGTTGT	62.2	
DMC1A		CCTGCAATGGTCTCATGATGCATA	63	
DMC1B		GATGCAATCGATATCAGCCAATTTTAGAC	62.4	
DMC1C		AGGTACTCTGTCTCTCAATG	55.3	
DMC1D		ACTAATCCTTCGCGTCAGCAATGC	62.7	
RAD51NO8LP		TTCAGGATGGTGTCTCAGAGC	59.8	
RAD51NO8RP		ATGCCAAGGTTGACAAGATTG	55.9	
SPO11F4		GAGGATATCCAGATGTCTC	54.5	

SPO11 R1		AGGAGAGCTTACTTCACGAC	52.2	
MSH4 F3		CGCATATGGAGATTGGTTTAGACACTTAC	63.9	
MSH4 R2		GCGTTGTGGAATGGATCAATG	57.9	
4AF1	AT1G10930EXF2	ACCTAAGACCTGGCGTTACTC	59.8	<i>AtRECQ4A</i> expression
4AR1	AT1G10930EXR1	CAGGTGTGACATATAGCAAC	55.3	
4BF1	BLMBEXFWD1	CTGGTTCTGAAGAGAGGGAAC	59.8	<i>AtRECQ4B</i> expression
4BR1	BLMBEXREV1	GCTGGTTGTTGCAGTAGCTG	59.4	
AT1G10930TDNA(2)		GCTCTGATCGTGTTGGACAG	59.4	<i>AtRECQ4A</i> genotyping
AT1G10930TDNA(2R)		GAATAAGAGACACAAGTGGAG	55.9	

At1g60930 F1		GCTGGTTGTTGCAGTAGCTG	59.4	<i>AtRECQ4B</i> genotyping
At1g60930R1		TTCAGGAGCTGAGCTAG	59.4	
ASY3-1-F1	676F1	AGGAGATGCTTCTGGAGAAC	57.3	<i>AtASY3</i> genotyping
ASY3-1-R1	676R1	CTGGTGCCAACTTAGGTCGC	61.4	
ASY3-2-F1	H01LP	CACGACACGTCCAATGCCC	61	
ASY3-2-R1	H01RP	CGAGCAAGAGCAATACTCCAC	59.8	
ASY3-3-F1	971LP	CCAGACTCTCATGTTCCACAAC	60.3	
ASY3-3-R1	971RP	GCGAGACTCAGATGGTTCAAG	59.8	
ASY3-EX-F1	ASY3-Ex-LP	GAAGAGCCATAGCGAACAATGC	60.3	
ASY3-EX-R1	ASY3-Ex-RP	CATCCACAGAGCAAAGCCCGG	63.7	

ASY3-CM-F1	RED1_CDNA_FWD 1	CCCTCGAGAACCGACACACCATTTTGAG	68	AtASY3 complementaio n
ASY3-CM-R1	RED1_CDNA_REV 1	GCACTAGTATATATCAAGATATCAATAACC	59.9	
COMP-GENO-676LP		GCCGCTTCAGTTTATGAAGG	57.3	
COMP-GENO-676RP		CGAGCAAGAGCAATACTCCAC	59.8	
ASY3-AB-F1	RED1F1	CCATATGATCAGCCCCGAAGAAAGAG	60	ASY3 antibody
ASY3-AB-R1	RED1R1	CGCTCGAGATCATCCCTCAAACATTCTGCGAC	65	
RED1 CDNA F1		GGTCTCCGAGATCGTCTCATCGG	66	AtASY3 cDNA sequencing
RED1 CDNA F2		GGTGCCAACTTAGGTCGCAAGTGC	66.1	
RED1 CDNA F3		CCTCTCAAGGGACAACAGGCC	63.7	

RED1 CDNA F4		GCCGAAACAAGATTACAAGAGC	58.4	
3RACE17AP		GACTCGAGTCGACATCGATTTTTTTTTTTTTTTT TT	62.6	<i>BoASY3</i> 3□ RACE
3RACE17AP		GACTCGAGTCGACATCGA	56	
BRA486-3RACEF1		GGGCAATGGACGTGTTACCTCGTC	66.1	
BRA486-3RACEF2		CAGAGGTGGATGAAGATGAAGGC	62.4	
BRAS4486F2		GCCATATGCCTGAAGCATCTCCTTTGC	66.5	
BRAS4486F3		ATGAGCGAATACAGAAGCTTCGGCAG	64.8	<i>BoASY3</i> sequencing
BRAS4486F4		GCACCAATCTCAAGTCCTTCCCCCTG	68	
BRAS4486R2		GCATTGTCCAGTTTTGTCTCGATGCCTCC	68.1	

BO486TAQF1		GATGGATAAGAGTCCTGAGAGG	60.3	
BO486TAQF2		GCTGTAAAATGCCGCAAGGTTC	60.3	
BO486TAQR1		GCGGCAAGACTGCAGATGGAGG	65.8	
BO486TAQR2		CAGAATCCCATCAGCTTCATCC	60.3	
BO486TAQR3		GGATGCAAAGGAGATGCTTCAGG	62.4	
ASY1-F		GCAGAGATCACTGAGCAGGACTCG	66.1	<i>AtASY1</i> genotyping
ASY1-R		CGGACCATCAACAGTTTCACATATGC	63.2	
ASY1TA-TRAN-IDF1		CGCTAAAGGTCAAGAGCGTG	53.8	<i>AtASY1</i> T295A sequencing
ASY1TA-TRAN-IDR1		GAGAGACAAGACACCAGAGAG	54.4	

9.3 List of publications and presentations

Publications

Ferdous, M., Higgins, J. D., Osman, K., Lambing, C., Roitinger, E., Mechtler K., Armstrong, S. J., Perry, R., Pradillo, M., Cuñado, N. and Franklin, F. C. H. (2012), Inter-homolog crossing-over and synapsis in *Arabidopsis* meiosis are dependent on the chromosome axis protein AtASY3. ***PLoS Genetics*** 8(2): e1002507.

Higgins, J. D., **Ferdous, M.**, Osman, K. and Franklin, F. C. H. (2011), The RecQ helicase AtRECQ4A is required to remove inter-chromosomal telomeric connections that arise during meiotic recombination in *Arabidopsis*. ***The Plant Journal***, 65: 492–502.

Lambing, C., Osman, K., Corredor E., Machlicova, A., Higgins, J.D., Ferdous, M., and Franklin, F. C. H., Phosphorylation of AtASY1 is required to ensure inter-homologue crossover formation in *Arabidopsis thaliana*. Project ongoing.

Oral presentations

Maheen Ferdous, James D. Higgins, Christophe Lambing, Kim Osman, F. Chris H. Franklin (2011), The axis protein ASY3 promotes inter-homolog recombination and synapsis in *Arabidopsis thaliana*. Bioscience Graduate Research School Symposium, University of Birmingham, (UK).

Maheen Ferdous, James D Higgins, F. Chris. H. Franklin (2010), ASY3 mediates interhomolog recombination and synapsis in *Arabidopsis*. Gordon-Kenan Research Seminar, New Hampshire, USA.

Maheen Ferdous, James D Higgins, F. Chris. H. Franklin (2010), ASY3, a novel component of the meiotic chromosome axes, is required for chromosome synapsis and crossover formation in *Arabidopsis thaliana*. British Meiosis Meeting, Leicester, UK.

Poster presentations

Maheen Ferdous, Christophe Lambing, James D. Higgins, Kim Osman, F. Chris H. Franklin (2011), The axis protein ASY3 promotes inter-homolog recombination and synapsis in *Arabidopsis thaliana*. Chromatin Research Symposium, Birmingham, UK.

Maheen Ferdous, Christophe Lambing, James D. Higgins, Kim Osman, F. Chris H. Franklin (2011), The axis protein ASY3 promotes inter-homolog recombination and synapsis in *Arabidopsis thaliana*. British Meiosis Meeting, Sheffield, UK.

Maheen Ferdous, James D Higgins, F. Chris. H. Franklin (2010), ASY3, a novel component of the meiotic chromosome axes that is required for chromosome synapsis and crossover formation during meiosis in *Arabidopsis thaliana*. Gordon Research Conference: Meiosis, New Hampshire, USA.

Maheen Ferdous, James D Higgins, F. Chris. H. Franklin (2010), ASY3, a novel component of the meiotic chromosome axes that is required for chromosome synapsis and crossover formation during meiosis in *Arabidopsis thaliana*. Gordon-Kenan Meiosis Research Seminar, New Hampshire, USA.

Maheen Ferdous, James D Higgins, F. Chris. H. Franklin (2009), ASY3, a novel component of the meiotic chromosome axes, is required for chromosome synapsis and crossover formation in *Arabidopsis thaliana*. Bioscience Graduate Research School Symposium, University of Birmingham, (UK).

Other scientific activities

Co-organizer of the student-led Chromatin Research Symposium, 2011, Birmingham, UK.